Unpeeling a homoclinic banana in the FitzHugh–Nagumo system

Paul Carter
Department of Mathematics
University of Arizona

Björn Sandstede
Division of Applied Mathematics
Brown University

Abstract

The FitzHugh–Nagumo equations are known to admit fast traveling pulse solutions with monotone tails. It is also known that this system admits traveling pulses with exponentially decaying oscillatory tails. Upon numerical continuation in parameter space, it has been observed that the oscillations in the tails of the pulses grow into a secondary excursion resembling a second copy of the primary pulse. In this paper, we outline in detail the geometric mechanism responsible for this single-to-double-pulse transition, and we construct the transition analytically using geometric singular perturbation theory and blow-up techniques.

Contents

1 Introduction

The FitzHugh–Nagumo system is a singularly perturbed reaction-diffusion partial differential equation (PDE) which arose as a simplification of the Hodgkin–Huxley model [17] for the propagation of nerve impulses in axons. We consider this system in the form

$$\begin{aligned} u_t &= u_{xx} + f(u) - w, \\ w_t &= \delta(u - \gamma w), \end{aligned} \tag{1.1}$$

for $x \in \mathbb{R}$, where $f(u) = u(u-a)(1-u)$, with $0 < a < \frac{1}{2}$, $0 < \delta \ll 1$, and $\gamma > 0$.

We are interested in solutions resembling nerve impulses. Such solutions, which we refer to as pulses, correspond to traveling waves that propagate with constant speed and are localized, i.e. the profiles converge to zero as $|x|$ goes to infinity.

To find traveling waves, we search for solutions of the form $(u, w)(x, t) = (u, w)(x + ct)$ for wavespeeds $c > 0$. Finding traveling pulse solutions to (1.1) is equivalent to finding localized solutions of the traveling wave ODE

$$\begin{aligned} \dot{u} &= v \\ \dot{v} &= cv - f(u) + w \\ \dot{w} &= \epsilon(u - \gamma w) \ , \end{aligned} \tag{1.2}$$

where we denote by $\dot{} = \dfrac{d}{d\xi}$ differentiation with respect to the traveling wave variable $\xi = x + ct$, and where $0 < \epsilon = \delta/c \ll 1$. In addition, we take $\gamma > 0$ sufficiently small so that $(u, v, w) = (0, 0, 0)$ is the only equilibrium of the system (1.2). In all of our numerical computations, we fix $\gamma = 0.5$.

It is well known that for each $0 < a < 1/2$ and each sufficiently small $\epsilon > 0$, (1.1) admits "slow" and "fast" traveling pulse solutions. Equivalently, in (1.2) this corresponds to the existence of orbits homoclinic to the only equilibrium $(u, v, w) = (0, 0, 0)$ with constant wave speeds c: Slow pulses have wave speeds close to zero and arise as regular perturbations from the limit $\epsilon \to 0$. Fast pulses have speeds that are bounded away from zero as $\epsilon \to 0$ and cannot be constructed as regular perturbations from $\epsilon = 0$ as in the case of slow pulses. The existence result for fast pulses has been obtained using a number of different techniques: classical singular perturbation theory [15], Conley index [3], and geometric singular perturbation theory [20]. This last viewpoint is the one we shall adopt.

A schematic bifurcation diagram depicting the existence results for pulses is shown in Figure 1. The existence region is composed of two branches: the upper branch represents the fast pulses, and the lower branch represents the slow pulses. It has been shown in [21] that near the point $(c, a, \epsilon) = (0, 1/2, 0)$, these two branches coalesce and form a surface as shown.

In general, both slow and fast pulses as described above have monotone tails as $x \to \pm\infty$. However, it was shown in [5] that (1.1) also admits fast traveling pulses with small amplitude, exponentially decaying oscillatory tails in the region near the point $(c, a, \epsilon) = (1/\sqrt{2}, 0, 0)$, which corresponds to the upper left corner of the bifurcation diagram in Figure 1. In the linearization of (1.2) about $(u, v, w) = (0, 0, 0)$ this transition is characterized by two real eigenvalues which collide and then split as a complex conjugate pair; when a homoclinic orbit is present in this situation, it is referred to as a Belyakov transition [18, §5.1.4]. In [5], it was shown that for sufficiently small $a, \epsilon > 0$ this transition occurs when

$$\epsilon = \frac{\sqrt{2}a^2}{4} + \mathcal{O}\left(a^3\right), \tag{1.3}$$

and proving the existence of pulses with oscillatory tails amounted to showing that pulses exist on either side of this transition (see Figure 1 — the red curve denotes the location of the Belyakov transition).

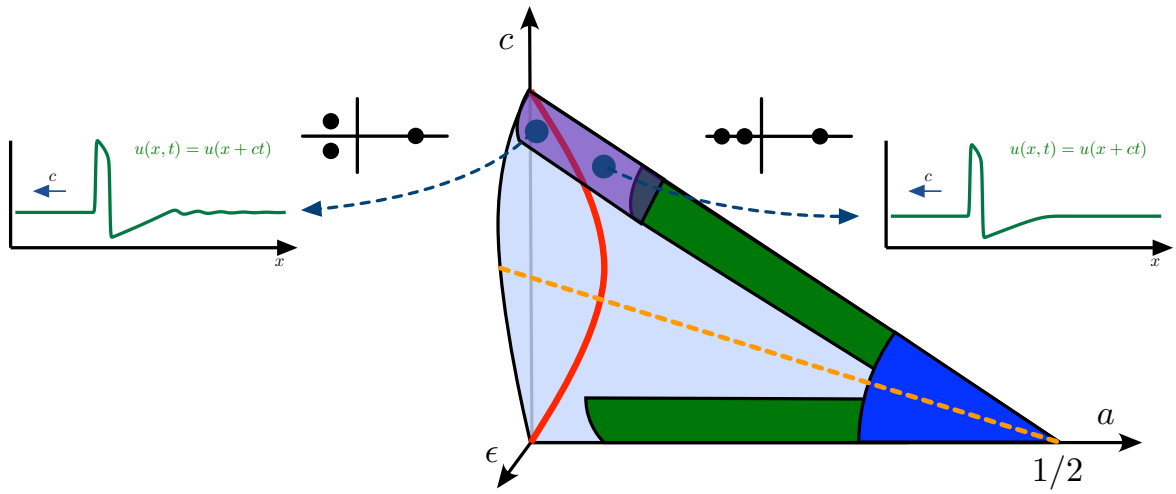

Figure 1: *Shown is the bifurcation diagram indicating the classical regions of existence for pulses in (1.2). Pulses on the upper green branch are referred to as "fast" pulses, while those along the lower green branch are called "slow" pulses. It is known [21] that these two branches coalesce near the point* $(c, a, \epsilon) = (0, 1/2, 0)$ *and form the blue surface shown. It has been conjectured [29] that these two branches connect globally and are in fact part of a larger surface (shown in light blue). The purple surface denotes the extension beyond the Belyakov transition (shown in red) to the region of pulses with oscillatory tails. Also shown are profiles of a fast pulse with monotone tail and fast pulse with oscillatory tail obtained numerically for the parameter values* $(c, a, \epsilon) = (0.593, 0.069, 0.0036)$ *and* $(c, a, \epsilon) = (0.689, 0.002, 0.0036)$*, respectively.*

Figure 1 also shows profiles of a fast monotone and fast oscillatory pulse obtained numerically. Such pulse solutions with oscillatory tails are interesting due to the possibility of constructing multi-pulses, which consist of several well-separated copies of the original pulse [18, §5.1.2]. We also note that pulses with oscillatory tails have been observed in FitzHugh–Nagumo-type systems with cross diffusion terms [30].

Combining these two different existence results for fast pulses, the well known classical existence result [20] in the region where $0 < \epsilon \ll a < \frac{1}{2}$, and the extension [5] to the regime $0 < a, \epsilon \ll 1$, encompassing the onset of oscillations in the tails of the pulses, we have the following theorem.

Theorem 1.1 ([5, 20])**.** *There exists* $K^* > 0$ *such that for each* $0 < \kappa < 1/2$ *and* $K > K^*$ *the following holds. There exists* $\epsilon_0 > 0$ *such that for each* $(a, \epsilon) \in [0, \frac{1}{2} - \kappa] \times (0, \epsilon_0)$ *satisfying* $\epsilon < Ka^2$ *system* (1.2) *admits a traveling-pulse solution with wave speed* $c = \check{c}(a, \epsilon)$ *approximated uniformly in* a *by*

$$\check{c} = \sqrt{2}\left(\tfrac{1}{2} - a\right) + \mathcal{O}(\epsilon).$$

Furthermore, if we have in addition $\epsilon > K^* a^2$*, then the tail of the pulse decays in an oscillatory fashion.*

We remark that while the slow pulses are known to be unstable in the PDE (1.1), it was proved independently by Jones [19] and Yanagida [29] that the fast pulses (with monotone tails) are stable for each fixed $0 < a < \frac{1}{2}$ provided $\epsilon > 0$ is sufficiently small. This stability result has also been recently extended in [4] to all pulses in Theorem 1.1, including those with oscillatory tails.

This paper is concerned with understanding the following phenomenon associated with the above traveling pulses: when continuing these pulses numerically in the parameters (c, a) for fixed ϵ, the continuation traces out a C-shaped (or rather, backwards C-shaped) curve; see Figure 2a. This is to be expected when considering an $\epsilon =$ const slice of the bifurcation diagram in Figure 1. When approaching the upper left corner of this bifurcation diagram, the pulses develop oscillations in the tails as described above, but the curve does not terminate; instead, as shown in Figure 2, the curve turns back sharply, and the oscillations in the tails of the pulses grow into a secondary pulse resembling the primary pulse via a mechanism resembling a canard explosion. The curve then

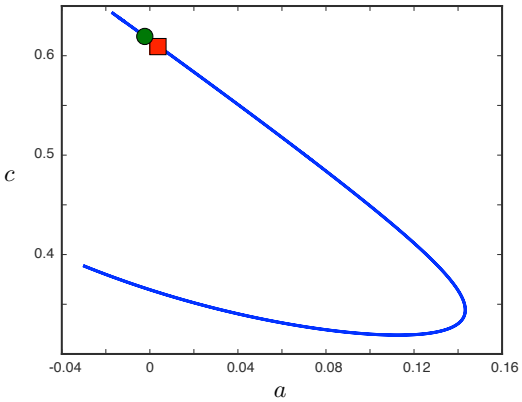

(a) *Homoclinic C-curve: c vs. a*

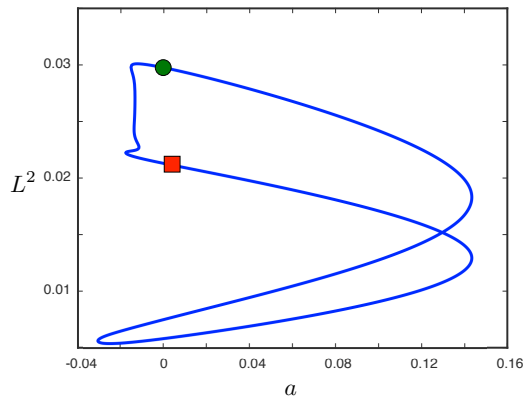

(b) *Homoclinic banana : L^2-norm vs. a*

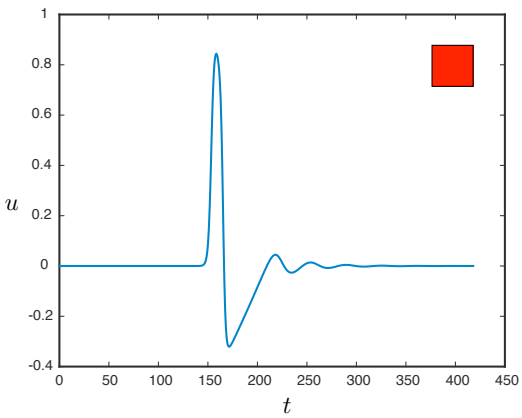

(c) *Shown is a pulse with oscillatory tail for* $(c, a, \epsilon) = (0.005, 0.608, 0.021)$.

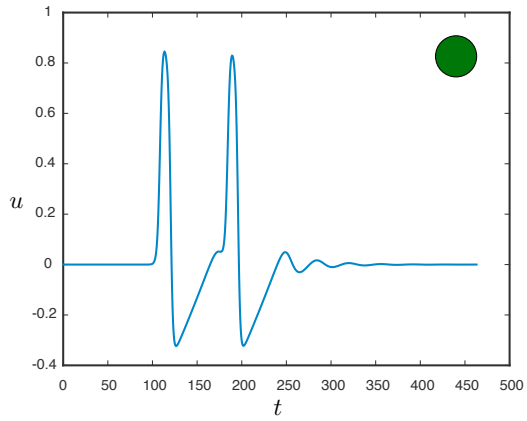

(d) *Shown is a double pulse for* $(c, a, \epsilon) = (0.001, 0.612, 0.021)$.

Figure 2: *Plotted are the homoclinic C-curve (a) and banana (b) obtained by continuing the pulse solution in the parameters* (a, c) *for* $\epsilon = 0.021$. *The red square and green circle refer to the locations of an example oscillatory pulse (c) and double pulse (d), respectively.*

retraces itself, and the double pulse transitions back into a single pulse near the lower left corner of the bifurcation diagram. Plotting the parameter a versus the L^2-norm of the solution as in Figure 2b shows that this C-curve is indeed composed of two curves forming a so-called homoclinic banana [6]. This homoclinic C-curve and banana are shown in Figure 2, as well as a single and double pulse on either side of this sharp transition.

Numerical explorations of the FitzHugh–Nagumo system have resulted in possible explanations for the termination of the branch of pulses in the upper left corner of the C-curve and the structure of the homoclinic banana [6, 12, 13]. There are several mechanisms at work, including a singular Hopf bifurcation occurring at the equilibrium as well as the presence of canard orbits and maximal canards (tangency of attracting and repelling slow manifolds). Figure 3 shows a schematic bifurcation diagram projected into (a, ϵ)-space. Shown are curves representing the location of a Hopf bifurcation (indicating exchange of stability of two complex conjugate eigenvalues) and the Belyakov transition occurring in the linearization of the vector field at the equilibrium, as well as the location of a maximal canard denoting the tangency of a repelling slow manifold and an attracting slow manifold near the equilibrium.

When continuing the classical branch of fast 1-pulses (green curve), the oscillations in the tails develop after crossing the Belyakov transition due to the change in eigenvalue structure near the equilibrium. Continuing further, it is clear that the branch cannot continue forever for decreasing a as it is blocked by the Hopf bifurcation. In fact, as stated above, this branch instead undergoes a 1-to-2-pulse transition and turns back sharply before

reaching the Hopf bifurcation.

In [13], the authors identified the proximity of this sharp turn to the tangency of certain invariant manifolds, namely the stable manifold of the equilibrium and the unstable manifold of a saddle slow manifold. However, the exact nature of the sharp turn in the C-curve, and in particular the continuous transition between the single and double pulse, is not fully understood; it is our aim in this work to fully unfold this transition – we will also explain the tangency observed in [13] (see Remark 4.6). In [5], we proposed a geometric mechanism which explains this transition, best visualized in the three-dimensional phase space: Figure 4 shows a zoom of the upper left part of the banana for a lower value of ϵ as well as six different pulses along the curve plotted together. See the accompanying animation M108070_01.mp4 [local/web 5.49MB] for a visualization of the transition.

The goal of this paper is to construct this transition analytically using geometric singular perturbation theory and blow up techniques as in the construction of the oscillatory pulses in [5, Theorem 1.1]. Specifically we aim to extend the existence result Theorem 1.1 for fast pulses to include this transition by proving the following theorem, which for now we state informally.

Theorem. *For each sufficiently small $\epsilon > 0$, there exists a one-parameter family*

$$s \to (c, a, \Gamma)\,(s, \sqrt{\epsilon}), \quad s \in (0, s_{end})$$

of traveling pulse solutions $\Gamma(s, \sqrt{\epsilon})$ to (1.2), which is C^1 in $(s, \sqrt{\epsilon})$. Furthermore, for s sufficiently small, the solutions $\Gamma(s, \sqrt{\epsilon})$ coincide with the single pulses with oscillatory tails from Theorem 1.1, while the solutions $\Gamma(s, \sqrt{\epsilon})$ are double pulses for s sufficiently close to s_{end}.

The construction is based on the slow-fast decomposition of the traveling wave ODE (1.2):

$$\begin{aligned}
\dot{u} &= v \\
\dot{v} &= cv - f(u) + w \\
\dot{w} &= \epsilon(u - \gamma w),
\end{aligned}$$

The singular $\epsilon = 0$ limit consists of slow flow on the critical manifold $\{(u, v, w) = (u, 0, f(u))\}$ and fast layer dynamics restricted to planes $w =$ const in which there exist front solutions connecting different branches of the critical manifold. The transitional pulses are then obtained as perturbations from singular limit structures obtained by concatenating fast jumps along front solutions in the layer dynamics and slow evolution along portions of the critical manifold. The geometric setup can be seen in Figure 4 where the slow (resp. fast) portions of the flow are labelled by single (resp. double) arrows. The corresponding singular limit structure is also shown in Figure 8 below.

Obtaining the transitional pulse solutions as perturbations from the singular structure poses a number of challenges, and the techniques required to construct such solutions extend beyond standard methods of geometric singular perturbation theory. A primary challenge arises from the fact that normal hyperbolicity is lost at two fold points on the critical manifold, and as the pulses in question pass near these points, blow-up techniques are needed to understand the flow in these regions. The resulting geometric matching procedure used to construct the pulses, while tailored to this particular problem, is in fact quite general: The slow/fast pieces of the pulse and passages through fold points are all matched together to construct the full solution, taking into account both hyperbolic and nonhyperbolic aspects of the flow near the folds.

We now comment on a number of phenomena that are apparent in Figure 4:

- The first is the observation that much of the transition occurs along a nearly vertical path in parameter space (see Figure 4a). We will show that this is due to the fact that the transition from a single to a double pulse is organized by a canard mechanism similar to that which generates a canard explosion of periodic orbits [23]. In particular, we show that for each fixed ϵ, much of the transition occurs exponentially close

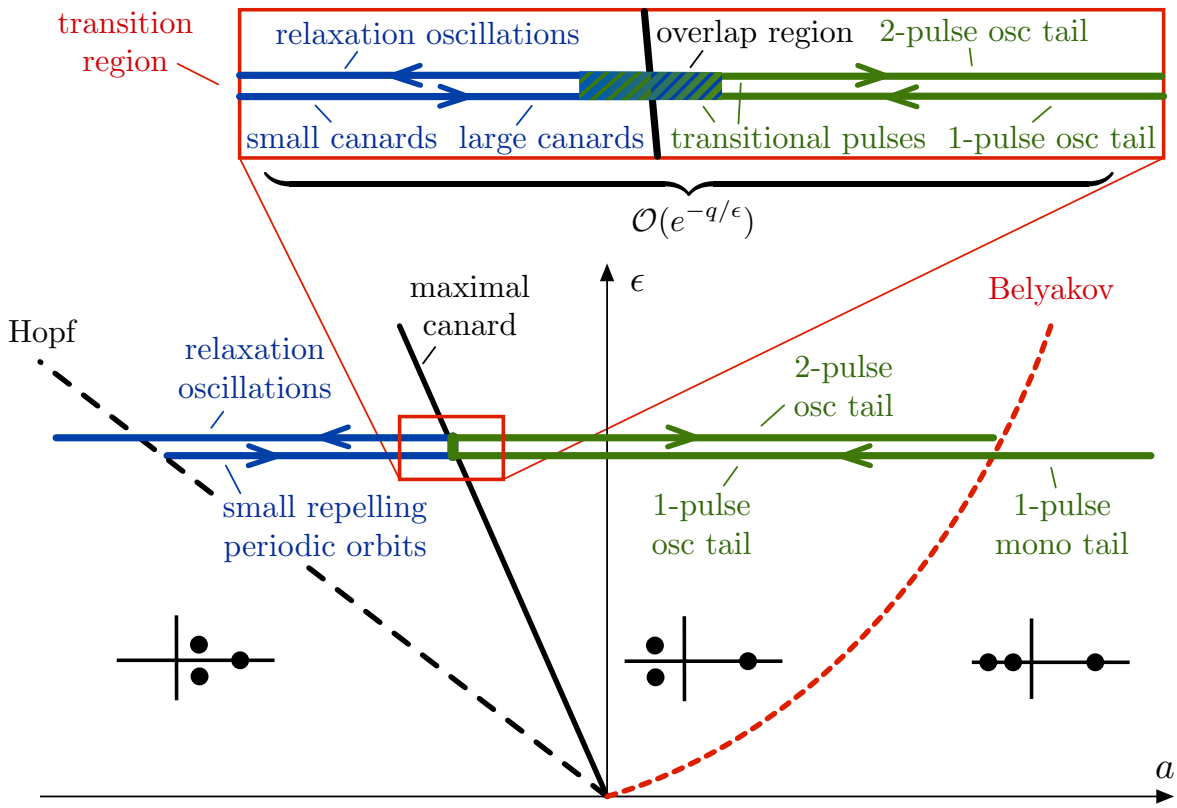

Figure 3: *Plotted is a schematic bifurcation diagram associated with the* 1*-to-*2*-pulse transition along the homoclinic banana projected into* (a, ϵ)*-space. The location of the Hopf bifurcation (dashed black), maximal canard (solid black), and Belyakov transition (dashed red) are shown along with the eigenvalue structure of the equilibrium in the relevant regions. The green branch of solutions corresponds to the pulse solutions for a fixed value of* ϵ*, and the arrows indicate the direction of continuation along the transition. Starting as a* 1*-pulse with monotone tail, the branch continues beyond the Belyakov transition (red dashed curve) and the pulses develop small oscillatory exponentially decaying tails before undergoing a sharp transition near the canard region and returning as a* 2*-pulse with oscillatory tail. We conjecture that this branch of* 2 *pulses then terminates at the Belyakov transition for sufficiently small* ϵ *(see Remark 4.13). We note that there is dependence on the wavespeed* c *along the branch of pulses, and further that the locations of the Belyakov, canard, and Hopf regions also depend on the value of* c*. Hence this picture is actually valid on some two-dimensional surface in* (c, a, ϵ)*-space; for clarity we have projected this onto the* (a, ϵ)*-plane. Also indicated are small amplitude repelling periodic orbits which bifurcate for each fixed* $c \approx 1/\sqrt{2}$ *from the subcritical Hopf bifurcation. These periodic solutions undergo a canard explosion and reemerge as large relaxation oscillations.*

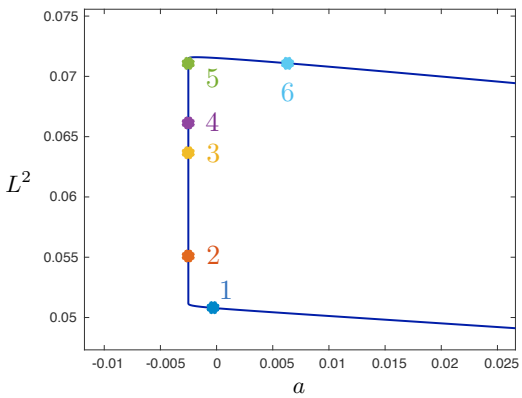

(a) *Zoom of homoclinic banana: L^2-norm vs. a*

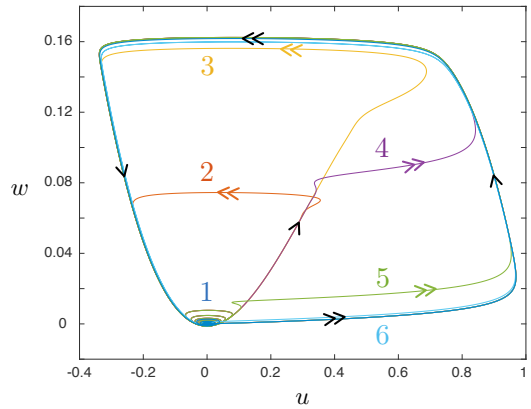

(b) *Six pulses along the banana projected onto the uw-plane showing the transition from a single to a double pulse.*

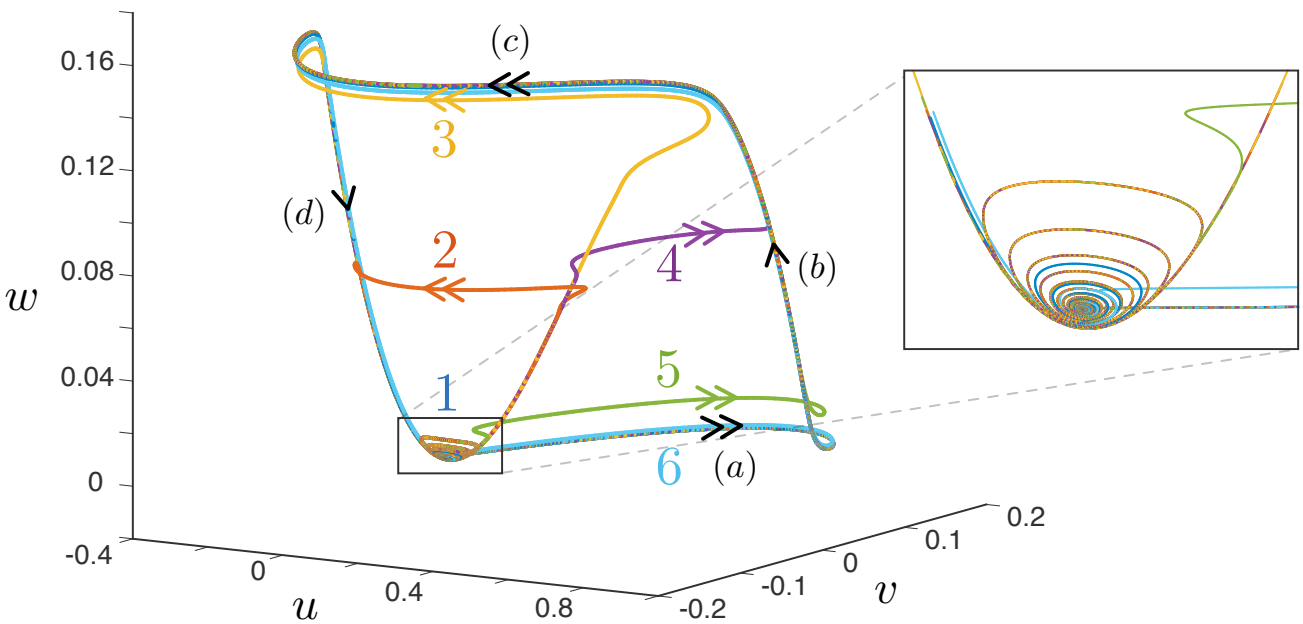

(c) *Six pulses along the banana in the full uvw-space showing the transition from a single to a double pulse.*

Figure 4: *Transition from single to double pulse in the top left of the homoclinic banana for $\epsilon = 0.0036$ (a visualization of this transition is shown in the accompanying animation* M108070_01.mp4 [local/web 5.49MB]*). The solutions labelled $1, 2$ are left pulses, and those labelled $4, 5, 6$ are right pulses. The solution labelled 3 lies in the transition between left/right pulses. The six pulses are representative of six different pulse types which we will construct in §4. Pulse 1 follows the sequence $(a), (b), (c), (d)$, followed by an oscillatory tail. Pulses $2, 3, 4, 5, 6$ first follow the sequence $(a), (b), (c), (d)$, followed by a secondary pulse along the corresponding colored trajectory, followed by an oscillatory tail. Note in the zoomed in portion of (c) that pulses labelled $2, 3, 4, 5$ appear to have nearly identical/overlapping tail trajectories. We will show that this due to the presence of an "Airy point" along the middle branch at which the dynamics transverse to the middle branch transitions from node to focus behavior.*

(in (a, c) parameter space) to a maximal canard representing the tangency of repelling and attracting slow manifolds. In this sense the transition can be viewed as a "canard explosion of homoclinic orbits."

This raises several technical challenges in constructing and parameterizing the pulse solutions due to dependence on exponentially small terms. Further, the proximity of the transition to the maximal canard and the subcritical Hopf bifurcations complicates matters, in particular in identifying the stable manifold of the equilibrium (a homoclinic solution must lie on this manifold). Bifurcating from the Hopf bifurcation are small amplitude repelling periodic orbits (see Figure 3): hence near the Hopf bifurcation, the stable manifold takes the form of a disc whose boundary is one such periodic orbit. Therefore any potential pulse solution could never reach the equilibrium in this region. However, moving further from the Hopf for increasing a, the periodic orbits grow in amplitude, undergo a canard transition near the maximal canard, and return as large relaxation oscillations; once these periodic orbits are sufficiently large, they no longer form the boundary of the stable manifold of the equilibrium as the full three-dimensional dynamics take over. Hence the structure of the stable manifold of the equilibrium is very sensitive and difficult to characterize in this region, and there is delicate interplay between the homoclinic pulse solutions and canard periodic orbits near the equilibrium. In order to construct the pulse solutions, in §3 we will determine geometric criteria which guarantee that certain solutions must lie on the stable manifold, and as a result we show that the periodic orbits bifurcating from the Hopf cannot cause obstructions.

- The second observation is that the transitional pulses all have oscillatory tails. As in [5], we will show that the oscillations in the tails are due to the presence of the Belyakov transition occurring at the equilibrium at the origin. The presence of the oscillatory tails in the single-to-double-pulse transition indicates that this transition occurs to the left of the Belyakov transition (see Figure 3). For ϵ large enough, the entire banana occurs on the left (complex side) of the Belyakov transition depicted in Figure 1 (hence all pulses have oscillatory tails), though for sufficiently small ϵ, we see numerically (Figure 5) that the banana splits, and only single pulses exist to the right of the Belyakov transition. We will show that our construction indeed breaks down near the Belyakov transition, and we conjecture that this is where the branch terminates for sufficiently small ϵ (see Remark 4.13).

- Finally, many of the pulses appear to have nearly identical/overlapping tails (see Figure 4c, in particular the zoomed-in portion). More precisely, it seems that along the vertical portion of the transition (see Figure 4a), after completing the secondary excursion, all of the transitional pulses jump off at nearly the same w-value and follow almost identical tail trajectories. Understanding this phenomenon is essential for the construction of the single-to-double-pulse transition. It turns out that the jump-off behavior is determined by the structure of the middle branch of the critical manifold. While the entire branch is completely unstable, we will see in §2.1 below that there is a point along the middle branch (in fact two due to symmetry) at which the flow changes from node to focus behavior: it is near this transition point that transitional pulses jump off to the left branch and thereby begin to form the tails. We refer to this point as the Airy point (as solutions near this point are governed by the Airy equation) and will introduce another blow up to examine the flow in this region (see §5).

The remainder of this paper is organized as follows. In §2, we outline the setup and give a precise statement of the main result, Theorem 2.2. In §3, we study the relevant two-dimensional dynamics near the equilibrium in order to characterize its stable manifold. The pulse solutions are then constructed in §4 save for the technical results on the dynamics near the Airy point which are proved in §5.

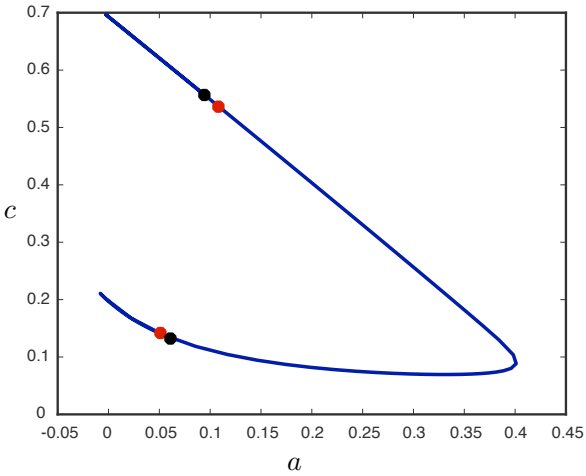

(a) *Plotted is the full C-curve for* $\epsilon = 0.0036$. *Also shown are the locations of the Belyakov transitions (red) obtained numerically, and the points where the branch of double pulses terminates (black).*

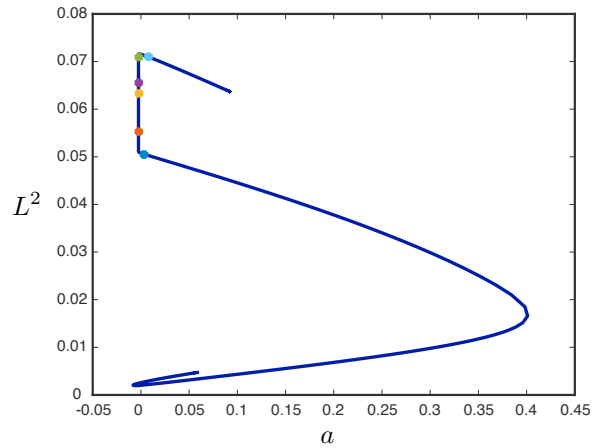

(b) *Plotted is the banana split obtained for* $\epsilon = 0.0036$. *The colored points correspond to the location of the transitional pulses as in Figure 4a.*

Figure 5: *Termination of the homoclinic banana and C-curve near the Belyakov transition for* $\epsilon = 0.0036$.

2 Setup and statement of the main result

In this section, we outline the setup and statement of the problem in the context of geometric singular perturbation theory. In §2.1, we describe fronts and backs of the reduced layer problems, which provide the building blocks of the transitional pulses. In §2.2, we state our main result: it is based on singular transitional pulses that form the backbone of the single-to-double pulse transition and which are based on the singular solutions constructed in §2.1. An outline of the proof is given in §2.3, and we collect several results in §2.4 that follow from standard geometric singular perturbation theory and from our previous work [5] for future reference.

2.1 Singular building blocks of transitional pulses

We separately consider the traveling wave ODE

$$\begin{aligned} \dot{u} &= v \\ \dot{v} &= cv - f(u) + w \\ \dot{w} &= \epsilon(u - \gamma w), \end{aligned} \tag{2.1}$$

which we call the fast system, and the system below obtained by rescaling $\tau = \epsilon\xi$, which we refer to as the slow system:

$$\begin{aligned} \epsilon u' &= v \\ \epsilon v' &= cv - f(u) + w \\ w' &= (u - \gamma w), \end{aligned} \tag{2.2}$$

where $'$ denotes $\dfrac{d}{d\tau}$. The two systems (2.1) and (2.2) are equivalent for any $\epsilon > 0$. The idea of geometric singular perturbation theory is to determine properties of the $\epsilon > 0$ system by piecing together information from the simpler equations obtained by separately considering the fast and slow systems in the singular limit $\epsilon = 0$.

2.1.1 The critical manifold $\mathcal{M}_0(a)$

We first set $\epsilon = 0$ in (2.2) and obtain the *reduced* system

$$\begin{aligned} 0 &= v \\ 0 &= cv - f(u) + w \\ w' &= (u - \gamma w), \end{aligned} \tag{2.3}$$

where the flow is now restricted to the set

$$\mathcal{M}_0(a) = \{(u, v, w) : v = 0,\ w = f(u) = u(u-a)(1-u)\}, \tag{2.4}$$

called the critical manifold with flow determined by the equation for w. Since $w = f(u)$ is cubic, there are two extrema, or *folds*, at

$$u^*_\pm(a) = \frac{1}{3}\left(a + 1 \pm \sqrt{a^2 - a + 1}\right). \tag{2.5}$$

Hence the manifold $\mathcal{M}_0(a)$ is S-shaped and consists of three branches

$$\mathcal{M}_0(a) = \mathcal{M}_0^\ell(a) \cup \mathcal{M}_0^m(a) \cup \mathcal{M}_0^r(a), \tag{2.6}$$

where

$$\begin{aligned} \mathcal{M}_0^\ell(a) &= \{(u, v, w) : v = 0,\ w = f(u), u \in (-\infty, u^*_-(a))\} \\ \mathcal{M}_0^m(a) &= \{(u, v, w) : v = 0,\ w = f(u), u \in [u^*_-(a), u^*_+(a)]\} \\ \mathcal{M}_0^r(a) &= \{(u, v, w) : v = 0,\ w = f(u), u \in (u^*_+(a), \infty)\}. \end{aligned}$$

We now set $\epsilon = 0$ in (2.1), and we obtain the *layer* problem

$$\begin{aligned} \dot{u} &= v \\ \dot{v} &= cv - f(u) + w \\ \dot{w} &= 0, \end{aligned} \tag{2.7}$$

so that w becomes a parameter for the flow and $\mathcal{M}_0(a)$ is the corresponding set of equilibria.

2.1.2 The fronts ϕ_f, ϕ_b

Considering (2.7) system in the plane $w = 0$, we obtain the Nagumo system

$$\begin{aligned} \dot{u} &= v \\ \dot{v} &= cv - f(u). \end{aligned} \tag{2.8}$$

Fix a_0 sufficiently small. It can then be shown that for each $-a_0 \le a \le 1/2$, this system possesses a heteroclinic connection ϕ_f (the Nagumo front) between the critical points $(u, v) = (0, 0)$ and $(u, v) = (1, 0)$ with wavespeed $c = c^*(a) = \sqrt{2}(1/2 - a)$.

For $a > 0$, in (2.7), the Nagumo front manifests as a connection between normally hyperbolic segments of the left and right branches, $\mathcal{M}_0^r(a)$ and $\mathcal{M}_0^\ell(a)$, of the critical manifold $\mathcal{M}_0(a)$, in the plane $w = 0$. By symmetry, there exists $w_b(a)$ such that there is a connection ϕ_b (the Nagumo back) in the plane $w = w_b(a)$ between the right and left branches of $\mathcal{M}_0(a)$ traveling with the same speed $c = c^*(a)$ (see Figure 6). In the case $a = 1/2$, ϕ_f and ϕ_b form a heteroclinic loop, though we do not consider this case here; see [21].

For $-a_0 < a \le 0$, this system possesses front type solutions for any $c > 1/\sqrt{2}(1 + a)$ connecting $u = 0$ to $u = 1$. For the critical value $c = c^*(a) = \sqrt{2}(1/2 - a)$ the front leaves the origin along the strong unstable manifold of

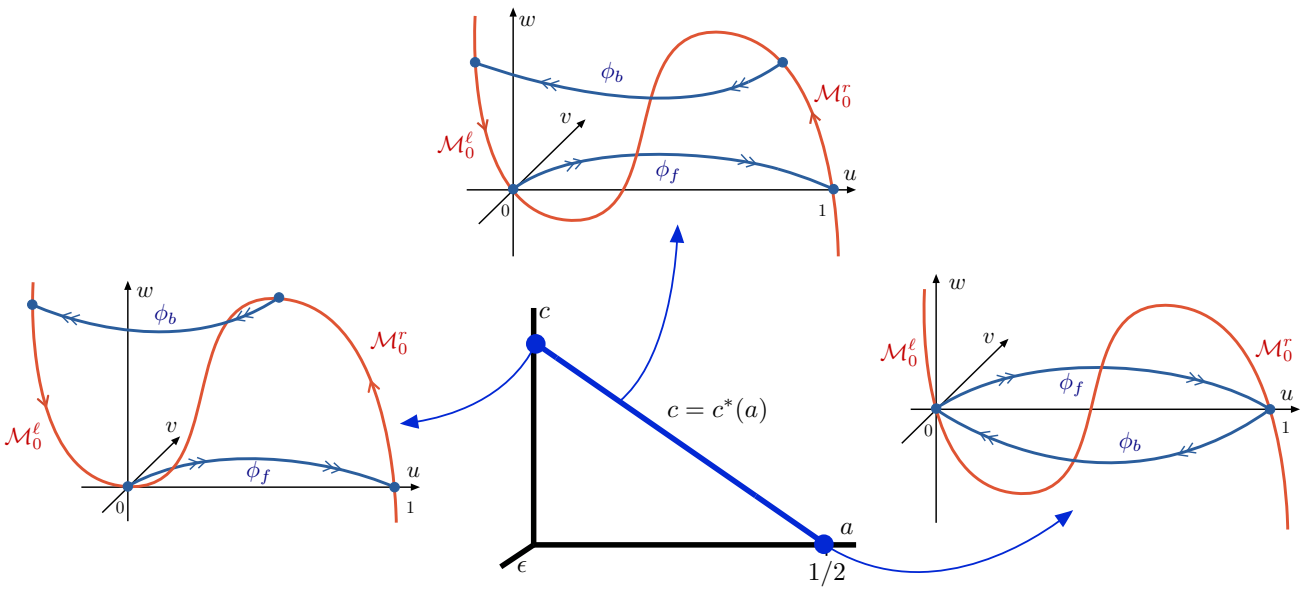

Figure 6: *Shown are the singular fronts ϕ_f and ϕ_b for the layer problem (2.7) for $\epsilon = 0$ and $0 \le a \le 1/2$.*

the origin, and for all other values of c, the front leaves the origin along a weak unstable direction. In the case of $a = 0$, (2.8) reduces to a Fisher–KPP type equation

$$\begin{aligned} \dot{u} &= v \\ \dot{v} &= cv - u^2(1-u), \end{aligned} \tag{2.9}$$

and the front/back solutions ϕ_f, ϕ_b leave $\mathcal{M}_0^\ell(a)$ and $\mathcal{M}_0^r(a)$ from the nonhyperbolic fold points (see Figure 6). For the critical value $c = 1/\sqrt{2}$ the front ϕ_f leaves the origin along the strong unstable manifold of the origin, and for $c > 1/\sqrt{2}$, the front leaves the origin along a center manifold. We are concerned with the case of $(c, a) = (1/\sqrt{2}, 0)$ (see Figure 6, left inset) in which the singular fast front solution ϕ_f leaves the origin along the strong unstable manifold. Note that by symmetry, for $(c, a) = (1/\sqrt{2}, 0)$, the fast singular back solution ϕ_b also leaves the upper right fold point along the strong unstable direction.

Remark 2.1. *For each $0 \le a < 1/2$, there exists a singular pulse solution obtained by following the sequence ϕ_f, $\mathcal{M}_0^r(a)$, ϕ_b, $\mathcal{M}_0^\ell(a)$ (see Figure 6). The existence Theorem 1.1 is obtained by searching for perturbations from these singular pulses for sufficiently small $\epsilon > 0$. The classical monotone pulses are obtained as perturbations from the case of $0 < a < 1/2$, whereas the onset of oscillations in the tails is found by perturbing from $\epsilon = a = 0$.*

2.1.3 The fronts $\phi_\ell(w), \phi_r(w)$

To understand the single to double pulse transition, we need more information from the layer problem (2.7), specifically regarding properties of the middle branch $\mathcal{M}_0^m(a)$ of the critical manifold $\mathcal{M}_0(a)$. For $a = 0$ there are also fronts connecting $\mathcal{M}_0^m(a)$ to $\mathcal{M}_0^\ell(a)$ and $\mathcal{M}_0^r(a)$ for values of $w \in [0, w^\dagger]$, where $(u^\dagger, 0, w^\dagger) = (2/3, 0, 8/27)$ denotes the location of the upper right fold point for $(c, a) = (1/\sqrt{2}, 0)$ (see Figure 7). To see this, we study the two-dimensional system

$$\begin{aligned} \dot{u} &= v \\ \dot{v} &= cv - u^2(1-u) + w, \end{aligned} \tag{2.10}$$

From §2.1.2 above, when $w = 0$, (2.10) has two equilibria at $(u, v) = (1, 0)$ and $(u, v) = (0, 0)$, which corresponds to the lower fold point in the left inset of Figure 6; when $c = 1/\sqrt{2}$, there is a front ϕ_f connecting these

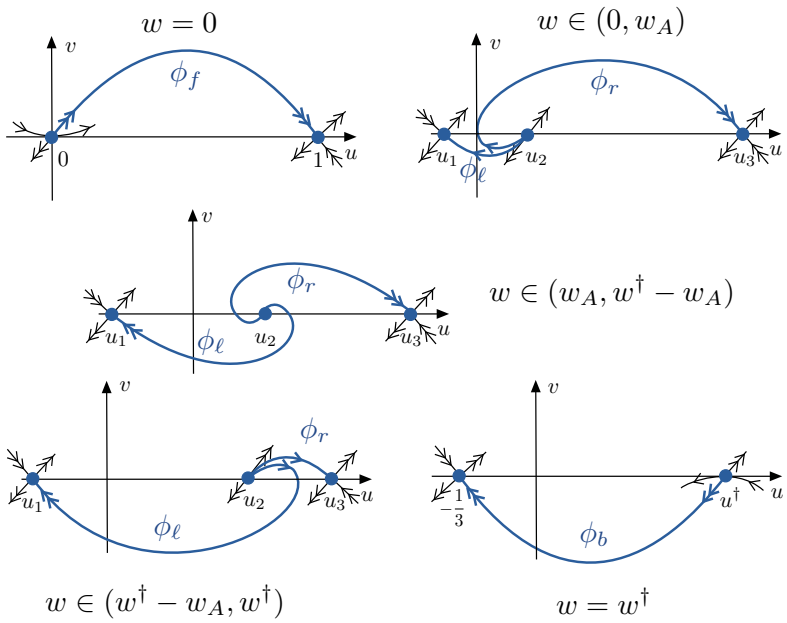

Figure 7: *Shown is the structure of the fronts $\phi_\ell, \phi_r, \phi_f, \phi_b$ for values of $w \in [0, w^\dagger]$ (see Proposition A.1).*

two equilibria. When $w = w^\dagger$ there are two equilibria at $(u, v) = (-1/3, 0)$ and $(u, v) = (2/3, 0)$, the latter corresponding to the upper fold point in the left inset of Figure 6; as discussed in §2.1.2 there is a 'back' ϕ_b which connects these two equilibria.

For values of $w \in (0, w^\dagger)$, (2.10) has three equilibria $p_i = (u_i(w), 0)$, where $u_i(w), i = 1, 2, 3$ are the three solutions of $f(u) = w$ in increasing order. The outer equilibria are saddles, while the middle equilibrium p_2 is completely unstable. To compute the type, we note that the eigenvalues at p_2 are given by

$$\lambda_\pm(p_2) = \frac{c \pm \sqrt{c^2 - 4f'(u_2(w))}}{2}. \tag{2.11}$$

We define w_A to be the lesser of the two solutions of $c^2 = 4f'(u_2(w))$, and we refer to the point $(u_2(w_A), 0, w_A)$ as the Airy point (by symmetry there is a second Airy point higher on $\mathcal{M}_0^m(a)$ corresponding to the larger solution, but for the forthcoming analysis, we will see that the lower Airy point is the only important one). Hence for $(c, a) = (1/\sqrt{2}, 0)$, the equilibrium p_2 is an unstable node for $w \in (0, w_A) \cup (w^\dagger - w_A, w^\dagger)$, a degenerate node at $w = w_A, w^\dagger - w_A$, and an unstable spiral for $w \in (w_A, w^\dagger - w_A)$. For each $w \in (0, w^\dagger)$, there exists a front $\phi_\ell(w)$ connecting the equilibria p_2 and p_1, and a front $\phi_r(w)$, connecting the equilibria p_2 and p_3 (see Figure 7). The existence of these fronts as well as their properties are outlined in Proposition A.1 in Appendix A.

2.2 Statement of the main result

The goal of this section is to state our main result that encompasses the transition from the single pulses with oscillatory tails from Theorem 1.1 to double pulse solutions comprised of a single pulse followed by a secondary excursion that is close to the original pulse.

These solutions will be close to singular transitional pulses, and we begin by constructing these singular transitional pulses for $(c, a, \epsilon) = (1/\sqrt{2}, 0, 0)$ using the layer analysis above: we refer to Figure 8 for the underlying geometry. We define

$$\mathcal{M}(u_1, u_2) := \{(u, 0, f(u)) : u \in [u_1, u_2]\} \tag{2.12}$$

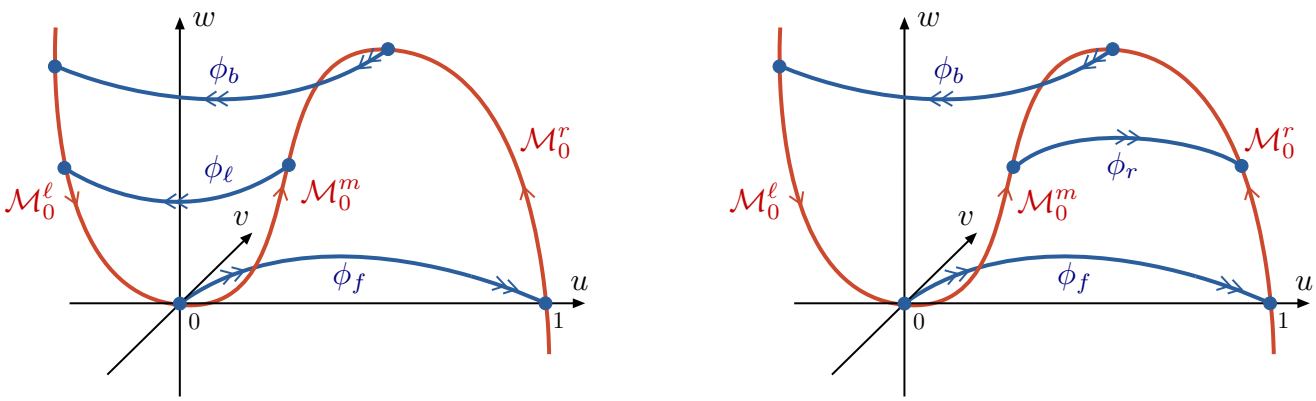

(a) *Singular left double pulse follows the sequence:* ϕ_f, $\mathcal{M}_0^r$, ϕ_b, $\mathcal{M}_0^\ell$, $\mathcal{M}_0^m$ ϕ_ℓ, $\mathcal{M}_0^\ell$.

(b) *Singular right double pulse follows the sequence:* ϕ_f, $\mathcal{M}_0^r$, ϕ_b, $\mathcal{M}_0^\ell$, $\mathcal{M}_0^m$ ϕ_r, $\mathcal{M}_0^r$, ϕ_b, $\mathcal{M}_0^\ell$.

Figure 8: *Singular* $\epsilon = 0$ *double pulses for* $(c, a) = (1/\sqrt{2}, 0)$.

All singular pulses will consist of a primary pulse

$$\Gamma_0^1 = \phi_f \cup \underbrace{\mathcal{M}(u^\dagger, 1)}_{=\mathcal{M}_0^r} \cup \phi_b \cup \underbrace{\mathcal{M}(u^\dagger - 1, 0)}_{=\mathcal{M}_0^\ell}, \tag{2.13}$$

followed by a secondary pulse. The secondary pulse follows a canard-like explosion which we parametrize by $s \in (0, 2w^\dagger)$. We define the singular secondary pulses

$$\Gamma_0^2(s) := \begin{cases} \mathcal{M}(0, u_2(s)) \cup \phi_\ell(s) \cup \mathcal{M}(u_1(s), 0), & s \in (0, w^\dagger) \\ \mathcal{M}(0, u^\dagger) \cup \phi_b \cup \mathcal{M}(u^\dagger - 1, 0), & s = w^\dagger \\ \mathcal{M}(0, u_2(2w^\dagger - s)) \cup \phi_r(2w^\dagger - s) \cup \mathcal{M}(u^\dagger, u_3(2w^\dagger - s)) \cup \phi_b \cup \mathcal{M}(u^\dagger - 1, 0), & s \in (w^\dagger, 2w^\dagger). \end{cases} \tag{2.14}$$

We refer to singular transitional pulses $\Gamma_0(s) = \Gamma_0^1 \cup \Gamma_0^2(s)$ as "left" transitional pulses for $s \in (0, w^\dagger)$ and "right" transitional pulses for $s \in (w^\dagger, 2w^\dagger)$. The left/right descriptor refers to whether the double pulse involves a jump from $\mathcal{M}_0^m$ to the left branch $\mathcal{M}_0^\ell$ or a jump to the right branch $\mathcal{M}_0^r$. These two types of singular pulses are shown in Figure 8.

We can now state the following existence theorem for a one-parameter family of homoclinic solutions to (1.2) that connects the single pulses with oscillatory tails with double pulses that resemble two copies of the original pulse.

Theorem 2.2. *Fix a small neighborhood* $\mathcal{V}$ *of the origin. For each sufficiently small* $\Delta_w > 0$*, there exists* $\epsilon_0, q, C > 0$ *such that the following holds. For each* $0 < \epsilon < \epsilon_0$*, there exists* $s_{end}(\sqrt{\epsilon}) = 2w^\dagger + \mathcal{O}(\epsilon)$ *and a one-parameter family of traveling pulse solutions to* (1.2)

$$s \to \left(c(s, \sqrt{\epsilon}), a(s, \sqrt{\epsilon}), \Gamma(s, \sqrt{\epsilon})\right), \quad s \in \left(0, s_{end}(\sqrt{\epsilon})\right] \tag{2.15}$$

which is C^1 *in* $(s, \sqrt{\epsilon})$*. Furthermore:*

(i) (Approximation by singular transitional pulses) *The family* $\Gamma(s, \sqrt{\epsilon})$ *is approximated by the singular transitional pulses* $\Gamma_0(s) = \Gamma_0^1 \cup \Gamma_0^2(s)$ *in the following sense:*

- *For* $s \in (0, \Delta_w)$*, the solution* $\Gamma(s, \sqrt{\epsilon})$ *consists of a primary excursion which lies within* $\mathcal{O}(\sqrt{\epsilon})$ *of* Γ_0^1*, followed by an oscillatory tail.*

- *For $s \in \big(\Delta_w, s_{end}(\sqrt{\epsilon})\big)$, the solution $\Gamma(s,\sqrt{\epsilon})$ consists of a primary excursion which lies within $\mathcal{O}(\sqrt{\epsilon})$ of Γ_0^1, followed by a secondary excursion which lies within $\mathcal{O}(\sqrt{\epsilon})$ of $\Gamma_0^2(s)$, followed by an oscillatory tail.*
- *For $s = s_{end}(\sqrt{\epsilon})$ the solution $\Gamma(s,\sqrt{\epsilon})$ consists of a primary excursion which lies within $\mathcal{O}(\sqrt{\epsilon})$ of Γ_0^1, followed by a secondary excursion which again lies within $\mathcal{O}(\sqrt{\epsilon})$ of Γ_0^1, followed by an oscillatory tail which remains in $\mathcal{V}$.*

(ii) (Behavior of tail trajectories) *For $s \in (0,\Delta_w) \cup \big(2w^\dagger - \Delta_w, s_{end}(\sqrt{\epsilon})\big]$, the oscillatory tail of $\Gamma(s,\sqrt{\epsilon})$ is confined to $\mathcal{V}$. For $s \in (\Delta_w, 2w^\dagger - \Delta_w)$, there exists $N(s) \in \mathbb{N}$ such that the oscillatory tail of $\Gamma(s,\sqrt{\epsilon})$ completes a sequence of excursions which reach the set $\{u = 0\}$ at heights $w = w_i(s,\epsilon)$, where*

$$w_1(s,\epsilon) > w_2(s,\epsilon) > \ldots > w_{N(s)-2}(s,\epsilon) > w_{N(s)-1}(s,\epsilon) \geq \Delta_w > w_{N(s)}(s,\epsilon) > 0, \tag{2.16}$$

after which the tail is confined to $\mathcal{V}$. We have that $w_i(s,\epsilon) \to w_i(s,0)$ as $\epsilon \to 0$ where $w_i(s,0)$ are successive zeros of a way-in-way-out function*, that is,*

$$R(w_1(s,0), w_2(s,0)) = R(w_2(s,0), w_3(s,0)) = \ldots = R(w_{N(s)-1}(s,0), w_{N(s)}(s,0)) = 0, \tag{2.17}$$

where the function R is defined by

$$R(w^-, w^+) := \frac{1}{2}\int_{u_1(w^-)}^{u_2(w^+)} \left(c - \sqrt{c^2 - 4f'(u)}\right) \frac{f'(u)}{u - \gamma f(u)} du, \tag{2.18}$$

where $u_1(w), u_2(w)$ denote the smallest two solutions of $f(u) = w$ in increasing order. Furthermore, the functions $w_i(s,0), i = 1,\ldots,N(s)$ are constant for $s \in [w_R^0, 2w^\dagger - w_A]$, where $w_R^0 > w_A$ is defined by $R(w_R^0, w_A) = 0$.

(iii) (Continuation of classical branch of 1-pulses) *For all sufficiently small $s > 0$, $a(s,\sqrt{\epsilon})$ is monotone decreasing in s and the pulses $\Gamma(s,\sqrt{\epsilon})$ correspond to the classical 1-pulses from Theorem 1.1 with*

$$c(s,\sqrt{\epsilon}) = \check{c}(a(s,\sqrt{\epsilon}),\epsilon). \tag{2.19}$$

(iv) (Exponential closeness of parameters) *There exists $(c_E, a_E) = (c_E, a_E)(\sqrt{\epsilon})$ such that for all $s \in (\Delta_w, 2w^\dagger - \Delta_w)$, we have that*

$$\big|(c,a)(s,\sqrt{\epsilon}) - (c_E, a_E)(\sqrt{\epsilon})\big| \leq Ce^{-q/\epsilon}. \tag{2.20}$$

Remark 2.3. *We note the appearance of the way-in-way-out type function R which determines the behavior of the tail trajectories of the pulses. In §3, we will show that solutions on the stable manifold $\mathcal{W}_\epsilon^s(0;c,a)$ of the equilibrium complete a series of excursions within a certain two-dimensional invariant manifold. These excursions are determined by a balance of exponential contraction/expansion along canard trajectories near the critical manifold $\mathcal{M}_0$, and we we will show that this balance is captured by the function R.*

Remark 2.4. *The exponential closeness of the parameter values (c,a) along the transition in Theorem 2.2(iv) is related to the existence of maximal canards in a center manifold of the equilibrium, similarly to the case of the classical canard explosion [23].*

Remark 2.5. *The termination of the branch of transitional pulses in Theorem 2.2 at $s = s_{end}(\sqrt{\epsilon})$ is related to the presence of the Belyakov transition (1.3) discussed in the introduction and the split banana appearing in the numerical continuation for sufficiently small ϵ (see Figure 5). As a perturbation from the $\epsilon = 0$ limit, we are able to construct pulses encompassing the transition from the single pulse to the double pulse up to a neighborhood of the Belyakov transition, but not the entire banana. We will see that our construction indeed breaks down in this region (see Remark 4.13 for further details).*

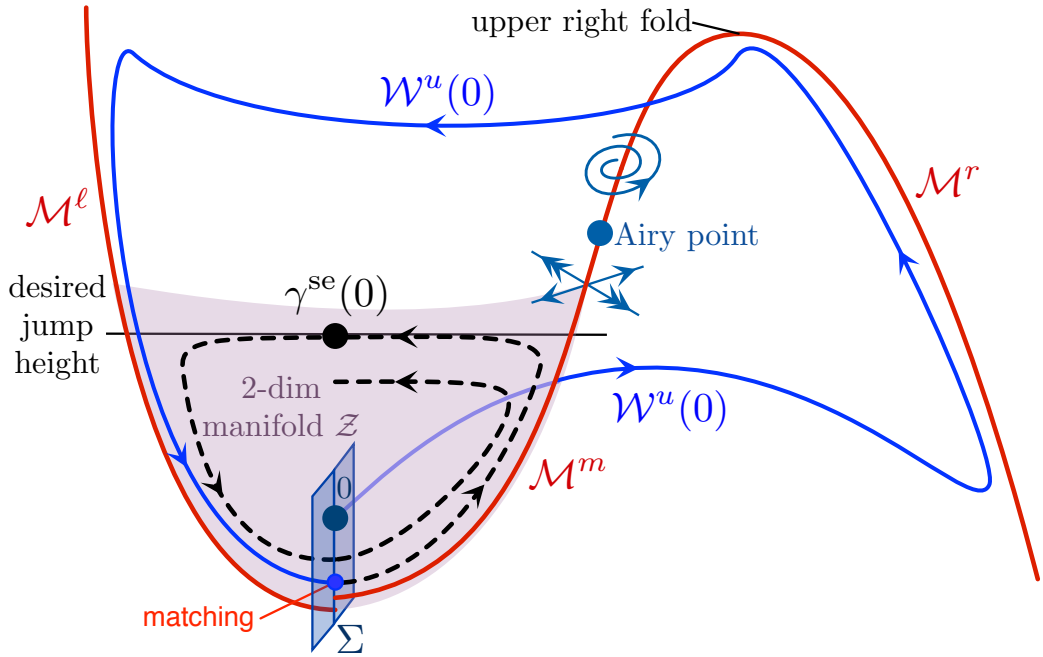

Figure 9: *Illustrated is the construction of transition pulses consisting of the primary pulse (denoted by $\mathcal{W}^u(0)$), which is matched in the transverse section Σ near the origin with a secondary excursion $\gamma^{\mathrm{se}}(\xi)$ that crosses at a given jump height. Also shown are the two-dimensional manifold $\mathcal{Z}$ (in purple) that contains the tail trajectory $\gamma^{\mathrm{se}}(\xi)$, and the Airy point at which the dynamics transverse to the slow manifold changes from node to spiral. Note that the lower Airy point is drawn much higher along the middle branch than it actually occurs; this is to leave room for the complex dynamics happening below the Airy point, which are relevant to the current discussion.*

2.3 Overview of the proof of Theorem 2.2

The remainder of this paper is devoted to the proof of Theorem 2.2. In this section, we provide a brief nontechnical outline of this proof. Our strategy is illustrated in Figure 9, and we refer readers to this illustration for the following description of the proof.

First, we follow the construction in [5] to track the unstable manifold $\mathcal{W}^u(0)$ of the equilibrium at the origin for each (c, a, ϵ) near $(1/\sqrt{2}, 0, 0)$ as it jumps to the right slow manifold $\mathcal{M}^r$, proceeds upwards along $\mathcal{M}^r$, jumps at the upper right fold back to $\mathcal{M}^\ell$, and then proceeds downwards along $\mathcal{M}^\ell$ until it reaches the boundary of a small neighborhood of the origin. We will then use geometric blow-up techniques to prove that the unstable manifold $\mathcal{W}^u(0)$ can be tracked into this neighborhood until it hits the section Σ shown in Figure 9. The end point of the unstable manifold in the section Σ will be $\mathcal{O}(e^{-q/\epsilon})$ close to the point at which the left branch $\mathcal{M}^\ell$ intersects Σ. This will complete the construction of the primary excursion of the homoclinic orbit, which, as mentioned above, can be carried out for each (c, a, ϵ) near $(1/\sqrt{2}, 0, 0)$.

Next, we consider the secondary excursion of the homoclinic orbit. We will first consider secondary canard-like solutions that will follow the middle branch $\mathcal{M}^m$ for some time before jumping at a specified height back to the left branch $\mathcal{M}^\ell$ and then spiral into the equilibrium at the origin as $\xi \to \infty$. There are three tasks that we need to carry out to complete this construction:

(i) show that canard-like solutions that jump off at a specified height exist;
(ii) match their start point in the section Σ with the end point of the unstable manifold $\mathcal{W}^u(0)$;
(iii) show that the canard-like solutions converge to the origin as $\xi \to \infty$.

The technical tool that we shall employ to complete these tasks is the two-dimensional locally invariant manifold $\mathcal{Z}$ shown in Figure 9, which can be thought of as an extension of the local center manifold of the origin. It

extends up to the height of the Airy point on the middle branch $\mathcal{M}^m$ at which the dynamics transverse to the middle branch changes from unstable node to unstable spiral: normal hyperbolicity is lost at the Airy point as we can no longer distinguish the weak from the strong unstable direction transverse to the middle branch, and we can therefore not continue this manifold beyond the Airy point. The manifold $\mathcal{Z}$ will be constructed using the graph transform and will be of class C^1.

We can use this manifold as follows to establish the existence of solutions that satisfy (i)-(iii) above for jump heights that are lower than the Airy point; we refer to these solutions as type 1 pulses. First, pick the initial condition $\gamma^{\mathrm{se}}(0) \in \mathcal{Z}$ that has the specified jump height below the Airy point. We can trace the resulting solution backwards in time until it hits the section Σ at a point $\gamma^{\mathrm{se}}_{\mathrm{start}}$ that is $\mathcal{O}(e^{-q/\epsilon})$ close to the point at which the middle branch $\mathcal{M}^m$ intersects this section: this will be shown using again the geometric blow-up mentioned above (and, in fact, the entire analysis near the origin will be done in appropriate blow-up coordinates). For each fixed $\epsilon > 0$, we can now vary (c, a) to match the end point of the unstable manifold $\mathcal{W}^u(0)$ with the point $\gamma^{\mathrm{se}}_{\mathrm{start}}$: these parameters will be exponentially close in ϵ to parameter values (c_E, a_E) at which the system has a maximal canard, that is, where the left and middle branches match, coinciding with an intersection of $\mathcal{W}^u(0)$ and stable manifold of $\mathcal{M}^\ell$. Thus, matching the first and secondary excursions will uniquely determine (c, a) for each fixed $0 < \epsilon \ll 1$. This establishes (i) and (ii), and it remains to show that the solution $\gamma^{\mathrm{se}}(\xi)$ converges to the origin as $\xi \to \infty$. The key is now that this solution stays in $\mathcal{Z}$ as this manifold is locally invariant, and the geometry requires that $\gamma^{\mathrm{se}}(\xi)$ continues to spiral inwards around the origin as ξ increases. The Poincaré–Bendixson theorem applied inside $\mathcal{Z}$ then shows that $\gamma^{\mathrm{se}}(\xi)$ converges either to the origin or else to a periodic orbit that surrounds the origin. However, it was shown in [23] that any periodic orbit that lies in $\mathcal{Z}$ must be repelling, and we can therefore exclude the second alternative. We will show in §3.2 that it is the existence of the canard-like excursion that jumps off at positive height that precludes the simultaneous existence of periodic canard orbits that could block solutions from reaching the origin.

The final step is to construct homoclinic orbits with secondary excursions that jump above the Airy point and that may also contain intermediate jumps to the left and right branches as shown in Figures 4 and 8: we again need to go through the three steps (i)-(iii) listed above as for type 1 pulses. The construction is illustrated in Figure 10. Due to various interactions with the nonhyperbolic fold points and the Airy point, the remaining solutions break down into 5 further types (types 2–6), which we describe in more detail in §4.

To address (i), we construct a secondary excursion γ^{se} which begins in Σ, and we track forward in time until it intersects Σ again; the construction uses standard geometric perturbation theory combined with blow-up analyses near the Airy point and the upper right fold for those excursions that pass through these points. Once such a solution is constructed, we denote by $\mathcal{B}_{\mathrm{end}}$ the unstable fiber of its end point in the section Σ. We can now follow the entire fiber backwards in time: this will result in a family of secondary excursions, which will intersect Σ in an exponentially small curve $\mathcal{B}_{\mathrm{start}}$; see Figure 10. Similarly, we can take an entire vertical segment $\mathcal{Y}_{\mathrm{end}}$ of tail solutions in the manifold $\mathcal{Z}$ and follow it backwards in time to get an exponentially small curve $\mathcal{Y}_{\mathrm{start}}$ in Σ.

Step (ii) involves matching $\mathcal{W}^u(0)$ with $\mathcal{B}_{\mathrm{start}}$, and $\mathcal{B}_{\mathrm{end}}$ with $\mathcal{Y}_{\mathrm{start}}$. The idea is to prove that the two curves $\mathcal{B}_{\mathrm{end}}$ with $\mathcal{Y}_{\mathrm{start}}$ intersect transversely (and can therefore be matched) and that $\mathcal{W}^u(0)$ can be matched with each solution in $\mathcal{B}_{\mathrm{start}}$ upon adjusting the parameters (c, a) appropriately. Implementing this idea is quite intricate though as we need to make sure that the two intersection points lie on the same trajectory, and we therefore provide more details of the actual matching process and refer again to Figure 10 for an illustration. First, we parametrize $\mathcal{B}_{\mathrm{end}}$ as $b_{\mathrm{end}}(c, a, z)$ using the unstable-fiber direction z shown in Figure 10. The corresponding points in $\mathcal{B}_{\mathrm{start}}$ are denoted by $b_{\mathrm{start}}(c, a, z)$, and we will show that the latter points lie in a ball of size $\mathcal{O}(e^{-q/\epsilon})$ uniformly in (c, a, z). Similarly, following $\mathcal{Y}_{\mathrm{end}}$ backwards in time results in a curve $Y_{\mathrm{start}}(c, a, y)$ in Σ that is parametrized by y and also lies in a ball of size $\mathcal{O}(e^{-q/\epsilon})$ uniformly in (c, a, y). For each fixed z, we can then proceed as before and match $\mathcal{W}^u(0)$ with $b_{\mathrm{start}}(c, a, z)$ by choosing $(c, a) = (c, a)(z)$ appropriately: since $\mathcal{B}_{\mathrm{start}}$ lies in a ball of size $\mathcal{O}(e^{-q/\epsilon})$, we will show that $(c, a)(z)$ will also lie in a ball of size $\mathcal{O}(e^{-q/\epsilon})$. It then remains

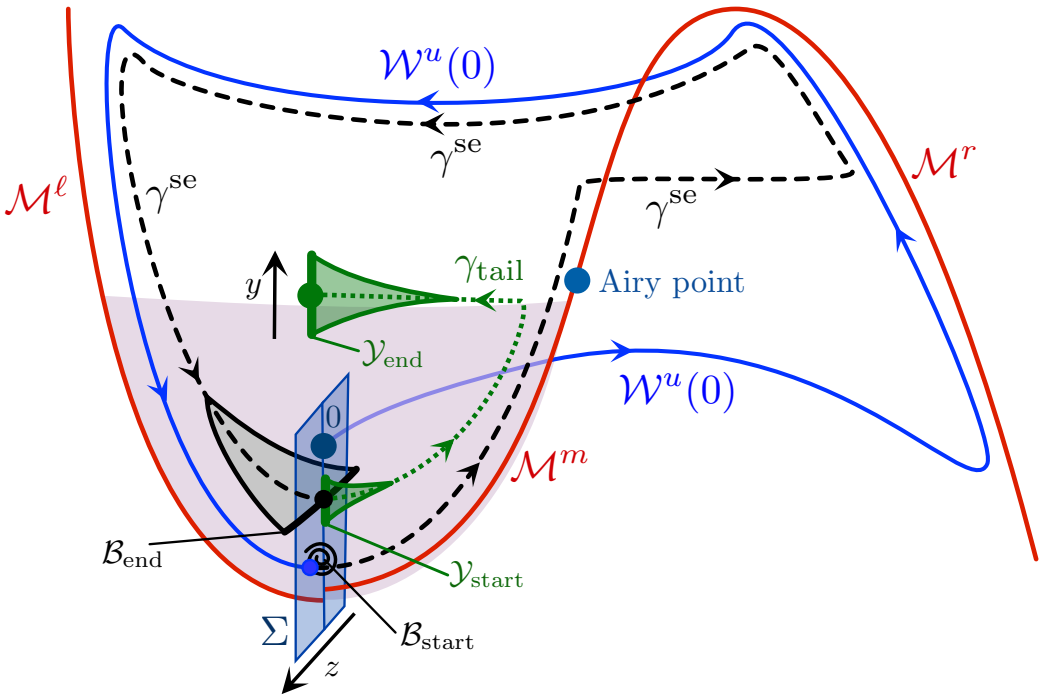

Figure 10: *Shown is a transitional pulse that consists of the primary pulse* $\mathcal{W}^u(0)$*, a large secondary excursion* $\gamma^{\mathrm{se}}(\xi)$*, and a tail solution* $\gamma^{\mathrm{tail}}(\xi)$ *that will converge to the origin as* $\xi \to \infty$*. To show the existence of these solutions, we construct an entire one-parameter family of secondary excursions that end in the unstable fiber* $\mathcal{B}_{\mathrm{end}}$ *in the section* Σ*: following this line segment backwards in time yields the curve* $\mathcal{B}_{\mathrm{start}}$ *in* Σ*, which will form an exponentially thin spiral due to the passage near the Airy point. Similarly, we construct a one-parameter family of tail solutions that end in the vertical segment* $\mathcal{Y}_{\mathrm{end}}$*, which, when continued backwards in time, yields an exponentially small line segment* $\mathcal{Y}_{\mathrm{start}}$ *in* Σ*. We then match* $\mathcal{W}^u(0)$ *with* $\mathcal{B}_{\mathrm{start}}$*, and* $\mathcal{B}_{\mathrm{end}}$ *with* $\mathcal{Y}_{\mathrm{start}}$*, using the parameters* (c, a) *and transversality of the intersection of* $\mathcal{B}_{\mathrm{end}}$ *and* $\mathcal{Y}_{\mathrm{start}}$*.*

to find y and z so that

$$b_{\text{end}}((c,a)(z),z) = Y_{\text{start}}((c,a)(z),y),$$

which is the matching condition for $\mathcal{B}_{\text{end}}$ and $\mathcal{Y}_{\text{start}}$. It turns out that we can always match the vertical direction in the section Σ by choosing y appropriately due to the transversality of these curves, and it remains to match their z-components. Using the exponential closeness of $(c,a)(z)$, the resulting condition is of the form

$$z + \mathcal{O}(e^{-q/\epsilon}) = \mathcal{O}(e^{-q/\epsilon})$$

uniformly in z, and the implicit function theorem provides a unique solution z as desired. The proof that the tail solutions converge to the origin follows as before, thus completing step (iii).

There are several technical challenges in this construction. First, the transitional pulses pass near the two fold points where the exchange lemma fails: as in the proof of [5, Theorem 1.1], we will use blow-up techniques to analyze the flow near these fold points. Secondly, many of the transitional pulses jump off near the Airy point after their second excursion: understanding this phenomenon is crucial to the analysis, and we will use blow-up techniques to analyze the passage near the Airy point. Thirdly, the transition from single to double pulses arises in an exponentially small parameter region, and it is therefore essential that we identify the right variables to parametrize the branch of pulses as we cannot use the (c,a) variables: it turns out that the jump-off heights provide a parametrization that allows us to use (c,a) as unfolding parameters in implicit function theorems. We remark that the first challenge mentioned above arose already in [5]; however, the remaining two challenges are unique to the construction of transitional pulses and indeed constitute the main technical innovation compared to the proofs in [5].

2.4 Results from standard geometric singular perturbation theory

We now fix some notation and collect a few results which follow from standard geometric singular perturbation theory and the analysis in [5]. Define the closed intervals $I_a = [-a_0, a_0]$ for sufficiently small $a_0 > 0$ and $I_c = \{c^*(a) : a \in I_a\}$; here $c^*(a) = 1/\sqrt{2}(1-2a)$ is the wavespeed for which the Nagumo front exists for this choice of a. Then for sufficiently small ϵ_0, a_0, we have the following:

1. The origin has a one-dimensional strong unstable manifold $\mathcal{W}_0^u(0;c,a)$ for $c \in I_c$, $a \in I_a$, and $\epsilon = 0$ which persists for a, c in the same range and $\epsilon \in [0, \epsilon_0]$.

2. Near the origin there is a local two-dimensional center manifold $\mathcal{W}_0^c(0;c)$ for $c \in I_c$, and $a = \epsilon = 0$. This manifold persists as a local invariant manifold $\mathcal{W}_\epsilon^c(0;c,a)$ for $(c,a,\epsilon) \in I_c \times I_a \times (0,\epsilon_0)$. The manifold $\mathcal{W}_\epsilon^c(0;c,a)$ can be taken to be C^k for any $k > 0$.

3. We consider the critical manifold $\mathcal{M}_0(a) = \{(u,v,w) : v = 0, w = f(u)\}$. For each $a \in I_a$, we consider the right branch $\mathcal{M}_0^r(a)$ of the critical manifold up to a neighborhood of the upper right fold point for $\epsilon = 0$. This manifold persists as a one-dimensional slow manifold $\mathcal{M}_\epsilon^r(c,a)$ for $\epsilon \in [0,\epsilon_0]$. In addition, $\mathcal{M}_0^r(a)$ possesses two-dimensional stable and unstable manifolds $\mathcal{W}^s(\mathcal{M}_0^r, c, a)$ and $\mathcal{W}^u(\mathcal{M}_0^r, c, a)$ which also persist for $\epsilon \in [0,\epsilon_0]$ as invariant manifolds which we denote by $\mathcal{W}_\epsilon^{s,r}(c,a)$ and $\mathcal{W}_\epsilon^{u,r}(c,a)$.

4. In addition, we consider the left branch of the critical manifold $\mathcal{M}_0^\ell(a)$ up to a neighborhood of the origin for $\epsilon = 0$. This manifold persists as a one-dimensional slow manifold $\mathcal{M}_\epsilon^\ell(c,a)$ for $\epsilon \in [0,\epsilon_0]$. In addition, $\mathcal{M}_0^\ell(a)$ possesses a two-dimensional stable manifold $\mathcal{W}^s(\mathcal{M}_0^\ell, c, a)$ which also persists for $\epsilon \in [0,\epsilon_0]$ as an invariant manifold which we denote by $\mathcal{W}_\epsilon^{s,\ell}(c,a)$. By evolving trajectories on the local center manifold $\mathcal{W}_\epsilon^c(0;c,a)$ backwards in time, it was shown in [5, §6] that the manifolds $\mathcal{W}_\epsilon^c(0;c,a)$ and $\mathcal{W}_\epsilon^{s,\ell}(c,a)$ can be chosen to overlap to form a larger center-like manifold which we call $\mathcal{W}_\epsilon^{c,\ell}(c,a)$. The manifold $\mathcal{W}_\epsilon^{c,\ell}(c,a) = \mathcal{W}_\epsilon^c(0;c,a) \cup \mathcal{W}_\epsilon^{s,\ell}(c,a)$ can be thought of as an extension of the stable manifold $\mathcal{W}_\epsilon^{s,\ell}(c,a)$ of $\mathcal{M}_\epsilon^\ell(c,a)$ into a neighborhood of the equilibrium.

5. Finally, we consider the middle branch of the critical manifold $\mathcal{M}_0^m(a)$ away from neighborhoods of the origin and the upper right fold point for $\epsilon = 0$. This manifold persists as a one-dimensional slow manifold $\mathcal{M}_\epsilon^m(a)$ for $\epsilon \in [0, \epsilon_0]$. In addition, $\mathcal{M}_0^m(c, a)$ possesses a three-dimensional unstable manifold $\mathcal{W}^u(\mathcal{M}_0^m, c, a)$ which also persists for $\epsilon \in [0, \epsilon_0]$ as an invariant manifold which we denote by $\mathcal{W}_\epsilon^{u,m}(c, a)$. Away from the folds, the stable manifolds $\mathcal{W}^s(\mathcal{M}_0^r, c, a)$ and $\mathcal{W}^s(\mathcal{M}_0^\ell, c, a)$ form part of $\mathcal{W}^u(\mathcal{M}_0^m, c, a)$ for $\epsilon = 0$ and hence for sufficiently small $\epsilon > 0$, we have that the foliations $\mathcal{W}_\epsilon^{s,r}(c, a)$ and $\mathcal{W}_\epsilon^{s,\ell}(c, a)$ along the slow manifolds $\mathcal{M}_\epsilon^r(c, a), \mathcal{M}_\epsilon^\ell(c, a)$ are contained in $\mathcal{W}_\epsilon^{u,m}(c, a)$.

Within the two-dimensional manifold $\mathcal{W}_\epsilon^{c,\ell}(c, a)$, there exist canard trajectories near the attracting slow manifold $\mathcal{M}_\epsilon^\ell(c, a)$ which pass near the origin and then follow the repelling slow manifold $\mathcal{M}_\epsilon^m(c, a)$ for some time. While in general the repelling slow manifold $\mathcal{M}_\epsilon^m(c, a)$ can not be chosen to lie inside the invariant manifold $\mathcal{W}_\epsilon^{c,\ell}(c, a)$, in the region where $\mathcal{W}_\epsilon^{c,\ell}(c, a)$ is defined, $\mathcal{M}_\epsilon^m(c, a)$ shadows a nearby orbit $\mathcal{M}_\epsilon^{m,c}(c, a)$ which does in fact lie on $\mathcal{W}_\epsilon^{c,\ell}(c, a)$ and which is exponentially close to $\mathcal{M}_\epsilon^m(c, a)$.

The results in [22] imply that there is a maximal canard solution which, by definition, occurs when $\mathcal{M}_\epsilon^\ell(c, a)$ and $\mathcal{M}_\epsilon^{m,c}(c, a)$ coincide within $\mathcal{W}_\epsilon^{c,\ell}(c, a)$. We have the following theorem, which will be proved in §4.1.

Theorem 2.6. *There exists $\epsilon_0 > 0$ and a smooth function $a^C(\sqrt{\epsilon}, c) : (0, \epsilon_0) \times I_c \to I_a$ such that there is a maximal canard solution connecting the manifolds $\mathcal{M}_\epsilon^\ell(c, a)$ and $\mathcal{M}_\epsilon^{m,c}(c, a)$ when $a = a^C(\sqrt{\epsilon}, c)$. We have that*

$$a^C(\sqrt{\epsilon}, c) = -m(c)\epsilon + \mathcal{O}\left(\epsilon^{3/2}\right) \tag{2.21}$$

where $m(c)$ is positively bounded away from zero uniformly in $c \in I_c$.

We also have the following proposition, which follows from the analysis in [5, §5]. The result is also illustrated in Figure 11.

Proposition 2.7. *There exists $\epsilon_0 > 0$ and $\mu > 0$ such that for each $a \in I_a$ and $\epsilon \in (0, \epsilon_0)$, the manifold $\bigcup_{c \in I_c} \mathcal{W}_\epsilon^u(0; c, a)$ intersects $\bigcup_{c \in I_c} \mathcal{W}_\epsilon^{s,\ell}(c, a)$ near the upper right fold point transversely in (u, v, w, c)-space with the intersection occurring at $c = \check{c}(a, \epsilon)$ for a smooth function $\check{c} : I_a \times (0, \epsilon_0) \to I_c$ where $\check{c}(a, \epsilon) = c^*(a) - \mu\epsilon + \mathcal{O}(\epsilon(|a| + \epsilon))$.*

Note that the intersection of $\bigcup_{c \in I_c} \mathcal{W}_\epsilon^u(0; c, a)$ and $\bigcup_{c \in I_c} \mathcal{W}_\epsilon^{s,\ell}(c, a)$ is at least one-dimensional as it consists of solutions, and transversality is equivalent to showing that this intersection is one-dimensional (and not higher-dimensional). The assertions of Proposition 2.7 were shown in [5] by tracking $\mathcal{W}_\epsilon^u(0; c, a)$ along ϕ_f, then along $\mathcal{M}_\epsilon^r(c, a)$ into a neighborhood of the upper right fold point using the exchange lemma. Since $\mathcal{W}_\epsilon^u(0; c, a)$ transversely intersects $\mathcal{W}_\epsilon^{s,\ell}(c, a)$ (and hence $\mathcal{W}_\epsilon^{c,\ell}(c, a)$) at $c = \check{c}(a, \epsilon)$, we can then track $\mathcal{W}_\epsilon^u(0; c, a)$ along ϕ_b whence it is exponentially attracted towards $\mathcal{M}_\epsilon^\ell(c, a)$ into a neighborhood of the equilibrium. Therefore, we deduce that for $a \in I_a$ and $\epsilon \in (0, \epsilon_0)$ and $c \approx \check{c}(a, \epsilon)$, $\mathcal{W}_\epsilon^u(0; c, a)$ follows a primary excursion which is close to Γ_0^1; see Figure 11.

3 The invariant manifold $\mathcal{Z}_\epsilon$ and its dynamics

The goal of this section is to construct a large two-dimensional normally hyperbolic invariant manifold $\mathcal{Z}_\epsilon(c, a)$ which contains the equilibrium. The main result of this section, Proposition 3.10, provides conditions under which solutions on this manifold also lie on the stable manifold $\mathcal{W}_\epsilon^s(0; c, a)$ of the equilibrium. Hence when constructing pulse solutions in §4, the goal is to ensure that they eventually become trapped on $\mathcal{Z}_\epsilon(c, a)$ in forward time.

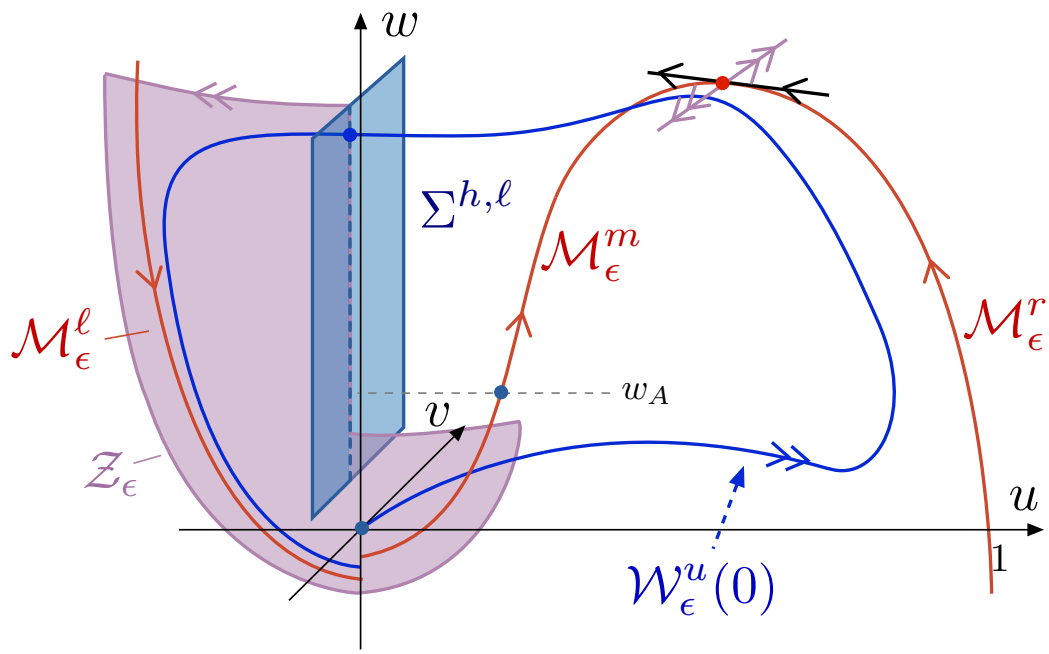

Figure 11: *Shown is the manifold $\mathcal{Z}_\epsilon(c,a)$ as well as the geometry of the primary pulse given by Proposition 2.7. The splitting of the (nonunique) slow manifolds $\mathcal{M}_\epsilon^\ell(c,a)$ and $\mathcal{M}_\epsilon^m(c,a)$ near the origin is due to the loss of normal hyperoblicity at the fold in the critical manifold, which produces a canard point. Canard trajectories are found by closing this splitting distance upon varying the parameter a; see Theorem 2.6. Note that $\mathcal{Z}_\epsilon(c,a)$ cannot be extended beyond the height of the Airy point along the middle branch due to loss of normal hyperbolicity: the weak/strong expansion rates cannot be separated beyond this point.*

3.1 Constructing the manifold $\mathcal{Z}_\epsilon(c,a)$

The idea behind the construction is to note that for any $\Delta_w > 0$, the fronts ϕ_ℓ for $w \in (0, w_A - \Delta_w]$ for $\epsilon = a = 0$ taken together form a two-dimensional invariant manifold which is normally hyperbolic in the sense that the rate of expansion in the normal direction is greater than the rate of expansion on the manifold itself. This is due to the separation of rates in the linearization of (1.2) for $u < u_A$; see below. We aim to understand in what sense this manifold perturbs when $0 < \epsilon \ll 1$. See Figure 11 as a guide for the geometry of the construction.

For $\epsilon = 0$, we define a singular invariant manifold as follows. For each $\Delta_w > 0$, suitable small intervals I_c, I_a can be chosen such that the following holds. The fronts $\phi_\ell(w)$ for $w \in [\Delta_w, w_A - \Delta_w]$ persist for $(c,a) \in I_c \times I_a$. From Appendix A, these fronts connect the unstable middle equilibrium $p_2(w)$ to the saddle equilibrium $p_1(w)$, leaving $p_2(w)$ along a weak unstable direction, and they depend smoothly on w. This means that each $\phi_\ell(w)$ lies on the stable manifold $\mathcal{W}^s(p_1(w))$ of $p_1(w)$ and a weak unstable manifold $\mathcal{W}^{wu}(p_2(w))$ of $p_2(w)$.

To determine expansion/contraction rates, we look at the linearization of (1.2) at $(c,a,\epsilon) = (1/\sqrt{2}, 0, 0)$ given by

$$A = \begin{pmatrix} 0 & 1 & 0 \\ -f'(u) & c & 1 \\ 0 & 0 & 0 \end{pmatrix}. \tag{3.1}$$

There are three eigenvalues

$$\lambda_0 = 0, \quad \lambda_\pm = \lambda_\pm(u) = \frac{c \pm \sqrt{c^2 - 4f'(u)}}{2}. \tag{3.2}$$

A quick computation shows that $\Re(\lambda_+) > \Re(\lambda_-)$ provided $c^2 > 4f'(u)$. In particular for $(c,a) = (1/\sqrt{2}, 0)$, this

holds for any $u < u_A = \frac{1}{3}\left(1 - \sqrt{\frac{5}{8}}\right)$.

Since the eigenvalues $\lambda_\pm$ are consistently separated in this region (at least if sufficiently close to $p_2(w)$), the weak unstable manifold $\mathcal{W}^{wu}(p_2(w))$ is at least C^1 smooth and can be taken to depend smoothly on w. Hence in each plane of fixed $w \in [\Delta_w, w_A - \Delta_w]$ there exists a one-dimensional C^1 manifold $\tilde{\mathcal{Z}}_0(c, a; w)$ which contains the intersection of $\mathcal{W}^s(p_1(w))$ and $\mathcal{W}^{wu}(p_2(w))$ with small neighborhoods of $p_1(w)$ and $p_2(w)$, respectively, as well as the entirely of $\phi_\ell(w)$. We define $\tilde{\mathcal{Z}}_0(c, a)$ to be the union of the manifolds $\tilde{\mathcal{Z}}_0(c, a; w)$ for $w \in [\Delta_w, w_A - \Delta_w]$.

Further, for each $(c, a) \in I_c \times I_a$, there is a local center manifold $\mathcal{W}_0^c(0; c, a)$ near the equilibrium [5, §6]. By taking Δ_w sufficiently small, it is clear that this manifold can be taken to overlap with $\tilde{\mathcal{Z}}_0(c, a)$ as defined above as $\mathcal{W}_0^c(0; c, a)$ contains the fronts $\phi_\ell(w)$ for small w. Hence we define $\mathcal{Z}_0(c, a)$ to be the union $\tilde{\mathcal{Z}}_0(c, a) \cup \mathcal{W}_0^c(0; c, a)$. With this definition, $\mathcal{Z}_0(c, a)$ is a locally invariant, normally hyperbolic two-dimensional manifold which is at least C^1 smooth.

Hence for sufficiently small $\epsilon > 0$, $\mathcal{Z}_0(c, a)$ perturbs to a C^1 normally hyperbolic invariant manifold $\mathcal{Z}_\epsilon(c, a)$ with a C^1 unstable manifold $\mathcal{W}^u(\mathcal{Z}_\epsilon(c, a))$ formed by a C^1 invariant foliation $\mathcal{W}^{uu}(\mathcal{Z}_\epsilon(c, a))$ of strong unstable fibers [16, 9]. The perturbed manifold $\mathcal{Z}_\epsilon(c, a) \to \mathcal{Z}_0(c, a)$ in the C^1 sense as $\epsilon \to 0$.

3.1.1 Extending the manifold $\mathcal{Z}_\epsilon(c, a)$

Note that in their common region of definition, in particular for $w \leq w_A - \Delta_w$, the two normally repelling invariant manifolds $\mathcal{Z}_\epsilon(c, a)$ and $\mathcal{W}_\epsilon^{c,\ell}(c, a)$ are the same up to exponentially small errors.

We now work to partially extend $\mathcal{Z}_\epsilon(c, a)$ into the region $w > w_A - \Delta_w$ using the (backwards) flow of (1.2). We define the section

$$\Sigma^{h,\ell} := \{u = 0, \Delta_w \leq w \leq w^\dagger + \Delta_w\}. \tag{3.3}$$

In the half space $u < 0$ (i.e. to the left of $\Sigma^{h,\ell}$), the manifold $\mathcal{Z}_\epsilon(c, a)$ intersects the plane $w = w_A - \Delta_w$ in a one-dimensional curve which is aligned exponentially close to the stable foliation $\mathcal{W}_\epsilon^{s,\ell}$ along $\mathcal{M}_\epsilon^\ell(c, a)$. We take this curve and evolve backwards in time until solutions intersect the section $\Sigma^{h,\ell}$. In doing this, $\mathcal{Z}_\epsilon(c, a)$ can be extended as a manifold which is also exponentially close to the stable foliation $\mathcal{W}_\epsilon^{s,\ell}(c, a)$ along $\mathcal{M}_\epsilon^\ell(c, a)$ in the region $w_A - \Delta_w < w < w^\dagger + \Delta_w$ and $u < 0$. We now fix this extended invariant manifold $\mathcal{Z}_\epsilon(c, a)$ once and for all; it is shown in Figure 11.

We sum up the results of this section in the following.

Proposition 3.1. *Fix $\Delta_w > 0$. For each $(c, a) \in I_c \times I_a$ and each sufficiently small $\epsilon > 0$, there exists a C^1 normally repelling invariant manifold $\mathcal{Z}_\epsilon(c, a)$ with a C^1 unstable manifold $\mathcal{W}^u(\mathcal{Z}_\epsilon(c, a))$ formed by an invariant foliation of strong unstable fibers. In the region $\{w \leq w_A - \Delta_w\}$, $\mathcal{Z}_\epsilon(c, a)$ is a C^1 perturbation of the manifold $\mathcal{Z}_0(c, a)$, while in the region $\{u < 0, w_A - \Delta_w < w < w^\dagger + \Delta_w\}$, $\mathcal{Z}_\epsilon(c, a)$ is $C^1 - \mathcal{O}(e^{-q/\epsilon})$ close to the stable foliation $\mathcal{W}_\epsilon^{s,\ell}(c, a)$.*

Remark 3.2. *By construction the two normally repelling invariant manifolds $\mathcal{Z}_\epsilon(c, a)$ and $\mathcal{W}_\epsilon^{c,\ell}(c, a)$ have a substantial overlapping region of definition; this region includes a neighborhood of the equilibrium and a neighborhood of the slow manifold $\mathcal{M}_\epsilon^\ell(c, a)$. Within this region, these two normally repelling manifolds coincide up to exponentially small errors in the C^1 sense, but in general are not the same. This may appear redundant, but in fact it is necessary to construct these two manifolds separately, as they serve different purposes.*

The primary purpose of constructing the large normally repelling manifold $\mathcal{Z}_\epsilon(c, a)$ is to be able to identify solutions far from the equilibrium which lie on the stable manifold $\mathcal{W}_\epsilon^s(0; c, a)$. The problem is that a priori the manifold $\mathcal{Z}_\epsilon(c, a)$ is in general only C^1-smooth, and hence when reducing the flow to this manifold or using coordinates which depend on a parametrization of this manifold, there are technical issues that arise in the local

blow-up analysis near the equilibrium due to the lack of smoothness. This is the reason we also identify the center-like manifold $\mathcal{W}_\epsilon^{c,\ell}(c,a)$; this manifold is constructed via standard Fenichel theory and center manifold theory and can be taken to be C^k for any k. Therefore, the manifold $\mathcal{W}_\epsilon^{c,\ell}(c,a)$ will serve as the basis for local coordinates near the equilibrium in which we will set up our matching conditions.

Remark 3.3. *The one-dimensional manifolds $\mathcal{M}_\epsilon^\ell(c,a), \mathcal{M}_\epsilon^m(c,a)$ shadow basepoint solutions $\mathcal{M}_\epsilon^{\ell,\mathcal{Z}}(c,a)$ and $\mathcal{M}_\epsilon^{m,\mathcal{Z}}(c,a)$ which lie on $\mathcal{Z}_\epsilon(c,a)$ and which are exponentially close to – but in general do not coincide with – the manifolds $\mathcal{M}_\epsilon^\ell(c,a), \mathcal{M}_\epsilon^m(c,a)$. Hence, when necessary we will distinguish the one-dimensional manifolds $\mathcal{M}_\epsilon^\ell(c,a), \mathcal{M}_\epsilon^m(c,a)$ from their counterparts $\mathcal{M}_\epsilon^{\ell,\mathcal{Z}}(c,a), \mathcal{M}_\epsilon^{m,\mathcal{Z}}(c,a)$.*

3.2 Characterizing the stable manifold $\mathcal{W}_\epsilon^s(0;c,a)$

In this section, we study the dynamics on the two-dimensional invariant manifold $\mathcal{Z}_\epsilon(c,a)$. We aim to find conditions which guarantee that certain solutions on $\mathcal{Z}_\epsilon(c,a)$ in fact lie in the stable manifold $\mathcal{W}_\epsilon^s(0;c,a)$ of the equilibrium $(u,v,w)=(0,0,0)$. In this sense we obtain an (incomplete) characterization of $\mathcal{W}_\epsilon^s(0;c,a)$, at least in the case when sufficiently long canard solutions are present. This characterization will be sufficient to construct the transitional pulses in the following sections.

The argument is broken down as follows: We first show in §3.2.1 that there are no nonrepelling periodic orbits lying entirely within $\mathcal{Z}_\epsilon(c,a)$. Then in §3.2.2, we define a way-in-way-out function R which we use in §3.2.3 to show that for sufficiently small $\epsilon>0$, in the presence of a suitable canard trajectory, solutions which enter $\mathcal{Z}_\epsilon(c,a)$ via $\Sigma^{h,\ell}$ at certain heights w remain in $\mathcal{Z}_\epsilon(c,a)$ for all forward time, with the height on each return to $\Sigma^{h,\ell}$ monotonically decreasing while approaching a small $\mathcal{O}(1)$ neighborhood of the equilibrium. The lack of nonrepelling periodic orbits then guarantees that such solutions must converge to the equilibrium in forward time and hence must lie on $\mathcal{W}_\epsilon^s(0;c,a)$.

3.2.1 Small amplitude periodic orbits on $\mathcal{Z}_\epsilon(c,a)$

The strategy for characterizing solutions on the stable manifold $\mathcal{W}_\epsilon^s(0;c,a)$ in the presence of canard solutions is to exploit monotonicity properties of solutions on $\mathcal{Z}_\epsilon(c,a)$ determined by a way-in-way-out function R. In §3.2.3 we will show that under certain conditions, such solutions remain on $\mathcal{Z}_\epsilon(c,a)$ with the height on each return to the section $\Sigma^{h,\ell}$ decreasing monotonically until the solution eventually becomes trapped in a small neighborhood of the equilibrium. Hence such a trajectory is approaching the equilibrium; the only way it can fail to lie in the stable manifold $\mathcal{W}_\epsilon^s(0;c,a)$ is if it is blocked by a periodic orbit (in this case $\mathcal{W}_\epsilon^s(0;c,a)$ would topologically take the form of a bounded disc). The aim of this section is to show that any such small amplitude periodic orbit lying in $\mathcal{Z}_\epsilon(c,a)$ must be repelling.

In [23], the authors constructed periodic canard orbits in a class of planar systems. Although the entire canard explosion is not possible to construct in the same manner in our case (there is no such two-dimensional invariant manifold which contains the entire S-shaped critical manifold $\mathcal{M}_0$), the results remains valid on a local center manifold in a small neighborhood of the equilibrium, and any such small amplitude periodic orbits must be contained in the two-dimensional normally repelling manifold $\mathcal{Z}_\epsilon(c,a)$. We quote the following result regarding such periodic solutions.

Proposition 3.4 ([23, Proposition 4.3])**.** *Fix a sufficiently small neighborhood $\mathcal{V}$ of the equilibrium in $\mathbb{R}^3$. There exists w_0 such that for each $c\in I_c$ and all sufficiently small $\epsilon>0$, there exists a family of periodic orbits*

$$(w,\epsilon)\to(a(w,\epsilon),\Gamma_p(w,\epsilon)) \tag{3.4}$$

parameterized by the height $w\in(0,w_0)$ such that $\Gamma_p(w,\epsilon)\subset\mathcal{Z}_\epsilon(c,a(w,\epsilon))$. Furthermore

(i) Any periodic orbit which is entirely contained in $\mathcal{V}\cap\mathcal{Z}_\epsilon(c,a)$ is part of this family.

(ii) All of the periodic orbits $\Gamma_p(w,\epsilon)$ are repelling.

In particular, the above implies that for any sufficiently small $\epsilon > 0$, there are no nonrepelling small amplitude periodic orbits on $\mathcal{Z}_\epsilon(c,a)$.

3.2.2 The way-in-way-out function R

We now define a way-in-way-out function as in [23] which essentially determines the difference in contraction/expansion rates along the critical manifold $\mathcal{M}_0$. We consider the reduced flow restricted to the critical manifold $\{v = 0, w = f(u)\}$ for $(a,\epsilon) = (0,0)$; the flow satisfies

$$u' = \frac{u - \gamma f(u)}{f'(u)}, \tag{3.5}$$

where $f(u) = u^2(1-u)$. For $w \in (0, w^\dagger)$, recall the equation $f(u) - w = 0$ has three solutions $u_i(w), i = 1,2,3$ which are indexed in increasing order. For $u < 2/3$, we have $u' > 0$ under the flow of (3.5). Hence given $w^- \in (0, w^\dagger)$ and $w^+ \in (0, w_A)$, there exists a solution $u = u(\tau; w^-, w^+)$ of (3.5) and time $T = T(w^-, w^+)$ such that $u(0; w^-, w^+) = u_1(w^-)$ and $u(T; w^-, w^+) = u_2(w^+)$.

To determine expansion/contraction rates, we recall the eigenvalues of the linearization of (1.2) at $\epsilon = a = 0$ given by

$$\lambda_0 = 0, \lambda_\pm = \lambda_\pm(u) = \frac{c \pm \sqrt{c^2 - 4f'(u)}}{2}. \tag{3.6}$$

Recall from §3.1 that $\Re(\lambda_+) > \Re(\lambda_-)$ provided $c^2 > 4f'(u)$. To measure the contraction/expansion along the critical manifold $\mathcal{M}_0$ occurring within $\mathcal{Z}_\epsilon(c,a)$, we choose the *smaller* rate λ_-.

So for $(w^-, w^+) \in (0, w^\dagger) \times (0, w_A)$, we now define the way-in-way-out function

$$R(w^-, w^+) := \int_0^{T(w^-,w^+)} \lambda_-(u(\tau; w^-, w^+))d\tau. \tag{3.7}$$

Hence for the solution $u = u(\tau; w^-, w^+)$ of (3.5), the quantity $R(w^-, w^+)$ is a measure of the contraction along the left branch $\mathcal{M}_0^\ell$ of the critical manifold from $w = w^-$ to $w = 0$ and the expansion along the middle branch $\mathcal{M}_0^m$ from $w = 0$ to $w = w^+$. For $R(w^-, w^+) > 0$, the interpretation is that the expansion along $\mathcal{M}_0^m$ from $w = 0$ to $w = w^+$ outweighs the contraction along $\mathcal{M}_0^\ell$ from $w = w^-$ to $w = 0$, yielding a net expansion, and vice versa for $R(w^-, w^+) < 0$.

Remark 3.5. *Recall from §3.1, we used the separation of the rates $\lambda_\pm$ to construct $\mathcal{Z}_\epsilon(c,a)$. In that context, the function R provides an estimate for the relative contraction/expansion along $\mathcal{M}_0$ within the manifold $\mathcal{Z}_\epsilon(c,a)$. We also note that the restriction of $w^+ \in (0, w_A)$ in the definition of $R(w^-, w^+)$ is due to the fact that the rates $\lambda_\pm$ cannot be separated near $\mathcal{M}_0^m$ for $w \in (w_A, w^\dagger - w_A)$ as $c^2 < 4f'(u)$ in this region.*

Using (3.6) and changing variables, we obtain the equivalent definition

$$R(w^-, w^+) := \frac{1}{2}\int_{u_1(w^-)}^{u_2(w^+)} \left(c - \sqrt{c^2 - 4f'(u)}\right) \frac{f'(u)}{u - \gamma f(u)} du, \tag{3.8}$$

We have the following lemma, which is proved in Appendix B.

Lemma 3.6. *When $a = 0$, the way-in-way-out function R satisfies*

(i) $R(w,w) > 0$ for all $w \in (0, w_A)$;

(ii) $R(w^\dagger, w_A) < 0$;

(iii) $\dfrac{dR}{dw^-}(w^-, w^+) < 0$ and $\dfrac{dR}{dw^+}(w^-, w^+) > 0$ for all $(w^-, w^+) \in (0, w^\dagger) \times (0, w_A)$.

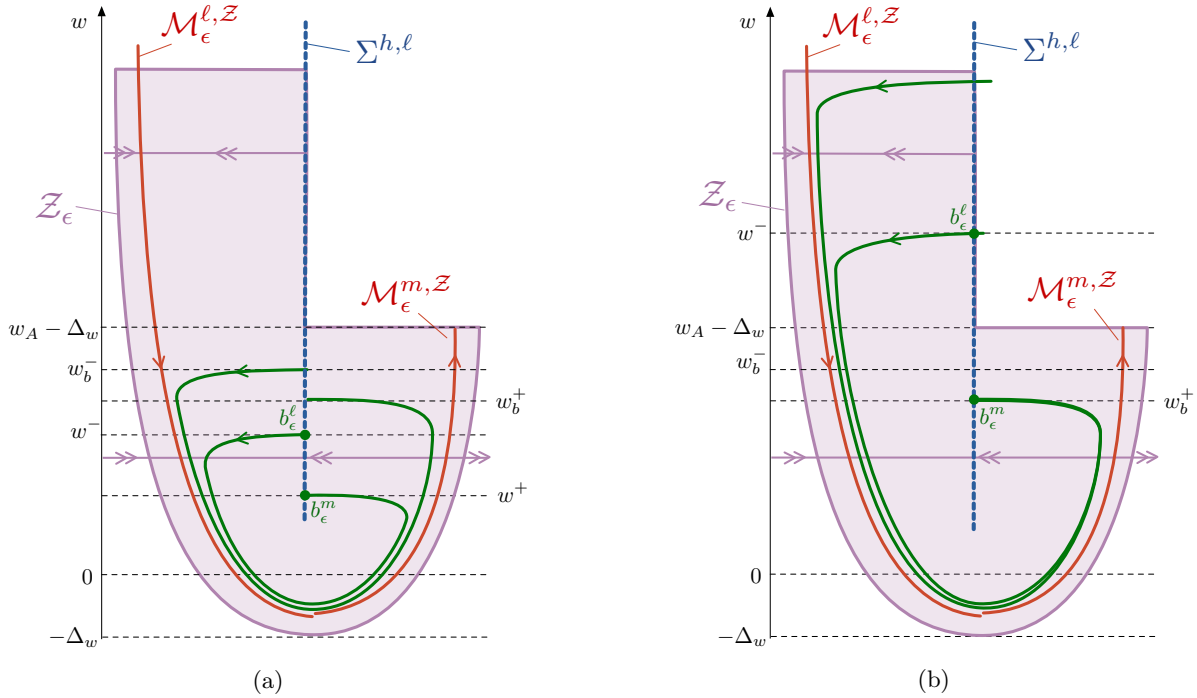

Figure 12: *Behavior of trajectories near the manifolds $\mathcal{M}_\epsilon^{\ell,\mathcal{Z}}(c,a), \mathcal{M}_\epsilon^{m,\mathcal{Z}}(c,a)$ in the presence of buffer heights (w_b^-, w_b^+). (a) Tunnel behavior for trajectories (green) entering along $\mathcal{M}_\epsilon^{\ell,\mathcal{Z}}(c,a)$ at height $w^- < w_b^-$. The exit height along $\mathcal{M}_\epsilon^{m,\mathcal{Z}}(c,a)$ is given by w^+ where $R(w^-, w^+) = 0$; see Definition 3.7(i). (b) Funnel behavior for trajectories (green) entering along $\mathcal{M}_\epsilon^{\ell,\mathcal{Z}}(c,a)$ at height $w^- > w_b^-$. The exit height along $\mathcal{M}_\epsilon^{m,\mathcal{Z}}(c,a)$ is given by w_b^+; see Definition 3.7(ii).*

3.2.3 Canard trajectories and the way-in-way-out function R

We aim to show that, in the presence of a canard trajectory, solutions which enter $\mathcal{Z}_\epsilon(c,a)$ via $\Sigma^{h,\ell}$ follow a sequence of excursions with the height on each return to $\Sigma^{h,\ell}$ monotonically decreasing until entering a small neighborhood of the equilibrium. Each such excursion begins in $\Sigma^{h,\ell}$, then is attracted to $\mathcal{M}_\epsilon^{\ell,\mathcal{Z}}(c,a)$, then follows $\mathcal{M}_\epsilon^{m,\mathcal{Z}}(c,a)$ for some time, before jumping off and returning to $\Sigma^{h,\ell}$ (see Remark 3.3 for the definition of $\mathcal{M}_\epsilon^{\ell,\mathcal{Z}}(c,a)$ and $\mathcal{M}_\epsilon^{m,\mathcal{Z}}(c,a)$). To construct this sequence of excursions, we need to determine the jump-off or exit height $w = w^+$ along $\mathcal{M}_\epsilon^{m,\mathcal{Z}}(c,a)$ given a starting height $w = w^-$ in $\Sigma^{h,\ell}$. To accomplish this, we use the way-in-way-out function R. The main idea is to show that the entry/exit heights are approximately related via the equation $R(w^-, w^+) = 0$. The sequence can then found by solving for successive zeros of R.

We begin by discussing the concept of 'buffer heights' [7] and the relation to canard trajectories on $\mathcal{Z}_\epsilon(c,a)$, that is, trajectories which first follow the attracting slow manifold $\mathcal{M}_\epsilon^{\ell,\mathcal{Z}}(c,a)$, and then the repelling slow manifold $\mathcal{M}_\epsilon^{m,\mathcal{Z}}(c,a)$ for some time. We will then use this notion of buffer heights in Proposition 3.10 to show that for certain solutions, the function R can be used to determine the sequence of excursions followed on $\mathcal{Z}_\epsilon(c,a)$.

Buffer heights essentially determine how the function R can be used to relate the entry/exit heights along $\mathcal{M}_\epsilon^{\ell,\mathcal{Z}}(c,a), \mathcal{M}_\epsilon^{m,\mathcal{Z}}(c,a)$: for entry heights w^- below these buffer heights, the entry/exit heights are related by zeros of R, while the behavior varies for entry heights above the buffer heights; see Figure 12. In fact, we define buffer heights via these properties.

Definition 3.7. *Suppose for each sufficiently small $\epsilon > 0$ there exists a canard trajectory γ_ϵ at the parameter values $(c,a) = (c_\epsilon^\diamond, a_\epsilon^\diamond)$ where the triplet $(\gamma_\epsilon, c_\epsilon^\diamond, a_\epsilon^\diamond)$ depends continuously on ϵ, and suppose γ_ϵ intersects $\Sigma^{h,\ell}$ at a point b_ϵ^ℓ satisfying $\lim_{\epsilon\to 0} b_\epsilon^\ell = b_0^\ell \in \Sigma^{h,\ell} \cap \{w = w^-\}$ so that the limit b_0^ℓ lies on the intersection of $\Sigma^{h,\ell}$ with the stable foliation of $\mathcal{M}_0^\ell$. A pair (w_b^-, w_b^+) satisfying $R(w_b^-, w_b^+) = 0$ are called* buffer heights *if the following*

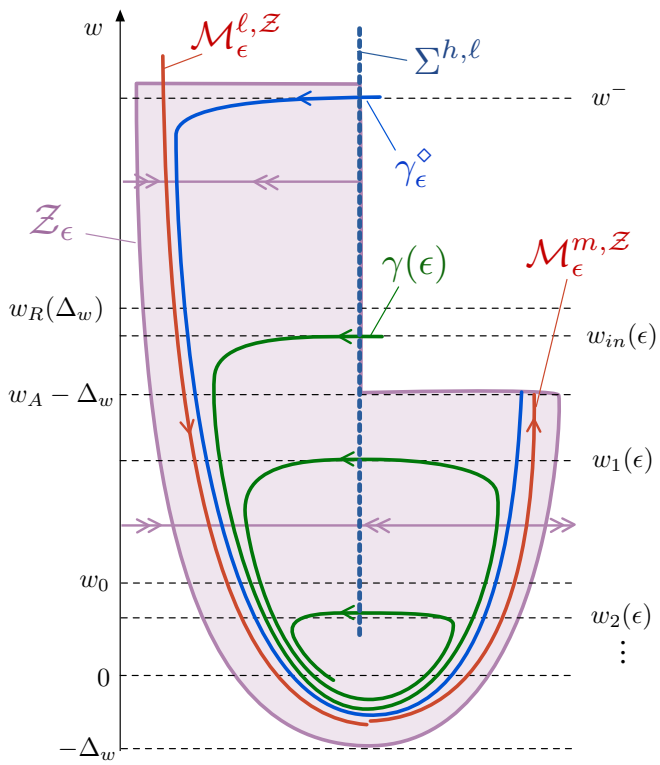

Figure 13: *Shown is a schematic of the manifold $\mathcal{Z}_\epsilon(c,a)$ and the section $\Sigma^{h,\ell}$ and the sequence $w_i(\epsilon)$ followed by a solution under the assumptions of Proposition 3.10. The specific trajectory shown corresponds to case* (B) *from the proof of Proposition 3.10: provided $w_{in} < w_R(\Delta_w)$, the trajectory $\gamma(\epsilon)$ returns to $\Sigma^{h,\ell}$ at heights $w = w_1, w_2, \ldots$ determined by successive zeros of the way-in-way-out function R, before eventually converging to the equilibrium.*

options hold for all such γ_ϵ.

(i) (Tunnel behavior): If $w^- < w_b^-$, then the corresponding exit point b_ϵ^m of γ_ϵ satisfies $\lim_{\epsilon\to 0} b_\epsilon^m = b_0^m \in \Sigma^{h,\ell} \cap \{w = w^+\}$ or $b_0^m \in \partial\mathcal{Z}_\epsilon(c_\epsilon^\diamond, a_\epsilon^\diamond) \cap \{w = w^+\}$, where $w^+ < w_b^+$ is the unique value satisfying $R(w^-, w^+) = 0$; see Figure 12a.

(ii) (Funnel behavior): If $w^- > w_b^-$, then the corresponding exit point b_ϵ^m of γ_ϵ satisfies $\lim_{\epsilon\to 0} b_\epsilon^m = b_0^m \in \Sigma^{h,\ell} \cap \{w = w_b^+\}$ or $b_0^m \in \partial\mathcal{Z}_\epsilon(c_\epsilon^\diamond, a_\epsilon^\diamond) \cap \{w = w_b^+\}$; see Figure 12b.

(iii) (Comb behavior): If $w^- = w_b^-$, then the corresponding exit point b_ϵ^m of γ_ϵ satisfies $\lim_{\epsilon\to 0} b_\epsilon^m = b_0^m \in \Sigma^{h,\ell} \cap \{w = w^+\}$ or $b_0^m \in \partial\mathcal{Z}_\epsilon(c_\epsilon^\diamond, a_\epsilon^\diamond) \cap \{w = w^+\}$ for some $w^+ \geq w_b^+$. (Comb behavior corresponds to funnel behavior when considering the flow in reverse time.)

A pair (w_b^-, w_b^+) satisfying only the condition (i) will be referred to as weak buffer heights.

Remark 3.8. *Note that the definition of buffer heights depends on the choice of parameters $(c, a) = (c_\epsilon^\diamond, a_\epsilon^\diamond)$, but not on the specific canard solution γ_ϵ.*

The next result is analogous to [7, Theorems 6 & 7] and relates the location of such buffer heights to the existence of a canard trajectory on $\mathcal{Z}_\epsilon(c, a)$ with specified entry/exit heights. Given entry/exit heights, one can find such a canard solution by varying the parameter $a = a^C(\sqrt{\epsilon}, c) + \mathcal{O}(e^{-q/\epsilon})$ [22]. Hence the next proposition can be thought of as relating the location of the buffer heights to different values of the parameter a; however given that a varies on an exponentially small interval, it is more natural to relate the buffer heights to the entry/exit heights of a given canard solution. A proof is given in Appendix C.

Proposition 3.9. *Suppose for each sufficiently small $\epsilon > 0$ there exists a canard trajectory $\gamma_\epsilon^\diamond$ at the parameter values $(c, a) = (c_\epsilon^\diamond, a_\epsilon^\diamond)$ where the triplet $(\gamma_\epsilon^\diamond, c_\epsilon^\diamond, a_\epsilon^\diamond)$ depends continuously on ϵ, and suppose $\gamma_\epsilon^\diamond$ intersects $\Sigma^{h,\ell}$ at the entry/exit points $b_\epsilon^\ell, b_\epsilon^m$ where*

$$\lim_{\epsilon\to 0} b_\epsilon^\ell = b_0^\ell \in \Sigma^{h,\ell} \cap \{w = w^-\}, \quad \lim_{\epsilon\to 0} b_\epsilon^m = b_0^m \in \Sigma^{h,\ell} \cap \{w = w^+\}.$$

Then exactly one of the following holds:

(i) Suppose $R(w^-, w^+) = 0$. Then w^- and w^+ are weak buffer heights.

(ii) Suppose $R(w^-, w^+) < 0$. Define $w_b^- < w^-$ to be the unique value satisfying $R(w_b^-, w^+) = 0$. Then w_b^- and w^+ are buffer heights.

(iii) Suppose $R(w^-, w^+) > 0$. Define $w_b^+ < w^+$ to be the unique value satisfying $R(w^-, w_b^+) = 0$. Then w^- and w_b^+ are buffer heights.

3.2.4 Convergence of trajectories to the equilibrium

Using the above notion of buffer heights and Proposition 3.9, we obtain the following proposition, describing the behavior of trajectories entering $\mathcal{Z}_\epsilon(c, a)$ via the section $\Sigma^{h,\ell}$ in the presence of a canard trajectory. See Figure 13 for a schematic depicting the results of Proposition 3.10.

Proposition 3.10. *Fix $w_0 > 0$ small. For each sufficiently small $\Delta_w = \Delta_w(w_0) > 0$, let $w_R(\Delta_w) > w_A + \Delta_w$ be defined by $R(w_R(\Delta_w), w_A - 3\Delta_w) = 0$, and set $w_R^0 = w_R(0)$. Suppose for each sufficiently small $\epsilon > 0$ there exists a canard trajectory $\gamma_\epsilon^\diamond$ at the parameter values $(c, a) = (c_\epsilon^\diamond, a_\epsilon^\diamond)$ where the triplet $(\gamma_\epsilon^\diamond, c_\epsilon^\diamond, a_\epsilon^\diamond)$ depends continuously on ϵ, and $\gamma_\epsilon^\diamond$ satisfies one of the following:*

(A) $\gamma_\epsilon^\diamond$ intersects $\Sigma^{h,\ell}$ at the entry/exit points $b_\epsilon^\ell, b_\epsilon^m$ where

$$\lim_{\epsilon\to 0} b_\epsilon^\ell = b_0^\ell \in \Sigma^{h,\ell} \cap \{w = w^-\}, \quad \lim_{\epsilon\to 0} b_\epsilon^m = b_0^m \in \Sigma^{h,\ell} \cap \{w = w^+\},$$

for some $w^- \geq w_R^0$ and $w^+ > 0$.

(B) $\gamma_\epsilon^\diamond$ intersects $\Sigma^{h,\ell}$ at the entry point b_ϵ^ℓ where

$$\lim_{\epsilon\to 0} b_\epsilon^\ell = b_0^\ell \in \Sigma^{h,\ell} \cap \{w = w^-\},$$

for some $w^- \geq w_R^0$, and $\gamma_\epsilon^\diamond$ exits $\mathcal{Z}_\epsilon(c_\epsilon^\diamond, a_\epsilon^\diamond)$ via $\{w = w_A - \Delta_w\}$.

Then at the same parameter values $(c, a) = (c_\epsilon^\diamond, a_\epsilon^\diamond)$, the following hold.

(i) Let $\gamma = \gamma(\epsilon)$ be another trajectory depending continuously on ϵ which intersects $\Sigma^{h,\ell} \cap \mathcal{Z}_\epsilon(c_\epsilon^\diamond, a_\epsilon^\diamond)$ at $w = w_{in}(\epsilon)$, where $w_{in}(0) = \lim_{\epsilon\to 0} w_{in}(\epsilon)$ satisfies $w_{in}(0) < w_R(\Delta_w)$.

Then γ remains in $\mathcal{Z}_\epsilon(c_\epsilon^\diamond, a_\epsilon^\diamond)$ for all forward time and lies on the stable manifold $\mathcal{W}_\epsilon^s(0; c_\epsilon^\diamond, a_\epsilon^\diamond)$. Furthermore, there exists $N \in \mathbb{N}$ such that γ returns to $\Sigma^{h,\ell}$ at a sequence of heights

$$w_1(\epsilon) > w_2(\epsilon) > \ldots > w_{N-2}(\epsilon) > w_{N-1}(\epsilon) > w_0 > w_N(\epsilon). \tag{3.9}$$

We have that $w_i(\epsilon) \to w_i(0)$ as $\epsilon \to 0$ where $w_i(0)$ are successive zeros of the way-in-way-out function R, that is,

$$R(w_1(0), w_2(0)) = R(w_2(0), w_3(0)) = \ldots = R(w_{N-1}(0), w_N(0)) = 0. \tag{3.10}$$

(ii) Any trajectory meeting the set $\mathcal{Z}_\epsilon(c_\epsilon^\diamond, a_\epsilon^\diamond) \cap \{u = 0, 0 < w \leq \Delta_w\}$ lies on the stable manifold $\mathcal{W}_\epsilon^s(0; c_\epsilon^\diamond, a_\epsilon^\diamond)$.

Proof. We first consider (A). To prove (i), since the exit point b_ϵ^m of the canard trajectory $\gamma_\epsilon^\diamond$ lies on $\Sigma^{h,\ell}$, we have $w^+ < w_A - \Delta_w$. By assumption, we have $w^- \geq w_R^0$, and hence $R(w^-, w^+) < 0$ due to the definition of w_R^0 and Lemma 3.6(iii). Proposition 3.9(ii) therefore implies the existence of w_b^- such that that the pair (w_b^-, w^+) are buffer heights, where $w_b^- < w^-$ satisfies $R(w_b^-, w^+) = 0$. The solution γ enters $\Sigma^{h,\ell}$ at $w = w_{in}(\epsilon)$, where $w_{in}(0) < w_R(\Delta_w)$. Since γ enters $\Sigma^{h,\ell}$ at a lower height than $\gamma_\epsilon^\diamond$, we know that γ must exit via $\Sigma^{h,\ell}$ at a height $w_1(\epsilon) \leq w^+$; this is merely due to the fact that on the two-dimensional manifold $\mathcal{Z}_\epsilon(c_\epsilon^\diamond, a_\epsilon^\diamond)$, the trajectory $\gamma_\epsilon^\diamond$ blocks γ from exiting higher than w^+ or via the boundary of $\mathcal{Z}_\epsilon(c_\epsilon^\diamond, a_\epsilon^\diamond)$. It remains to determine $w_1(\epsilon)$ via the properties of the buffer heights (w_b^-, w^+) from Definition 3.7.

There are two cases to consider: If $w_{in}(0) \geq w_b^-$, then γ subsequently exits via $\Sigma^{h,\ell}$ at $w_1(\epsilon)$, where $\lim_{\epsilon\to 0} w_1(\epsilon) = w_1(0) = w^+$. If $w_{in}(0) < w_b^-$, then γ subsequently exits via $\Sigma^{h,\ell}$ at $w_1(\epsilon)$, where $w_1(0) = \lim_{\epsilon\to 0} w_1(\epsilon)$ satisfies $R(w_{in}(0), w_1(0)) = 0$.

Now since $R(w, w) > 0$ for $0 < w \leq w_A$ by Lemma 3.6, on each subsequent return to $\Sigma^{h,\ell}$, the solution γ reaches $w = w_i(\epsilon)$, where $w_{i+1}(\epsilon) < w_i(\epsilon)$ for each i and $\lim_{\epsilon\to 0} w_i(\epsilon) = w_i(0)$ where $R(w_i(0), w_{i+1}(0)) = 0$. Since we can bound the difference $w_i(\epsilon) - w_{i+1}(\epsilon) > 0$ from below by a positive constant in the region $w \geq w_0$, we conclude that after finitely many, say N, such excursions, we have $w_N(0) < w_0$.

It is now apparent that γ is trapped in $\mathcal{Z}_\epsilon(c_\epsilon^\diamond, a_\epsilon^\diamond)$ for all forward time, returning to $\Sigma^{h,\ell}$ with the height w on each return decreasing monotonically. As w_0 was fixed arbitrarily small, we may assume that in forward time γ is trapped in a small fixed neighborhood $\mathcal{V}$ of the equilibrium. By Proposition 3.4, for any sufficiently small $\epsilon > 0$ there can be no nonrepelling periodic orbits lying entirely in $\mathcal{V}$. Hence the trajectory γ must converge to the equilibrium, and therefore γ lies in $\mathcal{W}_\epsilon^s(0; c_\epsilon^\diamond, a_\epsilon^\diamond)$. Using the monotonicity of γ, we see that the region in $\mathcal{Z}_\epsilon(c_\epsilon^\diamond, a_\epsilon^\diamond)$ that is enclosed by γ and the line segment $w_{N-1} < w < w_N$ is forward invariant and contains the

equilibrium that is situated at the origin for all (c, a, ϵ). The non-existence of nonrepelling periodic orbits in this region combined with Poincaré-Bendixson implies (ii).

We now consider case (B). In this case, since $\gamma_\epsilon^\diamond$ exits the manifold $\mathcal{Z}_\epsilon(c_\epsilon^\diamond, a_\epsilon^\diamond)$ via the boundary $\{w = w_A - \Delta_w\}$, it is not guaranteed that γ returns to $\Sigma^{h,\ell}$; that is, it is possible that γ follows $\gamma_\epsilon^\diamond$ and exits via $\{w = w_A - \Delta_w\}$, so we must rule out this possibility. Hence, we first show that γ must return to $\Sigma^{h,\ell}$ at a height $w \leq w_A - \Delta_w$. We consider the trajectory which meets $\Sigma^{h,\ell}$ at $w = w_A - 2\Delta_w$. Evolving *backwards* in time, this trajectory cannot cross $\gamma_\epsilon^\diamond$ and therefore must intersect $\Sigma^{h,\ell}$ at some height $w = w_C(\epsilon) \leq w_R^0$. Let $w_C^0 = \lim_{\epsilon \to 0} w_C(\epsilon)$. We claim that $R(w_C^0, w_A - 2\Delta_w) = 0$ and hence by Proposition 3.9, the pair $(w_C^0, w_A - 2\Delta_w)$ are weak buffer heights. To show this, we assume for contradiction that $R(w_C^0, w_A - 2\Delta_w) < 0$. By Proposition 3.9, we have that the pair $(w_b^-, w_A - 2\Delta_w)$ are buffer heights, where $w_b^- < w_C^0$ is the unique value satisfying $R(w_b^-, w_A - 2\Delta_w) = 0$. Thus any solution entering $\Sigma^{h,\ell}$ above $w = w_b^-$ exits $\Sigma^{h,\ell}$ or the boundary of $\mathcal{Z}_\epsilon(c_\epsilon^\diamond, a_\epsilon^\diamond)$ at height $w = w_A - 2\Delta_w$. This gives the desired contradiction: by assumption, we know that $\gamma_\epsilon^\diamond$ exits via $w = w_A - \Delta_w > w_A - 2\Delta_w$. The case $R(w_C^0, w_A - 2\Delta_w) > 0$ can be treated similarly.

Hence the pair $(w_C^0, w_A - 2\Delta_w)$ are weak buffer heights. Since $w_{in}(0) \leq w_R(\Delta_w) < w_C^0$, γ returns to $\Sigma^{h,\ell}$ at a height $w_1(\epsilon)$ where $w_1(0) = \lim_{\epsilon \to 0} w_1(\epsilon)$ satisfies $w_1(0) \leq w_A - 2\Delta_w$ and $R(w_{in}(0), w_1(0)) = 0$. The remainder of the argument follows as in case (A) above. □

Remark 3.11. *The above proposition essentially characterizes certain solutions on $\mathcal{W}_\epsilon^s(0; c, a)$ in the presence of a canard trajectory with suitable entry/exit points along the slow manifolds $\mathcal{M}_\epsilon^{\ell,\mathcal{Z}}(c, a)$ and $\mathcal{M}_\epsilon^{m,\mathcal{Z}}(c, a)$. In our application below, the basepoint trajectory on $\mathcal{Z}_\epsilon(c, a)$ shadowed by the primary excursion of the pulse will serve as this canard trajectory. In the forthcoming analysis, this geometric criterion regarding the existence of a suitable canard solution will suffice, though it is worth remarking that this condition can be translated into certain restrictions on the parameters (c, a).*

The entry/exit heights of a canard on $\mathcal{Z}_\epsilon(c, a)$ are adjusted via exponentially small changes in the parameters (c, a), and hence the structure of $\mathcal{W}_\epsilon^s(0; c, a)$ is very delicate and can change dramatically within very small intervals in parameter space. However, Proposition 3.10 guarantees that certain solutions must always lie on $\mathcal{W}_\epsilon^s(0; c, a)$, provided either:

(A) there is a canard trajectory with entry height suitably larger that the corresponding exit height
(B) there is a canard trajectory of sufficient length, i.e. we are sufficiently close to the maximal canard

It can be inferred from the proof of Theorem 2.6 in §4.1 that these conditions are roughly equivalent to the following conditions on the parameters (c, a) for fixed ϵ: for a fixed value of the wavespeed c, the parameter a cannot be too much lower than the value at which the maximal canard occurs (see Figure 3). While this statement could be made rigorous and the lower bound could in theory be computed, we do not attempt to proceed in this manner as the analysis is sensitive to exponentially small quantities and is unnecessary for our purposes.

4 Constructing transitional pulses

In this section, we construct the transitional pulses of Theorem 2.2 in pieces and obtain matching conditions near the equilibrium which are solved using an implicit function theorem.

The general construction for pulses of all types involves three pieces: the primary pulse, a secondary excursion, and a tail which is trapped in the manifold $\mathcal{Z}_\epsilon(c, a)$ in forward time. Hence the procedure involves obtaining two conditions: one which matches the primary pulse to the secondary excursion, and one matching the secondary excursion to the tail. Once these matching conditions are obtained, from the analysis in §3 we deduce that any such tail must lie in the stable manifold of the equilibrium, which completes the construction.

Due to various interactions of the pulses with the fold points and the Airy point, the construction of the

transitional pulses breaks down into six types. All pulse types have the same primary excursion Γ_0^1, and hence the pulse types are determined by properties of the secondary excursion $\Gamma_0^2(s)$. The different pulse types are as labelled in Figure 4 and are parametrized by s as in the statement of Theorem 2.2.

- Type 1: $\{\Gamma(s) : s \in (0, w_R(\Delta_w)\}$

  Type 1 pulses are left pulses with a secondary excursion of height $w \in (0, w_R(\Delta_w))$, where $w_R(\Delta_w)$ is defined in terms of the way-in-way-out function R via $R(w_R(\Delta_w), w_A - 3\Delta_w) = 0$, where w_A represents the height of the Airy point and Δ_w is sufficiently small. For these pulses, we show that this secondary excursion meets $\mathcal{Z}_\epsilon(c, a)$ in the section $\Sigma^{h,\ell}$, and due to Proposition 3.10, lies on the stable manifold $\mathcal{W}_\epsilon^s(0; c, a)$.

- Type 2: $\{\Gamma(s) : s \in (w_R(\Delta_w), w^\dagger - \Delta_w)\}$

  Type 2 pulses are left pulses with a secondary excursion of height $w \in (w_R(\Delta_w), w^\dagger - \Delta_w)$, where $w^\dagger$ is the height of the upper right fold point. For these pulses, the secondary pulse cannot be taken to lie on $\mathcal{Z}_\epsilon(c, a)$ in the section $\Sigma^{h,\ell}$, due to the fact that Proposition 3.10 can not be applied, and in general such a trajectory can not be expected to lie on $\mathcal{W}_\epsilon^s(0; c, a)$. In this case we consider a one-dimensional family of potential secondary pulse candidates and select one member of this family by imposing a second matching condition which ensures that the solution meets $\mathcal{Z}_\epsilon(c, a)$ on its next return to the section $\Sigma^{h,\ell}$ under circumstances where the results of Proposition 3.10 hold.

- Type 3: $\{\Gamma(s) : s \in (w^\dagger - \Delta_w, w^\dagger + \Delta_w)\}$

  Type 3 pulses pass near the upper right fold point and encompass the transition between left and right pulses. These are constructed in much the same way as type 2 pulses, but there are additional difficulties encountered in parameterizing these pulses (w is not a natural parameter in this regime), and in verifying that the interaction with the upper right fold does not cause the argument to break down.

- Type 4: $\{\Gamma(s) : s \in (w^\dagger + \Delta_w, 2w^\dagger - w_A - \Delta_w)\}$

  Type 4 pulses are right pulses with secondary excursion of height $w \in (w_A + \Delta_w, w^\dagger - \Delta_w)$. An additional technical difficulty arises in this regime: solving the first matching condition requires showing that there is a net contraction in backwards time along the slow manifolds $\mathcal{M}_\epsilon^\ell(c, a), \mathcal{M}_\epsilon^r(c, a)$.

- Type 5: $\{\Gamma(s) : s \in (2w^\dagger - w_A - \Delta_w, 2w^\dagger - \Delta_w)\}$

  Type 5 pulses are right pulses with a secondary excursion of height $w \in (\Delta_w, w_A + \Delta_w)$. For these pulses, the secondary excursions have a more delicate interaction with the Airy point and therefore introduce complications when trying to determine the final matching condition with the tail.

- Type 6: $\{\Gamma(s) : s \in (2w^\dagger - \Delta_w, 2w^\dagger)\}$

  Type 6 pulses consist of essentially two copies of the primary pulse. In this parameter regime, we are close to the Belyakov transition at which the double pulses are expected to terminate for ϵ sufficiently small [6]. While we are able to construct some type 6 pulses, our results do not cover all type 6 pulses up to the Belyakov point. See §4.7 and Remark 4.13 for more details on where the construction breaks down.

  At a technical level, the analysis in understanding the precise nature of the termination at the Belyakov point likely requires additional blow-ups near the origin to account for the changing eigenvalue structure. We believe that this regime is technically more challenging and therefore did not pursue a complete analysis of the termination of the branch of double pulses.

We begin with setting up the blown-up coordinate system near the canard point at the origin in which the matching will occur, followed by constructing pulses of type 1 and 2. We then outline the difficulties/differences

in constructing pulses of type 3-6 and how to overcome these. The construction is then complete up to several technical results involving transversality conditions which arise due to interaction with the Airy point; these are proved in §5.

We note that we will use the parameters (c, a) as free bifurcation parameters in order to solve matching conditions whose solutions correspond to the transitional pulse solutions. In describing certain solutions and invariant manifolds, we will omit their dependence on ϵ to avoid cumbersome notation and to emphasize their dependence on the free variables (c, a).

4.1 Flow near the canard point

We collect some results from [22, 5] which will be useful in the forthcoming analysis for obtaining matching conditions for the transitional pulses near the equilibrium. We will choose our coordinate system relative to the invariant manifold $\mathcal{W}_\epsilon^{c,\ell}(c, a)$ (see §2.4), which is C^k-smooth, rather than the larger (but only C^1-smooth) manifold $\mathcal{Z}_\epsilon(c, a)$ constructed in §3. However, we emphasize that in a neighborhood of the equilibrium, these manifolds are C^1 equivalent up to exponentially small errors; see Remark 3.2.

In [5], it was shown that in a neighborhood of the origin, after a change of coordinates, we obtain the system

$$\begin{aligned}
\dot{x} &= -y + x^2 + \mathcal{O}(\epsilon, xy, y^2, x^3) \\
\dot{y} &= \epsilon\left[x\left(1 + \mathcal{O}(x, y, \alpha, \epsilon)\right) + \alpha\left(1 + \mathcal{O}(x, y, \alpha, \epsilon)\right) + \mathcal{O}(y)\right] \\
\dot{z} &= z\left(c^{3/2} + \mathcal{O}(x, y, z, \epsilon)\right) \\
\dot{\alpha} &= 0 \\
\dot{\epsilon} &= 0\ ,
\end{aligned} \tag{4.1}$$

where $\alpha = \dfrac{a}{2c^{1/2}}$. The manifold $\mathcal{W}_\epsilon^{c,\ell}(c, a)$ is given by $z = 0$, where the strong unstable fibers have been straightened; we recall that by construction $\mathcal{W}_\epsilon^{c,\ell}(c, a)$ contains the one-dimensional slow manifolds $\mathcal{M}_\epsilon^{\ell}(c, a)$ and $\mathcal{M}_\epsilon^{m,c}(c, a)$. We note that the (x, y) coordinates are in the canonical form for a canard point (compare [22]), that is,

$$\begin{aligned}
\dot{x} &= -yh_1(x, y, \alpha, \epsilon, c) + x^2 h_2(x, y, \alpha, \epsilon, c) + \epsilon h_3(x, y, \alpha, \epsilon, c) \\
\dot{y} &= \epsilon\left(xh_4(x, y, \alpha, \epsilon, c) + \alpha h_5(x, y, \alpha, \epsilon, c) + yh_6(x, y, \alpha, \epsilon, c)\right) \\
\dot{z} &= z\left(c^{3/2} + \mathcal{O}(x, y, z, \alpha, \epsilon)\right) \\
\dot{\alpha} &= 0 \\
\dot{\epsilon} &= 0\ ,
\end{aligned} \tag{4.2}$$

where we have

$$\begin{aligned}
&h_3(x, y, \alpha, \epsilon, c) = \mathcal{O}(x, y, \alpha, \epsilon) \\
&h_j(x, y, \alpha, \epsilon, c) = 1 + \mathcal{O}(x, y, \alpha, \epsilon), \quad j = 1, 2, 4, 5\ .
\end{aligned} \tag{4.3}$$

We have now separated the hyperbolic dynamics (given by the z-coordinate) from the nonhyperbolic dynamics which are isolated on a four-dimensional center manifold parameterized by the variables (x, y, ϵ, α) on which the origin is a canard point in the sense of [22]. Such points are characterized by canard trajectories which follow a strongly attracting manifold (in this case $\mathcal{M}_\epsilon^{\ell}(c, a)$), pass near the equilibrium and continue along a strongly repelling manifold (in this case $\mathcal{M}_\epsilon^{m,c}(c, a)$) for some time; see Figure 14 for an illustration. To understand the flow near this point, we use blowup methods as in [22]. Restricting to the center manifold $z = 0$, the blow up transformation is given by

$$x = \bar{r}\bar{x}, \quad y = \bar{r}^2\bar{y}, \quad \alpha = \bar{r}\bar{\alpha}, \quad \epsilon = \bar{r}^2\bar{\epsilon}\ , \tag{4.4}$$

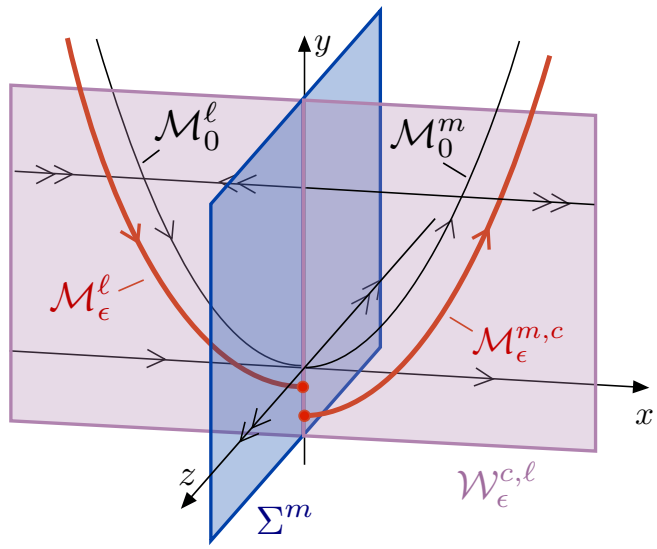

Figure 14: *The local coordinates near the section Σ^m. The manifold $\mathcal{W}_\epsilon^{c,\ell}(c,a)$ coincides with the subspace $z=0$. Within this subspace, the origin takes the form of a canard point [22].*

defined on the manifold $B_c = S^2 \times [0,\bar{r}_0] \times [-\bar{\alpha}_0, \bar{\alpha}_0]$ for sufficiently small $\bar{r}_0, \bar{\alpha}_0$ with $(\bar{x},\bar{y},\bar{\epsilon}) \in S^2$. There is one relevant coordinate chart which will be needed for the matching analysis. Keeping the same notation as in [22] and [23], the chart $\mathcal{K}_2$ uses the coordinates

$$x = r_2 x_2, \quad y = r_2^2 y_2, \quad \alpha = r_2 \alpha_2, \quad \epsilon = r_2^2. \tag{4.5}$$

Using these blow-up charts, the authors of [22] studied the behavior of the manifolds $\mathcal{M}_\epsilon^\ell(c,a)$ and $\mathcal{M}_\epsilon^{m,c}(c,a)$ near the equilibrium, and in particular determined conditions under which these manifolds coincide along a canard trajectory. We place a section $\Sigma^m = \{x=0, |y|<\Delta_y, |z| \le \Delta_z\}$ for small fixed Δ_z and $\Delta_y = 2\Delta_w$ in which most of our computations will take place (see Figure 14).

In the chart $\mathcal{K}_2$, the section Σ^m is given by $\Sigma_2^m = \left\{x_2 = 0, |r_2^2 y_2| < \Delta_y, |z| \le \Delta_z\right\}$. It was shown in [22] that for all sufficiently small r_2, α_2, the manifolds $\mathcal{M}_\epsilon^\ell(c,a)$ and $\mathcal{M}_\epsilon^{m,c}(c,a)$ reach Σ_2^m at $y = y_2^{\mathcal{M},\ell}(c,\alpha_2,r_2)$ and $y = y_2^{\mathcal{M},m}(c,\alpha_2,r_2)$, respectively. Furthermore, we have the following result which will be useful in the coming analysis.

Proposition 4.1. *[22, Proposition 3.5] The distance between the slow manifolds $\mathcal{M}_\epsilon^\ell(c,a)$ and $\mathcal{M}_\epsilon^{m,c}(c,a)$ in Σ^m is given by*

$$y_2^{\mathcal{M},\ell} - y_2^{\mathcal{M},m} = \mathcal{D}_0(\alpha_2, r_2; c) = d_{\alpha_2}\alpha_2 + d_{r_2} r_2 + \mathcal{O}(r_2^2 + \alpha_2^2)\ , \tag{4.6}$$

where the coefficients d_{α_2}, d_{r_2} are positive constants. Hence we can solve for when this distance vanishes which occurs when

$$\alpha_2 = \alpha_2^C = -\frac{d_{r_2}}{d_{\alpha_2}} r_2 + \mathcal{O}(r_2^2). \tag{4.7}$$

Theorem 2.6 then follows from the above proposition.

Remark 4.2. *In the following, many computations will be performed in the $\mathcal{K}_2$ coordinates before transforming back into the original coordinates/parameters as the results of Theorem 2.2 are stated in terms of the original parameters (c,a,ϵ), rather than (c,α_2,r_2). To obtain (a,ϵ) from (α_2,r_2), we have*

$$\begin{aligned} a &= 2c^{1/2}\alpha_2 r_2 \\ \epsilon &= r_2^2, \end{aligned} \tag{4.8}$$

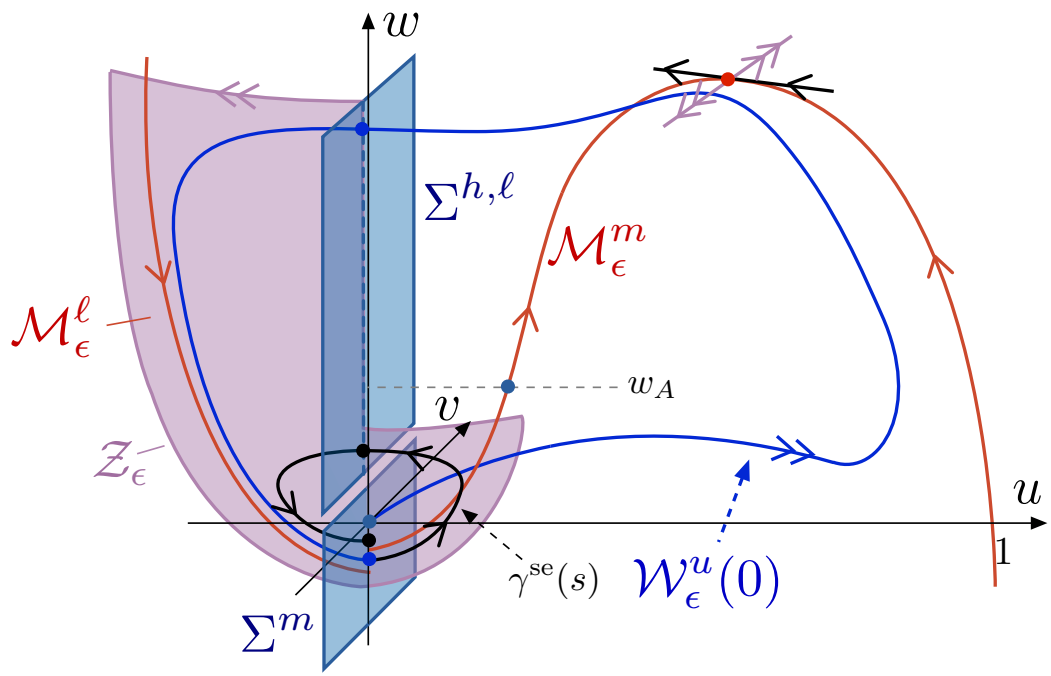

Figure 15: *Shown is the geometry for constructing a type* 1 *left transitional pulse.*

which are smooth functions of (c, α_2, r_2) *for* (c, α_2, r_2) *near* $(1/\sqrt{2}, 0, 0)$.

We remark that results involving transversality with respect to parameter variations due to the exchange lemma [26] which are obtained for the original system (1.2) *can likewise be shown to hold in the* $\mathcal{K}_2$ *coordinates by instead considering the system*

$$\begin{aligned} \dot{u} &= v \\ \dot{v} &= cv - f(u) + w \\ \dot{w} &= r_2^2(u - \gamma w), \end{aligned} \tag{4.9}$$

where $f(u) = u(u - 2c^{1/2}\alpha_2 r_2)(1-u)$ *for* (c, α_2, r_2) *near* $(1/\sqrt{2}, 0, 0)$.

4.2 Type 1 pulses

Type 1 pulses are the simplest of the transitional pulses and are really just single pulses with 'large' oscillatory tails. In this section, we deduce the existence of transitional left pulses with secondary excursion of height $w \leq w_R(\Delta_w)$ and show that these pulses are in fact a continuation of the family of pulses with oscillatory tails constructed in [5]. To construct a type 1 pulse, we need a single matching condition which matches the primary pulse with a secondary pulse of height $w \leq w_R(\Delta_w)$; see Figure 15. The fact that this secondary excursion lies in the stable manifold $\mathcal{W}_\epsilon^s(0; c, a)$ of the equilibrium will follow from Proposition 3.10.

We break this into two parts. We first construct pulses of height $w \in (\Delta_w, w_R(\Delta_w))$ and then move onto pulses with 'small' oscillatory tails, that is, pulses with tails of height $w \leq \Delta_w$ and show that this branch of pulses is a continuation of the classical branch of pulses given by Theorem 1.1.

4.2.1 Matching condition for pulses $\Gamma(s, \sqrt{\epsilon})$, $s \in (\Delta_w, w_R(\Delta_w))$

The desired transitional pulse solution consists of a primary excursion, followed by a secondary excursion $\gamma^{\mathrm{se}}(s; c, a)$ intersecting the section $\Sigma^{h,\ell}$ at height $w = s$ (see Figure 15). We can ensure that the unstable

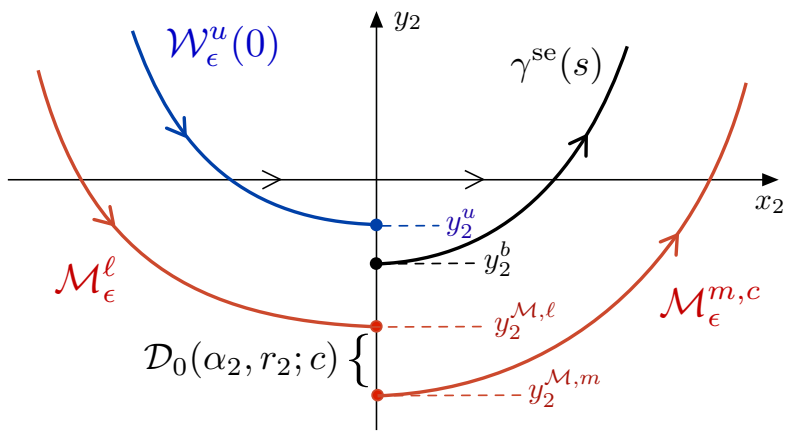

Figure 16: *Shown is the setup for the matching conditions* (4.12) *projected onto the* (x_2, y_2)*-plane.*

manifold $\mathcal{W}_\epsilon^u(0;c,a)$ completes the primary excursion and returns to a neighborhood of the equilibrium by using Proposition 2.7; see Figure 11. As $\mathcal{W}_\epsilon^u(0;c,a)$ is exponentially close to $\mathcal{M}_\epsilon^\ell(c,a)$ upon enterting this neighborhood, we can track $\mathcal{W}_\epsilon^u(0;c,a)$ along $\mathcal{M}_\epsilon^\ell(c,a)$ to where it intersects the section Σ^m (see §4.1). The goal is then to match $\mathcal{W}_\epsilon^u(0;c,a)$ with $\gamma^{\rm se}(s;c,a)$. The setup is shown in Figure 15. For $s \in (\Delta_w, w_R(\Delta_w))$, the fact that this secondary excursion $\gamma^{\rm se}(s;c,a)$ lies in the stable manifold $\mathcal{W}_\epsilon^s(0;c,a)$ of the equilibrium is due to Proposition 3.10.

We will match the various components of the solution in the section Σ^m in the $\mathcal{K}_2$ coordinates. Figure 16 shows the setup for the matching conditions projected onto the (x_2, y_2)-plane.

First, in order to match $\mathcal{W}_\epsilon^u(0;c,a)$ with $\gamma^{\rm se}(s;c,a)$, we have the following lemma describing the location of $\mathcal{W}_\epsilon^u(0;c,a)$ in Σ^m.

Lemma 4.3. *For each sufficiently small $\Delta_z > 0$, there exists $C, q, \epsilon_0 > 0$ and $q_1 > q_2 > 0$ such that the following holds. For each $0 < \epsilon < \epsilon_0$ and each $|z| < \Delta_z$, there exists $c = c(z)$ with $|c(z) - \check{c}(a,\epsilon)| = \mathcal{O}(e^{-q/\epsilon})$ such that $\mathcal{W}_\epsilon^u(0;c(z),a)$ intersects Σ^m at the point $(y_2^u(z;c(z),a), z)$ where*

$$\begin{aligned} e^{-q_1/\epsilon}/C \le y_2^u(0;c(z),a) - y_2^{\mathcal{M},\ell} &\le Ce^{-q_2/\epsilon} \\ |y_2^u(z;c(z),a) - y_2^u(0;c(0),a)| &= \mathcal{O}(ze^{-q/\epsilon}). \end{aligned} \tag{4.10}$$

Proof. We have that $\mathcal{W}_\epsilon^u(0;\check{c}(a,\epsilon),a)$ is $\mathcal{O}(e^{-q/\epsilon})$-close to $\mathcal{M}_\epsilon^\ell(c,a)$ in Σ^m. Since by Proposition 2.7, $\mathcal{W}_\epsilon^u(0;c,a)$ transversely intersects $\mathcal{W}_\epsilon^{s,\ell}(c,a)$ upon varying $c \approx \check{c}(a,\epsilon)$, the result follows from the exchange lemma [26]. □

We now construct the candidate 'secondary pulse' solution: Consider the solution $\gamma^{\rm se}(s;c,a)$ on $\mathcal{Z}_\epsilon(c,a)$ which intersects $\Sigma^{h,\ell}$ at height $w = s \in (\Delta_w, w_R(\Delta_w))$; this intersection occurs at a point $(u,v,w) = (0, v^{\rm se}(s;c,a), s)$. Since $\gamma^{\rm se}(s;c,a)$ in exponentially contracted to $\mathcal{M}_\epsilon^m(c,a)$ in backwards time from $\Sigma^{h,\ell}$ to Σ^m, we have that the backwards evolution of $\gamma^{\rm se}(s;c,a)$ meets Σ^m at a point $\gamma_{\rm start}^{\rm se}(s;c,a) := (0, y_2^b, z^b)(s;c,a)$ where

$$\begin{aligned} |y_2^b(s;c,a) - y_2^{\mathcal{M},m}| &= \mathcal{O}(e^{-q/\epsilon}) \\ |z^b(s;c,a)| &= \mathcal{O}(e^{-q/\epsilon}), \end{aligned} \tag{4.11}$$

uniformly in (c,a). Thus by Proposition 4.1 we can match $\mathcal{W}_\epsilon^u(0;c,a)$ with $\gamma_{\rm start}^{\rm se}(s;c,a)$ in Σ^m by solving for when $z = z^b(s;c,a)$ and

$$\begin{aligned} 0 &= y_2^u(z;c,a) - y_2^b(s;c,a) \\ &= \mathcal{D}_0(\alpha_2, r_2; c) - \left(y_2^{\mathcal{M},\ell} - y_2^u(z;c,a) + y_2^b(s;c,a) - y_2^{\mathcal{M},m}\right) \\ &= \mathcal{D}_0(\alpha_2, r_2; c) + \mathcal{O}(e^{-q/\epsilon}). \end{aligned}$$

Therefore we must solve the system

$$\begin{aligned} \mathcal{D}_0(\alpha_2, r_2; c) &= \left(y_2^{\mathcal{M},\ell} - y_2^u(z; c, a)\right) + \left(y_2^b(s; c, a) - y_2^{\mathcal{M},m}\right) = \mathcal{O}(e^{-q/\epsilon}) \\ z &= z^b(s; c, a). \end{aligned} \tag{4.12}$$

See Figure 16 for the setup of the matching conditions (4.12) projected onto the (x_2, y_2)-plane.

Before tackling (4.12), we first consider solving the simpler equations

$$\begin{aligned} \mathcal{D}_0(\alpha_2, r_2; c) &= 0 \\ c &= \breve{c}\,(a, \epsilon)\,, \end{aligned} \tag{4.13}$$

for which, by Proposition 4.1, there is a solution when

$$\begin{aligned} a &= 2c^{1/2}\epsilon^{1/2}\alpha_2^C \\ c &= \breve{c}\,(a, \epsilon)\,, \end{aligned} \tag{4.14}$$

which we can solve by the implicit function theorem at $(c, a) = (c_E, a_E)(\sqrt{\epsilon})$ for sufficiently small $\epsilon > 0$.

Remark 4.4. *Geometrically, the parameter values $(c, a) = (c_E, a_E)$ capture an intersection of the manifolds $\mathcal{W}_\epsilon^u(0; c, a)$ and $\mathcal{W}_\epsilon^{c,\ell}(c, a)$ (as in Proposition 2.7) coinciding with the existence of a maximal canard in $\mathcal{W}_\epsilon^{c,\ell}(c, a)$ (as in Theorem 2.6).*

The solution of (4.12) is then obtained by solving

$$\begin{aligned} a &= 2c^{1/2}\epsilon^{1/2}(\alpha_2^C + \mathcal{O}(e^{-q/\epsilon})) \\ c &= \breve{c}\,(a, \epsilon) + \mathcal{O}(e^{-q/\epsilon}) \end{aligned} \tag{4.15}$$

by the implicit function theorem to find $(c, a) = (c, a)(s, \sqrt{\epsilon})$ where

$$(c, a)(s, \sqrt{\epsilon}) = (c_E, a_E)(\sqrt{\epsilon}) + \mathcal{O}(e^{-q/\epsilon}). \tag{4.16}$$

This fixes the parameters $(c, a) = (c, a)(s, \sqrt{\epsilon})$; we now argue that this solution lies on the stable manifold $\mathcal{W}_\epsilon^s(0; c, a)$ using Proposition 3.10. By construction, the unstable manifold $\mathcal{W}_\epsilon^u(c, a)$ follows the slow manifold $\mathcal{M}_\epsilon^\ell(c, a)$ where it meets $\gamma_{\text{start}}^{\text{se}}(s; c, a)$ in Σ^m, then follows $\mathcal{M}_\epsilon^m(c, a)$ before jumping off to meet the section $\Sigma^{h,\ell}$ at height $w = s \in (\Delta_w, w_R(\Delta_w)$. This portion of the solution therefore shadows a canard $\gamma_\epsilon^\diamond$ which satisfies (A) or (B) in Proposition 3.10 depending on whether $s < w_A - \Delta_w$ or $s > w_A - \Delta_w$, respectively. The forward evolution of $\gamma^{\text{se}}(s; c, a)$ then gives a solution $\gamma(\epsilon)$ satisfying the conditions of Proposition 3.10 and hence remains in $\mathcal{Z}_\epsilon(c, a)$, eventually converging to the equilibrium.

4.2.2 Continuation of the known branch of fast 1-pulses

We now consider the case of pulses with tails of height $w \leq \Delta_w$. In [5], it was shown that there exists K^*, such that for each K and each sufficiently small (a, ϵ) satisfying $\epsilon < Ka^2$, there exists a pulse solution with wave speed $c = \breve{c}(a, \epsilon)$. For $\epsilon > K^* a^2$, the tail of the pulse decays exponentially to zero in an oscillatory fashion.

We deduce that such pulses exist for (α_2, r_2) for any $r_2 > 0$ sufficiently small and $\alpha_2 > \dfrac{1}{2c\sqrt{K}} > \dfrac{1}{2\sqrt{K}}$, since

$$c = 1/\sqrt{2} + \mathcal{O}(\alpha_2 r_2, r_2^2) < 1 \tag{4.17}$$

for α_2 bounded and $r_2 > 0$ sufficiently small. In this section we show that these pulses overlap with the type 1 pulses constructed above, forming a continuous one-parameter family. It turns out that this family is naturally parameterized by α_2.

To see this, we proceed as follows. Setting $s = \Delta_w$, for sufficiently small $\epsilon > 0$, we can follow the procedure above in constructing a type 1 pulse with a tail of height $s = \Delta_w$, though we now choose the solution $\gamma^{\mathrm{se}}(\Delta_w; c, a)$ so that it meets $\mathcal{W}_\epsilon^{c,\ell}(c, a)$ in the section $\Sigma^{h,\ell}$. We note that in this case, the backwards evolution of $\gamma^{\mathrm{se}}(\Delta_w; c, a)$ remains in $\mathcal{W}_\epsilon^{c,\ell}(c, a)$ until reaching the section Σ^m and therefore intersects this section at a point $\gamma^{\mathrm{se}}_{\mathrm{start}}(\Delta_w; c, a) := (0, y_2^b(\Delta_w; c, a), 0)$ which satisfies

$$e^{-q_1/\epsilon}/C \leq y_2^b(\Delta_w; c, a) - y_2^{\mathcal{M},m} \leq Ce^{-q_2/\epsilon} \tag{4.18}$$

for some $q_1 > q_2 > 0$. Thus we can match $\mathcal{W}_\epsilon^u(0; c, a)$ with $\gamma^{\mathrm{se}}_{\mathrm{start}}(\Delta_w; c, a)$ by solving

$$\mathcal{D}_0(\alpha_2, r_2; c) = \left(y_2^{\mathcal{M},\ell} - y_2^u(0; c, a)\right) + \left(y_2^b(\Delta_w; c, a) - y_2^{\mathcal{M},m}\right) \tag{4.19}$$

We obtain a solution by solving

$$\begin{aligned} \alpha_2 &= \alpha_2^C + \mathcal{O}(e^{-q/\epsilon}) \\ c &= \check{c}\left(2c^{1/2} r_2 \alpha_2, r_2^2\right), \end{aligned} \tag{4.20}$$

by the implicit function theorem to find a solution at $(c, \alpha_2) = (c^u, \alpha_2^u)(r_2)$. We now consider the function $\bar{\mathcal{D}}(\alpha_2, r_2, c)$ defined to be the difference

$$\bar{\mathcal{D}}(\alpha_2, r_2, c) = y_2^u(0; c, a) - y_2^b(\Delta_w; c, a) \tag{4.21}$$

in Σ^m. From the construction above for the pulse with tail of height $\bar{w} = \Delta_w$, we have that

$$\bar{\mathcal{D}}(\alpha_2^u, r_2, c^u) = 0 \tag{4.22}$$

and

$$\begin{aligned} \bar{\mathcal{D}}(\alpha_2, r_2, c) &= y_2^u(0; c, a) - y_2^b(\Delta_w; c, a) \\ &= y_2^{\mathcal{M},\ell} - y_2^{\mathcal{M},m} + \mathcal{O}\left(e^{-q/\epsilon}\right) \\ &= \mathcal{D}_0(\alpha_2, r_2; c) + \mathcal{O}\left(e^{-q/\epsilon}\right) \\ &= d_{\alpha_2}\alpha_2 + d_{r_2} r_2 + \mathcal{O}(\alpha_2^2, \alpha_2 r_2, r_2^2). \end{aligned} \tag{4.23}$$

Hence we have that

$$\frac{\partial}{\partial \alpha_2} \bar{\mathcal{D}}(\alpha_2, r_2, c) = d_{\alpha_2} + \mathcal{O}(\alpha_2, r_2) > 0 \tag{4.24}$$

for any sufficiently small $r_2 > 0$ and $|\alpha_2| \leq \kappa$, uniformly in $c \approx 1/\sqrt{2}$.

Hence for sufficiently small $r_2 > 0$, for $\alpha_2^u < \alpha_2 < \kappa$, we can ensure that $\mathcal{W}_\epsilon^u(0; c, a)$ lands in $\mathcal{W}_\epsilon^{c,\ell}(c, a)$ by solving

$$c = \check{c}(2c^{1/2} r_2 \alpha_2, r_2^2), \tag{4.25}$$

for $c = c(\alpha_2, r_2)$ by the implicit function theorem. Furthermore, we have that the distance $\bar{\mathcal{D}}(\alpha_2, r_2, c)$ is positive, and hence we obtain a pulse whose tail reaches a height lower than Δ_w, but remains in $\mathcal{W}_\epsilon^{c,\ell}(c, a)$ and converges to the equilibrium. For fixed r_2, such pulses are therefore parameterized by $\alpha_2^u < \alpha_2 < \kappa$.

By taking $K > \dfrac{1}{4\kappa^2}$ in Theorem 1.1, we deduce that these pulses form a continuation of the classical branch of pulses for $\alpha_2 > \dfrac{1}{2\sqrt{K}}$.

4.3 Pulses of type 2-6: a second matching condition

In §4.2, we proved the existence of type 1 pulses using a single matching condition. This condition ensured that $\mathcal{W}^u_\epsilon(0;c,a)$ completes a second excursion $\gamma^{\mathrm{se}}(s;c,a)$ which meets $\mathcal{Z}_\epsilon(c,a)$ in the section $\Sigma^{h,\ell}$. Proposition 3.10 then ensures that this solution also lies in $\mathcal{W}^s_\epsilon(0;c,a)$.

This procedure breaks down when attempting to construct left pulses with secondary excursions of height $w \geq w_R(\Delta_w)$ (or any of the right pulses), due to the fact that trajectories which meet $\mathcal{Z}_\epsilon(c,a)$ in the section $\Sigma^{h,\ell}$ at $w \geq w_R(\Delta_w)$ do not necessarily lie in $\mathcal{W}^s_\epsilon(0;c,a)$. However, by adjusting the choice of the secondary excursion slightly, we can ensure that this solution meets $\mathcal{Z}_\epsilon(c,a)$ at a height $w < w_R(\Delta_w)$ on its subsequent return to $\Sigma^{h,\ell}$, and hence we may apply the results of Proposition 3.10.

Therefore, construction of pulses of type $2-6$ will involve two matching conditions: The first matches $\mathcal{W}^u_\epsilon(0;c,a)$ in the section Σ^m with a secondary excursion which follows $\mathcal{M}^m_\epsilon(c,a)$ then jumps from $\mathcal{M}^m_\epsilon(c,a)$ to either the left or right at the appropriate height determined by s, then returns to the section Σ^m. The second condition matches this secondary excursion with $\mathcal{Z}_\epsilon(c,a)$ on its next return to $\Sigma^{h,\ell}$.

As was the case with type 1 pulses, it is natural to set up all matching conditions in the section Σ^m, as this avoids various issues arising from exponentially small errors in the estimates needed in employing the implicit function theorem. Therefore, to ensure that the secondary excursion reaches $\mathcal{Z}_\epsilon(c,a)$ in $\Sigma^{h,\ell}$, we must understand which solutions starting in Σ^m will meet $\mathcal{Z}_\epsilon(c,a)$ in $\Sigma^{h,\ell}$. Alternatively, to the same effect we may consider the one-dimensional intersection $\mathcal{Y}_{\mathrm{end}}(c,a,\epsilon)$ of $\mathcal{Z}_\epsilon(c,a)$ with $\Sigma^{h,\ell}$ and evolve this *backwards*: this traces out a two-dimensional invariant manifold $\mathcal{Y}(c,a,\epsilon)$ which intersects Σ^m in a one-dimensional curve $\mathcal{Y}_{\mathrm{start}}(c,a,\epsilon)$, determining precisely the initial conditions in Σ^m which will subsequently meet $\mathcal{Z}_\epsilon(c,a)$ in $\Sigma^{h,\ell}$. Further, in order to be able to match the secondary pulse in Σ^m with a point on this curve, we require certain transversality conditions, namely that this curve should be transverse to the strong unstable fibers $y_2 = \text{const}$ in Σ^m.

Hence we are concerned with the backwards evolution of the intersection $\mathcal{Y}_{\mathrm{end}}(c,a,\epsilon) = \mathcal{Z}_\epsilon(c,a) \cap \Sigma^{h,\ell}$ from $\Sigma^{h,\ell}$ to Σ^m. Due to the invariance of $\mathcal{Z}_\epsilon(c,a)$, the backwards evolution of a trajectory on $\mathcal{Y}(c,a,\epsilon)$ meeting $\Sigma^{h,\ell}$ at a height $w < w_A - \Delta_w$ in fact remains in the manifold $\mathcal{Z}_\epsilon(c,a)$ until reaching Σ^m. Hence we only need to take care with understanding the behavior of trajectories on $\mathcal{Y}(c,a,\epsilon)$ which meet $\Sigma^{h,\ell}$ at $w \geq w_A - \Delta_w$ evolved backwards to Σ^m.

Under this backwards evolution, the two-dimensional manifold $\mathcal{Y}(c,a,\epsilon)$ will intersect Σ^m in a curve $\mathcal{Y}_{\mathrm{start}}(c,a,\epsilon)$. The intersection $\mathcal{Y}_{\mathrm{start}}(c,a,\epsilon)$ of $\mathcal{Y}(c,a,\epsilon)$ with the section Σ^m is shown in Figure 17. Except for an exponentially thin region around $\mathcal{M}^{m,c}_\epsilon(c,a)$, this curve coincides with $\mathcal{Z}_\epsilon(c,a)$ due to the invariance of the manifold $\mathcal{Z}_\epsilon(c,a)$. However, due to the rotational behavior of $\mathcal{M}^m_\epsilon(c,a)$ near and above the Airy point, this curve must at some point deviate from $z = 0$ and "spiral" around $\mathcal{M}^m_\epsilon(c,a)$, eventually losing transversality with respect to the strong unstable fibers $y_2 = \text{const}$.

The intersection $\mathcal{Y}_{\mathrm{end}}(c,a,\epsilon)$ of $\mathcal{Z}_\epsilon(c,a)$ with $\Sigma^{h,\ell}$ can most naturally be parametrized by the height w. When evolved backwards to Σ^m, this height corresponds with the time spent near the manifold $\mathcal{M}^m_\epsilon(c,a)$ and hence also the corresponding amount of contraction in backwards time. Therefore, the expectation is that points on $\mathcal{Y}_{\mathrm{end}}(c,a,\epsilon)$ with larger w-values, when evolved backwards to Σ^m, will land "deeper" in the spiral formed by the curve $\mathcal{Y}_{\mathrm{start}}(c,a,\epsilon)$; from this, one expects that there is a maximum height $w = w^{\pitchfork}$ for which the trajectory in $\Sigma^{h,\ell}$ on $\mathcal{Y}_{\mathrm{end}}(c,a,\epsilon)$ at $w \leq w^{\pitchfork}$ lands on the part of the curve $\mathcal{Y}_{\mathrm{start}}(c,a,\epsilon)$ which is transverse to the strong unstable fibers y_2=const.

In the following proposition, these ideas are made precise, and we identify a portion $\mathcal{Y}^{\pitchfork}_{\mathrm{end}}(c,a,\epsilon)$ of the manifold $\mathcal{Y}_{\mathrm{end}}(c,a,\epsilon)$ in $\Sigma^{h,\ell}$, which when evolved backwards to Σ^m, lands on the part of the curve $\mathcal{Y}_{\mathrm{start}}(c,a,\epsilon)$ which is transverse to the strong unstable fibers.

Proposition 4.5. *For each sufficiently small $\Delta_w > 0$, there exists $C, \kappa, \epsilon_0, q > 0$ and sufficiently small intervals I_c, I_a such that for each $(c,a,\epsilon) \in I_c \times I_a \times (0,\epsilon_0)$, there exists $w^\Delta_\epsilon(c,a) \in [w_A - 3\Delta_w, w_A - \Delta_w]$ and $w^{\pitchfork}_\epsilon(c,a) >$*

$w_A+\kappa\epsilon^{2/3}$ such that the following holds. Let $\mathcal{Y}^{\pitchfork}_{\text{end}}(c,a,\epsilon)$ denote the portion of $\mathcal{Y}_{\text{end}}(c,a,\epsilon)$ in $\Sigma^{h,\ell}$ between $w^{\Delta}_{\epsilon} \leq w \leq w^{\pitchfork}_{\epsilon}$ and let $\mathcal{Y}^{\pitchfork}(c,a,\epsilon) \subset \mathcal{Y}(c,a,\epsilon)$ denote the two-dimensional manifold traced out by the backward evolution of $\mathcal{Y}^{\pitchfork}_{\text{end}}(c,a,\epsilon)$. Evolved backwards to Σ^m, $\mathcal{Y}^{\pitchfork}(c,a,\epsilon)$ intersects Σ^m in a one-dimensional curve $\mathcal{Y}^{\pitchfork}_{\text{start}}(c,a,\epsilon)$ which can be represented as a graph $z = z^{\mathcal{Y}}(y_2;c,a)$ for $y_2^{\mathcal{T}}(c,a) \leq y_2 \leq y_2^{\Sigma}(c,a)$ where

(i) The interval $[y_2^{\mathcal{T}}(c,a), y_2^{\Sigma}(c,a)]$ satisfies $0 < y_2^{\Sigma}(c,a) - y_2^{\mathcal{T}}(c,a) < Ce^{-q/\epsilon}$ uniformly in $(c,a) \in I_c \times I_a$.

(ii) There exists $y_2^{\mathcal{Z}}(c,a) \in [y_2^{\mathcal{T}}(c,a), y_2^{\Sigma}(c,a)]$ such that $\mathcal{Y}_{\text{start}}(c,a,\epsilon) \subset \mathcal{Z}_{\epsilon}(c,a) \cap \Sigma^m$ for $y_2 \in [y_2^{\mathcal{Z}}(c,a), y_2^{\Sigma}(c,a)]$.

(iii) The function $z^{\mathcal{Y}}(y_2;c,a)$ and its derivatives are $\mathcal{O}(e^{-q/\epsilon})$ uniformly in $y_2 \in [y_2^{\mathcal{T}}(c,a), y_2^{\Sigma}(c,a)]$ and $(c,a) \in I_c \times I_a$.

Hence we have that the two-dimensional manifold $\mathcal{Y}^{\pitchfork}(c,a,\epsilon)$ intersects Σ^m in a curve $\mathcal{Y}^{\pitchfork}_{\text{start}}(c,a,\epsilon)$ which can be represented as a graph $z = z^{\mathcal{Y}}(y_2;c,a)$ for $y_2 \geq y_2^{\mathcal{T}}(c,a)$ where the function $z^{\mathcal{Y}}$ and its derivatives are $\mathcal{O}(e^{-q/\epsilon})$. The proof of this proposition will be given in §5.6.

We recall that $\mathcal{Z}_{\epsilon}(c,a)$ is C^1 exponentially close to $\mathcal{W}^{c,\ell}_{\epsilon}(c,a)$ and hence $\mathcal{Z}_{\epsilon}(c,a)$ intersects Σ^m in the graph of a C^1-function $z = z^{\Sigma}(y_2;c,a) = \mathcal{O}(e^{-q/\epsilon})$ for $|r_2^2 y_2| < \Delta_y$. Hence by Proposition 4.5 and the invariance properties of the manifold $\mathcal{Z}_{\epsilon}(c,a)$,we may now determine all trajectories starting in Σ^m which meet $\mathcal{Z}_{\epsilon}(c,a)$ in $\Sigma^{h,\ell}$ with $w \leq w^{\pitchfork}_{\epsilon}$. We define $\mathcal{T}_{\epsilon}(c,a)$ to be the curve in Σ^m defined by the graph of the smooth function $z = z^{\mathcal{T}}_{\epsilon}(y_2;c,a)$ for $y_2 \geq y_2^{\mathcal{T}}(c,a)$ where

$$z^{\mathcal{T}}_{\epsilon}(y_2;c,a) := \begin{cases} z^{\Sigma}(y_2;c,a) & y_2^{\Sigma}(c,a) \leq y_2 \\ z^{\mathcal{Y}}(y_2;c,a) & y_2^{\mathcal{T}}(c,a) \leq y_2 \leq y_2^{\Sigma}(c,a), \end{cases} \qquad z^{\mathcal{T}}_{\epsilon}(y_2;c,a) = \mathcal{O}(e^{-q/\epsilon}). \tag{4.26}$$

The curve $\mathcal{T}_{\epsilon}(c,a)$ in the section Σ^m is shown in Figure 17. By Proposition 4.5 combined with the invariance of the manifold $\mathcal{Z}_{\epsilon}(c,a)$, the forward evolution of trajectories on $\mathcal{T}_{\epsilon}(c,a)$ will meet $\mathcal{Z}_{\epsilon}(c,a)$ in either $\{u = 0, 0 < w \leq \Delta_w\}$ or in $\Sigma^{h,\ell}$ with $w \leq w^{\pitchfork}_{\epsilon}$ where $w^{\pitchfork}_{\epsilon} = w_A + \mathcal{O}(\epsilon^{2/3}) < w_R(\Delta_w)$. Therefore in light of Proposition 3.10, in the presence of a suitable canard trajectory $\gamma^{\diamond}_{\epsilon}$ on $\mathcal{Z}_{\epsilon}(c,a)$, any trajectory which meets Σ^m on the curve $\mathcal{T}_{\epsilon}(c,a)$ in fact lies on the stable manifold $\mathcal{W}^s_{\epsilon}(0;c,a)$ of the equilibrium $(u,v,w) = (0,0,0)$.

Thus in order to construct pulses of type $2-6$, we impose two matching conditions in Σ^m: the first matches the unstable manifold $\mathcal{W}^u_{\epsilon}(0;c,a)$ with a solution which completes a secondary excursion and returns to Σ^m, and the second matches this secondary excursion with the curve $\mathcal{T}_{\epsilon}(c,a)$.

Remark 4.6. *We recall from Proposition 3.10 that (under certain conditions) solutions which meet $\mathcal{Z}_{\epsilon}(c,a)$ in the set $\{u = 0, 0 < w \leq \Delta_w\}$ or in the section $\Sigma^{h,\ell} \cap \{w < w_R(\Delta_w)\}$ in fact lie on the stable manifold $\mathcal{W}^s_{\epsilon}(0;c,a)$. With the definitions above, when evolved back to the section Σ^m, these trajectories will be contained in the union of the curves $\mathcal{T}_{\epsilon}(c,a)$ and $\mathcal{Y}_{\text{start}}(c,a,\epsilon)$. Hence a portion of the spiraling curve in Figure 17 consists of solutions on the stable manifold $\mathcal{W}^s_{\epsilon}(0;c,a)$, on which any homoclinic orbits must lie.*

As stated above, the strategy for constructing pulses consists of two matching conditions. The first matches $\mathcal{W}^u_{\epsilon}(0;c,a)$ in Σ^m with a secondary excursion; this secondary excursion will in fact meet $\Sigma^{h,\ell}$ exponentially close to the manifold $\mathcal{Z}_{\epsilon}(c,a)$. The second condition then matches this secondary excursion with $\mathcal{T}_{\epsilon}(c,a)$, which we noted in the previous paragraph consists of solutions on $\mathcal{W}^s_{\epsilon}(0;c,a)$, due to Proposition 3.10.

Therefore, for the first matching condition, the first intersection of the manifold $\mathcal{W}^u_{\epsilon}(0;c,a)$ with Σ^m must occur at some point near the spiral $\mathcal{T}_{\epsilon}(c,a) \cup \mathcal{Y}_{\text{start}}(c,a,\epsilon)$ (see Figure 17), and the matching for pulses further along in the 1-to-2-pulse transition (i.e. with larger s) occurs deeper in the spiral. We recall that $\mathcal{W}^u_{\epsilon}(0;c,a)$ enters Σ^m exponentially close to $\mathcal{M}^{\ell}_{\epsilon}(c,a)$, and due to Proposition 4.1, the parameter $\alpha_2 \sim a/\epsilon^{1/2}$ determines the splitting of the manifolds $\mathcal{M}^{\ell}_{\epsilon}(c,a), \mathcal{M}^{m,c}_{\epsilon}(c,a)$ to leading order. Thus, as the 1-to-2-pulse transition progresses, the parameter a must wiggle back and forth near the maximal canard value (see Theorem 2.6) to accommodate the first matching condition. This explains the folds observed along the transition in Figure 2b. Further, since

solutions are contracted exponentially in backwards time towards $\mathcal{M}_\epsilon^{m,c}(c,a)$, the spiral formed by $\mathcal{Y}_{\text{start}}(c,a,\epsilon)$ is exponentially small and hence the parameter a varies by $\mathcal{O}(e^{-q/\epsilon})$ along the transition, which explains why the folds are not visible in Figure 4a, which was obtained for a smaller value of ϵ.

Therefore, the first fold, and hence the first turning point along the transition, occurs when the parameter a approaches the value at which the strong unstable fiber of $\mathcal{M}_\epsilon^\ell(c,a)$ becomes tangent to the 'bottom' of the spiral in Σ^m, since beyond this point (up to some exponentially small quantities) it is no longer possible to match $\mathcal{W}_\epsilon^u(0;c,a)$ with a secondary excursion; thus the curve turns back, and we see the first fold. As stated above, this portion of the spiral contains solutions on the stable manifold $\mathcal{W}_\epsilon^s(0;c,a)$. This explains why the authors of [13] observe numerically that this first turning point occurs near a tangency of $\mathcal{W}_\epsilon^s(0;c,a)$ and the unstable manifold $\mathcal{W}_\epsilon^{u,\ell}(c,a)$ of $\mathcal{M}_\epsilon^\ell(c,a)$.

4.4 Type 2 pulses

To construct a left transitional pulse with secondary excursion of height $s \in (w_R(\Delta_w), w^\dagger - \Delta_w)$, we consider a one-parameter family (to be chosen below) of candidate secondary pulses which start in Σ^m and return to Σ^m after completing an excursion of height (approximately) $w = s$; this family thus forms a two-dimensional manifold $\mathcal{B}(s;c,a)$ which meets Σ^m in two curves, namely initially at $\mathcal{B}_{\text{start}}(s;c,a)$ and then at $\mathcal{B}_{\text{end}}(s;c,a)$ after the excursion. Further, the manifold $\mathcal{B}(s;c,a)$ can be chosen so that the curves $\mathcal{B}_{\text{end}}(s;c,a)$ and $\mathcal{T}_\epsilon(c,a)$ intersect transversely in Σ^m.

The idea is now to show that $\mathcal{W}_\epsilon^u(0;c,a)$ can be matched in Σ^m with any solution on the curve $\mathcal{B}_{\text{start}}(s;c,a)$ by choosing (c,a) appropriately, and consequently $\mathcal{W}_\epsilon^u(0;c,a)$ can be chosen to return to Σ^m at any desired point on the curve $\mathcal{B}_{\text{end}}(s;c,a)$. Since $\mathcal{B}_{\text{end}}(s;c,a)$ and $\mathcal{T}_\epsilon(c,a)$ intersect transversely in Σ^m, exactly one of these choices is guaranteed to lie on the stable manifold $\mathcal{W}_\epsilon^s(0;c,a)$ due to Proposition 3.10. The setup is shown in Figure 18.

Therefore, to construct a transitional pulse we need two matching conditions near the equilibrium: the first matches $\mathcal{W}_\epsilon^u(0;c,a)$ with $\mathcal{B}_{\text{start}}(s;c,a)$ to guarantee height s for the second excursion, and the second matches $\mathcal{B}_{\text{end}}(s;c,a)$ with $\mathcal{T}_\epsilon(c,a)$. The local geometry for the matching conditions is shown in Figure 19. The setup for the matching conditions in the section Σ^m is shown in Figure 17.

4.4.1 Matching conditions for pulses $\Gamma(s,\sqrt{\epsilon})$, $s \in (w_R(\Delta_w), w^\dagger - \Delta_w)$

We match the various components of the solution in the section Σ^m in the $\mathcal{K}_2$ coordinates. From Lemma 4.3, for each $|z| < \Delta_z$, there exists c with $|c - \check{c}(a,\epsilon)| = \mathcal{O}(e^{-q/\epsilon})$ such that $\mathcal{W}_\epsilon^u(0;c,a)$ intersects Σ^m at the point $(y_2^u(z;c,a), z)$ where

$$\begin{aligned} e^{-q_1/\epsilon}/C \le y_2^u(0;c,a) - y_2^{\mathcal{M},\ell} \le Ce^{-q_2/\epsilon} \\ |y_2^u(z;c,a) - y_2^u(0;c,a)| = \mathcal{O}(ze^{-q/\epsilon}), \end{aligned} \tag{4.27}$$

for some $q_1 > q_2 > 0$.

Consider the solution $\gamma^{\text{se}}(s;c,a)$ on the manifold $\mathcal{W}_\epsilon^{c,\ell}(c,a)$ which intersects the section $\Sigma^{h,\ell}$ at height $w = s$. This intersection occurs at a point $(u,v,w) = (0, v^{\text{se}}(s;c,a), s)$. This solution is exponentially attracted in forward time to $\mathcal{M}_\epsilon^\ell(c,a)$ and hence intersects Σ^m at the point $\gamma_{\text{end}}^{\text{se}}(s;c,a) = (0, y_2^{\text{se}}(s;c,a), 0)$ where

$$\frac{1}{C}e^{-q_1/\epsilon} \le y_2^{\text{se}}(s;c,a) - y_2^u(0;c,a) \le Ce^{-q_2/\epsilon}. \tag{4.28}$$

The geometry of the setup for type 2 pulses and the solution $\gamma^{\text{se}}(s;c,a)$ is shown in Figure 18.

In Σ^m, we now consider the one-dimensional fiber associated with the basepoint $\gamma_{\text{end}}^{\text{se}}(s;c,a)$

$$\{(0, y_2^{\text{se}}(s;c,a), z) : |z| \le \Delta_z\} \subseteq \Sigma^m. \tag{4.29}$$

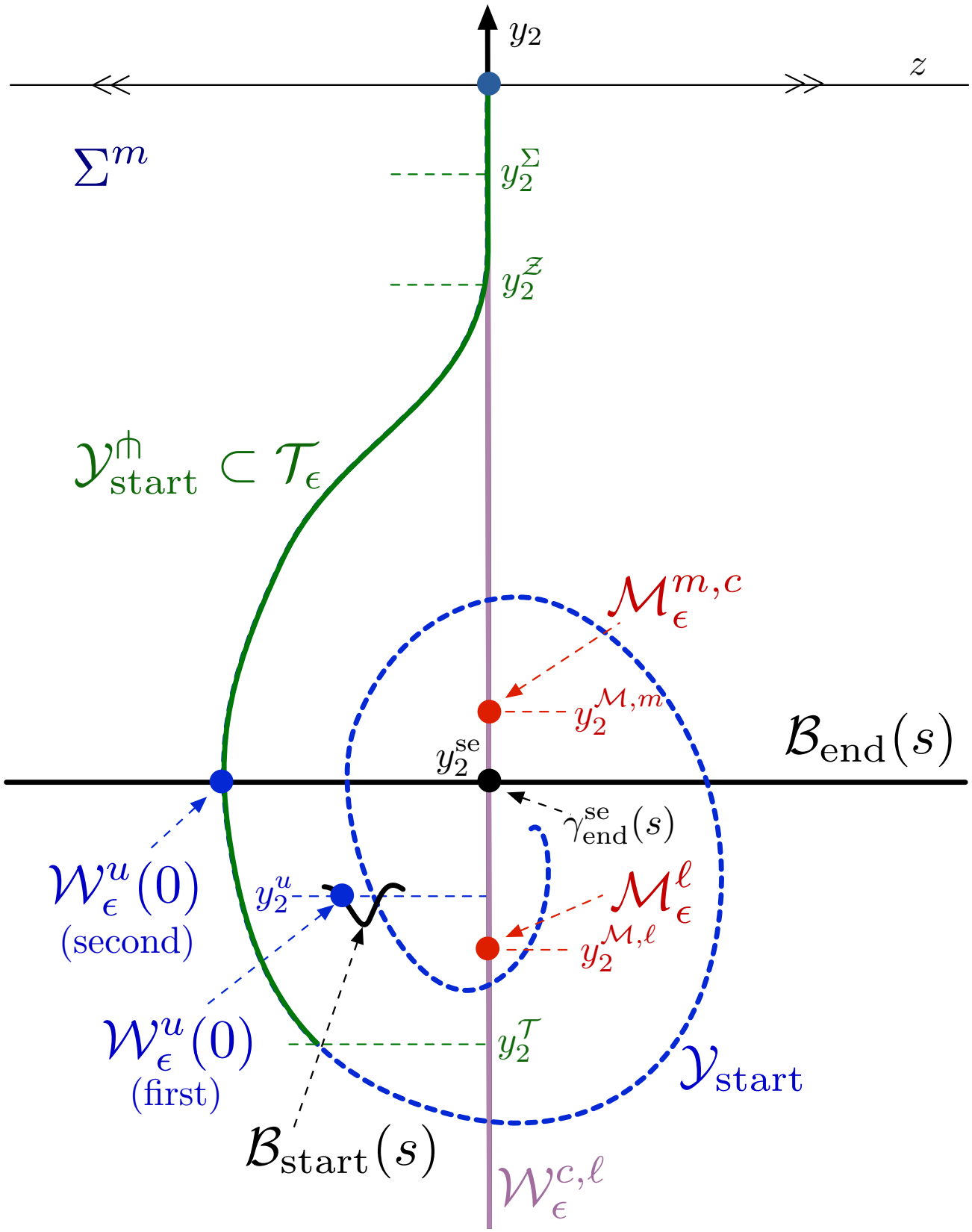

Figure 17: *Shown is the setup for the matching conditions in the section Σ^m. The "first/second" labels for the unstable manifold $\mathcal{W}_\epsilon^u(0;c,a)$ refer to the first and second intersections of $\mathcal{W}_\epsilon^u(0;c,a)$ with Σ^m after completing the primary and secondary excursions, respectively. There are two matching conditions: (i) match $\mathcal{W}_\epsilon^u(0;c,a)$ (first) with $\mathcal{B}_{\text{start}}(s;c,a)$, and (ii) match $\mathcal{B}_{\text{end}}(s;c,a)$ with $\mathcal{T}_\epsilon(c,a)$.*

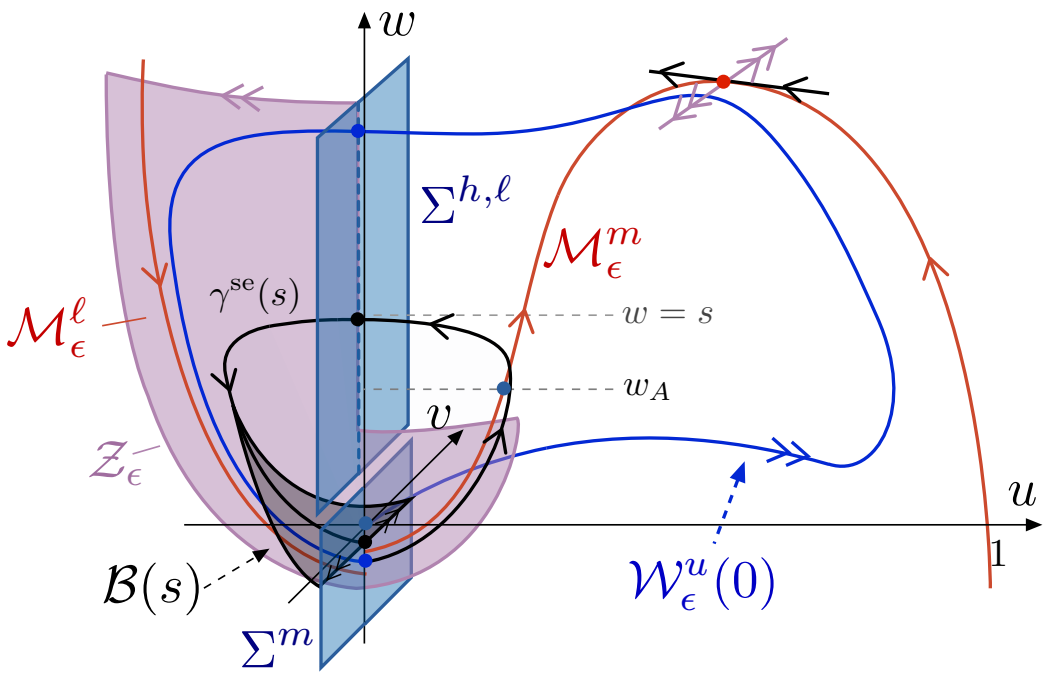

Figure 18: *Shown is the geometry for constructing a type 2 left transitional pulse.*

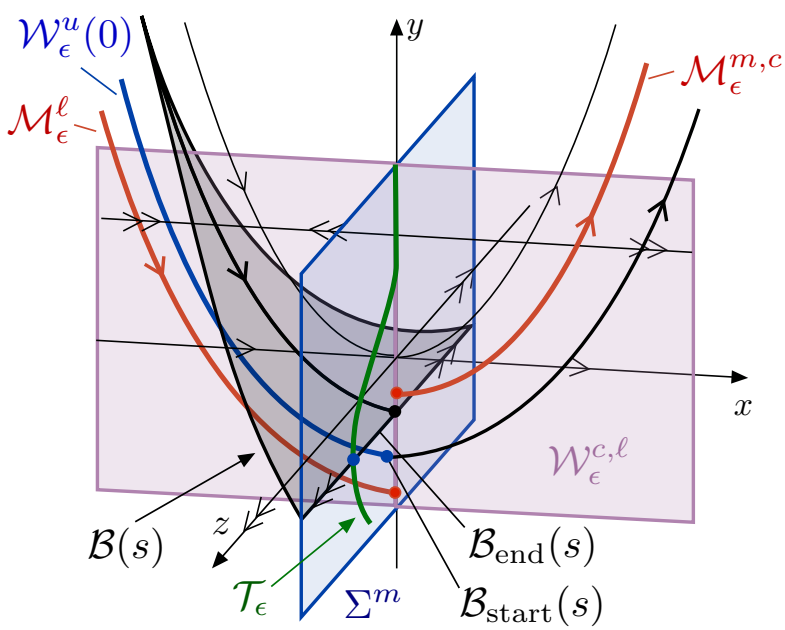

Figure 19: *Shown is the setup for the matching conditions in the section Σ^m. The curves $\mathcal{B}_{\mathrm{start}}(s;c,a)$ and $\mathcal{B}_{\mathrm{end}}(s;c,a)$ denote the first and second intersections, respectively, of the two-dimensional manifold $\mathcal{B}(s;c,a)$ with the section Σ^m. Note that due to the exponential contraction in backwards time, the curve $\mathcal{B}_{\mathrm{start}}(s;c,a)$ consists of points which are exponentially close together. In order to construct a pulse, there are two matching conditions to be satisfied: (i) match $\mathcal{W}_\epsilon^u(0;c,a)$ with $\mathcal{B}_{\mathrm{start}}(s;c,a)$, and (ii) match $\mathcal{B}_{\mathrm{end}}(s;c,a)$ with $\mathcal{T}_\epsilon(c,a)$.*

which we denote by $\mathcal{B}_{\text{end}}(s;c,a)$. We then define the two-dimensional manifold $\mathcal{B}(s;c,a)$ to be the backwards evolution of the one-dimensional curve $\mathcal{B}_{\text{end}}(s;c,a)$. We can parameterize trajectories on $\mathcal{B}(s;c,a)$ by $|z_{\text{end}}| \leq \Delta_z$, where z_{end} denotes the eventual z-value along the fiber $\mathcal{B}_{\text{end}}(s;c,a)$. In backwards time, this fiber is exponentially contracted to the solution $\gamma^{\text{se}}(s;c,a)$ and hence the manifold $\mathcal{B}(s;c,a)$ intersects $\Sigma^{h,\ell}$ in a one-dimensional curve which is $\mathcal{O}(e^{-q/\epsilon})$-close to $(u,v,w) = (0, v^{\text{se}}(s;c,a), s)$, uniformly in (c,a). A schematic of the manifold $\mathcal{B}(s;c,a)$ and its relation to $\gamma^{\text{se}}(s;c,a)$ is shown in Figure 18.

The final matching conditions are obtained as follows: Starting in $\Sigma^{h,\ell}$, we consider the backwards evolution of $\mathcal{B}(s;c,a)$ back to the section Σ^m where it intersects in a curve $\mathcal{B}_{\text{start}}(s;c,a)$ parameterized by $|z_{\text{end}}| \leq \Delta_z$; we then show that for each $|z_{\text{end}}| \leq \Delta_z$, $\mathcal{W}^u_\epsilon(0;c,a)$ can be matched with the corresponding point on $\mathcal{B}_{\text{start}}(s;c,a)$ by adjusting (c,a). We then recall that by construction, the forwards evolution of initial conditions on $\mathcal{B}_{\text{start}}(s;c,a)$ intersect Σ^m again, this time on the curve $\mathcal{B}_{\text{end}}(s;c,a)$. We then show that $\mathcal{B}_{\text{end}}(s;c,a)$ transversely intersects $\mathcal{T}_\epsilon(c,a)$ for each such (c,a) as z_{end} varies. This implies the existence of parameter values (c,a) for which $\mathcal{W}^u_\epsilon(0;c,a)$ completes one full pulse and a secondary pulse of height s before reaching $\mathcal{T}_\epsilon(c,a)$. We then verify the conditions of Proposition 3.10 to ensure that this solution lies in the stable manifold $\mathcal{W}^s_\epsilon(0;c,a)$. The setup for the matching conditions is shown in Figures 17 and 19.

Starting with the fiber $\mathcal{B}_{\text{end}}(s;c,a)$ and evolving backwards, we have that the two-dimensional manifold $\mathcal{B}(s;c,a)$ is exponentially contracted to $\mathcal{M}^m_\epsilon(c,a)$ by the time it reaches Σ^m (and hence is exponentially close to $\mathcal{M}^{m,c}_\epsilon(c,a)$ also). Thus we have that in Σ^m, $\mathcal{B}_{\text{start}}(s;c,a)$ is given by a curve $(y_2,z) = (y_2^b, z^b)(z_{\text{end}}, s; c, a)$ which satisfies

$$\begin{aligned} |y_2^b(z_{\text{end}}, s; c, a) - y_2^{\mathcal{M},m}| &= \mathcal{O}(e^{-q/\epsilon}) \\ |z^b(z_{\text{end}}, s; c, a)| &= \mathcal{O}(e^{-q/\epsilon}), \end{aligned} \tag{4.30}$$

uniformly in $|z_{\text{end}}| \leq \Delta_z$ and $(c,a) \in I_c \times I_a$. The derivatives of the above expressions with respect to (c,a,z_{end}) are also $\mathcal{O}(e^{-q/\epsilon})$, by taking q a bit smaller if necessary.

We showed in (4.26) that, in the section Σ^m, the curve $\mathcal{T}_\epsilon(c,a)$ is defined by the graph of a smooth function $z = z^{\mathcal{T}}_\epsilon(y_2;c,a)$ for $y_2 \geq y_2^{\mathcal{T}}(c,a)$ which is $\mathcal{O}(e^{-q/\epsilon})$ along with its derivatives. We have the following.

Lemma 4.7. *For each sufficiently small $\Delta_w > 0$, there exists $\epsilon_0, \Delta_z, q > 0$ and sufficiently small choice of the intervals I_c, I_a such that for each $s \in (w_R(\Delta_w), w^\dagger - \Delta_w)$ and each $0 < \epsilon < \epsilon_0$, the following hold. Firstly, the backwards evolution of the manifold $\mathcal{B}(s;c,a)$ intersects Σ^m in a curve $\mathcal{B}_{\text{start}}(s;c,a) = \{(y_2,z) = (y_2^b, z^b)(z_{\text{end}}, s; c, a); |z_{\text{end}}| \leq \Delta_z\}$ where*

$$\begin{aligned} |y_2^b(z_{\text{end}}, s; c, a) - y_2^{\mathcal{M},m}| &= \mathcal{O}(e^{-q/\epsilon}) \\ |z^b(z_{\text{end}}, s; c, a)| &= \mathcal{O}(e^{-q/\epsilon}), \end{aligned} \tag{4.31}$$

uniformly in $|z_{\text{end}}| \leq \Delta_z$ and $(c,a) \in I_c \times I_a$; the derivatives of the above expressions with respect to (c,a,z_{end}) are also $\mathcal{O}(e^{-q/\epsilon})$. Secondly,

$$y_2^{\mathcal{T}}(c,a) < \inf_{|z_{\text{end}}| \leq \Delta_z} y_2^b(z_{\text{end}}, s; c, a), \tag{4.32}$$

for all $(c,a) \in I_c \times I_a$.

The first assertion of Lemma 4.7 follows from the analysis above; the proof of the second assertion will be given in §5.6.

From Proposition 4.1, we have that the distance between the manifolds $\mathcal{M}^\ell_\epsilon(c,a)$ and $\mathcal{M}^{m,c}_\epsilon(c,a)$ in Σ^m is given by

$$y_2^{\mathcal{M},\ell} - y_2^{\mathcal{M},m} = \mathcal{D}_0(\alpha_2, r_2; c) = d_{\alpha_2}\alpha_2 + d_{r_2} r_2 + \mathcal{O}(2) \ . \tag{4.33}$$

Using Lemma 4.3 and Proposition 4.1, by varying c, α_2 we can match $\mathcal{W}^u_\epsilon(0;c,a)$ with any solution in $\mathcal{B}_{\text{start}}(s;c,a)$ by solving

$$\begin{aligned} \mathcal{D}_0(\alpha_2, r_2; c) &= \left(y_2^{\mathcal{M},\ell} - y_2^u(z;c,a)\right) + \left(y_2^b(z_{\text{end}}, s; c, a) - y_2^{\mathcal{M},m}\right) = \mathcal{O}(e^{-q/\epsilon}) \\ z &= z^b(z_{\text{end}}, s; c, a), \end{aligned} \tag{4.34}$$

for each $|z_{\text{end}}| \leq \Delta_z$. For each such z_{end}, we obtain a solution by solving

$$\begin{aligned} a &= 2c^{1/2}\epsilon^{1/2}(\alpha_2^C + \mathcal{O}(e^{-q/\epsilon})) \\ c &= \check{c}(a,\epsilon) + \mathcal{O}(e^{-q/\epsilon}), \end{aligned} \tag{4.35}$$

by the implicit function theorem to find $(a,c) = (a^u, c^u)(z_{\text{end}}; s, \sqrt{\epsilon})$ where we have

$$(c^u, a^u)(z_{\text{end}}; s, \sqrt{\epsilon}) = (c_E, a_E)(\sqrt{\epsilon}) + \mathcal{O}(e^{-q/\epsilon}), \tag{4.36}$$

uniformly in (z_{end}, s), where (c_E, a_E) is the unique solution of (4.14) (see §4.2.1).

We now evolve $\mathcal{W}^u_\epsilon(0;c,a)$ forwards; for each z_{end} we can ensure that $\mathcal{W}^u_\epsilon(0;c,a)$ reaches the corresponding point on the fiber $\mathcal{B}_{\text{end}}(s;c,a)$ on the subsequent return to Σ^m by adjusting (c,a); hence $\mathcal{W}^u_\epsilon(0;c,a)$ intersects Σ^m at the point $(y_2^{\text{se}}(s;c,a), z_{\text{end}})$ when $(c,a) = (c^u, a^u)(z_{\text{end}})$ defined above. We now match with the curve $\mathcal{T}_\epsilon(c,a)$ by solving

$$z_{\text{end}} = z_\epsilon^{\mathcal{T}}(y_2^{\text{se}}(s;c,a); c^u(z_{\text{end}}), a^u(z_{\text{end}})), \tag{4.37}$$

which, using (4.26) and Lemma 4.7, we can solve by the implicit function theorem for $z_{\text{end}} = z^s_{\text{end}} = \mathcal{O}(e^{-q/\epsilon})$ to find the desired solution at

$$\begin{aligned} a &= a(s, \sqrt{\epsilon}) := a^u(z^s_{\text{end}}; s, \sqrt{\epsilon}) \\ c &= c(s, \sqrt{\epsilon}) := c^u(z^s_{\text{end}}; s, \sqrt{\epsilon}). \end{aligned} \tag{4.38}$$

4.4.2 Convergence of tails

Finally, to ensure that this solution lies in $\mathcal{W}^s_\epsilon(0;c,a)$, we verify the assumptions of Proposition 3.10. Every solution which meets Σ^m on the curve $\mathcal{T}_\epsilon(c,a)$ lies on the stable manifold $\mathcal{W}^s_\epsilon(0;c,a)$ provided there exists a canard trajectory $\gamma^\diamond_\epsilon$ satisfying the conditions of Proposition 3.10. By construction, the solution $\gamma^{\text{se}}(s;c,a)$ shadows a canard trajectory lying on $\mathcal{Z}_\epsilon(c,a)$ which satisfies these conditions.

4.5 Type 4 & 5 pulses

In this section we consider pulses of type 4 & 5; type 3 pulses will be considered in §4.6. Type 4 & 5 pulses correspond to $\Gamma(s)$ for $s \in (w^\dagger + \Delta_w, 2w^\dagger - \Delta_w)$. Type 4 pulses are right transitional pulses with a secondary pulse of heights $w \in (w_A + \Delta_w, w^\dagger - \Delta_w)$, and type 5 pulses are right transitional pulses with a secondary pulse of height $w \in (\Delta_w, w_A + \Delta_w)$. For type 4 & 5 pulses, the secondary pulses pass close to the upper right fold point. These pulses are constructed in much the same way as type 2 pulses, except with a different definition of the solution $\gamma^{\text{se}}(s;c,a)$ and the associated manifold $\mathcal{B}(s;c,a)$. In terms of the actual construction of the pulses, there is no distinction between pulses of type 4 and 5. We distinguish these pulses, however, due to the technical difficulties associated with proving Lemma 4.9 below for the case of type 5 pulses, which is crucial to solving the final matching conditions.

To construct a right transitional pulse with secondary height $w = 2w^\dagger - s$, we first consider the plane $w = 2w^\dagger - s$ which intersects the section $\Sigma^{h,r} := \{u = 2/3, \Delta_w < w < w^\dagger - \Delta_w\}$ in a line $\{u = 2/3, w = 2w^\dagger - s\}$. This line transversely intersects the manifold $\mathcal{W}^{s,r}_\epsilon(c,a)$ for all $(c,a) \in I_c \times I_a$. Using arguments similar to those in [5, §5]

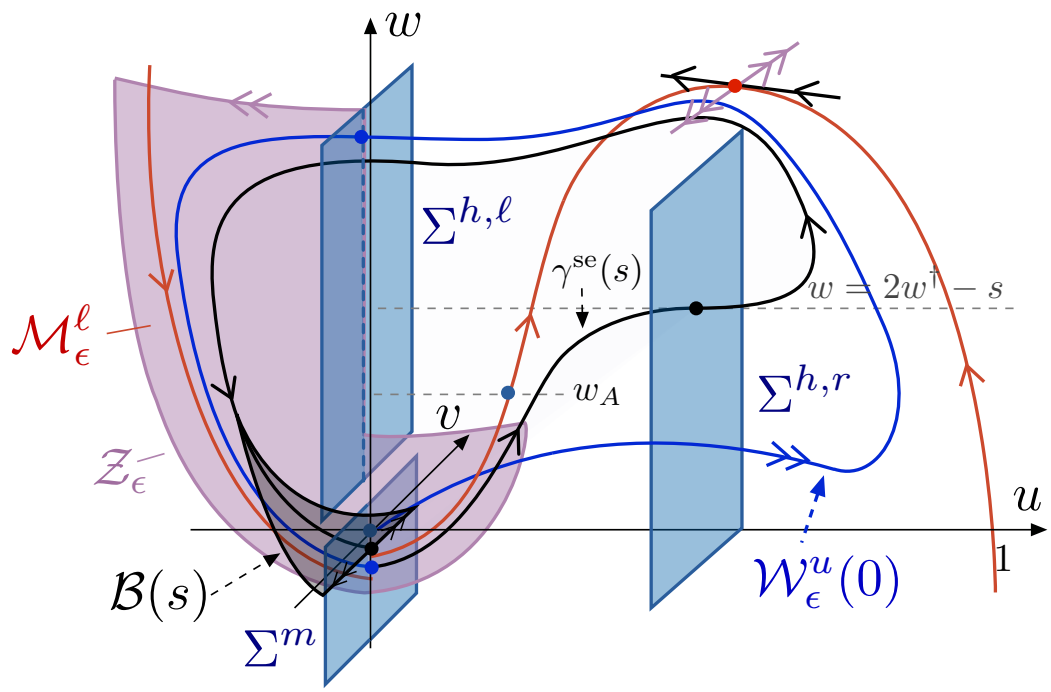

Figure 20: *Shown is the geometry for constructing a type 4 right transitional pulse.*

in the proof of Proposition 2.7, it follows that the forward evolution of this line transversely intersects $\mathcal{W}_{\epsilon}^{s,\ell}(c,a)$ for each $(c,a) \in I_c \times I_a$ and each sufficiently small $\epsilon > 0$ along a trajectory $\gamma^{\mathrm{se}}(s;c,a)$. Furthermore, the solution $\gamma^{\mathrm{se}}(s;c,a)$ is exponentially close to $\mathcal{W}_{\epsilon}^{s,r}(c,a)$ in $\Sigma^{h,r}$ and passes $\mathcal{O}(\epsilon^{2/3} + |a|)$ close to the fold before intersecting $\mathcal{W}_{\epsilon}^{s,\ell}(c,a)$.

The geometry of the setup for type 4 pulses and the solution $\gamma^{\mathrm{se}}(s;c,a)$ is shown in Figure 20.

Proceeding as with type 2 pulses, we follow $\gamma^{\mathrm{se}}(s;c,a)$ along $\mathcal{W}_{\epsilon}^{c,\ell}(c,a)$ where it is exponentially contracted to $\mathcal{M}_{\epsilon}^{\ell}(c,a)$ and intersects the section Σ^m at a point $\gamma_{\mathrm{end}}^{\mathrm{se}}(s;c,a) = (0, y_2^{\mathrm{se}}(s;c,a), 0)$. We again define the two-dimensional manifold $\mathcal{B}(s;c,a)$ to be the backwards evolution of the one-dimensional fiber $\mathcal{B}_{\mathrm{end}}(s;c,a) := \{(0, y_2^{\mathrm{se}}(s;c,a), z) : |z| \leq \Delta_z\}$ in the section Σ^m. We parametrize the trajectories on $\mathcal{B}(s;c,a)$ by $\{z_{\mathrm{end}}, |z_{\mathrm{end}}| \leq \Delta_z\}$ corresponding to the eventual z-value reached along the fiber $\mathcal{B}_{\mathrm{end}}(s;c,a)$ in Σ^m. Assuming this manifold is well defined and exponentially close to $\gamma^{\mathrm{se}}(s;c,a)$ in $\Sigma^{h,r}$ (and the derivatives of the transition maps with respect to (c,a,z_{end}) are also exponentially small), the remainder of the construction is similar to the case of type 2 pulses. A schematic of the manifold $\mathcal{B}(s;c,a)$ and its relation to $\gamma^{\mathrm{se}}(s;c,a)$ is shown in Figure 20.

The fact that $\mathcal{B}(s;c,a)$ is exponentially close to $\gamma^{\mathrm{se}}(s;c,a)$ in $\Sigma^{h,r}$ is due to the following lemma, proved in Appendix D.

Lemma 4.8. *For each sufficiently small Δ_w, there exists $\epsilon_0, q > 0$ and sufficiently small choice of the intervals I_c, I_a, such that for each $0 < \epsilon < \epsilon_0$, each $(c,a) \in I_c \times I_a$, and each $s \in (w^{\dagger} + \Delta_w, 2w^{\dagger} - \Delta_w)$, the following holds. The backwards evolution of the fiber $\mathcal{B}_{\mathrm{end}}(s;c,a)$ traces out a two-dimensional manifold $\mathcal{B}(s;c,a)$ which meets $\Sigma^{h,r}$ in a curve defined by*

$$(u,v,w) = \left(2/3, v^{\mathrm{se}}(s;c,a), 2w^{\dagger} - s\right) + \left(0, v_B(z_{\mathrm{end}}, s; c, a), w_B(z_{\mathrm{end}}, s; c, a)\right), \tag{4.39}$$

where

$$|v_B(z_{\mathrm{end}}, s; c, a)|, |w_B(z_{\mathrm{end}}, s; c, a)| = \mathcal{O}(e^{-q/\epsilon}), \tag{4.40}$$

along with their derivatives with respect to (z_{end}, c, a) uniformly in $|z_{\mathrm{end}}| \leq \Delta_z$ and $(c,a) \in I_c \times I_a$.

4.5.1 Matching conditions for pulses $\Gamma(s,\sqrt{\epsilon})$, $s \in (w^\dagger + \Delta_w, 2w^\dagger - \Delta_w)$

Evolving $\mathcal{B}(s;c,a)$ backwards and using Lemma 4.8, we have that the backwards evolution of $\mathcal{B}(s;c,a)$ intersects Σ^m in a curve $\mathcal{B}_{\text{start}}(s;c,a)$ which is exponentially close to $\mathcal{M}_\epsilon^m(c,a)$ (and hence also exponentially close to $\mathcal{M}_\epsilon^{m,c}(c,a)$). Thus we have that in Σ^m, $\mathcal{B}_{\text{start}}(s;c,a) = \{(0,y_2,z) = (y_2^b,z^b)(z_{\text{end}},s;c,a); |z_{\text{end}}| \le \Delta_z\}$ where

$$\begin{aligned} |y_2^b(z_{\text{end}},s;c,a) - y_2^{\mathcal{M},m}| &= \mathcal{O}(e^{-q/\epsilon}) \\ |z^b(z_{\text{end}},s;c,a)| &= \mathcal{O}(e^{-q/\epsilon}), \end{aligned} \tag{4.41}$$

uniformly in $|z_{\text{end}}| \le \Delta_z$.

We had shown in (4.26) that the curve $\mathcal{T}_\epsilon(c,a) \subset \Sigma^m$ is defined by the graph of a smooth function given by $z = z_\epsilon^{\mathcal{T}}(y_2;c,a)$ for $y_2 \ge y_2^{\mathcal{T}}(c,a)$ which is $\mathcal{O}(e^{-q/\epsilon})$ along with its derivatives. We have the following analogue of Lemma 4.7 which will be proved in §5.

Lemma 4.9. *For each sufficiently small $\Delta_w > 0$, there exists $\epsilon_0, \Delta_z, q > 0$ and sufficiently small choice of the intervals I_c, I_a such that for each $s \in (w^\dagger + \Delta_w, 2w^\dagger - \Delta_w)$ and each $0 < \epsilon < \epsilon_0$, the following hold. Firstly, the backwards evolution of the manifold $\mathcal{B}(s;c,a)$ intersects Σ^m in a curve $\mathcal{B}_{\text{start}}(s;c,a) = \{(0,y_2,z) = (y_2^b,z^b)(z_{\text{end}},s;c,a); |z_{\text{end}}| \le \Delta_z\}$ where*

$$\begin{aligned} |y_2^b(z_{\text{end}},s;c,a) - y_2^{\mathcal{M},m}| &= \mathcal{O}(e^{-q/\epsilon}) \\ |z^b(z_{\text{end}},s;c,a)| &= \mathcal{O}(e^{-q/\epsilon}), \end{aligned} \tag{4.42}$$

uniformly in $|z_{\text{end}}| \le \Delta_z$ and $(c,a) \in I_c \times I_a$; the derivatives of the above expressions with respect to (c,a,z_{end}) are also $\mathcal{O}(e^{-q/\epsilon})$. Secondly,

$$y_2^{\mathcal{T}}(c,a) < \inf_{|z_{\text{end}}| \le \Delta_z} y_2^b(z_{\text{end}},s;c,a), \tag{4.43}$$

for all $(c,a) \in I_c \times I_a$.

The first assertion of Lemma 4.9 follows from the analysis above; the proof of the second assertion will be given in §5.6.

From Proposition 4.1, we have that the distance between the manifolds $\mathcal{M}_\epsilon^\ell(c,a)$ and $\mathcal{M}_\epsilon^{m,c}(c,a)$ in Σ^m is given by

$$y_2^{\mathcal{M},\ell} - y_2^{\mathcal{M},m} = \mathcal{D}_0(\alpha_2,r_2;c) = d_{\alpha_2}\alpha_2 + d_{r_2}r_2 + \mathcal{O}(2)\ . \tag{4.44}$$

Thus we can match $\mathcal{W}_\epsilon^u(0;c,a)$ with any solution in $\mathcal{B}_{\text{start}}(s;c,a)$ by solving

$$\begin{aligned} \mathcal{D}_0(\alpha_2,r_2;c) &= y_2^u(z;c,a) - y_2^{\mathcal{M},\ell} - \left(y_2^b(z_{\text{end}},s;c,a) - y_2^{\mathcal{M},m}\right) \\ z &= z^b(z_{\text{end}},s;c,a), \end{aligned} \tag{4.45}$$

for each $|z_{\text{end}}| \le \Delta_z$. For each such z_{end}, we obtain a solution by solving

$$\begin{aligned} a &= 2c^{1/2}\epsilon^{1/2}(\alpha_2^C + \mathcal{O}(e^{-q/\epsilon})) \\ c &= \breve{c}(a,\epsilon) + \mathcal{O}(e^{-q/\epsilon}), \end{aligned} \tag{4.46}$$

by the implicit function theorem to find $(a,c) = (a^u,c^u)(z_{\text{end}};s,\sqrt{\epsilon})$ where we have

$$(c^u,a^u)(z_{\text{end}};s,\sqrt{\epsilon}) = (c_E,a_E)(\sqrt{\epsilon}) + \mathcal{O}(e^{-q/\epsilon}), \tag{4.47}$$

uniformly in (z_{end},s), where (c_E,a_E) is the unique solution of (4.14).

We now evolve $\mathcal{W}^u_\epsilon(0;c,a)$ forwards; for each z_{end} we can hit the corresponding point on $\mathcal{B}_{\text{end}}(s;c,a)$, hence $\mathcal{W}^u_\epsilon(0;c,a)$ intersects Σ^m at the point $(y_2^{\text{se}}(s;c,a), z_{\text{end}})$ when $(c,a) = (c^u, a^u)(z_{\text{end}})$ defined above. We now match with $\mathcal{T}_\epsilon(c,a)$ by solving

$$z_{\text{end}} = z_\epsilon^{\mathcal{T}}(y_2^{\text{se}}(s;c,a); c^u(z_{\text{end}}), a^u(z_{\text{end}})), \tag{4.48}$$

which, using (4.26) and Lemma 4.9, we can solve by the implicit function theorem when $z_{\text{end}} = z^s_{\text{end}} = \mathcal{O}(e^{-q/\epsilon})$ to find the desired pulse solution when

$$\begin{aligned} a &= a(s,\sqrt{\epsilon}) := a^u(z^s_{\text{end}}; s, \sqrt{\epsilon}) \\ c &= c(s,\sqrt{\epsilon}) := c^u(z^s_{\text{end}}; s, \sqrt{\epsilon}). \end{aligned} \tag{4.49}$$

The argument that the solution constructed above lies on the stable manifold $\mathcal{W}^s_\epsilon(0;c,a)$ is the same as the case of type 2 pulses.

4.6 Type 3 pulses

We now consider type 3 pulses. Type 3 pulses are those with secondary heights which are close to the upper right fold point; these pulses encompass the transition from left pulses to right pulses and hence form a bridge between type 2 and type 4 pulses. We construct these in a manner similar to type 2 pulses, but they are not parametrized naturally by the height of the secondary pulse. To set up a parametrization of these pulses, we change to local coordinates in a neighborhood of the upper right fold point [5, §4].

The fold point is given by the fixed point $(u_+^*(a), 0, w_+^*(a))$ of the layer problem (2.7) where

$$u_+^*(a) = \tfrac{1}{3}\left(a + 1 + \sqrt{a^2 - a + 1}\right),$$

and $w_+^* = f(u_+^*)$. The linearization of (2.7) about this fixed point has one positive real eigenvalue $c > 0$ and a double zero eigenvalue, since $f'(u_+^*) = 0$. As in [5], there exists a neighborhood $\mathcal{U}_F$ of the upper right fold point, in which we can perform the following C^k-change of coordinates $\Phi_\epsilon \colon \mathcal{U}_F \to \mathbb{R}^3$ to (1.2), which is C^k-smooth in c, a and ϵ for (c,a,ϵ)-values restricted to the set $I_c \times I_a \times [0, \epsilon_0]$, where $\epsilon_0 > 0$ is chosen sufficiently small. We apply Φ_ϵ in the neighborhood $\mathcal{U}_F$ of the fold point and rescale time by a positive constant θ_0 given by

$$\theta_0 = \frac{1}{c^{2/3}}\left(a^2 - a + 1\right)^{1/6}\left(u_+^* - \gamma w_+^*\right)^{1/3} > 0, \tag{4.50}$$

uniformly in $(c,a) \in I_c \times I_a$, so that (1.2) becomes

$$\begin{aligned} x' &= \left(y + x^2 + h(x,y,\epsilon;c,a)\right), \\ y' &= \epsilon g(x,y,\epsilon;c,a), \\ z' &= z\left(\frac{c}{\theta_0} + \mathcal{O}(x,y,z,\epsilon)\right), \end{aligned} \tag{4.51}$$

where h, g are C^k-functions satisfying

$$\begin{aligned} h(x,y,\epsilon;c,a) &= \mathcal{O}(\epsilon, xy, y^2, x^3), \\ g(x,y,\epsilon;c,a) &= 1 + \mathcal{O}(x,y,\epsilon), \end{aligned}$$

uniformly in $(c,a) \in I_c \times I_a$. In the transformed system (4.51), the x, y-dynamics is decoupled from the dynamics in the z-direction along the straightened out strong unstable fibers. Thus, the flow is fully described by the dynamics on the two-dimensional invariant manifold $z = 0$ and by the one-dimensional dynamics along the fibers in the z-direction.

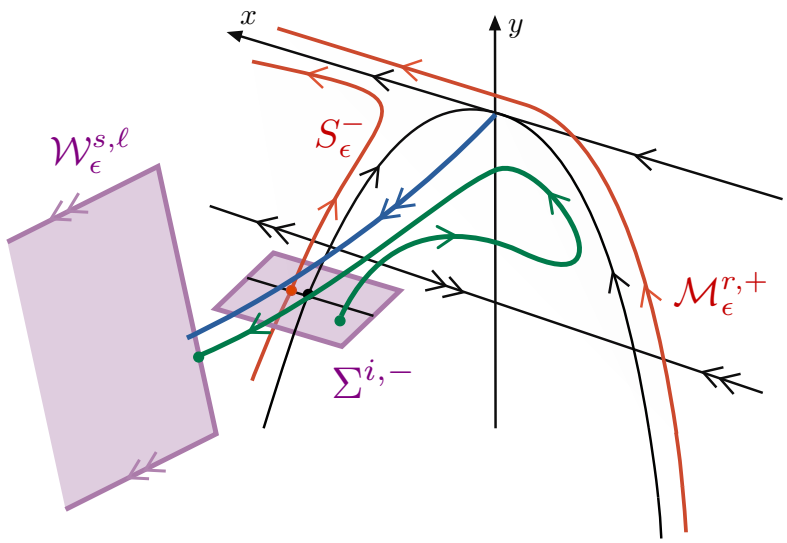

Figure 21: *Shown is the setup near the upper right fold point. Note that x increases to the left.*

We consider the flow of (4.51) on the invariant manifold $z = 0$. We append an equation for ϵ, arriving at the system

$$\begin{aligned} x' &= y + x^2 + h(x, y, \epsilon; c, a), \\ y' &= \epsilon g(x, y, \epsilon; c, a), \\ \epsilon' &= 0. \end{aligned} \tag{4.52}$$

For $\epsilon = 0$, this system possesses a critical manifold given by $\{(x, y) : y + x^2 + h(x, y, 0, c, a) = 0\}$, which in a sufficiently small neighborhood of the origin is shaped as a parabola opening downwards. The branch of this parabola for $x < 0$ is attracting and corresponds to the manifold $\mathcal{M}_0^r$. We define $\mathcal{M}_0^{r,+}$ to be the singular trajectory obtained by appending the fast trajectory given by the line $\{(x, 0) : x > 0\}$ to the attracting branch $\mathcal{M}_0^r$ of the critical manifold. In [5] it was shown that, for sufficiently small $\epsilon > 0$, $\mathcal{M}_0^{r,+}$ perturbs to a trajectory $\mathcal{M}_\epsilon^{r,+}$ on $z = 0$, represented as a graph $y = s_\epsilon(x; c, a)$, which is a-uniformly $C^0 - \mathcal{O}\left(\epsilon^{2/3}\right)$-close to $\mathcal{M}_0^{r,+}$ (see Figure 21 – note that in this figure, x increases to the left). The branch of the critical manifold corresponding to $x > 0$, which we denote by $S_0^-(c, a)$, is repelling and corresponds to the manifold $\mathcal{M}_0^m$ and is normally hyperbolic away from the fold point. Thus by Fenichel theory, this critical manifold persists as a slow manifold $S_\epsilon^-(c, a)$ for sufficiently small $\epsilon > 0$ and consists of a single solution. This slow manifold is unique up to exponentially small errors. We will be concerned with trajectories which are exponentially contracted to $S_\epsilon^-(c, a)$ in backwards time (see Figure 21).

Remark 4.10. *We use the notation $S_\epsilon^-(c, a)$ rather than $\mathcal{M}_\epsilon^m(c, a)$ as in general these manifolds only coincide up to exponentially small errors.*

We determine the location of $\mathcal{W}_\epsilon^{s,\ell}(c, a)$ in the neighborhood $\mathcal{U}_F$. From [5, §5], we know that $\mathcal{W}^s(\mathcal{M}_0^\ell(c^*(0), 0))$ intersects $\mathcal{W}^u(\mathcal{M}_0^{r,+}(c^*(0), 0))$ transversely for $\epsilon = 0$ along the Nagumo back ϕ_b, and this intersection persists for $(c, a, \epsilon) \in I_c \times I_a \times (0, \epsilon_0)$. This means that $\mathcal{W}_\epsilon^{s,\ell}(c, a)$ will transversely intersect the manifold $\mathcal{W}_\epsilon^{u,r}(c, a)$ which is composed of the union of the unstable fibers of the continuation of the slow manifold $\mathcal{M}_\epsilon^{r,+}(c, a)$ found in [5, §4]. We define the exit section Σ^{out} by

$$\Sigma^{out} = \{z = \Delta'\}. \tag{4.53}$$

For $(c, a, \epsilon) \in I_c \times I_a \times (0, \epsilon_0)$, the intersection of $\mathcal{W}_\epsilon^{s,\ell}(c, a)$ and $\mathcal{W}_\epsilon^{u,r}(c, a)$ occurs at a point

$$(x, y, z) = (x_\ell(c, a, \epsilon), s_\epsilon(x_\ell(c, a, \epsilon); c, a), \Delta') \in \Sigma^{out}, \tag{4.54}$$

and thus we may expand $\mathcal{W}_\epsilon^{s,\ell}(c,a)$ in Σ^{out} as

$$(x,y) = (x_\ell(c,a,\epsilon) + \mathcal{O}(y - s_\epsilon(x;c,a),\epsilon), y), \quad y \in [-\Delta_y, \Delta_y], \tag{4.55}$$

for some small $\Delta_y > 0$. The goal is now to parametrize the construction of type 3 pulses by the coordinate y, which parametrizes trajectories on the manifold $\mathcal{W}_\epsilon^{s,\ell}(c,a)$. By taking Δ_w sufficiently small, it is clear that there is overlap with the construction of type 2 pulses. We will argue that there is also overlap with the construction of type 4 pulses by considering an appropriate range of y-values.

We now place a section $\Sigma^{i,-}$ defined by

$$\Sigma^{i,-} = \{(x,y,z) : 0 \le x \le 2\rho, y = -\rho^2, |z| \le \Delta'\}, \tag{4.56}$$

and we note that the manifold $S_\epsilon^-(c,a)$ intersects $\Sigma^{i,-}$ for all sufficiently small $\epsilon > 0$. We define two other sections

$$\Sigma^{i,+} = \{(x,y,z) : -2\rho \le x \le 0, y = -\rho^2, |z| \le \Delta'\} \tag{4.57}$$

$$\Sigma^{i,v} = \{(x,y,z) : x = -2\rho, |y| \le \rho^2, |z| \le \Delta'\}. \tag{4.58}$$

We now note that, provided Δ_y is sufficiently small, any trajectory $\mathcal{W}_\epsilon^{s,\ell}(c,a)$ in Σ^{out} leaves a neighborhood of the fold point through one of the sections $\Sigma^{i,-}, \Sigma^{i,+}, \Sigma^{i,v}$ in backwards time. We construct type 3 pulses by considering only heights y which correspond to trajectories on $\mathcal{W}_\epsilon^{s,\ell}(c,a)$ which exit via $\Sigma^{i,-}$ in backwards time. The setup is shown in Figure 21.

Firstly, all solutions in $\Sigma^{i,-}$ are exponentially contracted in backwards time to $\mathcal{M}_\epsilon^m(c,a)$ upon arrival in the section Σ^m near the lower left fold point. We first consider the trajectory $S_\epsilon^-(c,a)$. Tracking backwards down the middle slow manifold, we have that $S_\epsilon^-(c,a)$ is uniformly $\mathcal{O}(e^{-q/\epsilon})$-close to $\mathcal{M}_\epsilon^m(c,a)$ in Σ^m for $(c,a) \in I_c \times I_a$.

Using similar arguments as in the construction of type 2 pulses, for each sufficiently small $\epsilon > 0$ we can find values of $(c,a) = (c^-,a^-)(\sqrt{\epsilon})$ such that the backwards evolution of $S_\epsilon^-(c,a)$ can be matched with $\mathcal{W}_\epsilon^u(0;c,a)$ in the section Σ^m. We now consider trajectories on $\mathcal{W}_\epsilon^{s,\ell}(c,a)$ in Σ^{out} which pass through $\Sigma^{i,-}$ in backwards time. As stated above, trajectories on $\mathcal{W}_\epsilon^{s,\ell}(c,a)$ in Σ^{out} are parametrized by $y \in [-\Delta_y, \Delta_y]$. For $(c,a) = (c^-,a^-)$, for each $\bar{y}$ sufficiently small, (for instance, $-\Delta_y < \bar{y} < -\Delta_y/2$), for all $\epsilon \in (0,\epsilon_0)$, the trajectory which intersects $\mathcal{W}_\epsilon^{s,\ell}(c,a)$ in Σ^{out} at $\bar{y}$ contracts exponentially in backwards time to $S_\epsilon^-(c,a)$ and therefore passes through $\Sigma^{i,-}$. We can therefore define the supremum of all such values of $\bar{y}$ to be y_ϵ^-. That is, y_ϵ^- is defined as the supremum of $\bar{y}$-values such that the trajectory which intersects $\mathcal{W}_\epsilon^{s,\ell}(c^-,a^-)$ in Σ^{out} at height $\bar{y}$ passes through $\Sigma^{i,-}$ in backwards time.

We now show that for each sufficiently small $\epsilon > 0$ and each $\bar{y} \in [-\Delta_y, y_\epsilon^-]$, we can construct a transitional pulse with secondary excursion which passes near the upper right fold and intersects the section Σ^{out} passing exponentially close to the point $(x,y) = (x_\ell(c,a,\epsilon) + \mathcal{O}(\bar{y} - s_\epsilon(x;c,a),\epsilon), \bar{y})$ on the manifold $\mathcal{W}_\epsilon^{s,\ell}(c,a)$. In this sense, $\bar{y}$ will serve as a parameterization of such transitional pulses passing near the fold. We then argue below that there is overlap between these and the construction of pulses of type 2 and 4.

To proceed, we show that for each such $\bar{y}$, a transitional pulse can be constructed following the same procedure as with type 2 pulses, though extra care is needed to make sure that the passage near the fold does not cause the argument to break down. We define the solution $\gamma^{\text{se}}(\bar{y};c^-,a^-)$ on the stable foliation $\mathcal{W}_\epsilon^{s,\ell}(c^-,a^-)$ which intersects the section Σ^{out} at height $y = \bar{y}$. This solution is exponentially attracted in forward time to $\mathcal{M}_\epsilon^\ell(c^-,a^-)$ and hence intersects Σ^m at the point $(0, y_2^{\text{se}}(c^-,a^-), 0)$ where

$$e^{-q_1/\epsilon}/C \le y_2^{\text{se}}(c^-,a^-) - y_2^u(0;c^-,a^-) \le Ce^{-q_2/\epsilon}. \tag{4.59}$$

Define the two-dimensional manifold $\mathcal{B}(\bar{y};c^-,a^-)$ to be the backwards evolution of the fiber

$$\mathcal{B}_{\text{end}}(\bar{y};c^-,a^-) := \{(0, y_2^{\text{se}}(c^-,a^-), z) : |z| \le \Delta_z\} \subseteq \Sigma^m. \tag{4.60}$$

In backwards time, this $\mathcal{B}(\bar{y}; c^-, a^-)$ is exponentially contracted to the solution $\gamma^{\rm se}(\bar{y}; c^-, a^-)$ and hence intersects Σ^{out} in a one-dimensional curve which is $\mathcal{O}(e^{-q/\epsilon})$-close to $\gamma^{\rm se}(\bar{y}; c^-, a^-)$. Because $\bar{y} < y_\epsilon^-$, in backwards time $\gamma^{\rm se}(\bar{y}; c^-, a^-)$ hits the section $\Sigma^{i,-}$. The passage in backwards time from Σ^{out} to $\Sigma^{i,-}$ defines a map which at worst expands exponentially at a rate $e^{\eta/\epsilon}$, where η can be made arbitrarily small by shrinking the fold neighborhood. In particular, we can ensure that $\eta \ll q$. Hence we can ensure that this potential expansion is always compensated by the contraction occurring along the fibers of $\mathcal{W}_\epsilon^{s,\ell}(c, a)$ in the passage in backwards time from Σ^m to Σ^{out}. Hence the intersection of the backwards evolution of $\mathcal{B}(\bar{y}; c^-, a^-)$ with $\Sigma^{i,-}$ also defines a one-dimensional manifold which is $\mathcal{O}(e^{-q/\epsilon})$-close to $\gamma^{\rm se}(\bar{y}; c^-, a^-)$, where q may have to be slightly decreased.

We will now show that the results above hold for an interval of parameters (c, a) exponentially close to (c^-, a^-), that is, we write $(c, a) = (c^-, a^-) + (\tilde{c}, \tilde{a})$ and consider values $|\tilde{c}|, |\tilde{a}| \leq Ce^{-2\eta/\epsilon}$. For all sufficiently small $\epsilon > 0$, we claim that the above assertions continue to hold uniformly for all such $(\tilde{c}, \tilde{a})$. We define the solution $\gamma^{\rm se}(\bar{y}; c, a)$ on $\mathcal{W}_\epsilon^{s,\ell}(c, a)$ which intersects the section Σ^{out} at height $y = \bar{y}$. This solution intersects Σ^m at the point $(y_2^{\rm se}(\bar{y}; c, a), 0)$ where

$$e^{-q_1/\epsilon}/C \leq y_2^{\rm se}(\bar{y}; c, a) - y_2^u(0; c, a) \leq Ce^{-q_2/\epsilon}. \tag{4.61}$$

uniformly in (c, a). Again we define the manifold $\mathcal{B}(\bar{y}; c, a)$ to be the backwards evolution of the fiber $\mathcal{B}_{\rm end}(\bar{y}; c, a) := \{(0, y_2^{\rm se}(\bar{y}; c, a), z) : |z| \leq \Delta_z\} \subseteq \Sigma^m$. In backwards time, this fiber is exponentially contracted to the solution $\gamma^{\rm se}(\bar{y}; c, a)$ and hence intersects Σ^{out} in a one-dimensional curve which is $\mathcal{O}(e^{-q/\epsilon})$-close to $\gamma^{\rm se}(\bar{y}; c, a)$. In backwards time, for any $|\tilde{c}|, |\tilde{a}| \leq Ce^{-2\eta/\epsilon}$, $\gamma^{\rm se}(\bar{y}; c, a)$ hits the section $\Sigma^{i,-}$, and the backwards evolution of $\mathcal{B}(\bar{y}; c, a)$ also meets $\Sigma^{i,-}$ in a curve which is $\mathcal{O}(e^{-q/\epsilon})$-close to $\gamma^{\rm se}(\bar{y}; c, a)$ uniformly in $|\tilde{c}|, |\tilde{a}| \leq Ce^{-2\eta/\epsilon}$, where q may have to be slightly decreased. Similar estimates also hold for the derivatives of the transition maps from Σ^m to $\Sigma^{i,-}$.

Since $\mathcal{B}(\bar{y}; c, a)$ intersects Σ^m in a vertical fiber $\mathcal{B}_{\rm end}(\bar{y}; c, a) = \{(0, y_2^{\rm se}(\bar{y}; c, a), z) : |z| \leq \Delta_z\}$, we parameterize the trajectories on $\mathcal{B}(\bar{y}; c, a)$ by $|z_{\rm end}| \leq \Delta_z$, where $z_{\rm end}$ denotes the eventual height along the fiber. We now consider the backwards evolution of $\mathcal{B}(\bar{y}; c, a)$ back to Σ^m, where it intersects in a curve $\mathcal{B}_{\rm start}(\bar{y}; c, a)$. For any $|\tilde{c}|, |\tilde{a}| \leq Ce^{-2\eta/\epsilon}$, we have that $\mathcal{B}_{\rm start}(\bar{y}; c, a)$ is $\mathcal{O}(e^{-q/\epsilon})$-close to $\mathcal{M}_\epsilon^m(c, a)$ in Σ^m. Thus we have that in Σ^m, $\mathcal{B}_{\rm start}(\bar{y}; c, a) = \{(0, y_2, z) = (y_2^b, z^b)(z_{\rm end}, \bar{y}; c, a); |z_{\rm end}| \leq \Delta_z\}$ where

$$\begin{aligned} |y_2^b(z_{\rm end}, \bar{y}; c, a) - y_2^{\mathcal{M},m}| &= \mathcal{O}(e^{-q/\epsilon}) \\ |z^b(z_{\rm end}, \bar{y}; c, a)| &= \mathcal{O}(e^{-q/\epsilon}), \end{aligned} \tag{4.62}$$

uniformly in $|z_{\rm end}| \leq \Delta_z$ and $|\tilde{c}|, |\tilde{a}| \leq Ce^{-2\eta/\epsilon}$.

We can now repeat argument in the construction of type 2 pulses, given the uniformity of the above estimates in $|\tilde{c}|, |\tilde{a}| \leq Ce^{-2\eta/\epsilon}$ and the fact that we only need freedom in the variation in the bifurcation parameters (c, a) of $\mathcal{O}(e^{-q/\epsilon})$ for perhaps a slightly smaller value of q to solve the corresponding matching conditions.

4.6.1 Overlap with pulses of type $2, 4$

The pulses now form a one-parameter family parametrized by the height $\bar{y}$. By taking Δ_w sufficiently small with respect to Δ_y, it is clear that there is overlap in the construction of type 3 pulses above and the construction of type 2 pulses. That is, type 3 pulses for $\bar{y}$ near Δ_y are constructed in much the same manner as type 2 pulses for s near $w^\dagger - \Delta_w$. Furthermore, again with Δ_w sufficiently small with respect to Δ_y, there is also overlap in the construction of type 4 pulses. Type 4 pulses constructed for s near $w^\dagger + \Delta_w$ will pass through the section $\Sigma^{i,-}$ before passing $\mathcal{O}(\epsilon^{2/3} + |a|)$-close to the fold and leaving the section Σ^{out} exponentially close to $\mathcal{W}_\epsilon^{s,\ell}(c, a)$. These pulses therefore overlap with the construction of type 3 pulses for $\bar{y}$ near y_ϵ^-.

As all pulses of types $2, 3, 4$ were constructed using the implicit function theorem, by local uniqueness the one-parameter families of pulses of types $2, 3, 4$ in fact form one continuous family. Hence we reparameterize the family of type 3 pulses by $s \in (w^\dagger - \Delta_w, w^\dagger + \Delta_w)$ rather than the height $\bar{y}$.

4.7 Type 6 pulses

Finally, we consider type 6 pulses, which are right transitional pulses corresponding to $s \in (2w^\dagger - \Delta_w, 2w^\dagger)$. To construct type 6 pulses, we proceed as in the case of type 4/5 pulses and analogously define the solution $\gamma^{\mathrm{se}}(s; c, a)$; this solution is well defined and exponentially close to $\mathcal{W}_\epsilon^{s,r}(c, a)$ in $\Sigma^{h,r}$ (and the derivatives of the transition maps with respect to (c, a) are also exponentially small). However, the challenge comes from the fact that the backwards evolution of $\gamma^{\mathrm{se}}(s; c, a)$ does not necessarily meet the section Σ^m at a distance $\mathcal{O}(e^{-q/\epsilon})$-close to $\mathcal{M}_\epsilon^{m,c}(c, a)$, and hence more care is required to obtain the corresponding matching conditions.

We begin by describing the manifold $\mathcal{W}_\epsilon^{s,r}(c, a)$ in a neighborhood of the origin. We first write $c = \check{c}(a, \epsilon) + c_2\epsilon = 1/\sqrt{2} + \mathcal{O}(a, \epsilon)$, for $|c_2|$ small and $(a, \epsilon) \in I_a \times (0, \epsilon_0)$, that is, we only allow c to vary from the value $\check{c}(a, \epsilon)$ by an $\mathcal{O}(\epsilon)$ amount. Since $\mathcal{W}_0^u(0; c, a)$ lies in $\mathcal{W}_0^s(\mathcal{M}_0^r; c, a)$ for $(c, a) = (1/\sqrt{2}, 0)$, by standard geometric singular perturbation theory, we have that for $(a, \epsilon) \in I_a \times (0, \epsilon_0)$, in the section $\Sigma^z = \{z = \Delta_z\}$, we can write $\mathcal{W}_\epsilon^{s,r}(c, a)$ as a graph

$$x = x^r(y, \alpha, \epsilon, c) = \mathcal{O}(y, \alpha, \epsilon), \quad y \in [-2\Delta_y, 2\Delta_y], \tag{4.63}$$

for sufficiently small $\Delta_y > 0$.

Since the coordinate transformation $x \to x + g(y, \alpha, \epsilon)$ for a function $g(y, \alpha, \epsilon) = \mathcal{O}(y)$ does not change the form of the equations (4.2), we can assume without loss of generality that $\mathcal{W}_\epsilon^{s,r}(c, a)$ is given by the line

$$x = x^r(\alpha, \epsilon, c) = \mathcal{O}(\alpha, \epsilon), \quad y \in [-2\Delta_y, 2\Delta_y], \tag{4.64}$$

or, equivalently, in the $\mathcal{K}_2$ coordinates

$$x_2 = x_2^r(\alpha_2, r_2, c_2) = \mathcal{O}(\alpha_2, r_2). \tag{4.65}$$

4.7.1 Dynamics in $\mathcal{K}_2$

The desingularized flow in the $\mathcal{K}_2$ coordinates is given by

$$\begin{aligned} x_2' &= -y_2 + x_2^2 + r_2 G_1(x_2, y_2) + \mathcal{O}(r_2(\alpha_2 + r_2)) \\ y_2' &= x_2 + \alpha_2 + r_2 G_2(x_2, y_2) + \mathcal{O}(r_2(\alpha_2 + r_2)) \\ r_2' &= 0 \\ \alpha_2' &= 0, \end{aligned} \tag{4.66}$$

where $' = \dfrac{d}{dt_2}$, $t_2 = r_2 t$, and

$$G(x_2, y_2) = \begin{pmatrix} G_1(x_2, y_2) \\ G_2(x_2, y_2) \end{pmatrix} = \begin{pmatrix} a_1 x_2 - a_2 x_2 y_2 + a_3 x_2^3 \\ a_4 x_2^2 + a_5 y_2 \end{pmatrix}, \tag{4.67}$$

where

$$\begin{aligned} a_1 &= \frac{\partial h_3}{\partial x}(0, 0, 0, 0, c), \quad a_2 = \frac{\partial h_2}{\partial x}(0, 0, 0, 0, c), \quad a_3 = \frac{\partial h_1}{\partial x}(0, 0, 0, 0, c), \\ a_4 &= \frac{\partial h_4}{\partial x}(0, 0, 0, 0, c), \quad a_5 = h_6(0, 0, 0, 0, c) \end{aligned}$$

and the functions h_i are as in (4.2). For $r_2 = \alpha_2 = 0$, the system is integrable with constant of motion

$$H(x_2, y_2) = \frac{1}{2} e^{-2y_2} \left(y_2 - x_2^2 + \frac{1}{2} \right). \tag{4.68}$$

The function H has a continuous family of closed level curves

$$\Gamma_2^h = \{(x_2, y_2) : H(x_2, y_2) = h\}, \quad h \in (0, 1/4) \tag{4.69}$$

contained in the interior of the parabola $y_2 = x_2^2 - 1/2$, which is the level curve for $h = 0$. We define the trajectories $\gamma_2^h(t) = (x_2^h(t), y_2^h(t))$ to be the closed orbits corresponding to Γ_2^h, satisfying $x_2^h(0) = 0$ and $y_2^h(0) > 0$, and we let T^h denote the half period of the orbit Γ_2^h. For $h = 0$, we parametrize the parabola $\gamma_2^0(t)$ as

$$(x_2^0(t), y_2^0(t)) = \left(\frac{t}{2}, \frac{t^2}{4} - \frac{1}{2}\right). \tag{4.70}$$

For (α_2, r_2) sufficiently small and $y_2^h(0) > 0$ bounded away from zero uniformly in (α_2, r_2), define $\gamma_{\alpha_2,r_2}^{h,r}(t), \widehat{\gamma}_{\alpha_2,r_2}^{h,r}(t)$ to be the forward/backward solutions of (4.66) satisfying $\gamma_{\alpha_2,r_2}^{h,r}(0) = \widehat{\gamma}_{\alpha_2,r_2}^{h}(0) = (x_2^r(\alpha_2, r_2, c_2), y_2^h(0))$ so that $\gamma_{0,0}^{h,r}(0) = \widehat{\gamma}_{0,0}^{h}(0) = \gamma_2^h(0)$. Denote by $y_{\alpha_2,r_2}^{h,r}, \widehat{y}_{\alpha_2,r_2}^{h,r} < 0$ the y_2 values at which $\gamma_{\alpha_2,r_2}^{h,r}(t), \widehat{\gamma}_{\alpha_2,r_2}^{h,r}(t)$ reach $x_2 = 0$.

For $h \in (0, h_0)$, where h_0 is sufficiently small, we are interested in the distance function

$$\mathcal{D}_h(\alpha_2, r_2, h) := H(0, y_2^{\mathcal{M},\ell}) - H(0, \widehat{y}_{\alpha_2,r_2}^{r,h}). \tag{4.71}$$

A zero of this function corresponds to a connection between $\mathcal{M}_\epsilon^\ell(c, a)$ and a trajectory reaching $(x_2^r(\alpha_2, r_2, c_2), y_2^h(0))$ in the chart $\mathcal{K}_2$. We have the following

Proposition 4.11. *Fix $h_0, \Delta_y > 0$ sufficiently small. There exists $\epsilon_0 > 0$ such that for each $r_2 \in (0, \sqrt{\epsilon_0})$, there exists $h_L > 0$ and a curve $\alpha_2 = \alpha_2^h(r_2, c_2)$ satisfying*

$$\mathcal{D}_h(\alpha_2^h(r_2, c_2), r_2, h) = 0, \quad h \in (h_L, h_0). \tag{4.72}$$

Furthermore, we have that $r_2^2 y_2^{h_L}(0) = \Delta_y(1 + \mathcal{O}(\Delta_y))$.

Proof. The proof follows from similar arguments as in [22] and in the proof of [23, Theorem 4.2]; here we briefly outline the differences.

Proceeding as in [22, §3.6], we compute that

$$H(0, y_2^{\mathcal{M},\ell}) = r_2 \int_{-\infty}^0 \nabla H(\gamma_2^0(t)) \cdot G(\gamma_2^0(t)) dt + \alpha_2 \int_{-\infty}^0 \nabla H(\gamma_2^0(t)) \cdot \begin{pmatrix} 0 \\ 1 \end{pmatrix} dt + \mathcal{O}((r_2 + |\alpha_2|)^2), \tag{4.73}$$

and following the proof of [23, Proposition 4.1], we have that

$$H(0, \widehat{y}_{\alpha_2,r_2}^{h,r}) = h - r_2 \int_{-T^h}^0 \nabla H(\gamma_2^h(t)) \cdot G(\gamma_2^h(t)) dt - \alpha_2 \int_{-T^h}^0 \nabla H(\gamma_2^h(t)) \cdot \begin{pmatrix} 0 \\ 1 \end{pmatrix} dt + \mathcal{O}((r_2 + |\alpha_2|)^2). \tag{4.74}$$

The main distinction between the argument in [23] and the derivation of the expression (4.74) above is that there are errors incurred due to the choice $\widehat{\gamma}_{\alpha_2,r_2}^h(0) = (x_2^r(\alpha_2, r_2, c_2), y_2^h(0)) = \big(\mathcal{O}(\alpha_2, r_2), y_2^h(0)\big)$ instead of $\widehat{\gamma}_{\alpha_2,r_2}^h(0) = (0, y_2^h(0))$; however, by tracking the argument in the proof of [23, Proposition 4.1], we see that these errors can be absorbed into the quadratic terms, and we omit the details.

It follows that

$$\mathcal{D}_h(\alpha_2, r_2, h) = -h + d_{\alpha_2}^h \alpha_2 + d_{r_2}^h r_2 + \mathcal{O}((r_2 + |\alpha_2|)^2), \tag{4.75}$$

where

$$\begin{aligned} d_{r_2}^h &= \int_{-\infty}^0 \nabla H(\gamma_2^0(t)) \cdot G(\gamma_2^0(t)) dt + \int_{-T^h}^0 \nabla H(\gamma_2^h(t)) \cdot G(\gamma_2^h(t)) dt \\ d_{\alpha_2}^h &= \int_{-\infty}^0 \nabla H(\gamma_2^0(t)) \cdot \begin{pmatrix} 0 \\ 1 \end{pmatrix} dt + \int_{-T^h}^0 \nabla H(\gamma_2^h(t)) \cdot \begin{pmatrix} 0 \\ 1 \end{pmatrix} dt, \end{aligned} \tag{4.76}$$

with $d_{\alpha_2}^h > 0$ uniformly in $h \in (0, h_0)$. Though the difference function $\mathcal{D}_h$ differs from that in [23] due to the presence of the $-h$ term, we may carry though the argument as in the proof of [23, Theorem 4.1] and see that analogous estimates hold for $\mathcal{D}_h$ and its derivatives in order to obtain the function $\alpha_2^h(r_2, c_2)$ with the desired properties. □

4.7.2 Matching conditions for pulses $\Gamma(s, \sqrt{\epsilon})$, $s \in (2w^\dagger - \Delta_w, 2w^\dagger)$

The backwards evolution of $\gamma^{\rm se}(s; c, a)$ is exponentially close to $\mathcal{W}^{s,r}_\epsilon(c, a)$ in $\Sigma^z := \{z = \Delta_z\}$. Rather than parameterizing $\gamma^{\rm se}(s; c, a)$ by s, it is more natural to use $h \in (h_L, h_0)$ along $\mathcal{W}^{s,r}_\epsilon(c, a)$ from Lemma 4.11 as a parameter (this is in one-to-one correspondence with the height y along $\mathcal{W}^{s,r}_\epsilon(c, a)$ in the section Σ^m). Thus we have that in Σ^z, $\gamma^{\rm se}_{\rm start}(h; c, a)$ is given by a point $(x, y) = (x^b(h; c, a, \epsilon), \epsilon y^h_2(0))$ which satisfies

$$|x^b(\bar{y}; c, a, \epsilon) - x^r(a, \epsilon)| = \mathcal{O}(e^{-q/\epsilon}), \tag{4.77}$$

uniformly in (c, a). We have the following

Lemma 4.12. *The backwards evolution of $\gamma^{\rm se}(s; c, a)$ intersects Σ^m at a point $\gamma^{\rm se}_{\rm start}(s; c, a) = (0, \widehat{y}^{\rm se}_2(\alpha_2, r_2), \widehat{z}^{\rm se}(\alpha_2, r_2))$ satisfying*

$$\begin{aligned} |\widehat{y}^{\rm se}_2(\alpha_2, r_2) - \widehat{y}^{h,r}_{\alpha_2, r_2}| &= \mathcal{O}(e^{-q/r_2^2}) \\ |\widehat{z}^{\rm se}(\alpha_2, r_2)| &= \mathcal{O}(e^{-q/r_2}), \end{aligned} \tag{4.78}$$

along with their derivatives uniformly in (α_2, r_2) sufficiently small.

Proof. To see this, we first recall that $\gamma^{\rm se}(h; c, a)$ intersects Σ^z at a point $(x, y) = (x^b(h; c, a, \epsilon), \epsilon y^h_2(0))$ which is $\mathcal{O}(e^{-q/\epsilon})$-close to $\mathcal{W}^{s,r}_\epsilon(c, a)$ satisfying (4.77). Recalling in the $\mathcal{K}_2$ coordinates that $t_2 = r_2 t$, we obtain the desired estimates by evolving backwards by time $t_2 = T^h + \mathcal{O}(\alpha_2, r_2)$, noting from (4.2) that the z-coordinate evolves according to

$$\dot{z} = z\left(c^{3/2} + \mathcal{O}(x, y, z, \alpha, \epsilon)\right), \tag{4.79}$$

where $\cdot = \dfrac{d}{dt}$, hence decaying exponentially in backwards time. □

The final matching conditions can then be obtained as follows. Starting in Σ^z, we consider the backwards evolution of $\gamma^{\rm se}(s; c, a)$ back to the section Σ^m where it intersects at a point $\gamma^{\rm se}_{\rm start}(s; c, a)$; we then show that for $h \in (h_L, h_0)$, $\mathcal{W}^u_\epsilon(0; c, a)$ can be matched with $\gamma^{\rm se}_{\rm start}(h; c, a)$ by adjusting (c, a) using Lemma 4.9. We then evolve $\gamma^{\rm se}(h; c, a)$ forwards to its next return to Σ^m; by construction, $\gamma^{\rm se}(h; c, a)$ meets Σ^m at a point $\gamma^{\rm se}_{\rm end}(h; c, a)$ which lies on the manifold $\mathcal{Z}_\epsilon(c, a)$ and in forward time will not reach a height higher than $\epsilon y^h_2(0)$. By Proposition 3.10, this gives a tail which lies in $\mathcal{W}^s_\epsilon(0; c, a)$, completing the construction.

From Proposition 4.11, for $h \in (h_L, h_0)$ we can match $\mathcal{W}^u_\epsilon(0; c, a)$ with $\gamma^{\rm se}_{\rm start}(h; c, a)$ by solving

$$\begin{aligned} \mathcal{D}_h(\alpha_2, r_2, h) &= \left(H(0, y_2^{\mathcal{M},\ell}) - H(0, y^u_2(z; c, a))\right) + \left(H(0, \widehat{y}^{\rm se}_2(\alpha_2, r_2)) - H(0, \widehat{y}^{r,h}_{\alpha_2, r_2})\right) \\ z &= \widehat{z}^{\rm se}(\alpha_2, r_2), \end{aligned} \tag{4.80}$$

Using Lemma 4.3, we obtain a solution by solving

$$\begin{aligned} a &= 2c^{1/2}\epsilon^{1/2}(\alpha^h_2(r_2, c_2) + \mathcal{O}(e^{-q/\epsilon})) \\ c &= \breve{c}\,(a, \epsilon) + \mathcal{O}(e^{-q/\epsilon}), \end{aligned} \tag{4.81}$$

Recalling

$$c = \breve{c}(a, \epsilon) + c_2\epsilon, \tag{4.82}$$

by the implicit function theorem we obtain a solution

$$\begin{aligned} a &= a(h, \sqrt{\epsilon}) \\ c &= c(h, \sqrt{\epsilon}), \end{aligned} \tag{4.83}$$

to (4.81) for each $h \in (h_L, h_0)$.

We can naturally reparameterize these solutions via the invertible map $h \to y_2^h(0)$ so that they are parameterized by the height $y = \epsilon y_2^h(0)$ at which the secondary pulse leaves the neighborhood of the origin along $\mathcal{W}_\epsilon^{s,r}(c,a)$. This y-coordinate ranges from $y \in [y^{h_0}, y^{h_L}]$ where $y^{h_0} = \epsilon y_2^{h_0}(0) = \mathcal{O}(\epsilon)$ and $y^{h_L} = \epsilon y_2^{h_L}(0) = \Delta_y(1 + \mathcal{O}(\Delta_y))$. From this, we first deduce that for the solution in this family reaching Σ^z at $(x,y) = (x^r(\alpha,\epsilon), y^{h_L}) = \mathcal{O}(\sqrt{\epsilon})$, the secondary pulse leaves along $\mathcal{W}_\epsilon^{s,r}(c,a)$ at an $\mathcal{O}(\sqrt{\epsilon})$ distance from the primary pulse. Secondly, from the endpoint at $y^{h_L} = \mathcal{O}(1)$, we see that there is overlap with the construction of type 5 pulses.

Hence we can reparameterize these pulses by s so that they form one continuous family with the previously constructed type 5 pulses. For type 6 pulses, s ranges from $s = 2w^\dagger - \Delta_w$ to $s = s_{end}(\sqrt{\epsilon})$, the end of this family marked by the solution described above with a secondary pulse which is $\mathcal{O}(\sqrt{\epsilon})$-close to the primary pulse.

Remark 4.13. *We have shown above that type* 6 *pulses form a bridge between type* 5 *pulses at $h = h_L$ and double pulses at $h = h_0$ for some small fixed h_0. Beyond this, our construction procedure breaks down. Using* (4.81) *and the fact that $\alpha_2^{h_0}(r_2, c_2)$ solves*

$$\mathcal{D}_h(\alpha_2^{h_0}, r_2, h_0) = 0, \tag{4.84}$$

where $\mathcal{D}_h$ is defined by (4.75)*, we note that the corresponding a-value is given by*

$$a(h_0, \sqrt{\epsilon}) = 2^{3/4} h_0 \sqrt{\epsilon} + \mathcal{O}(\epsilon). \tag{4.85}$$

We note that this value is less than, but close to the value at which the Belyakov transition (1.3) *occurs at*

$$a = 2^{3/4}\sqrt{\epsilon} + \mathcal{O}(\epsilon). \tag{4.86}$$

This corresponds with the split banana we see in Figure 5. It may be possible to fully understand the termination of this branch of double pulses by unfolding the Belyakov point. We do not develop this further here, but we note that the above construction indeed fails near this region.

4.8 Proof of Theorem 2.2

We briefly conclude the proof of Theorem 2.2. For each sufficiently small $\epsilon > 0$, the existence of the desired one parameter family of pulse solutions $\Gamma(s, \sqrt{\epsilon})$ and their approximation by the singular pulses $\Gamma_0(s)$ follows from the constructions of pulses of type $1, 2, 3, 4, 5, 6$ in §4.2-4.7. As all of these were constructed using the implicit function theorem, and the constructions can be taken to have overlapping regions of validity, we obtain a single continuous family of solutions which satisfy the singular approximations (i). The overlap of the family $\Gamma(s, \sqrt{\epsilon})$ with the classical branch of 1-pulses from Theorem 1.1 for sufficiently small s was shown in §4.2.2, proving (iii).

The statement (ii) follows directly from Proposition 3.10 for the case of pulses of type $1-5$. We now prove the final statement, regarding the fact that the functions $w_i(s,0)$ are constant for $s \in [w_R^0, 2w^\dagger - w_A]$. As constructed in §4.2-4.6, a transitional pulse $\Gamma(s, \sqrt{\epsilon})$, $s \in [w_R^0, 2w^\dagger - w_A]$, completes a primary excursion, followed by a secondary excursion (determined by s), followed by a trajectory which meets $\mathcal{Z}_\epsilon(c,a)$ in the section $\Sigma^{h,\ell}$ at some height $w_1(s,\epsilon) < w_\epsilon^{\pitchfork}$ where $w_\epsilon^{\pitchfork} = w_A + \mathcal{O}(\epsilon^{2/3}) \leq w_A + \Delta_w$ for all sufficiently small $\epsilon > 0$. We first claim that $\lim_{\epsilon \to 0} w_1(s,\epsilon) = w_1(s,0) \geq w_A - 3\Delta_w$.

To see this, we consider the backwards evolution of the trajectory starting in $\Sigma^{h,\ell}$ at height $w = w_A - 3\Delta_w$, which ends up in $\Sigma^{h,\ell}$ at some height $w = w_C(\epsilon)$. Let $w_C^0 = \lim_{\epsilon \to 0} w_C(\epsilon)$. We claim that $R(w_C^0, w_A - 3\Delta_w) = 0$, i.e. $w_0^C = w_R(\Delta_w)$. To show this, we assume for contradiction that $R(w_C^0, w_A - 3\Delta_w) < 0$. By Proposition 3.9, we have that the pair $(w_R(\Delta_w), w_A - 3\Delta_w)$ are buffer heights. Thus any solution entering $\Sigma^{h,\ell}$ above $w = w_R(\Delta_w)$ exits $\Sigma^{h,\ell}$ at height $w_A - 3\Delta_w$. This gives the desired contradiction: any transitional pulse $\Gamma(s, \sqrt{\epsilon})$, $s \in [w_R(\Delta_w), 2w^\dagger - w_A + \Delta_w]$, must first complete a primary pulse which intersects $\Sigma^{h,\ell}$ near $w = w^\dagger$. This primary

excursion therefore subsequently shadows a canard solution on $\mathcal{Z}_\epsilon(c,a)$ which enters via $\Sigma^{h,\ell}$ near $w = w^\dagger$; however this solution does not exit at the buffer height $w_A - 3\Delta_w$ but rather must exit $\mathcal{Z}_\epsilon(c,a)$ through the boundary $w = w_A - \Delta_w$ in order for $\Gamma(s,\sqrt{\epsilon})$ to complete the secondary excursion. The case $R(w_C^0, w_A - 3\Delta_w) > 0$ can be treated similarly.

Hence there is a canard trajectory on $\mathcal{Z}_\epsilon(c,a)$ which enters via $\Sigma^{h,\ell}$ at $w = w_C(\epsilon)$, then exits via $\Sigma^{h,\ell}$ at $w = w_A - 3\Delta_w$, and $w_C(\epsilon)$ satisfies $\lim_{\epsilon\to 0} w_C(\epsilon) = w_R(\Delta_w)$. Since the secondary excursion of a transitional pulse $\Gamma(s,\sqrt{\epsilon})$, $s \in [w_R^0, 2w^\dagger - w_A]$ meets $\Sigma^{h,\ell}$ at a height $w \geq w_R^0 > w_R(\Delta_w)$, the subsequent return to $\Sigma^{h,\ell}$ must occur at a height $w_A - 3\Delta_w \leq w < w_\epsilon^{\pitchfork}$ as claimed, and subsequent returns to $\Sigma^{h,\ell}$ are similarly determined by successive zeros of the way-in-way-out function R. We note that the choice of Δ_w in the above argument is arbitrary. Hence the argument can be repeated for arbitrarily small Δ_w for pulses $\Gamma(s,\sqrt{\epsilon})$,$s \in [w_R^0, 2w^\dagger - w_A]$ without affecting the limits $w_i(s,0)$, provided ϵ is correspondingly taken sufficiently small. Hence $w_1(s,0) = w_A$ for $s \in [w_R^0, 2w^\dagger - w_A]$ and the sequence $w_i(s), i = 2,\ldots,N(s)$ follows.

Finally, the estimates (iv) follow directly from the final matching conditions (4.16), (4.36), (4.47) for each of the pulse of type 1-5, where (c_E, a_E) are as defined in §4.2.1.

5 Flow near the Airy point

The goal of this section is to prove Proposition 4.5, as well as Lemma 4.7 and Lemma 4.9, regarding properties of the backwards evolution of certain trajectories on the manifolds $\mathcal{Y}(c,a,\epsilon), \mathcal{W}_\epsilon^{s,r}(c,a)$ which pass near the Airy point.

In particular, we need to track the manifold $\mathcal{Y}(c,a,\epsilon)$ in backwards time into a neighborhood of $\mathcal{M}_\epsilon^m(c,a)$ and determine its behavior near the canard point, in particular its transversality with respect to the strong unstable fibers in the section Σ^m. We recall that the intersection $\mathcal{Y}_{\text{end}}(c,a,\epsilon)$ of $\mathcal{Y}(c,a,\epsilon)$ with $\Sigma^{h,\ell}$ coincides with the intersection of $\mathcal{Z}_\epsilon(c,a)$ with $\Sigma^{h,\ell}$. Hence for trajectories on $\mathcal{Y}_{\text{end}}(c,a,\epsilon)$ in $\Sigma^{h,\ell}$ with $w < w_A - \Delta_w$, this behavior is clear: these trajectories are attracted exponentially close to $\mathcal{M}_\epsilon^m(c,a)$ and remain in the invariant manifold $\mathcal{Z}_\epsilon(c,a)$ upon entering a neighborhood of the canard point. Hence there is transversality with respect to the strong unstable fibers in Σ^m.

However, for $w \geq w_A - \Delta_w$, the behavior is not so clear since near $\mathcal{M}_\epsilon^m(c,a)$, the manifold $\mathcal{Z}_\epsilon(c,a)$ is not defined for $w \geq w_A - \Delta_w$ due to the lack of spectral gap in the linearization of the vector field. Therefore, such trajectories on $\mathcal{Y}(c,a,\epsilon)$ are still exponentially attracted to $\mathcal{M}_\epsilon^m(c,a)$ in backwards time, but in general do not remain on $\mathcal{Z}_\epsilon(c,a)$ upon reaching $w = w_A - \Delta_w$ due to the interaction with the focus-like properties of the manifold $\mathcal{M}_\epsilon^m(c,a)$ (see Figure 22 – note that the flow direction is reversed in this figure). To understand the transition from node to focus, we must understand the flow near the Airy point. The goal is to show that even though the backwards evolution of $\mathcal{Y}(c,a,\epsilon)$ leaves the manifold $\mathcal{Z}_\epsilon(c,a)$ on the journey from $\Sigma^{h,\ell}$ to Σ^m, we retain the desired transversality properties for trajectories on $\mathcal{Y}(c,a,\epsilon)$ which meet $\Sigma^{h,\ell}$ a bit above the Airy point, specifically for $w < w_A + C\epsilon^{2/3}$ for some $C > 0$.

The Airy point (u_A, w_A) is defined by the conditions $c^2 = 4f'(u_A)$ and $w_A = f(u_A)$. In a neighborhood of this point, the manifold $\mathcal{M}_\epsilon^m(c,a)$ can be written as a graph $(u,v) = (u_A + h(w,\epsilon), g(w,\epsilon))$ where

$$\begin{aligned} h(w,\epsilon) &= \frac{1}{f'(u_A)}(w - w_A) + \mathcal{O}\left(\epsilon, (w - w_A)^2\right) \\ g(w,\epsilon) &= \mathcal{O}\left(\epsilon, (w - w_A)\right). \end{aligned} \tag{5.1}$$

We make the coordinate transformation

$$\begin{aligned} x &= \frac{2}{c}\left(v - g(w,\epsilon)\right) - \left(u - u_A - h(w,\epsilon)\right) \\ y &= \frac{4f''(u_A)}{c^2 f'(u_A)}(w - w_A) \\ z &= u - u_A - h(w,\epsilon), \end{aligned} \tag{5.2}$$

and rescale time by $-(c/2)$ to arrive at the system

$$\begin{aligned} \dot{x} &= -x + yz + H(y,z,\epsilon)z \\ \dot{z} &= -x - z + \mathcal{O}(\epsilon z) \\ \dot{y} &= \epsilon\left(-k + \mathcal{O}(y,z,\epsilon)\right), \end{aligned} \tag{5.3}$$

where

$$H(y,z,\epsilon) = \mathcal{O}(y^2, z, \epsilon), \tag{5.4}$$

and

$$k = \frac{2f''(u_A)}{cf'(u_A)^2}(u_A - \gamma w_A) > 0. \tag{5.5}$$

Note that the flow direction has been reversed. We make a final coordinate change $y \to y + \mathcal{O}(y^2, \epsilon)$ to simplify the equation for $\dot{x}$ and arrive at the system

$$\begin{aligned} \dot{x} &= -x + yz + \mathcal{O}(z^2) \\ \dot{z} &= -x - z + \mathcal{O}(\epsilon z) \\ \dot{y} &= \epsilon\left(-k + \mathcal{O}(x,y,z,\epsilon)\right), \end{aligned} \tag{5.6}$$

We consider solutions entering via the section

$$\Sigma_A^{in} = \{(x,y,z,\epsilon) : x = \rho^4,\ |y| \le \rho^2,\ |z| \le \rho^3\mu,\ 0 < \epsilon \le \rho^3\delta\}. \tag{5.7}$$

Such solutions exit via the section

$$\Sigma_A^{out} = \{(x,y,z,\epsilon) : |x| \le \rho^4,\ y = -\rho^2,\ |z| \le \rho^3\mu,\ 0 < \epsilon \le \rho^3\delta\}. \tag{5.8}$$

The goal of this section is to prove Proposition 4.5, that is, we track the backwards evolution of the manifolds $\mathcal{Y}(c,a,\epsilon), \mathcal{W}_\epsilon^{s,r}(c,a)$ near the Airy point until they exit via Σ_A^{out}, where we then use an exchange lemma type argument to track the rest of the way to Σ^m. In the following, we use the labels ℓ, r to refer to objects associated with the manifolds $\mathcal{Y}(c,a,\epsilon), \mathcal{W}_\epsilon^{s,r}(c,a)$, respectively, due to the fact that in solutions on $\mathcal{Y}(c,a,\epsilon)$ (resp. $\mathcal{W}_\epsilon^{s,r}(c,a)$) originate from the left (resp. right) of the Airy point.

To start, we have the following regarding the entry of the manifolds $\mathcal{Y}(c,a,\epsilon), \mathcal{W}_\epsilon^{s,r}(c,a)$ in Σ_A^{in}.

Lemma 5.1. *For each sufficiently small $\Delta_y > 0$ there exists $\epsilon_0 > 0$ and sufficiently small choice of the intervals $I_c \times I_a$, such that for $(c,a,\epsilon) \in I_c \times I_a \times (0,\epsilon_0)$, the manifolds $\mathcal{Y}(c,a,\epsilon), \mathcal{W}_\epsilon^{s,r}(c,a)$ intersect Σ_A^{in} in curves $z = z_\epsilon^{s,\ell}(y;c,a), z_\epsilon^{s,r}(y;c,a)$, respectively, for $|y| \le \Delta_y$. Furthermore, there exists a constant $\kappa = \kappa(\rho) > 0$ such that*

$$z_\epsilon^{s,r}(y;c,a) - z_\epsilon^{s,\ell}(y;c,a) > \rho^3\kappa(\rho) \tag{5.9}$$

uniformly in $|y| \le \Delta_y$.

Proof. Using Proposition A.1, we find that for $(c, a, \epsilon) = (1/\sqrt{2}, 0, 0)$, the front ϕ_ℓ is asymptotic (in forward time according to 5.6) to the Airy point $(x, y, z) = (0, 0, 0)$ and satisfies

$$\begin{aligned} x(s) &= 2\sqrt{2}B_\ell e^{\frac{-s}{2\sqrt{2}}} + \mathcal{O}(s^2 e^{\frac{-s}{\sqrt{2}}}) \\ z(s) &= (A_\ell - B_\ell s)e^{\frac{-s}{2\sqrt{2}}} + \mathcal{O}(s^2 e^{\frac{-s}{\sqrt{2}}}). \end{aligned} \tag{5.10}$$

Therefore, ϕ_ℓ intersects Σ_A^{in} at the point $(x, y, z) = (\rho^4, 0, z_0^\ell)$ where

$$\begin{aligned} z_0^\ell &= \rho^4 \left(\frac{A_\ell}{2\sqrt{2}B_\ell} + \log\left(\frac{\rho^4}{2\sqrt{2}B_\ell} \right) \right) + o(\rho^4) \\ &= 4\rho^4 \log\left(\frac{\rho}{2\sqrt{2}B_\ell} \right) + \mathcal{O}(\rho^4). \end{aligned} \tag{5.11}$$

Therefore, by a regular perturbation argument, we have for sufficiently small Δ_y and any $(c, a) \in I_c \times I_a$, for $|y| \leq \Delta_y$, the manifold $\mathcal{Y}(c, a, 0)$ intersects Σ_A^{in} in a curve $z = z_0^{s,\ell}(y; c, a)$ given by

$$z_0^{s,\ell}(y; c, a) = z_0^\ell + \mathcal{O}(y, (c - c^*), a). \tag{5.12}$$

By using standard geometric singular perturbation theory, for sufficiently small $\epsilon > 0$, the perturbed manifold $\mathcal{Y}(c, a, \epsilon)$ intersects Σ_A^{in} in a smooth curve $z = z_\epsilon^{s,\ell}(y; c, a)$ given by

$$z_\epsilon^{s,\ell}(y; c, a) = z_0^\ell + \mathcal{O}(y, (c - c^*), a, \epsilon), \tag{5.13}$$

for $|y| \leq \Delta_y$. We similarly obtain that $\mathcal{W}_\epsilon^{s,r}(c, a)$ intersects Σ_A^{in} in a smooth curve $z = z_\epsilon^{s,r}(y; c, a)$ given by

$$z_\epsilon^{s,r}(y; c, a) = z_0^r + \mathcal{O}(y, (c - c^*), a, \epsilon), \tag{5.14}$$

for $|y| \leq \Delta_y$. Using Proposition A.1, and taking $\Delta_y \ll \rho^4$ sufficiently small, we deduce that there exists $\kappa = \kappa(\rho) > 0$ such that

$$z_\epsilon^{s,r}(y; c, a) - z_\epsilon^{s,\ell}(y; c, a) > \rho^3 \kappa(\rho) \tag{5.15}$$

uniformly in $|y| \leq \Delta_y$. □

By taking $\Delta_y := 2k\Delta_w$ sufficiently small, we reduce the study of Proposition 4.5 to just understanding the passage of trajectories on $\mathcal{Y}(c, a, \epsilon)$ which enter a neighborhood of the Airy point in backwards time in a manner governed by Lemma 5.1; these solutions interact with the flow near the Airy point in a nontrivial manner (see Figure 22). All solutions on $\mathcal{Y}(c, a, \epsilon)$ entering a neighborhood of $\mathcal{M}_\epsilon^m(c, a)$ in backwards time at heights lower than this remain in $\mathcal{Z}_\epsilon(c, a)$ until arriving at the section Σ^m due to the nature of the construction of this manifold in §3.1.

To accomplish this, we need to understand detailed properties of the flow of (5.6). Ultimately, we will show that the flow of (5.6) is qualitatively similar to the flow of the simpler system

$$\begin{aligned} \dot{x} &= -x + yz \\ \dot{z} &= -x - z \\ \dot{y} &= -\epsilon, \end{aligned} \tag{5.16}$$

which are essentially the Airy equations on a slow timescale coupled with exponential decay. The solutions of this system are given in terms of the Airy functions Ai, Bi, and their derivatives, which are shown in Figure 23.

We begin by solving the simpler system (5.16) to demonstrate why it is reasonable to expect that the transversality properties of Proposition 4.5 should indeed hold. Then we will use blow up techniques to study (5.6) directly to show that Proposition 4.5 continues to be valid when including the higher order terms.

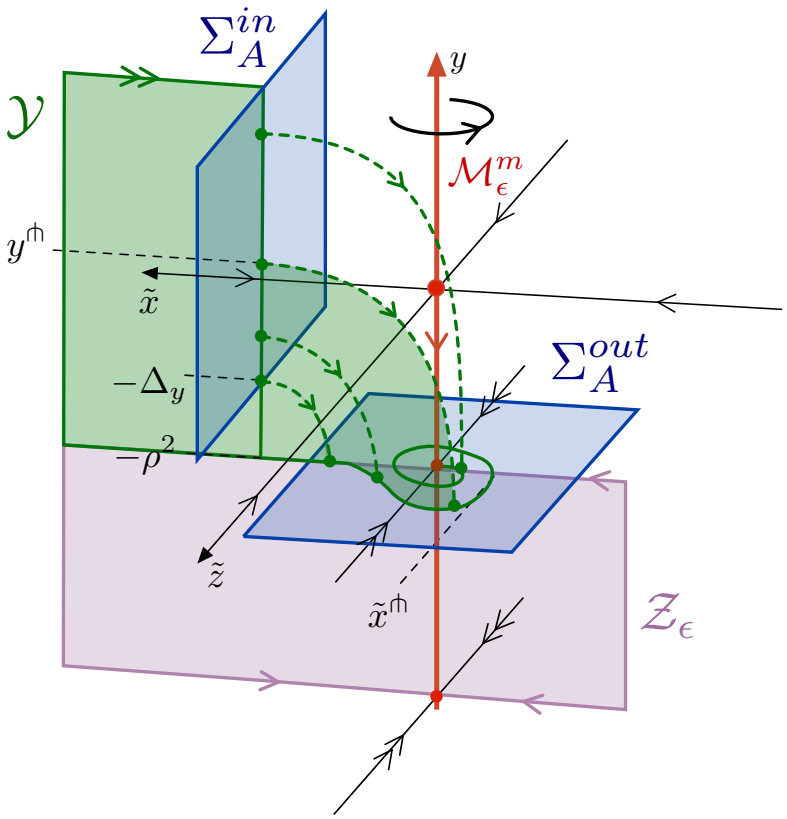

Figure 22: *Shown is the schematic of the flow near the Airy point. Note that the flow direction corresponds to that of* (5.6)*, which is the reverse of* (1.2)*.*

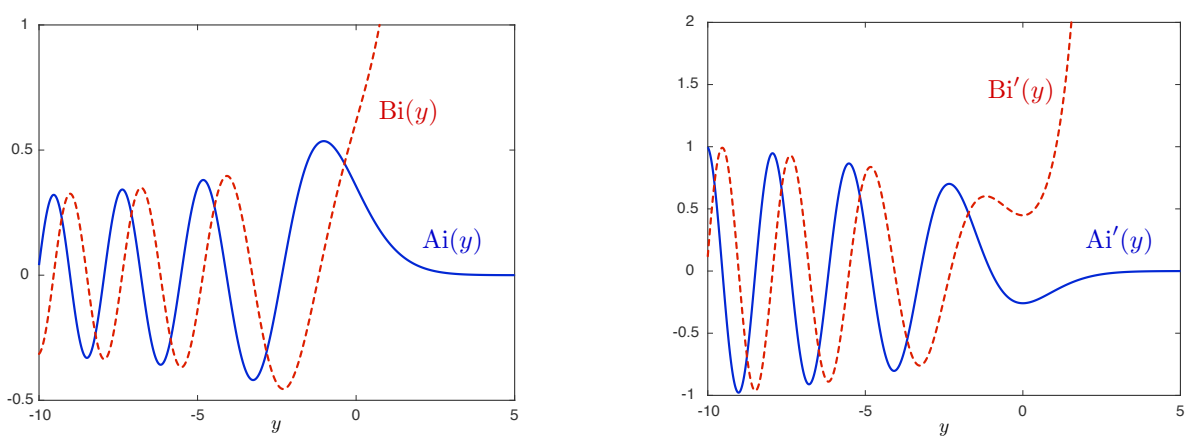

(a) *The Airy functions* Ai(y) *(blue) and* Bi(y) *(dashed red).*

(b) *The derivatives* Ai$'(y)$ *(blue) and* Bi$'(y)$ *(dashed red) of the Airy functions* Ai(y), Bi(y)*.*

Figure 23: *Shown are graphs of the Airy functions* Ai, Bi *and their derivatives.*

5.1 A simpler system

We are concerned with the passage of trajectories on $\mathcal{Y}(c,a,\epsilon)$ from Σ_A^{in} to Σ_A^{out}. In this section, as motivation for the full proof in the following sections for the system (5.6), we first consider the simpler system (5.16). The goal is to show that $\mathcal{Y}(c,a,\epsilon)$ intersects Σ_A^{out} in a curve transverse to the fibers of the manifold $\mathcal{Z}_\epsilon(c,a)$. Then, using the exchange lemma, we deduce that the transversality holds in the section Σ^m as well. We note that for trajectories entering Σ_A^{in} for $y < -\Delta_y$, this transversality is clear as due to the construction of the invariant manifold $\mathcal{Z}_\epsilon(c,a)$ in §3.1. Hence we are primarily concerned with the trajectories for $y_0 > -\Delta_y$, whose intersections with Σ_A^{out} we will explicitly compute below. This is precisely the regime in which the manifolds $\mathcal{Y}(c,a,\epsilon)$ and $\mathcal{Z}_\epsilon(c,a)$ begin to deviate.

The system (5.16) is essentially the Airy equation on a slow timescale coupled with exponential decay. To see this, we rescale $(x,z) = (e^{-t}\bar{x}, e^{-t}\bar{z})$ and obtain the equations

$$\begin{aligned}\dot{\bar{x}} &= y\bar{z}\\ \dot{\bar{z}} &= -\bar{x}\\ \dot{y} &= -\epsilon.\end{aligned} \tag{5.17}$$

The solutions of this system can be given explicitly in terms of Airy functions Ai, Bi (see Figure 23)

$$\begin{aligned}\bar{x}(t) &= \pi\left[\left(\mathrm{Ai}\left(-\frac{y_0}{\epsilon^{2/3}}\right)\mathrm{Bi}'\left(-\frac{y_0}{\epsilon^{2/3}}+\epsilon^{1/3}t\right) - \mathrm{Bi}\left(-\frac{y_0}{\epsilon^{2/3}}\right)\mathrm{Ai}'\left(-\frac{y_0}{\epsilon^{2/3}}+\epsilon^{1/3}t\right)\right)x_0\right.\\ &\quad\left.+\,\epsilon^{1/3}\left(\mathrm{Ai}'\left(-\frac{y_0}{\epsilon^{2/3}}\right)\mathrm{Bi}'\left(-\frac{y_0}{\epsilon^{2/3}}+\epsilon^{1/3}t\right) - \mathrm{Bi}'\left(-\frac{y_0}{\epsilon^{2/3}}\right)\mathrm{Ai}'\left(-\frac{y_0}{\epsilon^{2/3}}+\epsilon^{1/3}t\right)\right)z_0\right]\\ \bar{z}(t) &= \frac{\pi}{\epsilon^{1/3}}\left[\left(\mathrm{Bi}\left(-\frac{y_0}{\epsilon^{2/3}}\right)\mathrm{Ai}\left(-\frac{y_0}{\epsilon^{2/3}}+\epsilon^{1/3}t\right) - \mathrm{Ai}\left(-\frac{y_0}{\epsilon^{2/3}}\right)\mathrm{Bi}\left(-\frac{y_0}{\epsilon^{2/3}}+\epsilon^{1/3}t\right)\right)x_0\right.\\ &\quad\left.+\,\epsilon^{1/3}\left(\mathrm{Bi}'\left(-\frac{y_0}{\epsilon^{2/3}}\right)\mathrm{Ai}\left(-\frac{y_0}{\epsilon^{2/3}}+\epsilon^{1/3}t\right) - \mathrm{Ai}'\left(-\frac{y_0}{\epsilon^{2/3}}\right)\mathrm{Bi}\left(-\frac{y_0}{\epsilon^{2/3}}+\epsilon^{1/3}t\right)\right)z_0\right]\\ y(t) &= y_0 - \epsilon t,\end{aligned} \tag{5.18}$$

where $y_0 = y(0)$, $x_0 = \bar{x}(0) = x(0)$, and $z_0 = \bar{z}(0) = z(0)$. This solution reaches $y = -\rho^2$ at time $T = \dfrac{y_0+\rho^2}{\epsilon}$ with

$$\begin{aligned}x(T) &= \pi e^{-\frac{y_0+\rho^2}{\epsilon}}\left[\left(\mathrm{Ai}\left(-\frac{y_0}{\epsilon^{2/3}}\right)\mathrm{Bi}'\left(\frac{\rho^2}{\epsilon^{2/3}}\right) - \mathrm{Bi}\left(-\frac{y_0}{\epsilon^{2/3}}\right)\mathrm{Ai}'\left(\frac{\rho^2}{\epsilon^{2/3}}\right)\right)x_0\right.\\ &\quad\left.+\,\epsilon^{1/3}\left(\mathrm{Ai}'\left(-\frac{y_0}{\epsilon^{2/3}}\right)\mathrm{Bi}'\left(\frac{\rho^2}{\epsilon^{2/3}}\right) - \mathrm{Bi}'\left(-\frac{y_0}{\epsilon^{2/3}}\right)\mathrm{Ai}'\left(\frac{\rho^2}{\epsilon^{2/3}}\right)\right)z_0\right]\\ z(T) &= \frac{\pi}{\epsilon^{1/3}}e^{-\frac{y_0+\rho^2}{\epsilon}}\left[\left(\mathrm{Bi}\left(-\frac{y_0}{\epsilon^{2/3}}\right)\mathrm{Ai}\left(\frac{\rho^2}{\epsilon^{2/3}}\right) - \mathrm{Ai}\left(-\frac{y_0}{\epsilon^{2/3}}\right)\mathrm{Bi}\left(\frac{\rho^2}{\epsilon^{2/3}}\right)\right)x_0\right.\\ &\quad\left.+\,\epsilon^{1/3}\left(\mathrm{Bi}'\left(-\frac{y_0}{\epsilon^{2/3}}\right)\mathrm{Ai}\left(\frac{\rho^2}{\epsilon^{2/3}}\right) - \mathrm{Ai}'\left(-\frac{y_0}{\epsilon^{2/3}}\right)\mathrm{Bi}\left(\frac{\rho^2}{\epsilon^{2/3}}\right)\right)z_0\right]\\ y(T) &= -\rho^2.\end{aligned} \tag{5.19}$$

Using asymptotic properties of Airy functions [1, §10.4], we have the following

Lemma 5.2. *The Airy functions* $\mathrm{Ai}(y), \mathrm{Bi}(y)$ *have the following asymptotics for all sufficiently large* $y \gg 1$

$$\begin{aligned}\mathrm{Ai}(y) &= \frac{e^{-\frac{2}{3}y^{3/2}}}{2\sqrt{\pi}y^{1/4}}\left(1 - \frac{15}{144y^{3/2}} + \mathcal{O}\left(y^{-3}\right)\right),\\ \mathrm{Ai}'(y) &= \frac{-y^{1/4}e^{-\frac{2}{3}y^{3/2}}}{2\sqrt{\pi}}\left(1 + \frac{21}{144y^{3/2}} + \mathcal{O}\left(y^{-3}\right)\right),\\ \mathrm{Bi}(y) &= \frac{e^{\frac{2}{3}y^{3/2}}}{\sqrt{\pi}y^{1/4}}\left(1 + \frac{15}{144y^{3/2}} + \mathcal{O}\left(y^{-3}\right)\right),\\ \mathrm{Bi}'(y) &= \frac{y^{1/4}e^{\frac{2}{3}y^{3/2}}}{\sqrt{\pi}}\left(1 + \frac{21}{144y^{3/2}} + \mathcal{O}\left(y^{-3}\right)\right).\end{aligned} \tag{5.20}$$

Considering the linearization of (5.16) for $\epsilon = 0$ in the plane $y = -\rho^2$, we see that there are two eigenvalues $\lambda = -1 \pm \rho$ with corresponding eigenvectors $(\mp\rho, 1)$. We now change coordinates $\tilde{x} = x - \rho z, \tilde{z} = x + \rho z$ and using Lemma 5.2 under the assumption that $0 < \epsilon^{2/3} \ll \Delta_y \ll \rho^2 \ll 1$, we can expand the terms dependent on the fixed argument $\dfrac{\rho^2}{\epsilon^{2/3}}$ to obtain

$$\begin{aligned}
\tilde{x}(T) &= \frac{\rho^{1/2}\sqrt{\pi}}{\epsilon^{1/6}} e^{-\frac{y_0+\rho^2}{\epsilon}} \left[\left(x_0 \operatorname{Ai}\left(-\frac{y_0}{\epsilon^{2/3}}\right) + \epsilon^{1/3} z_0 \operatorname{Ai}'\left(-\frac{y_0}{\epsilon^{2/3}}\right)\right) e^{\frac{2\rho^3}{3\epsilon}} \left(2 + \mathcal{O}(\epsilon)\right) \right. \\
&\quad \left. + \left(x_0 \operatorname{Bi}\left(-\frac{y_0}{\epsilon^{2/3}}\right) + \epsilon^{1/3} z_0 \operatorname{Bi}'\left(-\frac{y_0}{\epsilon^{2/3}}\right)\right) e^{-\frac{2\rho^3}{3\epsilon}} \left(\frac{\epsilon}{8\rho^3} + \mathcal{O}\left(\epsilon^2\right)\right) \right] \\
\tilde{z}(T) &= \frac{\rho^{1/2}\sqrt{\pi}}{\epsilon^{1/6}} e^{-\frac{y_0+\rho^2}{\epsilon}} \left[\left(x_0 \operatorname{Ai}\left(-\frac{y_0}{\epsilon^{2/3}}\right) + \epsilon^{1/3} z_0 \operatorname{Ai}'\left(-\frac{y_0}{\epsilon^{2/3}}\right)\right) e^{\frac{2\rho^3}{3\epsilon}} \left(\frac{\epsilon}{24\rho^3} + \mathcal{O}\left(\epsilon^2\right)\right) \right. \\
&\quad \left. + \left(x_0 \operatorname{Bi}\left(-\frac{y_0}{\epsilon^{2/3}}\right) + \epsilon^{1/3} z_0 \operatorname{Bi}'\left(-\frac{y_0}{\epsilon^{2/3}}\right)\right) e^{-\frac{2\rho^3}{3\epsilon}} \left(1 + \mathcal{O}(\epsilon)\right) \right] \\
y(T) &= -\rho^2.
\end{aligned} \tag{5.21}$$

We now consider solutions on $\mathcal{Y}(c, a, \epsilon)$ which enter via Σ_A^{in}, with $(x, y, z)(0) = (x_0, y_0, z_0) = (\rho^4, y_0, z_\epsilon^{s,\ell}(y_0; c, a))$, where $z_\epsilon^{s,\ell}(y_0; c, a) < 0$, so that $\mathcal{Y}(c, a, \epsilon)$ is parameterized in Σ_A^{in} by $|y_0| \le \Delta_y$. Using the above analysis, $\mathcal{Y}(c, a, \epsilon)$ exits via Σ_A^{out} in a curve $(\tilde{x}, \tilde{z}) = (\tilde{x}^\ell, \tilde{z}^\ell)(y_0)$ given by

$$\begin{aligned}
\tilde{x}^\ell(y_0) &= \frac{\rho^{1/2}\sqrt{\pi}}{\epsilon^{1/6}} e^{-\frac{y_0+\rho^2}{\epsilon}} \tilde{X}^\ell(y_0) \\
\tilde{z}^\ell(y_0) &= \frac{\rho^{1/2}\sqrt{\pi}}{\epsilon^{1/6}} e^{-\frac{y_0+\rho^2}{\epsilon}} \tilde{Z}^\ell(y_0)
\end{aligned} \tag{5.22}$$

where

$$\begin{aligned}
\tilde{X}^\ell(y_0) &= \left(\rho^4 \operatorname{Ai}\left(-\frac{y_0}{\epsilon^{2/3}}\right) + \epsilon^{1/3} z_\epsilon^{s,\ell}(y_0) \operatorname{Ai}'\left(-\frac{y_0}{\epsilon^{2/3}}\right)\right) e^{\frac{2\rho^3}{3\epsilon}} \left(2 + \mathcal{O}(\epsilon)\right) \\
&\quad + \left(\rho^4 \operatorname{Bi}\left(-\frac{y_0}{\epsilon^{2/3}}\right) + \epsilon^{1/3} z_\epsilon^{s,\ell}(y_0) \operatorname{Bi}'\left(-\frac{y_0}{\epsilon^{2/3}}\right)\right) e^{-\frac{2\rho^3}{3\epsilon}} \left(\frac{\epsilon}{8\rho^3} + \mathcal{O}\left(\epsilon^2\right)\right) \\
\tilde{Z}^\ell(y_0) &= \left(\rho^4 \operatorname{Ai}\left(-\frac{y_0}{\epsilon^{2/3}}\right) + \epsilon^{1/3} z_\epsilon^{s,\ell}(y_0) \operatorname{Ai}'\left(-\frac{y_0}{\epsilon^{2/3}}\right)\right) e^{\frac{2\rho^3}{3\epsilon}} \left(\frac{\epsilon}{24\rho^3} + \mathcal{O}\left(\epsilon^2\right)\right) \\
&\quad + \left(\rho^4 \operatorname{Bi}\left(-\frac{y_0}{\epsilon^{2/3}}\right) + \epsilon^{1/3} z_\epsilon^{s,\ell}(y_0) \operatorname{Bi}'\left(-\frac{y_0}{\epsilon^{2/3}}\right)\right) e^{-\frac{2\rho^3}{3\epsilon}} \left(1 + \mathcal{O}(\epsilon)\right).
\end{aligned} \tag{5.23}$$

We now want to understand the transversality of this curve with respect to the fibers of the manifold $\mathcal{Z}_\epsilon(c, a)$ in the section Σ_A^{out}. Under the transformation to the $\sim$ coordinates corresponding to the strong/weak eigenspaces of the linearization of (5.16), the manifold $\mathcal{Z}_\epsilon(c, a)$ will manifest as a curve in Σ_A^{out} aligned approximately with the subspace $\tilde{z} = 0$ and its fibers will manifest as curves aligned approximately with $\tilde{x} \approx$ const. It is clear from the expressions above that the same does not hold for $\mathcal{Y}(c, a, \epsilon)$ when y_0 gets too large, as the Airy functions transition to oscillatory behavior.

We compute the derivatives

$$\begin{aligned}
(\tilde{x}^\ell)'(y_0) &= -\frac{\rho^{1/2}\sqrt{\pi}}{\epsilon^{7/6}} e^{-\frac{y_0+\rho^2}{\epsilon}} \left(\tilde{X}^\ell(y_0) + \epsilon(\tilde{X}^\ell)'(y_0)\right) \\
(\tilde{z}^\ell)'(y_0) &= -\frac{\rho^{1/2}\sqrt{\pi}}{\epsilon^{7/6}} e^{-\frac{y_0+\rho^2}{\epsilon}} \left(\tilde{Z}^\ell(y_0) + \epsilon(\tilde{Z}^\ell)'(y_0)\right),
\end{aligned} \tag{5.24}$$

and hence in Σ_A^{out}, $\mathcal{Y}(c, a, \epsilon)$ can be written as a graph $\tilde{z} = \tilde{z}(\tilde{x})$ with

$$\frac{d\tilde{z}}{d\tilde{x}} = \frac{(\tilde{z}^\ell)'(y_0)}{(\tilde{x}^\ell)'(y_0)} = \frac{\tilde{Z}^\ell(y_0) + \epsilon(\tilde{Z}^\ell)'(y_0)}{\tilde{X}^\ell(y_0) + \epsilon(\tilde{X}^\ell)'(y_0)}, \tag{5.25}$$

provided that the denominator does not vanish. Points at which the denominator vanishes are essentially those at which this curve becomes tangent to the fibers $\tilde{x} \approx$ const of $\mathcal{Z}_\epsilon(c,a)$. Hence we reduce our study to finding zeros of this expression. This will be carried out in detail in the following sections, but we note that they occur approximately at the zeros of $\tilde{X}^\ell(y_0)$, which are approximately the zeros of Ai $\left(-y_0/\epsilon^{2/3}\right)$ for all sufficiently small $\epsilon > 0$. Hence we are primarily concerned with studying the Airy function Ai. We have the following [1, §10.4]

Lemma 5.3. *There exists $y^* < 0$ such that the Airy function* Ai *satisfies the following*

(i) $\mathrm{Ai}(y^*) = 0$

(ii) $\mathrm{Ai}'(y^*) > 0$

(iii) $\mathrm{Ai}(y) > 0$ *for all* $y > y^*$.

We can therefore find the first zero of the denominator or equivalently, the first turning point of $\mathcal{Y}(c,a,\epsilon)$, which occurs when $y_0 = y_0^{\pitchfork} \approx -y^*\epsilon^{2/3} > 0$. Therefore $\mathcal{Y}(c,a,\epsilon)$ is transverse to the fibers of $\mathcal{Z}_\epsilon(c,a)$ in Σ_A^{out} up to the fiber passing through the point $(\tilde{x}^{\pitchfork}, \tilde{z}(\tilde{x}^{\pitchfork})) = (\tilde{x}^\ell(y_0^{\pitchfork}), \tilde{z}^\ell(y_0^{\pitchfork}))$. A schematic of this result is depicting in Figure 22.

Using an inclination lemma, we continue to track $\mathcal{Y}(c,a,\epsilon)$ backwards from Σ_A^{out} to the section Σ^m and deduce that this transversality holds there also.

In the coming sections, we consider the full system (5.6), and we make the above computations precise in this context.

5.2 Blow up transformation

To study the flow of the full equations (5.6)

$$\begin{aligned}\dot{x} &= -x + yz + \mathcal{O}(z^2)\\ \dot{z} &= -x - z + \mathcal{O}(\epsilon z)\\ \dot{y} &= \epsilon\left(-k + \mathcal{O}(x,y,z,\epsilon)\right),\end{aligned}$$

we will use blow up techniques. The blow up is a rescaling which blows up the degenerate point $(x,y,z,\epsilon) = (0,0,0,0)$ to a 3-sphere. The blow up transformation is given by

$$x = \bar{r}^4\bar{x}, \quad y = \bar{r}^2\bar{y}, \quad z = \bar{r}^3\bar{z}, \quad \epsilon = \bar{r}^3\bar{\epsilon}\ . \tag{5.26}$$

Defining $B_A = S^3 \times [0,\bar{r}_0]$ for some sufficiently small $\bar{r}_0$, we consider the blow up as a mapping $B_A \to \mathbb{R}^4$ with $(\bar{x},\bar{y},\bar{z},\bar{\epsilon}) \in S^3$ and $\bar{r} \in [0,\bar{r}_0]$. The point $(x,y,z,\epsilon) = (0,0,0,0)$ is now represented as a copy of S^3 (i.e. $\bar{r} = 0$) in the blow up transformation. To study the flow on the manifold B_A, there are three relevant coordinate charts. The first is the chart $\mathcal{K}_1$ which uses the coordinates

$$x = r_1^4, \quad y = r_1^2 y_1, \quad z = r_1^3 z_1, \quad \epsilon = r_1^3\epsilon_1\ , \tag{5.27}$$

the second chart $\mathcal{K}_2$ uses the coordinates

$$x = r_2^4 x_2, \quad y = r_2^2 y_2, \quad z = r_2^3 z_2, \quad \epsilon = r_2^3\ , \tag{5.28}$$

and the third chart $\mathcal{K}_3$ uses the coordinates

$$x = r_3^4 x_3, \quad y = -r_3^2, \quad z = r_3^3 z_3, \quad \epsilon = r_3^3\epsilon_3\ , \tag{5.29}$$

With these three sets of coordinates, a short calculation gives the following.

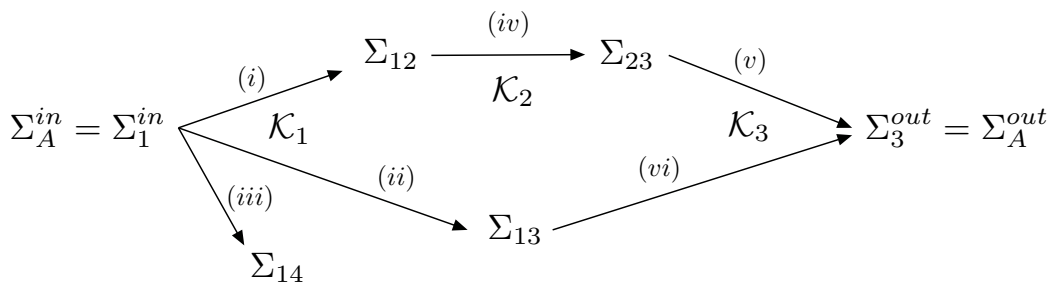

(i)	(ii)	(iii)	(iv)	(v)	(vi)
$\mathcal{K}_1$	$\mathcal{K}_1$	$\mathcal{K}_1$	$\mathcal{K}_2$	$\mathcal{K}_3$	$\mathcal{K}_3$
§5.3	§5.3	§5.3	§5.4	§5.5.1	§5.5.2

Figure 24: *Shown is the sequence of sections through which the manifold $\mathcal{Y}(c,a,\epsilon)$ will be tracked. The table displays the charts and sections in the text in which the various transitions will be studied.*

Lemma 5.4. *The transition map $\kappa_{12}:\mathcal{K}_1\to\mathcal{K}_2$ between the coordinates in $\mathcal{K}_1$ and $\mathcal{K}_2$ is given by*

$$x_2=\frac{1}{\epsilon_1^{4/3}},\quad y_2=\frac{y_1}{\epsilon_1^{2/3}},\quad z_2=\frac{z_1}{\epsilon_1},\quad r_2=r_1\epsilon_1^{1/3},\quad \text{for } \epsilon_1>0, \tag{5.30}$$

the transition map $\kappa_{13}:\mathcal{K}_1\to\mathcal{K}_3$ between the coordinates in $\mathcal{K}_1$ and $\mathcal{K}_3$ is given by

$$x_3=\frac{1}{y_1^2},\quad r_3=r_1(-y_1)^{1/2},\quad z_3=\frac{z_1}{(-y_1)^{3/2}},\quad \epsilon_3=\frac{\epsilon_1}{(-y_1)^{3/2}},\quad \text{for } y_1<0, \tag{5.31}$$

and the transition map $\kappa_{23}:\mathcal{K}_2\to\mathcal{K}_3$ between the coordinates in $\mathcal{K}_2$ and $\mathcal{K}_3$ is given by

$$x_3=\frac{x_2}{y_2^2},\quad r_3=r_2(-y_2)^{1/2},\quad z_3=\frac{z_2}{(-y_2)^{3/2}},\quad \epsilon_3=\frac{1}{(-y_2)^{3/2}},\quad \text{for } y_2<0. \tag{5.32}$$

Solutions on $\mathcal{Y}(c,a,\epsilon)$ will enter via the section Σ_A^{in} and exit via Σ_A^{out}. During this passage, it will be necessary to track different parts of the manifold $\mathcal{Y}(c,a,\epsilon)$ in the different charts $\mathcal{K}_1,\mathcal{K}_2,\mathcal{K}_3$. A diagram of the sequence through which the solutions will be tracked is shown in Figure 24. We begin in §5.3 with a study of the chart $\mathcal{K}_1$, where all solutions enter via the section Σ_A^{in}.

5.3 Dynamics in $\mathcal{K}_1$

In the $\mathcal{K}_1$ coordinates, the equations are given by

$$\begin{aligned}
\dot r_1&=-\frac14 r_1+\frac14 r_1^2y_1z_1+\mathcal{O}\left(r_1^3z_1^2\right)\\
\dot z_1&=-\frac14 z_1-r_1-\frac34 r_1y_1z_1^2+\mathcal{O}\left(r_1^3\epsilon_1z_1,r_1^2z_1^3\right)\\
\dot y_1&=\frac12 y_1-kr_1\epsilon_1-\frac12 r_1y_1^2z_1+\mathcal{O}\left(r_1^2y_1z_1^2,r_1^5\epsilon_1,r_1^3\epsilon_1y_1,r_1^4\epsilon_1z_1,r_1^4\epsilon_1^2\right)\\
\dot\epsilon_1&=\frac34\epsilon_1-\frac34 r_1y_1z_1\epsilon_1+\mathcal{O}\left(r_1^2z_1^2\epsilon_1\right).
\end{aligned} \tag{5.33}$$

In these coordinates, the section Σ_A^{in} is given by

$$\Sigma_1^{in}=\{(r_1,y_1,z_1,\epsilon_1):r_1=\rho,\ |y_1|\le 1,\ |z_1|\le\mu,\ 0<\epsilon_1\le\delta\}. \tag{5.34}$$

Define the set

$$D_1=\{(r_1,y_1,z_1,\epsilon_1):0\le r_1\le\rho,\ |y_1|\le 1,\ |z_1|\le\mu,\ 0\le\epsilon_1\le\delta\}. \tag{5.35}$$

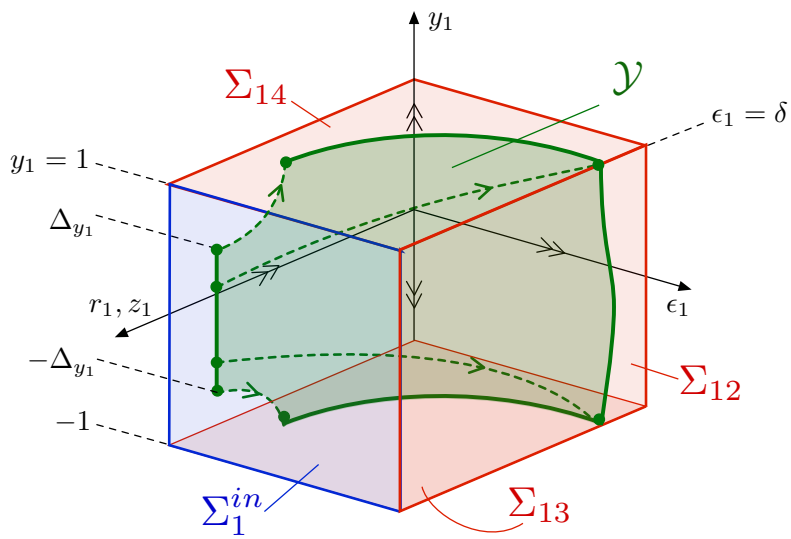

Figure 25: *Shown is the setup in the chart $\mathcal{K}_1$.*

Under the flow of (5.33), any solution starting in Σ_1^{in} exits D_1 via one of the sections

$$\Sigma_{12} = \{(r_1, y_1, z_1, \epsilon_1) : r_1 \leq \rho,\ |y_1| \leq 1,\ |z_1| \leq \mu,\ \epsilon_1 = \delta\} \tag{5.36}$$

$$\Sigma_{13} = \{(r_1, y_1, z_1, \epsilon_1) : r_1 \leq \rho,\ y_1 = -1,\ |z_1| \leq \mu,\ 0 < \epsilon_1 \leq \delta\} \tag{5.37}$$

$$\Sigma_{14} = \{(r_1, y_1, z_1, \epsilon_1) : r_1 \leq \rho,\ y_1 = 1,\ |z_1| \leq \mu,\ 0 < \epsilon_1 \leq \delta\}. \tag{5.38}$$

The setup in the chart $\mathcal{K}_1$ is shown in Figure 25. It turns out that we only need to consider those solutions exiting via Σ_{12} and Σ_{13}, which will be tracked in the charts $\mathcal{K}_2$ and $\mathcal{K}_3$, respectively (see Figure 24). Solutions exiting via Σ_{14} will not be analyzed.

The following result gives estimates for solutions on the manifolds $\mathcal{Y}(c, a, \epsilon)$ and $\mathcal{W}_\epsilon^{s,r}(c, a)$ which exit via the sections Σ_{12} and Σ_{13}.

Proposition 5.5. *For each sufficiently small $\rho, \delta > 0$, there exists $\epsilon_0 > 0$ and sufficiently small choice of the intervals I_c, I_a such that the following holds. For each sufficiently small $\Delta_{y_1} > 0$ and each $(c, a, \epsilon) \in I_c \times I_a \times (0, \epsilon_0)$, the manifolds $\mathcal{Y}(c, a, \epsilon)$ and $\mathcal{W}_\epsilon^{s,r}(c, a)$ intersect Σ_1^{in} in smooth curves $z_1 = z_{1,0}^{\ell}(y_1; c, a, \epsilon)$ and $z_1 = z_{1,0}^{r}(y_1; c, a, \epsilon)$ for $|y_1| \leq \Delta_{y_1}$. Furthermore, there exists $C > 0$ independent of c, a, ϵ and $0 < \kappa(\rho) \leq C_0 \rho\, |\log \rho|$ where C_0 is independent of $c, a, \epsilon, \rho, \delta$ such that for any $(c, a, \epsilon) \in I_c \times I_a \times (0, \epsilon_0)$, the following hold*

(i) The parts of the manifolds $\mathcal{Y}(c, a, \epsilon), \mathcal{W}_\epsilon^{s,r}(c, a)$ which exit via Σ_{13} intersect Σ_{13} in curves $z_1 = z_1^{\ell,r}(r_1)$ which satisfy $\left|\dfrac{dz_1^{\ell,r}}{dr_1}\right| \leq C|\log \epsilon|$ uniformly in y_1.

(ii) The parts of the manifolds $\mathcal{Y}(c, a, \epsilon), \mathcal{W}_\epsilon^{s,r}(c, a)$ which exit via Σ_{12} intersect Σ_{12} in curves $z_1 = z_1^{\ell,r}(y_1)$ which satisfy

$$\begin{aligned} \left|z_1^{\ell,r}\right| &\leq C\epsilon^{1/3}|\log \epsilon| \\ \left|\frac{dz_1^{\ell,r}}{dy_1}\right| &\leq C\epsilon|\log \epsilon| \end{aligned} \tag{5.39}$$

and

$$0 < \kappa(\rho)\epsilon^{1/3} < z_1^r(y_1) - z_1^\ell(y_1) < C\epsilon^{1/3}|\log \epsilon|. \tag{5.40}$$

uniformly in y_1.

Proof. We focus on the manifold $\mathcal{Y}(c,a,\epsilon)$; the computations for $\mathcal{W}^{s,r}_{\epsilon}(c,a)$ are similar.

First we consider the function $z^{\ell}_{1,0}(y_1;c,a,\epsilon)$. By taking $\Delta_{y_1} \ll \rho^2$, for any sufficiently small ρ we have that

$$\sup_{|y_1|\leq \Delta_{y_1}} |z^{\ell}_{1,0}(y_1;c,a,\epsilon)| \leq C_0\rho|\log\rho|$$
$$\sup_{|y_1|\leq \Delta_{y_1}} \left|\frac{dz^{\ell}_{1,0}(y_1;c,a,\epsilon)}{dy_1}\right| \leq C(\rho),$$

for some C_0 independent of $(c,a,\epsilon,\rho,\delta)$ and $C(\rho)$ independent of (c,a,ϵ,δ), provided ϵ and the intervals I_c, I_a are sufficiently small. This follows from Lemma 5.1 by taking $\rho^2\Delta_{y_1} = \Delta_y \ll \rho^4$.

To prove (i), for each sufficiently small $|y_{1,0}| \leq \Delta_{y_1}$, we consider solutions starting in Σ^{in}_A with $(r_1,z_1,y_1,\epsilon_1)(0) = (\rho, z^{\ell}_{1,0}(y_{1,0}), y_{1,0}, \epsilon/\rho^3)$ which exit via Σ_{13} at time $T^*_1(y_{1,0};c,a,\epsilon)$. As the solution exits via Σ_{13}, we must have $y_1(T^*_1) = -1$ and $\epsilon/\rho^3 < \epsilon_1(T^*_1) = \epsilon^*_1 \leq \delta$.

We define $\Phi_1(t,s)$ to be the linear evolution of the constant coefficient system

$$\begin{pmatrix} \dot{r}_1 \\ \dot{z}_1 \end{pmatrix} = \begin{pmatrix} -1/4 & 0 \\ -1 & -1/4 \end{pmatrix} \begin{pmatrix} r_1 \\ z_1 \end{pmatrix}. \tag{5.41}$$

We set

$$U_1 = \begin{pmatrix} r_1 \\ z_1 \end{pmatrix} \tag{5.42}$$

$$U_{1,0} = \begin{pmatrix} r_{1,0} \\ z^{\ell}_{1,0}(y_{1,0}) \end{pmatrix}, \tag{5.43}$$

and we rewrite (5.33) as the integral equation

$$\begin{aligned}
U_1(t) &= \Phi_1(t,0)U_{1,0} + \int_0^t \Phi_1(t,s) g_{U_1}(r_1(s),z_1(s),y_1(s),\epsilon_1(s))ds \\
&=: F_{U_1}(U_1,y_1,\epsilon_1,U_{1,0},T^*_1;c,a) \\
y_1(t) &= -e^{\frac{1}{2}(t-T^*_1)} + \int_{T^*_1}^t e^{\frac{1}{2}(t-s)} g_{y_1}(r_1(s),z_1(s),y_1(s),\epsilon_1(s))ds \\
&=: F_{y_1}(U_1,y_1,\epsilon_1,U_{1,0},T^*_1;c,a) \\
\epsilon_1(t) &= \frac{\epsilon}{\rho^3}e^{\frac{3}{4}t} + \int_0^t e^{\frac{3}{4}(t-s)} g_{\epsilon_1}(r_1(s),z_1(s),y_1(s),\epsilon_1(s))ds \\
&=: F_{\epsilon_1}(U_1,y_1,\epsilon_1,U_{1,0},T^*_1;c,a),
\end{aligned} \tag{5.44}$$

where

$$\begin{aligned}
g_{U_1}(r_1,z_1,y_1,\epsilon_1) &= \begin{pmatrix} \frac{1}{4}r_1^2y_1z_1 + \mathcal{O}\left(r_1^3z_1^2\right) \\ -\frac{3}{4}r_1y_1z_1^2 + \mathcal{O}\left(r_1^2z_1^3, r_1^3\epsilon_1z_1\right) \end{pmatrix} \\
&= \mathcal{O}\left(|U_1|^3\right) \\
g_{y_1}(r_1,z_1,y_1,\epsilon_1) &= -kr_1\epsilon_1 - \frac{1}{2}r_1y_1^2z_1 + \mathcal{O}\left(r_1^2y_1z_1^2, r_1^5\epsilon_1, r_1^3\epsilon_1y_1, r_1^4\epsilon_1z_1, r_1^4\epsilon_1^2\right) \\
&= \mathcal{O}\left(|U_1||\epsilon_1| + |U_1|^2|y_1|\right) \\
g_{\epsilon_1}(r_1,z_1,y_1,\epsilon_1) &= -\frac{3}{4}r_1y_1z_1\epsilon_1 + \mathcal{O}\left(r_1^2z_1^2\epsilon_1\right) \\
&= \mathcal{O}\left(|U_1|^2|\epsilon_1|\right),
\end{aligned} \tag{5.45}$$

and we assume $T_1^* \geq 0$ is such that $\left|\frac{\epsilon}{\rho^3} e^{\frac{3}{4}T_1^*}\right| \leq 2\delta$. We define the spaces

$$
\begin{aligned}
V_{\frac{1}{4}}^- &= \left\{ U_1 : [0, T_1^*] \to \mathbb{R}^2 : \|U_1\|_{\frac{1}{4}}^- = \sup_{t\in[0,T_1^*]} \frac{e^{\frac{1}{4}t}}{1+|t|} |U_1(t)| < \infty \right\} \\
V_{\frac{1}{2}}^+ &= \left\{ y_1 : [0, T_1^*] \to \mathbb{R} : \|y_1\|_{\frac{1}{2}}^+ = \sup_{t\in[0,T_1^*]} e^{\frac{1}{2}(T_1^*-t)} |y_1(t)| < \infty \right\} \\
V_{\frac{3}{4}}^+ &= \left\{ \epsilon_1 : [0, T_1^*] \to \mathbb{R} : \|\epsilon_1\|_{\frac{3}{4}}^+ = \sup_{t\in[0,T_1^*]} e^{\frac{3}{4}(T_1^*-t)} |\epsilon_1(t)| < \infty \right\},
\end{aligned}
\tag{5.46}
$$

and search for solutions $(U_1, y_1, \epsilon_1) \in V_{\frac{1}{4}}^- \times V_{\frac{1}{2}}^+ \times V_{\frac{3}{4}}^+$ to (5.44). We note that

$$
\|U_1\|_\infty \leq \|U_1\|_{\frac{1}{4}}^-, \quad \|y_1\|_\infty \leq \|y_1\|_{\frac{1}{2}}^+, \quad \|\epsilon_1\|_\infty \leq \|\epsilon_1\|_{\frac{3}{4}}^+, \tag{5.47}
$$

where $\|X\|_\infty = \sup_{t\in[0,T_1^*]} |X(t)|$ denotes the C^0-norm.

First we show that for each fixed $(U_{1,0}, T_1^*)$, the mapping

$$
(U_1, y_1, \epsilon_1) \to F_1(U_1, y_1, \epsilon_1, U_{1,0}, T_1^*; c, a), \tag{5.48}
$$

defined by

$$
F_1(U_1, y_1, \epsilon_1, U_{1,0}, T_1^*; c, a) = \begin{pmatrix} F_{U_1}(U_1, y_1, \epsilon_1, U_{1,0}, T_1^*; c, a) \\ F_{y_1}(U_1, y_1, \epsilon_1, U_{1,0}, T_1^*; c, a) \\ F_{\epsilon_1}(U_1, y_1, \epsilon_1, U_{1,0}, T_1^*; c, a) \end{pmatrix} \tag{5.49}
$$

maps the space $V_{\frac{1}{4}}^- \times V_{\frac{1}{2}}^+ \times V_{\frac{3}{4}}^+$ into itself. We compute

$$
\begin{aligned}
\|F_{U_1}(U_1, y_1, \epsilon_1, U_{1,0}, T_1^*; c, a)\|_{\frac{1}{4}}^- &= \sup_{t\in[0,T_1^*]} \frac{e^{\frac{1}{4}t}}{1+|t|} \left(\Phi_1(t,0)U_{1,0} + \int_0^t \Phi_1(t,s) g_{U_1}(r_1(s), z_1(s), y_1(s), \epsilon_1(s)) ds \right) \\
&\leq C|U_{1,0}| + C\left(\|U_1\|_{\frac{1}{4}}^-\right)^3,
\end{aligned}
\tag{5.50}
$$

where we used (5.47) and the fact that $|\Phi_1(t,s)| \leq |t-s| e^{-\frac{1}{4}(t-s)}$.

Similarly, we compute

$$
\begin{aligned}
\|F_{y_1}(U_1, y_1, \epsilon_1, U_{1,0}, T_1^*; c, a)\|_{\frac{1}{2}}^+ &= \sup_{t\in[0,T_1^*]} e^{\frac{1}{2}(T_1^*-t)} \left(e^{\frac{1}{2}(t-T_1^*)} + \int_{T_1^*}^t e^{\frac{1}{2}(t-s)} g_{y_1}(r_1(s), z_1(s), y_1(s), \epsilon_1(s)) ds \right) \\
&\leq 1 + Ce^{\frac{1}{2}T_1^*} \int_0^{T_1^*} e^{-\frac{1}{2}s} \left(|U_1(s)||\epsilon_1(s)| + |U_1(s)|^2 |y_1(s)| \right) ds \\
&\leq 1 + C\left(\|U_1\|_{\frac{1}{4}}^- \|\epsilon_1\|_{\frac{3}{4}}^+ + \left(\|U_1\|_{\frac{1}{4}}^-\right)^2 \|y_1\|_{\frac{1}{2}}^+ \right),
\end{aligned}
\tag{5.51}
$$

and

$$
\begin{aligned}
\|F_{\epsilon_1}(U_1, y_1, \epsilon_1, U_{1,0}, T_1^*; c, a)\|_{\frac{3}{4}}^+ &= \sup_{t\in[0,T_1^*]} e^{\frac{3}{4}(T_1^*-t)} \left(\frac{\epsilon}{\rho^3} e^{\frac{3}{4}t} + \int_0^t e^{\frac{3}{4}(t-s)} g_{\epsilon_1}(r_1(s), z_1(s), y_1(s), \epsilon_1(s)) ds \right) \\
&\leq \left| \frac{\epsilon}{\rho^3} e^{\frac{3}{4}T_1^*} \right| + Ce^{\frac{3}{4}T_1^*} \int_0^{T_1^*} e^{-\frac{3}{4}s} \left(|U_1(s)|^2 |\epsilon_1(s)| \right) ds \\
&\leq \left| \frac{\epsilon}{\rho^3} e^{\frac{3}{4}T_1^*} \right| + C\left(\|U_1\|_{\frac{1}{4}}^-\right)^2 \|\epsilon_1\|_{\frac{3}{4}}^+.
\end{aligned}
\tag{5.52}
$$

Provided ρ, δ are sufficiently small, for each sufficiently small $U_{1,0}$ and for $\left|\frac{\epsilon}{\rho^3}e^{\frac{3}{4}T_1^*}\right| \leq 2\delta$ sufficiently small, that is T_1^* is not too large, we can solve (5.44) to find a unique solution satisfying

$$\begin{aligned} \|U_1\|_{\frac{1}{4}}^- &= \mathcal{O}(|U_{1,0}|) \\ \|y_1\|_{\frac{1}{2}}^+ &= 1 + \mathcal{O}\left(|U_{1,0}|(\delta + |U_{1,0}|)\right) \\ \|\epsilon_1\|_{\frac{3}{4}}^+ &= \mathcal{O}(\delta) \end{aligned} \tag{5.53}$$

By our assumption that we consider only solutions exiting via Σ_{13}, and so $\epsilon_1 \leq \delta$, the time T_1^* satisfies $0 \leq T_1^* \leq C(\rho, \delta)|\log \epsilon|$ for all sufficiently small $\epsilon > 0$.

To obtain estimates on the derivatives of the solutions with respect to $U_{1,0}, c, a$, we consider the variational equation

$$\begin{aligned} d\dot{U}_1 &= \begin{pmatrix} -1/4 & 0 \\ -1 & -1/4 \end{pmatrix} dU_1 + dg_{U_1}(r_1, z_1, y_1, \epsilon_1) \\ \dot{dy}_1 &= \frac{1}{2}dy_1 + dg_{y_1}(r_1, z_1, y_1, \epsilon_1) \\ \dot{d\epsilon}_1 &= \frac{3}{4}d\epsilon_1 + dg_{\epsilon_1}(r_1, z_1, y_1, \epsilon_1), \end{aligned} \tag{5.54}$$

where

$$\begin{aligned} dg_{U_1}(r_1, z_1, y_1, \epsilon_1) &= \mathcal{O}\left(|U_1|^2 dU_1, |U_1|^3(|dy_1| + |d\epsilon_1|), |U_1|^3\right) \\ dg_{y_1}(r_1, z_1, y_1, \epsilon_1) &= \mathcal{O}\Big(|U_1|d\epsilon_1, (|\epsilon_1| + |U_1|)dU_1, (|U_1|^2 + |U_1||\epsilon_1|)|dy_1|, |U_1|^2|y_1|, |U_1||\epsilon_1|\Big) \\ dg_{\epsilon_1}(r_1, z_1, y_1, \epsilon_1) &= \mathcal{O}\left(|U_1||\epsilon_1|dU_1, |U_1|^2 d\epsilon_1, |U_1|^2|\epsilon_1|dy_1, |U_1|^2|\epsilon_1|\right). \end{aligned} \tag{5.55}$$

Proceeding as above, we can rewrite this as an integral equation; using the estimates obtained for the solutions (U_1, y_1, ϵ_1) and noting that the derivatives of k with respect to (c, a) are uniformly bounded, we can solve for the derivatives of the solutions on the same spaces and obtain

$$\|D_\nu U_1\|_{\frac{1}{4}}^-, \|D_\nu y_1\|_{\frac{1}{2}}^+, \|D_\nu \epsilon_1\|_{\frac{3}{4}}^+ \leq C, \tag{5.56}$$

$\nu = U_{1,0}, c, a$, uniformly in $(U_{1,0}, T_1^*, c, a, \epsilon)$ for all sufficiently small ρ, δ.

We also need estimates on the derivatives with respect to T_1^*. First, we show that these derivatives exist; then we show that they are in fact bounded uniformly in T_1^*. To compute the derivative with respect to T_1^* at some $T_1^* = T_0$, we rescale time by $t = (1+\omega)\tau$, which results in the differential equation

$$\dot{\hat{X}} = (1+\omega)F(\hat{X}), \tag{5.57}$$

where $X = (r_1, z_1, y_1, \epsilon_1)$ and $F(X)$ denotes the RHS of (5.33). Proceeding as above, we can now find solutions to this new system, keeping T_0 fixed and allowing ω to vary as a small parameter, with $|\omega| \leq \omega_0$, where ω_0 is sufficiently small. We obtain a new integral equation

$$\begin{aligned} U_1(t) &= \Phi_{1,\omega}(t,0)U_{1,0} + \int_0^t \Phi_{1,\omega}(t,s)g_{U_1}(r_1(s), z_1(s), y_1(s), \epsilon_1(s))ds \\ y_1(t) &= -e^{\frac{1}{2}(1+\omega)(t-T_0)} + \int_{T_0}^t e^{\frac{1}{2}(1+\omega)(t-s)}g_{y_1}(r_1(s), z_1(s), y_1(s), \epsilon_1(s))ds \\ \epsilon_1(t) &= \frac{\epsilon}{\rho^3}e^{\frac{3}{4}(1+\omega)t} + \int_0^t e^{\frac{3}{4}(1+\omega)(t-s)}g_{\epsilon_1}(r_1(s), z_1(s), y_1(s), \epsilon_1(s))ds, \end{aligned} \tag{5.58}$$

where the functions $g_{U_1}, g_{y_1}, g_{\epsilon_1}$ are defined as in (5.45), and $\Phi_{1,\omega}$ denotes the evolution of the constant coefficient system

$$\begin{pmatrix} \dot{r}_1 \\ \dot{z}_1 \end{pmatrix} = \begin{pmatrix} -(1+\omega)/4 & 0 \\ -(1+\omega) & -(1+\omega)/4 \end{pmatrix} \begin{pmatrix} r_1 \\ z_1 \end{pmatrix}. \tag{5.59}$$

We now slightly decrease the exponential weights and solve (5.58) for $(U_1, y_1, \epsilon_1) \in V^-_{\frac{1}{4}(1-\omega_0)} \times V^+_{\frac{1}{2}(1-\omega_0)} \times V^+_{\frac{3}{4}(1-\omega_0)}$, where the spaces $V^\pm_\eta$ are defined analogously to (5.46). Further, as above we can use the corresponding variational equation to estimate the derivatives of the solution with respect to the parameters, including ω, noting that they are bounded uniformly in T_0.

Let $\hat{X}(\tau; T_0, \omega, U_{1,0}, c, a) = (U_1, y_1, \epsilon_1)(\tau; T_0, \omega, U_{1,0}, c, a)$ denote a solution to (5.58), and let $X(t; T_1^*, U_{1,0}, c, a) = (U_1, y_1, \epsilon_1)(t; T_1^*, U_{1,0}, c, a)$ denote a solution to the original equation (5.44). By uniqueness, we have that $\hat{X}(T_0, \omega, U_{1,0}, c, a) = X((1+\omega)T_0, U_{1,0}, c, a)$. We now differentiate

$$\begin{aligned} D_\omega \hat{X}(\tau; T_0, \omega, U_{1,0}, c, a) = \tau \dot{X}((1+\omega)\tau; (1+\omega)T_0, U_{1,0}, c, a) \\ + T_0 D_{T_1^*} X((1+\omega)\tau; (1+\omega)T_0, U_{1,0}, c, a), \end{aligned} \tag{5.60}$$

from which we deduce that the derivative $D_{T_1^*} X$ exists and is bounded in the norms

$$\|D_{T_1^*} U_1\|^-_{\frac{1}{4}(1-\omega_0)}, \|D_{T_1^*} y_1\|^+_{\frac{1}{2}(1-\omega_0)}, \|D_{T_1^*} \epsilon_1\|^+_{\frac{3}{4}(1-\omega_0)} \leq C \tag{5.61}$$

uniformly in $(U_{1,0}, T_1^*, c, a, \epsilon)$ for all sufficiently small ρ, δ.

We can now write the unique solution of (5.44) satisfying

$$\begin{aligned} r_1(0) &= \rho \\ z_1(0) &= z^\ell_{1,0}(y_{1,0}), \end{aligned} \tag{5.62}$$

for sufficiently small $0 > y_{1,0} > -\Delta_{y_1}$ so that $z^\ell_1(y_{1,0}) = \mathcal{O}(\rho \log \rho)$. Recalling $U_1 = (r_1, z_1)$, we have that this solution is given by

$$\begin{pmatrix} r_1(t) \\ z_1(t) \end{pmatrix} = \begin{pmatrix} \rho e^{-\frac{1}{4}t} \\ z^\ell_{1,0}(y_{1,0}) e^{-\frac{1}{4}t} + \rho t e^{-\frac{1}{4}t} \end{pmatrix} + \int_0^t \Phi_1(t,s) g_{U_1}(r_1(s), z_1(s), y_1(s), \epsilon_1(s)) ds, \tag{5.63}$$

where

$$y_{1,0} = -e^{-\frac{1}{2}T_1^*} + \int_{T_1^*}^0 e^{-\frac{1}{2}s} g_{y_1}(r_1(s), z_1(s), y_1(s), \epsilon_1(s)) ds. \tag{5.64}$$

We consider only T_1^* large enough so that $y_{1,0} \geq -\Delta_{y_1}$. This gives

$$\begin{aligned} -\Delta_{y_1} &\leq -e^{-\frac{1}{2}T_1^*} + \int_{T_1^*}^0 e^{-\frac{1}{2}s} g_{y_1}(r_1(s), z_1(s), y_1(s), \epsilon_1(s)) ds \\ &= -e^{-\frac{1}{2}T_1^*} + \mathcal{O}\left(e^{-\frac{1}{2}T_1^*} \|U_1\|^-_{1/4} \left(\|\epsilon_1\|^+_{3/4} + \|U_1\|^-_{1/4}\right)\right) \\ &= -e^{-\frac{1}{2}T_1^*} \left(1 + \mathcal{O}(\rho^2, \rho\delta)\right), \end{aligned} \tag{5.65}$$

so that

$$e^{-\frac{1}{2}T_1^*} \leq \Delta_{y_1} \left(1 + \mathcal{O}\left(\rho^2, \rho\delta\right)\right), \tag{5.66}$$

and

$$\begin{aligned} \frac{dy_{1,0}}{dT_1^*} &= \frac{1}{2} e^{-\frac{1}{2}T_1^*} + e^{-\frac{1}{2}T_1^*} g_{y_1}(r_1(T_1^*), z_1(T_1^*), y_1(T_1^*), \epsilon_1(T_1^*)) \\ &\quad + \int_{T_1^*}^0 e^{-\frac{1}{2}s} \frac{d}{dT_1^*} [g_{y_1}(r_1(s), z_1(s), y_1(s), \epsilon_1(s))] ds \\ &= e^{-\frac{1}{2}T_1^*} \left(\frac{1}{2} + \mathcal{O}\left(\rho \log \rho, \delta\right)\right) \\ &= \Delta_{y_1} \left(1 + \mathcal{O}\left(\rho \log \rho, \delta\right)\right) \end{aligned} \tag{5.67}$$

where we used (5.45), (5.61), and (5.66).

We have

$$\begin{pmatrix} r_1(T_1^*) \\ z_1(T_1^*) \end{pmatrix} = \begin{pmatrix} \rho e^{-\frac{1}{4}T_1^*} \\ z_{1,0}^{\ell}(y_{1,0})e^{-\frac{1}{4}T_1^*} + \rho T_1^* e^{-\frac{1}{4}T_1^*} \end{pmatrix} + \int_0^{T_1^*} \Phi_1(T_1^*, s) g_{U_1}(r_1(s), z_1(s), y_1(s), \epsilon_1(s)) ds, \tag{5.68}$$

and we now compute

$$\begin{aligned} \frac{d}{dT_1^*}\begin{pmatrix} r_1(T_1^*) \\ z_1(T_1^*) \end{pmatrix} = & \begin{pmatrix} -\frac{\rho}{4}e^{-\frac{1}{4}T_1^*} \\ \left(-\frac{z_{1,0}^{\ell}(y_{1,0})}{4} + (z_{1,0}^{\ell})'(y_{1,0})\frac{dy_{1,0}}{dT_1^*} + \rho - \frac{\rho}{4}T_1^*\right)e^{-\frac{1}{4}T_1^*} \end{pmatrix} \\ & + g_{U_1}(r_1(T_1^*), z_1(T_1^*), y_1(T_1^*), \epsilon_1(T_1^*)) \\ & + \int_0^{T_1^*} \frac{d}{dT_1^*}\left[\Phi_1(T_1^*, s) g_{U_1}(r_1(s), z_1(s), y_1(s), \epsilon_1(s))\right] ds, \end{aligned} \tag{5.69}$$

where

$$\begin{aligned} z_{1,0}^{\ell}(y_{1,0}) &= \mathcal{O}(\rho \log \rho) \\ (z_{1,0}^{\ell})'(y_{1,0})\frac{dy_{1,0}}{dT_1^*} &= \mathcal{O}\left(C(\rho)e^{-\frac{1}{2}T_1^*}\left(1 + \mathcal{O}(\rho \log \rho, \delta)\right)\right) = \mathcal{O}(\rho), \end{aligned}$$

for Δ_{y_1} sufficiently small by (5.67), and

$$\begin{aligned} g_{U_1}(r_1(T_1^*), z_1(T_1^*), y_1(T_1^*), \epsilon_1(T_1^*)) &= \mathcal{O}\left((\rho \log \rho)^3 e^{-\frac{3}{4}T_1^*}\right) \\ \int_0^{T_1^*} \frac{d}{dT_1^*}\left[\Phi_1(T_1^*, s) g_{U_1}(r_1(s), z_1(s), y_1(s), \epsilon_1(s))\right] ds &= \begin{pmatrix} \mathcal{O}\left((\rho \log \rho)^2 e^{-\frac{1}{4}T_1^*}\right) \\ \mathcal{O}\left(T_1^*(\rho \log \rho)^2 e^{-\frac{1}{4}T_1^*}\right) \end{pmatrix}, \end{aligned}$$

by (5.45), (5.53), and (5.61).

Therefore we have that

$$\begin{aligned} \frac{dr_1(T_1^*)}{dT_1^*} &= \left(-\frac{\rho}{4} + \mathcal{O}\left((\rho \log \rho)^2\right)\right)e^{-\frac{1}{4}T_1^*} \\ \frac{dz_1(T_1^*)}{dT_1^*} &= \left(\mathcal{O}\left(\rho \log \rho, (1 + T_1^*)\rho\right)\right)e^{-\frac{1}{4}T_1^*} \end{aligned} \tag{5.70}$$

so that in Σ_{13}, for each fixed ρ, δ sufficiently small, we obtain a curve $z_1 = z_1(r_1)$ satisfying

$$\left|\frac{dz_1}{dr_1}\right| \leq C(\rho, \delta)(1 + T_1^*), \tag{5.71}$$

uniformly in $|y_{1,0}| < \Delta_{y_1}$, provided Δ_{y_1} is sufficiently small. Using the fact that $|T_1^*| \leq C(\rho, \delta)|\log \epsilon|$, we therefore obtain

$$\left|\frac{dz_1}{dr_1}\right| \leq C(\rho, \delta)|\log \epsilon|, \tag{5.72}$$

uniformly in (c, a, ϵ), which completes the proof of (i).

The proof of (ii) is similar and we omit the details. □

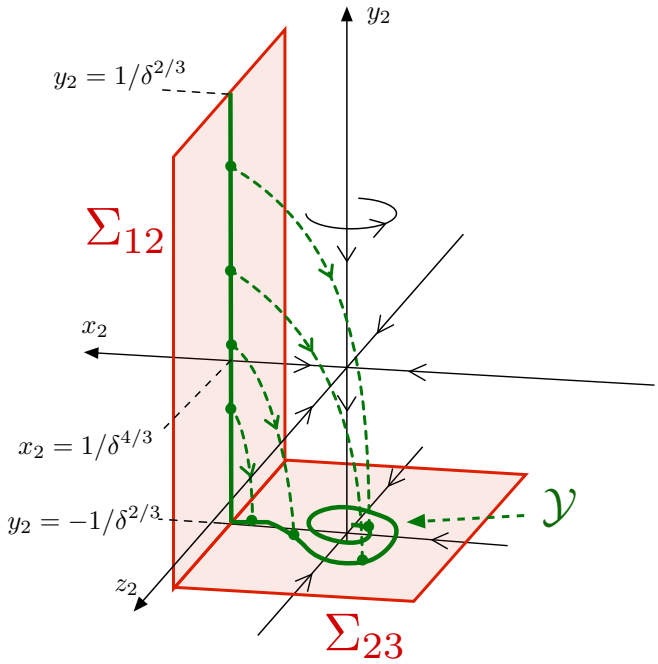

Figure 26: *Shown is the setup in the chart $\mathcal{K}_2$.*

5.4 Dynamics in $\mathcal{K}_2$

In the $\mathcal{K}_2$ coordinates, the equations are given by

$$\begin{aligned}
\dot{x}_2 &= -x_2 + r_2 y_2 z_2 + \mathcal{O}\left(r_2^2 z_2^2\right) \\
\dot{z}_2 &= -z_2 - r_2 x_2 + \mathcal{O}\left(r_2^3 z_2\right) \\
\dot{y}_2 &= -k r_2 + \mathcal{O}\left(r_2^3 y_2, r_2^4\right) \\
\dot{r}_2 &= 0.
\end{aligned} \tag{5.73}$$

Solutions enter via Σ_{12} which is given in the $\mathcal{K}_2$ coordinates by

$$\Sigma_{12} = \left\{(x_2, y_2, z_2, r_2) : x_2 = \frac{1}{\delta^{4/3}},\ |y_2| \leq \frac{1}{\delta^{2/3}},\ |z_2| \leq \frac{\mu}{\delta},\ 0 < r_2 \leq \rho\delta^{1/3}\right\}, \tag{5.74}$$

and exit via

$$\Sigma_{23} = \left\{(x_2, y_2, z_2, r_2) : |x_2| \leq \frac{1}{\delta^{4/3}},\ y_2 = -\frac{1}{\delta^{2/3}},\ |z_2| \leq \frac{\mu}{\delta},\ 0 < r_2 \leq \rho\delta^{1/3}\right\}. \tag{5.75}$$

The setup in the chart $\mathcal{K}_2$ is shown in Figure 26.

In this chart we can determine formulae for the solutions as follows. First, we consider solutions starting in Σ_{12} as time $t = 0$. We set $x_2 = e^{-t}\tilde{x}_2, z_2 = e^{-t}\tilde{z}_2$ and obtain the system

$$\begin{aligned}
\dot{\tilde{x}}_2 &= r_2 y_2 \tilde{z}_2 + \mathcal{O}\left(e^{-t} r_2^2 \tilde{z}_2^2\right) \\
\dot{\tilde{z}}_2 &= -r_2 \tilde{x}_2 + \mathcal{O}\left(r_2^3\right) \\
\dot{y}_2 &= -k r_2 + \mathcal{O}\left(r_2^3\right) \\
\dot{r}_2 &= 0.
\end{aligned} \tag{5.76}$$

We now rescale time by $t = t_2/r_2$ to desingularize the system

$$\begin{aligned}
\tilde{x}_2' &= y_2\tilde{z}_2 + \mathcal{O}(e^{-t_2/r_2}r_2)\\
\tilde{z}_2' &= -\tilde{x}_2 + \mathcal{O}\left(r_2^2\right)\\
y_2' &= -k + \mathcal{O}\left(r_2^2\right)\\
r_2' &= 0,
\end{aligned} \tag{5.77}$$

where $'$ denotes $\dfrac{d}{dt_2}$. Setting $r_2 = 0$ we obtain the Airy equations

$$\begin{aligned}
\tilde{x}_2' &= y_2\tilde{z}_2\\
\tilde{z}_2' &= -\tilde{x}_2\\
y_2' &= -k,
\end{aligned} \tag{5.78}$$

which have the following explicit solutions in terms of Airy functions Ai, Bi

$$\begin{aligned}
\tilde{x}_2 &= \pi\Bigg[\left(\mathrm{Ai}\left(-\frac{y_{2,0}}{k^{2/3}}\right)\mathrm{Bi}'\left(-\frac{y_{2,0}}{k^{2/3}} + k^{1/3}t_2\right) - \mathrm{Bi}\left(-\frac{y_{2,0}}{k^{2/3}}\right)\mathrm{Ai}'\left(-\frac{y_{2,0}}{k^{2/3}} + k^{1/3}t_2\right)\right)\frac{1}{\delta^{4/3}}\\
&\quad + k^{1/3}\left(\mathrm{Ai}'\left(-\frac{y_{2,0}}{k^{2/3}}\right)\mathrm{Bi}'\left(-\frac{y_{2,0}}{k^{2/3}} + k^{1/3}t_2\right) - \mathrm{Bi}'\left(-\frac{y_{2,0}}{k^{2/3}}\right)\mathrm{Ai}'\left(-\frac{y_{2,0}}{k^{2/3}} + k^{1/3}t_2\right)\right)z_{2,0}\Bigg]\\
\tilde{z}_2 &= \frac{\pi}{k^{1/3}}\Bigg[\left(\mathrm{Bi}\left(-\frac{y_{2,0}}{k^{2/3}}\right)\mathrm{Ai}\left(-\frac{y_{2,0}}{k^{2/3}} + k^{1/3}t_2\right) - \mathrm{Ai}\left(-\frac{y_{2,0}}{k^{2/3}}\right)\mathrm{Bi}\left(-\frac{y_{2,0}}{k^{2/3}} + k^{1/3}t_2\right)\right)\frac{1}{\delta^{4/3}}\\
&\quad + k^{1/3}\left(\mathrm{Bi}'\left(-\frac{y_{2,0}}{k^{2/3}}\right)\mathrm{Ai}\left(-\frac{y_{2,0}}{k^{2/3}} + k^{1/3}t_2\right) - \mathrm{Ai}'\left(-\frac{y_{2,0}}{k^{2/3}}\right)\mathrm{Bi}\left(-\frac{y_{2,0}}{k^{2/3}} + k^{1/3}t_2\right)\right)z_{2,0}\Bigg]\\
y_2 &= y_{2,0} - kt_2,
\end{aligned} \tag{5.79}$$

where $y_{2,0} = y_2(0)$ and $z_{2,0} = \tilde{z}_2(0) = z_2(0)$.

Lemma 5.6. *For each fixed $\delta, \mu > 0$, there exists $r_{2,0} > 0$ such that for any $0 < r_2 < r_{2,0}$, any solution of (5.76) with initial condition in Σ_{12} given by $(x_2, y_2, z_2)(0) = (1/\delta^{4/3}, y_{2,0}, z_{2,0})$ reaches Σ_{23} with*

$$\begin{aligned}
x_2 &= \pi e^{-\frac{\frac{1}{\delta^{2/3}} + y_{2,0}}{kr_2}}\Bigg[\left(\mathrm{Ai}\left(-\frac{y_{2,0}}{k^{2/3}}\right)\mathrm{Bi}'\left(\frac{1}{k^{2/3}\delta^{2/3}}\right) - \mathrm{Bi}\left(-\frac{y_{2,0}}{k^{2/3}}\right)\mathrm{Ai}'\left(\frac{1}{k^{2/3}\delta^{2/3}}\right)\right)\frac{1}{\delta^{4/3}}\\
&\quad + k^{1/3}\left(\mathrm{Ai}'\left(-\frac{y_{2,0}}{k^{2/3}}\right)\mathrm{Bi}'\left(\frac{1}{k^{2/3}\delta^{2/3}}\right) - \mathrm{Bi}'\left(-\frac{y_{2,0}}{k^{2/3}}\right)\mathrm{Ai}'\left(\frac{1}{k^{2/3}\delta^{2/3}}\right)\right)z_{2,0} + \mathcal{O}(r_2^2)\Bigg]\\
z_2 &= \frac{\pi e^{-\frac{\frac{1}{\delta^{2/3}} + y_{2,0}}{kr_2}}}{k^{1/3}}\Bigg[\left(\mathrm{Bi}\left(-\frac{y_{2,0}}{k^{2/3}}\right)\mathrm{Ai}\left(\frac{1}{k^{2/3}\delta^{2/3}}\right) - \mathrm{Ai}\left(-\frac{y_{2,0}}{k^{2/3}}\right)\mathrm{Bi}\left(\frac{1}{k^{2/3}\delta^{2/3}}\right)\right)\frac{1}{\delta^{4/3}}\\
&\quad + k^{1/3}\left(\mathrm{Bi}'\left(-\frac{y_{2,0}}{k^{2/3}}\right)\mathrm{Ai}\left(\frac{1}{k^{2/3}\delta^{2/3}}\right) - \mathrm{Ai}'\left(-\frac{y_{2,0}}{k^{2/3}}\right)\mathrm{Bi}\left(\frac{1}{k^{2/3}\delta^{2/3}}\right)\right)z_{2,0} + \mathcal{O}(r_2^2)\Bigg]\\
y_2 &= -\frac{1}{\delta^{2/3}}.
\end{aligned} \tag{5.80}$$

Proof. Considering the equations (5.78), solutions given by (5.79) with initial conditions $(x_2, y_2, z_2)(0) = (1/\delta^{4/3}, y_{2,0}, z_{2,0})$ in Σ_{12} exit Σ_{23} in time

$$T_2 = \frac{1}{k}\left(y_{2,0} + \frac{1}{\delta^{2/3}}\right). \tag{5.81}$$

For each fixed $\delta > 0$, T_2 is bounded uniformly in $|y_{2,0}| \leq 1/\delta^{2/3}$. Hence by a regular perturbation argument, and returning to the original coordinates x_2, z_2, we obtain the result. □

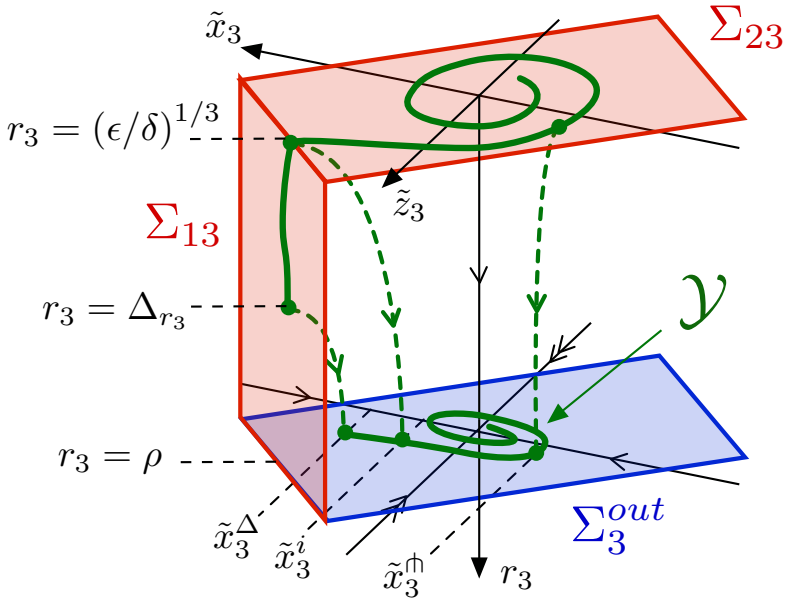

Figure 27: *Shown is the setup in the chart $\mathcal{K}_3$, including a schematic of the results of Lemma 5.10, Lemma 5.11, and Lemma 5.12.*

5.5 Dynamics in $\mathcal{K}_3$

In the $\mathcal{K}_3$ coordinates, the equations are given by

$$\begin{aligned}
\dot{x}_3 &= -x_3 - r_3 z_3 - 2k r_3 x_3 \epsilon_3 + \mathcal{O}\left(r_3^2 z_3^2, r_3^3 \epsilon_3 x_3\right) \\
\dot{z}_3 &= -z_3 - r_3 x_3 - \frac{3}{2} k r_3 \epsilon_3 z_3 + \mathcal{O}\left(r_3^3 z_3 \epsilon_3\right) \\
\dot{r}_3 &= \frac{1}{2} r_3^2 \epsilon_3 \left(k + \mathcal{O}\left(r_3^2\right)\right) \\
\dot{\epsilon}_3 &= -\frac{3}{2} r_3 \epsilon_3^2 \left(k + \mathcal{O}\left(r_3^2\right)\right)
\end{aligned} \tag{5.82}$$

Solutions enter via Σ_{13} or Σ_{23} which are given in the $\mathcal{K}_3$ coordinates by

$$\Sigma_{13} = \{(x_3, z_3, r_3, \epsilon_3) : x_3 = 1,\ |z_3| \leq \mu,\ 0 < r_3 \leq \rho,\ 0 < \epsilon_3 \leq \delta\} \tag{5.83}$$

$$\Sigma_{23} = \{(x_3, z_3, r_3, \epsilon_3) : |x_3| \leq 1,\ |z_3| \leq \mu,\ 0 < r_3 \leq \rho,\ \epsilon_3 = \delta\}, \tag{5.84}$$

respectively, and exit via

$$\Sigma_3^{out} = \{(x_3, z_3, r_3, \epsilon_3) : |x_3| \leq 1,\ |z_3| \leq \mu,\ r_3 = \rho,\ 0 < \epsilon_3 \leq \delta\}. \tag{5.85}$$

We need to determine the behavior of solutions which enter via Σ_{13} or Σ_{23} upon exit in Σ_3^{out}. The setup is shown in Figure 27. Between these sections, due to the relation $r_3^3 \epsilon_3 = \epsilon$, such solutions are restricted to the region $(\epsilon/\delta)^{1/3} \leq r_3 \leq \rho$ in which r_3 is strictly increasing. The linearization of (5.82) in the (x_3, z_3)-plane has approximate eigenvalues $(-1 \pm r_3)$. Hence, informally one expects that the flow should separate into strong and weak stable directions with an exponential separation that is initially $\mathcal{O}(\epsilon^{1/3})$ and grows to $\mathcal{O}(1)$ at Σ_3^{out}. We begin by deriving a change of coordinates $(x_3, z_3) \to (\tilde{x}_3, \tilde{z}_3)$ which more clearly separates these strong/weak directions.

To see this, we add an equation for the ratio $\theta_3 := z_3/x_3$

$$\begin{aligned}\dot{\theta}_3 &= \frac{\dot{z}_3}{x_3} - \theta_3 \frac{\dot{x}_3}{x_3} \\ &= -r_3 + r_3\theta_3^2 - \frac{3}{2}kr_3\epsilon_3\theta_3 + 2kr_3\epsilon_3\theta_3 + \mathcal{O}\left(r_3^3\theta_3\epsilon_3, r_3^2\theta_3^2\right) \\ &= r_3\left(\theta_3^2 - 1 + \frac{1}{2}k\epsilon_3\theta_3\right) + \mathcal{O}\left(r_3^2\right),\end{aligned} \tag{5.86}$$

and we consider the extended system

$$\begin{aligned}\dot{x}_3 &= -x_3 - r_3z_3 - 2kr_3x_3\epsilon_3 + \mathcal{O}\left(r_3^2(|x_3| + |z_3|)\right) \\ \dot{z}_3 &= -z_3 - r_3x_3 - \frac{3}{2}kr_3\epsilon_3z_3 + \mathcal{O}\left(r_3^3z_3\epsilon_3\right) \\ \dot{\theta}_3 &= r_3\left(\theta_3^2 - 1 + \frac{1}{2}k\epsilon_3\theta_3\right) + \mathcal{O}\left(r_3^2\right) \\ \dot{r}_3 &= \frac{1}{2}r_3^2\epsilon_3\left(k + \mathcal{O}\left(r_3^2\right)\right) \\ \dot{\epsilon}_3 &= -\frac{3}{2}r_3\epsilon_3^2\left(k + \mathcal{O}\left(r_3^2\right)\right).\end{aligned} \tag{5.87}$$

Solutions are exponentially attracted to the subspace $x_3 = z_3 = 0$ on which the flow is given by

$$\begin{aligned}\dot{\theta}_3 &= r_3\left(\theta_3^2 - 1 + \frac{1}{2}k\epsilon_3\theta_3\right) + \mathcal{O}\left(r_3^2\right) \\ \dot{r}_3 &= \frac{1}{2}r_3^2\epsilon_3\left(k + \mathcal{O}\left(r_3^2\right)\right) \\ \dot{\epsilon}_3 &= -\frac{3}{2}r_3\epsilon_3^2\left(k + \mathcal{O}\left(r_3^2\right)\right).\end{aligned} \tag{5.88}$$

Rescaling time by $t_3 = r_3t$, we obtain

$$\begin{aligned}\theta_3' &= \theta_3^2 - 1 + \frac{1}{2}k\epsilon_3\theta_3 + \mathcal{O}\left(r_3\right) \\ r_3' &= \frac{1}{2}r_3\epsilon_3\left(k + \mathcal{O}\left(r_3^2\right)\right) \\ \epsilon_3' &= -\frac{3}{2}\epsilon_3^2\left(k + \mathcal{O}\left(r_3^2\right)\right).\end{aligned} \tag{5.89}$$

Firstly, there are two invariant subspaces for the dynamics of (5.89): the plane $r_3 = 0$ and the plane $\epsilon_3 = 0$. Their intersection is the invariant line $l_3 = \{(\theta_3, 0, 0) : \theta_3 \in \mathbb{R}\}$, and the dynamics on l_3 evolve according to $\theta_3' = -1 + \theta_3^2$. There are two equilibria $p^- = (-1, 0, 0)$ and $p^+ = (1, 0, 0)$, with eigenvalues -2 and 2, respectively, for the flow along l_3. In the plane $\epsilon_3 = 0$, the dynamics are given by

$$\begin{aligned}\theta_3' &= \theta_3^2 - 1 + \mathcal{O}(r_3) \\ r_3' &= 0\ .\end{aligned} \tag{5.90}$$

This system has normally hyperbolic curves $S_{0,3}^{\pm}(c, a)$ of equilibria emanating from $p^{\pm}$ (see Figure 28). Along $S_{0,3}^{\pm}(c, a)$ the linearization has one zero eigenvalue and one eigenvalue close to ± 2 for small r_3.

In the invariant plane $r_3 = 0$, the dynamics are given by

$$\begin{aligned}\theta_3' &= \theta_3^2 - 1 + \frac{1}{2}k\epsilon_3\theta_3 \\ \epsilon_3' &= -\frac{3}{2}\epsilon_3^2\ .\end{aligned} \tag{5.91}$$

Here we still have the equilibria $p^{\pm}$ which now have an additional zero eigenvalue due to the second equation. The corresponding eigenvector is $(-k, 4)$ and hence there exist one-dimensional center manifolds $N_3^{\pm}(c, a)$ at $p^{\pm}$ along which ϵ_3 decreases. Note that the branch of $N_3^{+}(c, a)$ in the half space $\epsilon_1 > 0$ is unique.

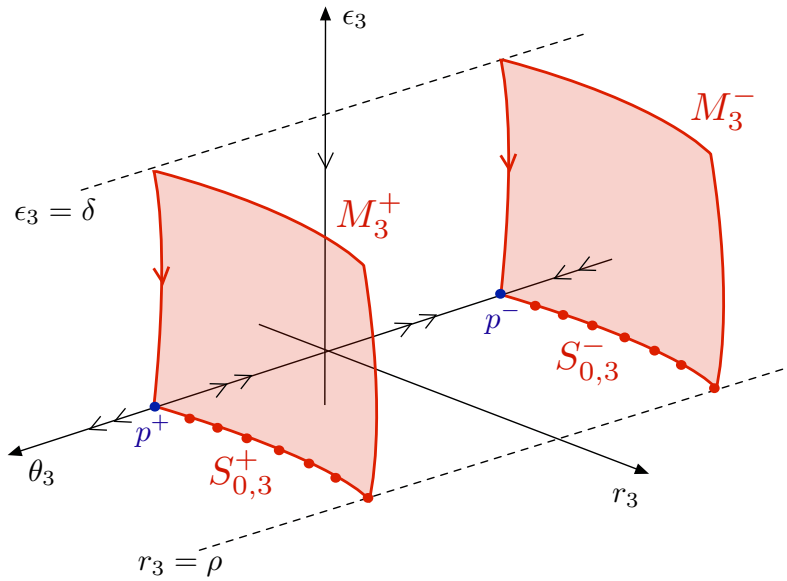

Figure 28: *Shown are the invariant manifolds $M_3^{\pm}(c,a)$ corresponding to the dynamics of (5.89).*

Restricting attention to the set

$$D_3 = \{(\theta_3, r_3, \epsilon_3) : \theta_3 \in \mathbb{R}, 0 \leq r_3 \leq \rho, 0 \leq \epsilon_1 \leq \delta\} \ , \tag{5.92}$$

we have the following (see Figure 28).

Proposition 5.7. *For any $(c,a) \in I_c \times I_a$ and any sufficiently small $\rho, \delta > 0$, the following assertions hold for the dynamics of (5.89):*

1. *There exists a repelling two-dimensional center manifold $M_3^+(c,a)$ at p^+ which contains the line of equilibria $S_{0,3}^+(c,a)$ and the center manifold $N_3^+(c,a)$. In D_3, $M_3^+(c,a)$ is given as a graph $\theta_3 = h^+(r_3, \epsilon_3, c, a) = 1 + \mathcal{O}(r_3, \epsilon_3)$. The branch of $N_3^+(c,a)$ in $r_3 = 0, \epsilon_3 > 0$ is unique.*

2. *There exists an attracting two-dimensional center manifold $M_3^-(c,a)$ at p^- which contains the line of equilibria $S_{0,3}^-(c,a)$ and the center manifold $N_3^-(c,a)$. In D_3, $M_3^-(c,a)$ is given as a graph $\theta_3 = h^-(r_3, \epsilon_3, c, a) = -1 + \mathcal{O}(r_3, \epsilon_3)$.*

We now return to the full system (5.87), in which the flow on the subspace $x_3 = z_3 = 0$ is foliated by flow along strong stable fibers. Hence in the full five-dimensional space, there exist four-dimensional invariant manifolds $\bar{M}_3^{\pm}(c,a)$ (see Figure 29) given by the strong stable foliations of the two-dimensional manifolds $M_3^{\pm}(c,a)$. The manifolds $\bar{M}_3^{\pm}(c,a)$ can be written as graphs $\theta_3 = H^{\pm}(x_3, z_3, r_3, \epsilon_3, c, a) = \pm 1 + \mathcal{O}(r_3, \epsilon_3)$.

Now using the relation $\theta_3 = z_3/x_3$, we see that the dynamics are in fact restricted to three-dimensional invariant submanifolds $\tilde{M}_3^{\pm}(c,a)$ of $\bar{M}_3^{\pm}(c,a)$. The manifolds $\tilde{M}_3^{\pm}(c,a)$ are given by $z_3 = x_3 H^{\pm}(x_3, z_3, r_3, \epsilon_3, c, a)$. By the implicit function theorem, for any sufficiently small $\rho, \delta > 0$, we can now solve to find $\tilde{M}_3^{\pm}(c,a)$ as graphs

$$\begin{aligned} z_3 &= F^-(x_3, r_3, \epsilon_3, c, a) = x_3(-1 + \mathcal{O}(r_3, \epsilon_3)) \\ x_3 &= F^+(z_3, r_3, \epsilon_3, c, a) = z_3(1 + \mathcal{O}(r_3, \epsilon_3)). \end{aligned} \tag{5.93}$$

We now change coordinates by

$$\begin{aligned} \tilde{z}_3 &= z_3 - F^-(x_3, r_3, \epsilon_3, c, a) = z_3 + x_3(1 + \mathcal{O}(r_3, \epsilon_3)) \\ \tilde{x}_3 &= x_3 - F^+(z_3, r_3, \epsilon_3, c, a) = x_3 - z_3(1 + \mathcal{O}(r_3, \epsilon_3)) \end{aligned} \tag{5.94}$$

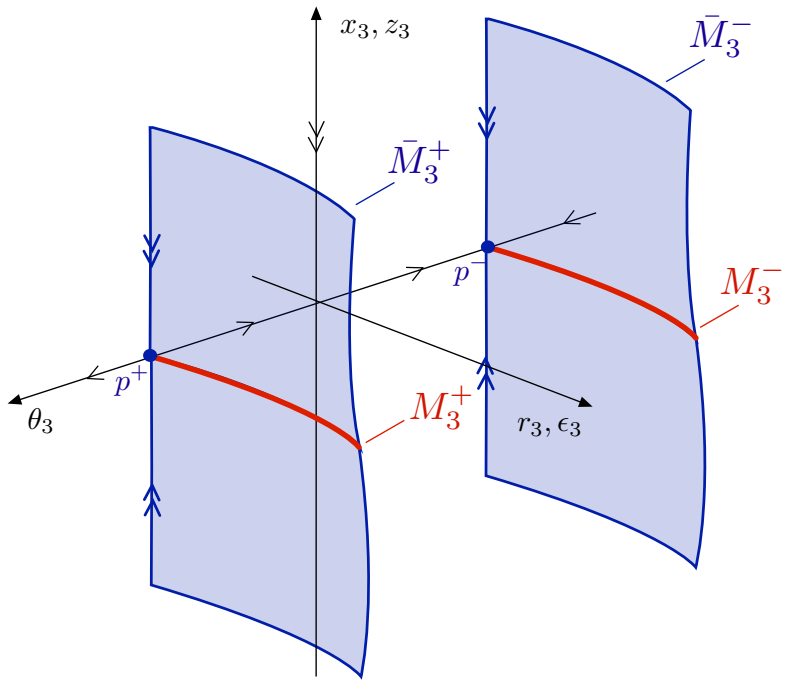

Figure 29: *Shown are the invariant manifolds $\bar{M}_3^{\pm}(c,a)$ corresponding to the dynamics of (5.87).*

In these coordinates, (5.82) becomes

$$\begin{aligned}
\dot{\tilde{x}}_3 &= \left(-1 + r_3 + r_3 h_+(\tilde{x}_3, \tilde{z}_3, r_3, \epsilon_3)\right) \tilde{x}_3 \\
\dot{\tilde{z}}_3 &= \left(-1 - r_3 + r_3 h_-(\tilde{x}_3, \tilde{z}_3, r_3, \epsilon_3)\right) \tilde{z}_3 \\
\dot{r}_3 &= \frac{1}{2} r_3^2 \epsilon_3 \left(k + g_1(\tilde{x}_3, \tilde{z}_3, r_3, \epsilon_3)\right) \\
\dot{\epsilon}_3 &= -\frac{3}{2} r_3 \epsilon_3^2 \left(k + g_2(\tilde{x}_3, \tilde{z}_3, r_3, \epsilon_3)\right),
\end{aligned} \tag{5.95}$$

where

$$\begin{aligned}
h_+(\tilde{x}_3, \tilde{z}_3, r_3, \epsilon_3) &= \mathcal{O}\left(r_3, \epsilon_3\right) \\
h_-(\tilde{x}_3, \tilde{z}_3, r_3, \epsilon_3) &= \mathcal{O}\left(r_3, \epsilon_3\right) \\
g_1(\tilde{x}_3, \tilde{z}_3, r_3, \epsilon_3) &= \mathcal{O}\left(r_3^2\right) \\
g_2(\tilde{x}_3, \tilde{z}_3, r_3, \epsilon_3) &= \mathcal{O}\left(r_3^2\right).
\end{aligned} \tag{5.96}$$

In (5.95), it is clear that the strong attraction in the variables (x_3, z_3) splits into strong/weak directions where the exponential splitting increases as r_3 increases. By changing coordinates to $(\tilde{x}_3, \tilde{z}_3)$, we straighten out the invariant manifolds $\tilde{M}_3^{\pm}(c,a)$ (see Figure 30).

5.5.1 Solutions with initial conditions in Σ_{23}

We first consider solutions entering $\mathcal{K}_3$ via Σ_{23}. Using $r_3^3 \epsilon_3 = \epsilon$, we have that such solutions satisfy $\epsilon_3 = \delta, r_3 = (\epsilon/\delta)^{1/3}$ in Σ_{23}. We have the following.

Lemma 5.8. *For all sufficiently small $\rho, \delta > 0$, any solution to (5.95) with initial condition $(\tilde{x}_3, \tilde{z}_3, r_3, \epsilon_3)(0) =$*

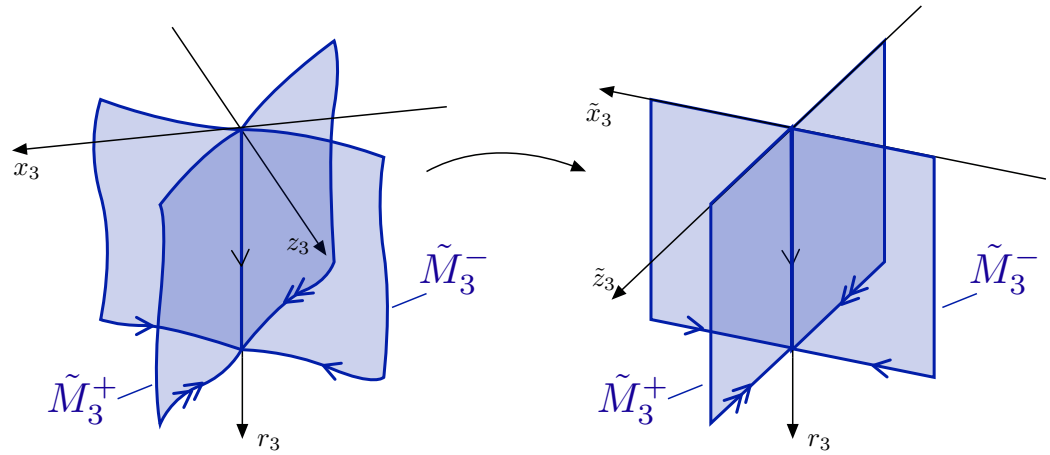

Figure 30: *Shown are the invariant manifolds $\tilde{M}_3^{\pm}(c,a)$ transformed to the $(\tilde{x}_3,\tilde{z}_3)$-coordinates.*

$(\tilde{x}_{3,0},\tilde{z}_{3,0},(\epsilon/\delta)^{1/3},\delta)\in\Sigma_{23}$ *which reaches the section* Σ_3^{out} *at time* $t=T^*=T^*(\rho,\delta,\tilde{x}_{3,0},\tilde{z}_{3,0},\epsilon)$ *satisfies*

$$\begin{aligned}
\tilde{x}_3(T^*) &= \tilde{x}_{3,0}\exp\left(\beta_+^2(\rho,\delta,\epsilon)+\eta_+^2(\rho,\delta,\tilde{x}_{3,0},\tilde{z}_{3,0},\epsilon)\right)\\
\tilde{z}_3(T^*) &= \tilde{z}_{3,0}\exp\left(\beta_-^2(\rho,\delta,\epsilon)+\eta_-^2(\rho,\delta,\tilde{x}_{3,0},\tilde{z}_{3,0},\epsilon)\right)\\
r_3(T^*) &= \rho\\
\epsilon_3(T^*) &= \frac{\epsilon}{\rho^3},
\end{aligned}\tag{5.97}$$

where

$$\begin{aligned}
\beta_-^2(\rho,\delta,\epsilon) &= \frac{\rho^2}{\epsilon}\left(-1-\frac{2\rho}{3}+\mathcal{O}(\rho^2,\rho\delta)\right)\\
\beta_+^2(\rho,\delta,\epsilon) &= \frac{\rho^2}{\epsilon}\left(-1+\frac{2\rho}{3}+\mathcal{O}(\rho^2,\rho\delta)\right)\\
\eta_\pm^2(\rho,\delta,\tilde{x}_{3,0},\tilde{z}_{3,0},\epsilon) &= \mathcal{O}\left(\left(\frac{\epsilon}{\delta}\right)^{1/3}\left(|\tilde{x}_{3,0}|+|\tilde{z}_{3,0}|\right)\right).
\end{aligned}\tag{5.98}$$

Proof. It is clear from (5.95) that the $(\tilde{x}_3,\tilde{z}_3)$-coordinates decay exponentially for all sufficiently small $\rho,\delta>0$. By directly integrating (5.95), we obtain the following expressions

$$\begin{aligned}
\tilde{x}_3(T^*) &= \tilde{x}_{3,0}\exp\left(-T^*+\int_0^{T^*} r_3(t)\left(1+h_+(\tilde{x}_3(t),\tilde{z}_3(t),r_3(t),\epsilon_3(t))\right)dt\right)\\
\tilde{z}_3(T^*) &= \tilde{z}_{3,0}\exp\left(-T^*-\int_0^{T^*} r_3(t)\left(1+h_-(\tilde{x}_3(t),\tilde{z}_3(t),r_3(t),\epsilon_3(t))\right)dt\right)\\
r_3(T^*) &= \rho\\
\epsilon_3(T^*) &= \frac{\epsilon}{\rho^3}.
\end{aligned}\tag{5.99}$$

We determine the functions β_+^2,η_+^2. The computation of β_-^2,η_-^2 is similar. We now write

$$\begin{aligned}
T^* &= \int_{(\epsilon/\delta)^{1/3}}^{\rho}\frac{1}{\dot{r}_3}dr_3\\
&= \frac{2}{\epsilon}\int_{(\epsilon/\delta)^{1/3}}^{\rho} r_3\left(1+\mathcal{O}\left(r_3^2\right)\right)dr_3,
\end{aligned}\tag{5.100}$$

using $r_3^3\epsilon_3=\epsilon$. We also have

$$\int_0^{T^*} r_3(t)\left(1+h_+(\tilde{x}_3(t),\tilde{z}_3(t),r_3(t),\epsilon_3(t))\right)dt = \frac{2}{\epsilon}\int_{(\epsilon/\delta)^{1/3}}^{\rho} r_3^2\left(1+\mathcal{O}\left(r_3,\epsilon_3\right)\right)dr_3,\tag{5.101}$$

and hence

$$
\begin{aligned}
-T^* + \int_0^{T^*} r_3(t)\left(1+\mathcal{O}\left(r_3(t),\epsilon_3(t)\right)\right)dt &= -\frac{2}{\epsilon}\int_{(\epsilon/\delta)^{1/3}}^{\rho} r_3 - r_3^2 + \mathcal{O}\left(r_3^3, r_3^2\epsilon_3\right) dr_3 \\
&= -\frac{2}{\epsilon}\int_{(\epsilon/\delta)^{1/3}}^{\rho} r_3 - r_3^2 + h_1(r_3,\epsilon_3) + h_2(r_3,\epsilon_3,\tilde{x}_3,\tilde{z}_3)dr_3,
\end{aligned}
\tag{5.102}
$$

where we have separated out the $\tilde{x}_3, \tilde{z}_3$ dependence through the functions h_1, h_2. That is, we have $\partial_{\tilde{x}_3} h_1 = \partial_{\tilde{z}_3} h_1 = 0$ and

$$
\begin{aligned}
h_1(r_3,\epsilon_3) &= \mathcal{O}\left(r_3^3, r_3^2\epsilon_3\right) \\
h_2(r_3,\epsilon_3,\tilde{x}_3,\tilde{z}_3) &= \mathcal{O}\left(r_3^2(|r_3|+|\epsilon_3|)(|\tilde{x}_3|+|\tilde{z}_3|)\right).
\end{aligned}
\tag{5.103}
$$

We now define

$$
\begin{aligned}
\beta_+^2(\rho,\delta,\epsilon) &= -\frac{2}{\epsilon}\int_{(\epsilon/\delta)^{1/3}}^{\rho} r_3 - r_3^2 + h_1(r_3,\epsilon_3)dr_3 \\
&= -\frac{2}{\epsilon}\left(\frac{\rho^2}{2} - \frac{\rho^3}{3} + \mathcal{O}\left(\rho^4, \rho^3\delta\right)\right) \\
\eta_+^2(\rho,\delta,\tilde{x}_{3,0},\tilde{z}_{3,0},\epsilon) &= -\frac{2}{\epsilon}\int_{(\epsilon/\delta)^{1/3}}^{\rho} h_2(r_3,\epsilon_3,\tilde{x}_3,\tilde{z}_3)dr_3.
\end{aligned}
\tag{5.104}
$$

To estimate η_+^2, we first note that for any sufficiently small ρ, δ, we can bound

$$
\begin{aligned}
|\tilde{x}_3(t)| &\leq \tilde{x}_{3,0}\exp\left(-t/2\right) \\
|\tilde{z}_3(t)| &\leq \tilde{z}_{3,0}\exp\left(-t/2\right),
\end{aligned}
\tag{5.105}
$$

for any $0 \leq t \leq T^*$. Furthermore, we have

$$
\begin{aligned}
t &= \int_{(\epsilon/\delta)^{1/3}}^{r_3(t)} \frac{1}{\dot{r}_3} dr_3 \\
&= \frac{2}{\epsilon}\int_{(\epsilon/\delta)^{1/3}}^{r_3(t)} r_3\left(1+\mathcal{O}\left(r_3^2\right)\right)dr_3 \\
&> \frac{1}{2\epsilon}\left(r_3(t)^2 - (\epsilon/\delta)^{2/3}\right),
\end{aligned}
\tag{5.106}
$$

for each sufficiently small fixed $\rho, \delta > 0$. Hence we have

$$
\begin{aligned}
\eta_+^2(\rho,\delta,\tilde{x}_{3,0},\tilde{z}_{3,0},\epsilon) &= -\frac{2}{\epsilon}\int_{(\epsilon/\delta)^{1/3}}^{\rho} h_2(r_3,\epsilon_3,\tilde{x}_3,\tilde{z}_3)dr_3 \\
&= -\frac{2}{\epsilon}\int_{(\epsilon/\delta)^{1/3}}^{\rho} \mathcal{O}\left(r_3^2(|r_3|+|\epsilon_3|)(|\tilde{x}_3|+|\tilde{z}_3|)\right)dr_3 \\
&= -\frac{2}{\epsilon}\int_{(\epsilon/\delta)^{1/3}}^{\rho} \mathcal{O}\left(r_3^2(|r_3|+|\epsilon_3|)(|\tilde{x}_{3,0}|+|\tilde{z}_{3,0}|)\exp\left(-\frac{1}{4\epsilon}\left(r_3^2 - (\epsilon/\delta)^{2/3}\right)\right)\right)dr_3 \\
&= \mathcal{O}\left(\left(\frac{\epsilon}{\delta}\right)^{1/3}(|\tilde{x}_{3,0}|+|\tilde{z}_{3,0}|)\right)
\end{aligned}
\tag{5.107}
$$

that is, the dependence on the initial $(\tilde{x}_{3,0}, \tilde{z}_{3,0})$ of the exponential contraction between Σ_{23} and Σ_3^{out} is very small. □

We now consider solutions on $\mathcal{Y}(c,a,\epsilon), \mathcal{W}_\epsilon^{s,r}(c,a)$ passing through $\Sigma_A^{in} = \Sigma_1^{in} \to \Sigma_{12} \to \Sigma_{23}$. We obtain estimates for these solutions upon entry in the chart $\mathcal{K}_3$ in Σ_{23} and exit via Σ_3^{out}.

Lemma 5.9. *Solutions on the manifolds $\mathcal{Y}(c,a,\epsilon), \mathcal{W}_\epsilon^{s,r}(c,a)$, which have initial conditions in Σ_{23} define curves $(\tilde{x}_{3,0}^\ell(y_{2,0}), \tilde{z}_{3,0}^\ell(y_{2,0}))$ and $(\tilde{x}_{3,0}^r(y_{2,0}), \tilde{z}_{3,0}^r(y_{2,0}))$, respectively, in Σ_{23} parametrized by $|y_{2,0}| \leq 1/\delta^{2/3}$ with*

$$\begin{aligned}\tilde{x}_{3,0}^j(y_{2,0}) &= \frac{\sqrt{\pi}e^{-\frac{\frac{1}{\delta^{2/3}}+y_{2,0}}{k\epsilon^{1/3}}}}{k^{1/6}\delta^{1/6}}\tilde{X}_3^j(y_{2,0})\\ \tilde{z}_{3,0}^j(y_{2,0}) &= \frac{\sqrt{\pi}e^{-\frac{\frac{1}{\delta^{2/3}}+y_{2,0}}{k\epsilon^{1/3}}}}{k^{1/6}\delta^{1/6}}\tilde{Z}_3^j(y_{2,0}),\end{aligned} \tag{5.108}$$

where

$$\begin{aligned}\tilde{X}_3^j(y_{2,0}) &= \left(\mathrm{Ai}\left(-\frac{y_{2,0}}{k^{2/3}}\right) + k^{1/3}\delta^{4/3}\,\mathrm{Ai}'\left(-\frac{y_{2,0}}{k^{2/3}}\right)z_{2,0}^j(y_{2,0})\right)e^{\frac{2}{3}\frac{1}{k\delta}}\left(2+\mathcal{O}(\delta)\right)\\ &\quad + \mathcal{O}(\delta)\left(\mathrm{Bi}\left(-\frac{y_{2,0}}{k^{2/3}}\right) + k^{1/3}\delta^{4/3}\,\mathrm{Bi}'\left(-\frac{y_{2,0}}{k^{2/3}}\right)z_{2,0}^j(y_{2,0})\right)e^{-\frac{2}{3}\frac{1}{k\delta}} + \mathcal{O}(\epsilon^{2/3})\\ \tilde{Z}_3^j(y_{2,0}) &= \left(\mathrm{Bi}\left(-\frac{y_{2,0}}{k^{2/3}}\right) + k^{1/3}\delta^{4/3}\,\mathrm{Bi}'\left(-\frac{y_{2,0}}{k^{2/3}}\right)z_{2,0}^j(y_{2,0})\right)e^{-\frac{2}{3}\frac{1}{k\delta}}\left(1+\mathcal{O}(\delta)\right)\\ &\quad + \mathcal{O}(\delta)\left(\mathrm{Ai}\left(-\frac{y_{2,0}}{k^{2/3}}\right) + k^{1/3}\delta^{4/3}\,\mathrm{Ai}'\left(-\frac{y_{2,0}}{k^{2/3}}\right)z_{2,0}^j(y_{2,0})\right)e^{\frac{2}{3}\frac{1}{k\delta}} + \mathcal{O}(\epsilon^{2/3}),\end{aligned} \tag{5.109}$$

for $j=\ell,r$,where

$$\begin{aligned}\left|z_{2,0}^j(y_{2,0})\right| &\leq C\epsilon^{1/3}|\log\epsilon|\\ \left|\frac{dz_{2,0}^j}{dy_{2,0}}\right| &\leq C\epsilon^{1/3}|\log\epsilon|\end{aligned} \tag{5.110}$$

and

$$\kappa\epsilon^{1/3} < z_{2,0}^r(y_{2,0}) - z_{2,0}^\ell(y_{2,0}) < C\epsilon^{1/3}|\log\epsilon|. \tag{5.111}$$

uniformly in $y_{2,0}$ for some $C,\kappa>0$ independent of c,a,ϵ.

Proof. Using the analysis in §5.4, Lemma 5.6 and the estimates in Proposition 5.5 (ii), we deduce that solutions on the manifolds $\mathcal{Y}(c,a,\epsilon), \mathcal{W}_\epsilon^{s,r}(c,a)$ define curves in Σ_{23} parametrized by $|y_{2,0}| \leq 1/\delta^{2/3}$ as

$$\begin{aligned}x_3 &= x_{3,0}^j(y_{2,0})\\ &= \pi e^{-\frac{\frac{1}{\delta^{2/3}}+y_{2,0}}{kr_2}}\Bigg(\mathrm{Ai}\left(-\frac{y_{2,0}}{k^{2/3}}\right)\mathrm{Bi}'\left(\frac{1}{k^{2/3}\delta^{2/3}}\right) - \mathrm{Bi}\left(-\frac{y_{2,0}}{k^{2/3}}\right)\mathrm{Ai}'\left(\frac{1}{k^{2/3}\delta^{2/3}}\right)\\ &\qquad + k^{1/3}\delta^{4/3}\left(\mathrm{Ai}'\left(-\frac{y_{2,0}}{k^{2/3}}\right)\mathrm{Bi}'\left(\frac{1}{k^{2/3}\delta^{2/3}}\right) - \mathrm{Bi}'\left(-\frac{y_{2,0}}{k^{2/3}}\right)\mathrm{Ai}'\left(\frac{1}{k^{2/3}\delta^{2/3}}\right)\right)z_{2,0}^j(y_{2,0}) + \mathcal{O}(r_2^2)\Bigg)\\ z_3 &= z_{3,0}^j(y_{2,0})\\ &= \frac{\pi e^{-\frac{\frac{1}{\delta^{2/3}}+y_{2,0}}{kr_2}}}{k^{1/3}\delta^{1/3}}\Bigg(\mathrm{Bi}\left(-\frac{y_{2,0}}{k^{2/3}}\right)\mathrm{Ai}\left(\frac{1}{k^{2/3}\delta^{2/3}}\right) - \mathrm{Ai}\left(-\frac{y_{2,0}}{k^{2/3}}\right)\mathrm{Bi}\left(\frac{1}{k^{2/3}\delta^{2/3}}\right)\\ &\qquad + k^{1/3}\delta^{4/3}\left(\mathrm{Bi}'\left(-\frac{y_{2,0}}{k^{2/3}}\right)\mathrm{Ai}\left(\frac{1}{k^{2/3}\delta^{2/3}}\right) - \mathrm{Ai}'\left(-\frac{y_{2,0}}{k^{2/3}}\right)\mathrm{Bi}\left(\frac{1}{k^{2/3}\delta^{2/3}}\right)\right)z_{2,0}^j(y_{2,0}) + \mathcal{O}(r_2^2)\Bigg)\\ \epsilon_3 &= \delta,\end{aligned} \tag{5.112}$$

for $j=\ell,r$, where

$$\begin{aligned}\left|z_{2,0}^j(y_{2,0})\right| &\leq C\epsilon^{1/3}|\log\epsilon|\\ \left|\frac{dz_{2,0}^j}{dy_{2,0}}\right| &\leq C\epsilon|\log\epsilon|\end{aligned} \tag{5.113}$$

and

$$\kappa\epsilon^{1/3} < z^r_{2,0}(y_{2,0}) - z^\ell_{2,0}(y_{2,0}) < C\epsilon^{1/3}|\log\epsilon|. \tag{5.114}$$

uniformly in $y_{2,0}$ for some $C, \kappa > 0$ independent of c, a, ϵ. Using asymptotic properties of Airy functions (5.20), we have

$$\begin{aligned} x^j_{3,0}(y_{2,0}) &= \frac{\sqrt{\pi}e^{-\frac{\frac{1}{\delta^{2/3}}+y_{2,0}}{kr_2}}}{k^{1/6}\delta^{1/6}} X^j_3(y_{2,0}) \\ z^j_{3,0}(y_{2,0}) &= \frac{\sqrt{\pi}e^{-\frac{\frac{1}{\delta^{2/3}}+y_{2,0}}{kr_2}}}{k^{1/6}\delta^{1/6}} Z^j_3(y_{2,0}), \end{aligned} \tag{5.115}$$

where

$$\begin{aligned} X^j_3(y_{2,0}) &= \left(\mathrm{Ai}\left(-\frac{y_{2,0}}{k^{2/3}}\right) + k^{1/3}\delta^{4/3}\,\mathrm{Ai}'\left(-\frac{y_{2,0}}{k^{2/3}}\right) z^j_{2,0}(y_{2,0})\right) e^{\frac{2}{3}\frac{1}{k\delta}}\left(1+\mathcal{O}(\delta)\right) \\ &\quad + \left(\mathrm{Bi}\left(-\frac{y_{2,0}}{k^{2/3}}\right) + k^{1/3}\delta^{4/3}\,\mathrm{Bi}'\left(-\frac{y_{2,0}}{k^{2/3}}\right) z^j_{2,0}(y_{2,0})\right)\frac{e^{-\frac{2}{3}\frac{1}{k\delta}}}{2}\left(1+\mathcal{O}(\delta)\right) + \mathcal{O}\left(r_2^2\right) \\ Z^j_3(y_{2,0}) &= -\left(\mathrm{Ai}\left(-\frac{y_{2,0}}{k^{2/3}}\right) + k^{1/3}\delta^{4/3}\,\mathrm{Ai}'\left(-\frac{y_{2,0}}{k^{2/3}}\right) z^j_{2,0}(y_{2,0})\right) e^{\frac{2}{3}\frac{1}{k\delta}}\left(1+\mathcal{O}(\delta)\right) \\ &\quad + \left(\mathrm{Bi}\left(-\frac{y_{2,0}}{k^{2/3}}\right) + k^{1/3}\delta^{4/3}\,\mathrm{Bi}'\left(-\frac{y_{2,0}}{k^{2/3}}\right) z^j_{2,0}(y_{2,0})\right)\frac{e^{-\frac{2}{3}\frac{1}{k\delta}}}{2}\left(1+\mathcal{O}(\delta)\right) + \mathcal{O}\left(r_2^2\right). \end{aligned} \tag{5.116}$$

Using (5.94), in the '$\sim$' coordinates we have

$$\begin{aligned} \tilde{z}^j_{3,0}(y_{2,0}) &= z^j_{3,0}(y_{2,0}) - F^-\left(x^j_{3,0}(y_{2,0}), (\epsilon/\delta)^{1/3}, \delta, c, a\right) \\ \tilde{x}^j_{3,0}(y_{2,0}) &= x^j_{3,0}(y_{2,0}) - F^+\left(z^j_{3,0}(y_{2,0}), (\epsilon/\delta)^{1/3}, \delta, c, a\right), \end{aligned} \tag{5.117}$$

from which the result follows, noting $r_2 = \epsilon^{1/3}$. □

We now obtain estimates for solutions on $\mathcal{Y}(c,a,\epsilon)$ with initial conditions in Σ_{23} upon exit in Σ_3^{out}. We have the following lemma regarding $\mathcal{Y}(c,a,\epsilon)$ (an analogous result holds for $\mathcal{W}^{s,r}_\epsilon(c,a)$).

Lemma 5.10. *Consider solutions on the manifold $\mathcal{Y}(c,a,\epsilon)$, with initial conditions as in Lemma 5.9 parameterized by $|y_{2,0}| \le 1/\delta^{2/3}$. Such solutions exit Σ_3^{out} in time $T^* = T^*(y_{2,0})$ in a curve $(\tilde{x}^\ell_3(T^*(y_{2,0})), \tilde{z}^\ell_3(T^*(y_{2,0})))$. For each sufficiently small $\delta, \rho > 0$, there exists $C > 0$ independent of (c,a,ϵ) and $y^\pitchfork_{2,0} > 0$ such that the following holds. Let $\tilde{x}^i_3 = \tilde{x}^\ell_3(T^*(-1/\delta^{2/3}))$, and let $\tilde{x}^\pitchfork_3 = \tilde{x}^\ell_3(T^*(y^\pitchfork_{2,0}))$. Then*

$$\tilde{x}^\pitchfork_3 \le -\frac{\epsilon^{1/3}}{C}\exp\left(\beta^2_+(\rho,\delta,\epsilon) - \frac{C}{\epsilon^{1/3}}\right), \tag{5.118}$$

and for $y_{2,0} \in (-1/\delta^{2/3}, y^\pitchfork_{2,0})$, the curve $(\tilde{x}^\ell_3(T^*(y_{2,0})), \tilde{z}^\ell_3(T^*(y_{2,0})))$ can be expressed as a graph $\tilde{z}_3 = \widehat{z}_3(\tilde{x}_3; c,a,\epsilon)$ for $\tilde{x}_3 \in (\tilde{x}^\pitchfork_3, \tilde{x}^i_3)$ which satisfies

$$\begin{aligned} |\widehat{z}_3(\tilde{x}_3; c,a,\epsilon)| &\le C\exp\left(-\frac{\rho^2}{\epsilon}\left(1+\frac{2\rho}{3}+\mathcal{O}(\rho^2,\rho\delta)\right)\right) \\ \frac{d\widehat{z}_3}{d\tilde{x}_3}(\tilde{x}_3; c,a,\epsilon) &\le \frac{C}{\epsilon^{2/3}}\exp\left(-\frac{4\rho^3}{3\epsilon}\left(1+\mathcal{O}(\rho,\delta)\right)\right) \end{aligned} \tag{5.119}$$

uniformly in $\tilde{x}_3 \in (\tilde{x}^\pitchfork_3(c,a,\epsilon), \tilde{x}^i_3(c,a,\epsilon))$ and (c,a,ϵ).

Proof. Using Lemma 5.8, we have that solutions with initial conditions given by Lemma 5.9 for $|y_{2,0}| \le 1/\delta^{2/3}$ reach Σ_3^{out} at time $T^* = T^*(y_{2,0})$ in curves

$$\begin{aligned} \tilde{x}^\ell_3(T^*(y_{2,0})) &= \tilde{x}^\ell_{3,0}(y_{2,0})\exp\left(\beta^2_+(\rho,\delta,\epsilon) + \eta^2_+(\rho,\delta,\tilde{x}^\ell_{3,0}(y_{2,0}),\tilde{z}^\ell_{3,0}(y_{2,0}),\epsilon)\right) \\ \tilde{z}^\ell_3(T^*(y_{2,0})) &= \tilde{z}^\ell_{3,0}(y_{2,0})\exp\left(\beta^2_-(\rho,\delta,\epsilon) + \eta^2_-(\rho,\delta,\tilde{x}^\ell_{3,0}(y_{2,0}),\tilde{z}^\ell_{3,0}(y_{2,0}),\epsilon)\right), \end{aligned} \tag{5.120}$$

where β_+^2, η_+^2 are given by the integrals (5.104) (and analogously for β_-^2, η_-^2). It remains to estimate the derivatives $\dfrac{d\tilde{x}_3^\ell(T^*)}{dy_{2,0}}, \dfrac{d\tilde{z}_3^\ell(T^*)}{dy_{2,0}}$.

To obtain estimates on the derivatives of the solutions with respect to $y_{2,0}, c, a$, we consider the variational equation of (5.95). Using the estimates (5.120), for $K = 1/2$ and each small $\kappa > 0$, there exists C such that for all sufficiently small ρ, δ, we can estimate

$$\begin{aligned}
\frac{d\tilde{x}_3^\ell(t)}{dy_{2,0}} &\leq C\left(\left|(\tilde{x}_{3,0}^\ell)'(y_{2,0})\right| + \left|(\tilde{z}_{3,0}^\ell)'(y_{2,0})\right|\right) e^{-Kt} \\
\frac{d\tilde{z}_3^\ell(t)}{dy_{2,0}} &\leq C\left(\left|(\tilde{x}_{3,0}^\ell)'(y_{2,0})\right| + \left|(\tilde{z}_{3,0}^\ell)'(y_{2,0})\right|\right) e^{-Kt} \\
\frac{dr_3^\ell(t)}{dy_{2,0}} &\leq C\left(\left|(\tilde{x}_{3,0}^\ell)'(y_{2,0})\right| + \left|(\tilde{z}_{3,0}^\ell)'(y_{2,0})\right|\right) e^{\kappa t} \\
\frac{d\epsilon_3^\ell(t)}{dy_{2,0}} &\leq C\left(\left|(\tilde{x}_{3,0}^\ell)'(y_{2,0})\right| + \left|(\tilde{z}_{3,0}^\ell)'(y_{2,0})\right|\right) e^{\kappa t}
\end{aligned} \tag{5.121}$$

for solutions on $\mathcal{Y}(c, a, \epsilon)$ with initial conditions

$$(\tilde{x}_3, \tilde{z}_3, r_3, \epsilon_3)(0) = (\tilde{x}_{3,0}^\ell(y_{2,0}), \tilde{z}_{3,0}^\ell(y_{2,0}), (\epsilon/\delta)^{1/3}, \delta) \in \Sigma_{23}. \tag{5.122}$$

Differentiating (5.120), we have that

$$\begin{aligned}
\frac{d\tilde{x}_3^\ell(T^*)}{dy_{2,0}} = &\left((\tilde{x}_{3,0}^\ell)'(y_{2,0}) + \tilde{x}_{3,0}^\ell \frac{d}{dy_{2,0}}\left(\frac{2}{\epsilon}\int_{r_{3,0}}^{\rho} \mathcal{O}\left(r_3^3(|\tilde{x}_3^\ell| + |\tilde{z}_3^\ell|), r_3^2\epsilon_3(|\tilde{x}_3^\ell| + |\tilde{z}_3^\ell|)\right) dr_3\right)\right) \\
&\times \exp\left(\beta_+^2(\rho, \delta, \epsilon) + \eta_+^2(\rho, \delta, \tilde{x}_{3,0}^\ell, \tilde{z}_{3,0}^\ell, \epsilon)\right),
\end{aligned} \tag{5.123}$$

where $r_{3,0} = (\epsilon/\delta)^{1/3}$. It remains to prove the following estimate for the second term

$$\left|\frac{d}{dy_{2,0}}\left(\frac{2}{\epsilon}\int_{r_{3,0}}^{\rho} \mathcal{O}\left(r_3^3(|\tilde{x}_3^\ell| + |\tilde{z}_3^\ell|), r_3^2\epsilon_3(|\tilde{x}_3^\ell| + |\tilde{z}_3^\ell|)\right) dr_3\right)\right| \leq C\delta\left(\left|(\tilde{x}_{3,0}^\ell)'(y_{2,0})\right| + \left|(\tilde{z}_{3,0}^\ell)'(y_{2,0})\right|\right), \tag{5.124}$$

where $C > 0$ is independent of δ, ρ, ϵ. We begin with estimating a term of the form

$$\frac{d}{dy_{2,0}}\left(\frac{2}{\epsilon}\int_{r_{3,0}}^{\rho} r_3^3\tilde{x}_3^\ell dr_3\right), \tag{5.125}$$

as the others will be similar. As the endpoints of the integral are fixed, we obtain

$$\frac{d}{dy_{2,0}}\left(\frac{2}{\epsilon}\int_{r_{3,0}}^{\rho} r_3^3\tilde{x}_3^\ell dr_3\right) = \frac{2}{\epsilon}\int_{r_{3,0}}^{\rho} r_3^3\frac{d\tilde{x}_3^\ell}{dy_{2,0}} dr_3 + \frac{2}{\epsilon}\int_{r_{3,0}}^{\rho} 3r_3^2\frac{dr_3}{dy_{2,0}}\tilde{x}_3^\ell dr_3. \tag{5.126}$$

Using the estimates (5.121) and noting that $t > \dfrac{1}{2\epsilon}(r_3(t)^2 - r_{3,0}^2)$ (as in the proof of Lemma 5.8), we see that we can bound the above integrals by an integral of the form

$$\begin{aligned}
&\frac{2}{\epsilon}\left(\left|(\tilde{x}_{3,0}^\ell)'(y_{2,0})\right| + \left|(\tilde{z}_{3,0}^\ell)'(y_{2,0})\right|\right)\left|\int_{r_{3,0}}^{\rho} r_3^2 \exp\left(-\frac{1}{4\epsilon}\left(r_3^2 - r_{3,0}^2\right)\right) dr_3\right| \\
&\qquad \leq C\left(\left|(\tilde{x}_{3,0}^\ell)'(y_{2,0})\right| + \left|(\tilde{z}_{3,0}^\ell)'(y_{2,0})\right|\right)\left(r_{3,0} + \mathcal{O}(r_{3,0}^2)\right),
\end{aligned} \tag{5.127}$$

where C is independent of ρ, δ, ϵ. Proceeding similarly, we estimate

$$\frac{d}{dy_{2,0}}\left(\frac{2}{\epsilon}\int_{r_{3,0}}^{\rho} r_3\epsilon_3\tilde{z}_3^\ell dr_3\right) \leq C\delta\left(\left|(\tilde{x}_{3,0}^\ell)'(y_{2,0})\right| + \left|(\tilde{z}_{3,0}^\ell)'(y_{2,0})\right|\right)\left(1 + \mathcal{O}(r_{3,0})\right), \tag{5.128}$$

where C is independent of ρ, δ, ϵ. Using the fact that $r_{3,0} = \left(\frac{\epsilon}{\delta}\right)^{1/3}$, we obtain

$$\begin{aligned}\frac{d\tilde{x}_3^\ell(T^*)}{dy_{2,0}} &= \left((\tilde{x}_{3,0}^\ell)'(y_{2,0}) + \mathcal{O}\left(\delta\tilde{x}_{3,0}^\ell(y_{2,0})\left(\left|(\tilde{x}_{3,0}^\ell)'(y_{2,0})\right| + \left|(\tilde{z}_{3,0}^\ell)'(y_{2,0})\right|\right)\right)\right) \\ &\quad \times \exp\left(\beta_+^2(\rho,\delta,\epsilon) + \eta_+^2(\rho,\delta,\tilde{x}_{3,0}^\ell(y_{2,0}),\tilde{z}_{3,0}^\ell(y_{2,0}),\epsilon)\right) \\ \frac{d\tilde{z}_3^\ell(T^*)}{dy_{2,0}} &= \left((\tilde{z}_{3,0}^\ell)'(y_{2,0}) + \mathcal{O}\left(\delta\tilde{z}_{3,0}^\ell(y_{2,0})\left(\left|(\tilde{x}_{3,0}^\ell)'(y_{2,0})\right| + \left|(\tilde{z}_{3,0}^\ell)'(y_{2,0})\right|\right)\right)\right) \\ &\quad \times \exp\left(\beta_-^2(\rho,\delta,\epsilon) + \eta_-^2(\rho,\delta,\tilde{x}_{3,0}^\ell(y_{2,0}),\tilde{z}_{3,0}^\ell(y_{2,0}),\epsilon)\right),\end{aligned} \tag{5.129}$$

for $j = \ell, r$, where $\beta_\pm^2, \eta_\pm^2$ are given by Lemma 5.8.

We now can compute the slope of the intersection of $\mathcal{Y}(c,a,\epsilon)$ with the section Σ_3^{out}

$$\begin{aligned}\frac{d\tilde{z}_3^\ell}{d\tilde{x}_3^\ell}(y_{2,0}) &= \frac{\left((\tilde{z}_{3,0}^\ell)'(y_{2,0}) + \mathcal{O}\left(\delta\tilde{z}_{3,0}^\ell\left(\left|(\tilde{x}_{3,0}^\ell)'(y_{2,0})\right| + \left|(\tilde{z}_{3,0}^\ell)'(y_{2,0})\right|\right)\right)\right)}{\left((\tilde{x}_{3,0}^\ell)'(y_{2,0}) + \mathcal{O}\left(\delta\tilde{x}_{3,0}^\ell\left(\left|(\tilde{x}_{3,0}^\ell)'(y_{2,0})\right| + \left|(\tilde{z}_{3,0}^\ell)'(y_{2,0})\right|\right)\right)\right)} e^{\left(-\frac{4\rho^3}{3\epsilon}(1+\mathcal{O}(\rho,\delta))\right)} \\ &= \frac{\left(\tilde{Z}_3^\ell - k\epsilon^{1/3}(\tilde{Z}_3^\ell)' + \mathcal{O}\left(\delta\tilde{z}_{3,0}^\ell\left(|\tilde{X}_3^\ell| + |\tilde{Z}_3^\ell| + \mathcal{O}(\epsilon^{1/3})\right)\right)\right)}{\left(\tilde{X}_3^\ell - k\epsilon^{1/3}(\tilde{X}_3^\ell)' + \mathcal{O}\left(\delta\tilde{x}_{3,0}^\ell\left(|\tilde{X}_3^\ell| + |\tilde{Z}_3^\ell| + \mathcal{O}(\epsilon^{1/3})\right)\right)\right)} e^{\left(-\frac{4\rho^3}{3\epsilon}(1+\mathcal{O}(\rho,\delta))\right)}\end{aligned} \tag{5.130}$$

where we used that $r_2 = \epsilon^{1/3}$. For each fixed small $\delta, \rho > 0$, the numerator in the above fraction is a bounded function for sufficiently small $\epsilon > 0$. Hence it is clear that the tangent space to $\mathcal{Y}(c,a,\epsilon)$ has exponentially small slope except near points where the denominator is also exponentially small. Hence we proceed by obtaining a lower bound for the denominator for an appropriate range of $y_{2,0}$.

From properties of Airy functions in Lemma 5.3 and the bounds in Lemma 5.9, we know that the function $\tilde{X}_3^\ell(y_{2,0})$ is smooth and is positive for $y_{2,0} \le 0$. For $y_{2,0} > 0$, $\tilde{X}_3^\ell(y_{2,0})$ transitions to oscillatory behavior: the first zero occurs at $y_{2,0} = y_{2,0}^\ell > 0$ and here $(\tilde{X}_3^\ell)'(y_{2,0}^\ell) < 0$. Hence by the implicit function theorem we can solve for the first zero of the denominator

$$\left(\tilde{X}_3^\ell - k\epsilon^{1/3}(\tilde{X}_3^\ell)' + \mathcal{O}\left(\delta\tilde{x}_{3,0}^\ell\left(|\tilde{X}_3^\ell| + |\tilde{Z}_3^\ell| + \mathcal{O}(\epsilon^{1/3})\right)\right)\right) = 0. \tag{5.131}$$

We first argue that the $\mathcal{O}$-term does not contribute to finding zeros in this expression. To see this, we note that for δ fixed sufficiently small, we can bound

$$|\tilde{X}_3^\ell| + |\tilde{Z}_3^\ell| + \mathcal{O}(\epsilon^{1/3}) \le 4|\tilde{X}_3^\ell| \tag{5.132}$$

uniformly in $y_{2,0} \in (-1/\delta^{2/3}, -1/\delta^{2/3} + \delta)$, provided ϵ is taken sufficiently small. Hence there are no zeros of (5.131) for $y_{2,0} \in (-1/\delta^{2/3}, -1/\delta^{2/3} + \delta)$ and ϵ sufficiently small. For $y_{2,0} > -1/\delta^{2/3} + \delta$, we have that

$$\tilde{x}_{3,0}^\ell = \frac{\sqrt{\pi}e^{-\frac{\frac{1}{\delta^{2/3}} + y_{2,0}}{k\epsilon^{1/3}}}}{k^{1/6}\delta^{1/6}}\tilde{X}_3^\ell(y_{2,0}), \tag{5.133}$$

where we used the fact that $r_2 = \epsilon^{1/3}$. Hence by taking ϵ sufficiently small, we can bound $\tilde{x}_{3,0}^\ell = \mathcal{O}(\epsilon^{2/3})$. Hence the first zero of (5.131) occurs when

$$y_{2,0} = y_{2,0}^\ell + k\epsilon^{1/3} + \mathcal{O}(\epsilon^{2/3}). \tag{5.134}$$

Hence there exists C such that for all

$$y_{2,0} \le y_{2,0}^{\pitchfork} := y_{2,0}^\ell + k\epsilon^{1/3} - C\epsilon^{2/3}, \tag{5.135}$$

the slope $\frac{d\tilde{z}}{d\tilde{x}}(y_{2,0})$ of the manifold $\mathcal{Y}(c,a,\epsilon)$ in Σ_3^{out} is exponentially small. We now define

$$\begin{aligned}\tilde{x}_3^{\pitchfork}(c,a,\epsilon) &= \tilde{x}_{3,0}(y_{2,0}^{\pitchfork})\exp\left(\beta_+^2(\rho,\delta,\epsilon) + \eta_+^2(\rho,\delta,\tilde{x}_{3,0}(y_{2,0}^{\pitchfork}),\tilde{z}_{3,0}(y_{2,0}^{\pitchfork}),\epsilon)\right) \\ &\le -\frac{\epsilon^{1/3}}{C}\exp\left(\beta_+^2(\rho,\delta,\epsilon) - \frac{C}{\epsilon^{1/3}}\right)\end{aligned} \tag{5.136}$$

for some $C > 0$ independent of (c,a,ϵ). The result follows. □

5.5.2 Solutions with initial conditions in Σ_{13}

The above takes care of the solutions on $\mathcal{Y}(c,a,\epsilon)$ entering via Σ_{23}, but we still have those which enter via Σ_{13} directly from chart $\mathcal{K}_1$. We have the following.

Lemma 5.11. *For each sufficiently small $\rho,\delta>0$, there exists $C,\eta,\epsilon_0>0$ and sufficiently small choice of the intervals I_a, I_c such that for each $(c,a,\epsilon)\in I_c\times I_a\times(0,\epsilon_0)$, there exists $x_3^{\Delta}(c,a,\epsilon)>0$ such that the following holds. Consider solutions on the manifold $\mathcal{Y}(c,a,\epsilon)$, with initial conditions in Σ_{13}. All such solutions exit Σ_3^{out} in a curve which can be represented as a graph $\tilde{z}_3=\widehat{z}_3(\tilde{x}_3;c,a,\epsilon)$ for $\tilde{x}_3\in(\tilde{x}_3^i(c,a,\epsilon),\tilde{x}_3^{\Delta}(c,a,\epsilon))$ which satisfies*

$$\begin{aligned}&|\widehat{z}_3(\tilde{x}_3;c,a,\epsilon)|\leq Ce^{-\eta/\epsilon}\\&\frac{d\widehat{z}_3}{d\tilde{x}_3}(\tilde{x}_3;c,a,\epsilon)\leq Ce^{-\eta/\epsilon},\end{aligned}\tag{5.137}$$

uniformly in $\tilde{x}_3\in(\tilde{x}_3^i(c,a,\epsilon),\tilde{x}_3^{\Delta}(c,a,\epsilon))$ and $(c,a,\epsilon)\in I_c\times I_a\times(0,\epsilon_0)$.

Proof. From Proposition 5.5 (i), we have that such solutions enter Σ_{13} in a curve $z_3=z_{3,0}(r_{3,0})$, for $r_{3,0}\in((\epsilon/\delta)^{1/3},\Delta_{r_3})$ which satisfies $|z_{3,0}'(r_{3,0})|\leq C|\log\epsilon|$ uniformly in $r_{3,0}$, where we may assume $\Delta_{r_3}\ll\rho$ by taking Δ_{y_1} smaller in Proposition 5.5 if necessary. In the $\sim$ coordinates, we have that this curve can be parameterized by $r_{3,0}$ as $(\tilde{x}_3,\tilde{z}_3)=(\tilde{x}_{3,0}(r_{3,0}),\tilde{z}_{3,0}(r_{3,0}))$ where

$$\begin{aligned}\tilde{x}_{3,0}(r_{3,0})&=1-F^+\left(z_{3,0}(r_{3,0}),r_{3,0},\epsilon_{3,0}(r_{3,0}),c,a\right)\\\tilde{z}_{3,0}(r_{3,0})&=z_{3,0}(r_{3,0})-F^-\left(1,r_{3,0},\epsilon_{3,0}(r_{3,0}),c,a\right)\\\epsilon_{3,0}(r_{3,0})&=\frac{\epsilon}{r_{3,0}^3}.\end{aligned}\tag{5.138}$$

Similarly to the proof of Lemma 5.8 we track these solutions through to Σ_3^{out}, where they intersect in a curve

$$\begin{aligned}\tilde{x}_3(r_{3,0})&=\tilde{x}_{3,0}(r_{3,0})\exp\left(\beta_+^1(\rho,\delta,r_{3,0},\epsilon)\right)\\\tilde{z}_3(r_{3,0})&=\tilde{z}_{3,0}(r_{3,0})\exp\left(\beta_-^1(\rho,\delta,r_{3,0},\epsilon)\right),\end{aligned}\tag{5.139}$$

where

$$\begin{aligned}\beta_-^1(\rho,\delta,r_{3,0},\epsilon)&=\frac{2}{\epsilon}\int_{r_{3,0}}^{\rho}\left(-r_3-r_3^2+\mathcal{O}(r_3^3,r_3^2\epsilon_3)\right)dr_3\\&=\frac{1}{\epsilon}\left(-\rho^2+r_{3,0}^2-\frac{2}{3}(\rho^3-r_{3,0}^3)+\mathcal{O}(\rho^4,\rho^3\delta,r_{3,0}^4)\right)\\\beta_+^1(\rho,\delta,r_{3,0},\epsilon)&=\frac{2}{\epsilon}\int_{r_{3,0}}^{\rho}\left(-r_3+r_3^2+\mathcal{O}(r_3^3,r_3^2\epsilon_3)\right)dr_3\\&=\frac{1}{\epsilon}\left(-\rho^2+r_{3,0}^2+\frac{2}{3}(\rho^3-r_{3,0}^3)+\mathcal{O}(\rho^4,\rho^3\delta,r_{3,0}^4)\right).\end{aligned}\tag{5.140}$$

Using similar arguments as in the proof of Lemma 5.10, we estimate

$$\begin{aligned}\frac{d\tilde{x}_3}{dr_{3,0}}&=\left(\frac{d\tilde{x}_{3,0}}{dr_{3,0}}+\frac{2}{\epsilon}\tilde{x}_{3,0}\left(r_{3,0}+\mathcal{O}(r_{3,0}^2)\right)+\mathcal{O}\left(\tilde{x}_{3,0}\left(\epsilon^{-1/3}+\left|\frac{d\tilde{x}_{3,0}}{dr_{3,0}}\right|+\left|\frac{d\tilde{z}_{3,0}}{dr_{3,0}}\right|\right)\right)\right)\\&\quad\times\exp\left(\beta_+^1(\rho,\delta,r_{3,0},\epsilon)\right)\\\frac{d\tilde{z}_3}{dr_{3,0}}&=\left(\frac{d\tilde{z}_{3,0}}{dr_{3,0}}+\frac{2}{\epsilon}\tilde{z}_{3,0}\left(r_{3,0}+\mathcal{O}(r_{3,0}^2)\right)+\mathcal{O}\left(\tilde{x}_{3,0}\left(\epsilon^{-1/3}+\left|\frac{d\tilde{x}_{3,0}}{dr_{3,0}}\right|+\left|\frac{d\tilde{z}_{3,0}}{dr_{3,0}}\right|\right)\right)\right)\\&\quad\times\exp\left(\beta_-^1(\rho,\delta,r_{3,0},\epsilon)\right),\end{aligned}\tag{5.141}$$

and we define

$$\begin{aligned}\tilde{x}_3^i(c,a,\epsilon)&:=\tilde{x}_{3,0}((\epsilon/\delta)^{1/3})\exp\left(\beta_+^1(\rho,\delta,(\epsilon/\delta)^{1/3},\epsilon)\right)\\\tilde{x}_3^{\Delta}(c,a,\epsilon)&:=\tilde{x}_{3,0}(\Delta_{r_3})\exp\left(\beta_+^1(\rho,\delta,\Delta_{r_3},\epsilon)\right),\end{aligned}\tag{5.142}$$

noting that the definition of $\tilde{x}_3^i(c,a,\epsilon)$ coincides with that in Lemma 5.10. We therefore can estimate

$$\frac{d\tilde{z}_3}{d\tilde{x}_3}(r_{3,0}) = \frac{\tilde{z}_{3,0} + \mathcal{O}\left(\epsilon^{1/3}\log\epsilon\right)}{\tilde{x}_{3,0} + \mathcal{O}\left(\epsilon^{1/3}\log\epsilon\right)} \exp\left(-\frac{4}{3\epsilon}\left(\rho^3 - r_{3,0}^3\right) + \mathcal{O}\left(\rho^4, \rho^3\delta, r_{3,0}^4\right)\right), \tag{5.143}$$

from which we obtain the required estimates, recalling the choice of $0 < \Delta_{r_3} \ll \rho$. □

5.5.3 Estimates for $\mathcal{Y}(c,a,\epsilon)$ in Σ_3^{out}

We now fix ρ, δ sufficiently small and combine the results of Lemma 5.9 and Lemma 5.11 into the following.

Lemma 5.12. *For each sufficiently small $\Delta_y > 0$, there exists $C, \eta, \epsilon_0 > 0$ and sufficiently small choice of the intervals I_a, I_c such that for each $(c,a,\epsilon) \in I_c \times I_a \times (0,\epsilon_0)$, there exists $y_\epsilon^*(c,a) > \epsilon^{2/3}/C$ such that the following holds. Define $\mathcal{Y}^{\pitchfork}(c,a,\epsilon)$ to be the backwards evolution of initial conditions $\{(\rho^4, y, z, \epsilon) : z = z_\epsilon^{s,\ell}(y;c,a), -\Delta_y \leq y \leq y_\epsilon^*(c,a)\}$ on $\mathcal{Y}(c,a,\epsilon)$ in Σ_A^{in}. The intersection of $\mathcal{Y}^{\pitchfork}(c,a,\epsilon)$ with $\Sigma_A^{out} = \Sigma_3^{out}$ is given by a curve $\tilde{z}_3 = \widehat{z}_3(\tilde{x}_3;c,a,\epsilon)$ in the $\mathcal{K}_3$ coordinates for $\tilde{x}_3 \in (\tilde{x}_3^{\pitchfork}(c,a,\epsilon), \tilde{x}_3^{\Delta}(c,a,\epsilon))$ which satisfies*

$$\begin{aligned} |\widehat{z}_3(\tilde{x}_3;c,a,\epsilon)| &\leq Ce^{-\eta/\epsilon} \\ \frac{d\widehat{z}_3}{d\tilde{x}_3}(\tilde{x}_3;c,a,\epsilon) &\leq Ce^{-\eta/\epsilon}, \end{aligned} \tag{5.144}$$

uniformly in $\tilde{x}_3 \in (\tilde{x}_3^{\pitchfork}(c,a,\epsilon), \tilde{x}_3^{\Delta}(c,a,\epsilon))$ and (c,a,ϵ). Here $\tilde{x}_3^{\pitchfork}(c,a,\epsilon), \tilde{x}_3^{\Delta}(c,a,\epsilon)$ are defined as in Lemma 5.9 and Lemma 5.11 and

$$\tilde{x}_3^{\pitchfork}(c,a,\epsilon) \leq -\frac{\epsilon^{1/3}}{C}\exp\left(\beta_+^2(\rho,\delta,\epsilon) - \frac{C}{\epsilon^{1/3}}\right). \tag{5.145}$$

5.6 Proofs of transversality results

To measure the transversality properties of $\mathcal{Y}^{\pitchfork}(c,a,\epsilon)$ with respect to the strong unstable fibers of $\mathcal{Z}_\epsilon(c,a)$ in the section Σ^m, we use the transversality results for the backwards evolution of fibers on $\mathcal{Y}(c,a,\epsilon)$ with height $y > -\Delta_y$ obtained above in the section Σ_3^{out} combined with the fact that trajectories on $\mathcal{Y}(c,a,\epsilon)$ for $y < -\Delta_w$ remain on the invariant manifold $\mathcal{Z}_\epsilon(c,a)$ when evolved backwards to Σ^m.

Remark 5.13. *We note a subtle distinction: the transversality we actually require is with respect to the fibers of $\mathcal{W}_\epsilon^{c,\ell}(c,a)$ in the section Σ^m. However by evolving these forward to Σ_3^{out}, they also provide a foliation over the manifold $\mathcal{Z}_\epsilon(c,a)$ in which the fibers are C^1 exponentially close to those of $\mathcal{Z}_\epsilon(c,a)$. The arguments in this section carry through with respect to any such foliation. Hence without loss of generality we work with the (nonunique) strong unstable fibers of $\mathcal{Z}_\epsilon(c,a)$.*

Proof of Proposition 4.5. We note that the manifold $\mathcal{Y}^{\pitchfork}(c,a,\epsilon)$ is defined in terms of the (u,v,w)-coordinates in $\Sigma^{h,\ell}$ in Proposition 4.5, but defined in terms of the (x,y,z)-coordinates in Σ_A^{in} in Lemma 5.12. In the analysis below, it is more natural to determine transversality properties in the section Σ_3^{out}, and hence also more natural to represent this manifold in the (x,y,z)-coordinates near the Airy point. To obtain the corresponding definition in $\Sigma^{h,\ell}$, we evolve $\mathcal{Y}^{\pitchfork}(c,a,\epsilon)$ *forwards* from Σ_A^{in} to $\Sigma^{h,\ell}$ to obtain the w-coordinate endpoints w_ϵ^{Δ} and $w_\epsilon^{\pitchfork}$ corresponding to the solutions on $\mathcal{Y}^{\pitchfork}(c,a,\epsilon)$ with initial conditions in Σ_A^{in} at $y = -\Delta_y$ and $y = y_\epsilon^*(c,a)$, respectively.

Using Lemma 5.12, we are able to track trajectories on $\mathcal{Y}(c,a,\epsilon)$ with initial conditions in Σ_A^{in} with $y \in (-\Delta_y, y_\epsilon^*)$ down to the section Σ_3^{out}. In the chart $\mathcal{K}_3$, the intersection of this manifold with Σ_3^{out} is given by a curve $\tilde{z}_3 = \widehat{z}_3(\tilde{x}_3;c,a,\epsilon)$ for $\tilde{x}_3 \in (\tilde{x}_3^{\pitchfork}(c,a,\epsilon), \tilde{x}_3^{\Delta}(c,a,\epsilon))$ which satisfies

$$|\widehat{z}_3(\tilde{x}_3;c,a,\epsilon)| \leq Ce^{-\eta/\epsilon}, \quad \frac{d\widehat{z}_3}{d\tilde{x}_3}(\tilde{x}_3;c,a,\epsilon) \leq Ce^{-\eta/\epsilon}, \tag{5.146}$$

uniformly in $\tilde{x}_3 \in (\tilde{x}_3^{\pitchfork}(c,a,\epsilon), \tilde{x}_3^{\Delta}(c,a,\epsilon))$ and (c,a,ϵ).

We now investigate the intersection of $\mathcal{Z}_\epsilon(c,a)$ with the section Σ_3^{out}. This manifold will intersect Σ_3^{out} in a curve $\tilde{z}_3 = \tilde{z}_3^s(\tilde{x}_3; c, a, \epsilon)$ which satisfies

$$\tilde{z}_3^s(0; c, a, \epsilon) = \mathcal{O}(e^{-q/\epsilon}), \tag{5.147}$$

and

$$\frac{d\tilde{z}_3^s}{d\tilde{x}}(\tilde{x}_3; c, a, \epsilon) \to 0 \quad \text{as} \quad |(\epsilon, \tilde{x}_3)| \to 0, \tag{5.148}$$

uniformly in (c,a). This follows from the fact that $\mathcal{Z}_\epsilon(c,a)$ contains a (non-unique) choice of the slow manifold $\mathcal{M}_\epsilon^m(c,a)$ which will be exponentially close to the point $(\tilde{x}_3, \tilde{z}_3) = (0,0)$, and that $\mathcal{Z}_\epsilon(c,a)$ is a C^1 perturbation of $\mathcal{Z}_0(c,a)$ which at $\epsilon = 0$ is tangent to the weak unstable subspace $\tilde{z}_3 = 0$ at the origin $(\tilde{x}_3, \tilde{z}_3) = (0,0)$.

The strong unstable fibers $\mathcal{W}^{uu}(\mathcal{Z}_\epsilon(c,a))$ of $\mathcal{Z}_\epsilon(c,a)$ are also a C^1 perturbation of $\mathcal{W}^{uu}(\mathcal{Z}_0(c,a))$ which at $\epsilon = 0$ is tangent to the strong unstable subspace $\tilde{x}_3 = 0$ at the origin $(\tilde{x}_3, \tilde{z}_3) = (0,0)$. Therefore, the strong unstable fiber of a passing through a point $(\tilde{x}_3^b, \tilde{z}_3^b)$ is given by a graph $\tilde{x}_3 = f_3^s(\tilde{z}_3; \tilde{x}_3^b, \tilde{z}_3^b, c, a, \epsilon)$, where

$$f_3^s(\tilde{z}_3^b; \tilde{x}_3^b, \tilde{z}_3^b, c, a, \epsilon) = \tilde{x}_3^b \tag{5.149}$$

and

$$\frac{df_3^s}{d\tilde{z}_3}(\tilde{z}_3; \tilde{x}_3^b, \tilde{z}_3^b, c, a, \epsilon) \to 0 \quad \text{as} \quad |(\epsilon, \tilde{x}_3^b, \tilde{z}_3^b, \tilde{z}_3)| \to 0 \tag{5.150}$$

Finally, since the manifold $\mathcal{Z}_\epsilon(c,a)$ is invariant and well defined for $y < -\Delta_y$, we have that $\tilde{z}_3^s(\tilde{x}_3^{\Delta}; c, a, \epsilon) = \widehat{z}_3(\tilde{x}_3^{\Delta}; c, a, \epsilon)$ and trajectories on $\mathcal{Y}(c,a,\epsilon)$ evolved backwards from Σ_A^{in} for $y < -\Delta_y$ in fact again *remain in* $\mathcal{Z}_\epsilon(c,a)$. Since $\mathcal{Z}_\epsilon(c,a)$ is certainly transverse to its own strong unstable fibers, we are only concerned for values $\tilde{x}_3 \in (\tilde{x}_3^{\pitchfork}(c,a,\epsilon), \tilde{x}_3^{\Delta}(c,a,\epsilon))$ as here the intersection of the manifolds $\mathcal{Y}(c,a,\epsilon)$ and $\mathcal{Z}_\epsilon(c,a)$ with the section Σ_3^{out} separate into curves given by the two functions described above.

From the estimates above, we can deduce that the backwards evolution of $\mathcal{Y}^{\pitchfork}(c,a,\epsilon)$ given by the curve $\tilde{z}_3 = \widehat{z}_3(\tilde{x}_3; c, a, \epsilon)$ in the section Σ_3^{out} remains transverse to the strong unstable fibers of $\mathcal{Z}_\epsilon(c,a)$ at least up to the fiber which passes through the point $(\tilde{x}_3^{\pitchfork}, \widehat{z}_3(\tilde{x}_3^{\pitchfork}))$.

We now evolve the manifold $\mathcal{Y}^{\pitchfork}(c,a,\epsilon)$ backwards from Σ_3^{out} to Σ^m. Using an inclination lemma, we deduce that the above transversality also holds in the section Σ^m and all trajectories are exponentially contracted to $\mathcal{M}_\epsilon^m(c,a)$. We denote by $y_2^{\Sigma}(c,a)$ the y_2 coordinate in Σ^m of the backwards evolution of the solution $\mathcal{Y}^{\pitchfork}(c,a,\epsilon)$ passing through $(\tilde{x}_3^{\Delta}(c,a,\epsilon), \widehat{z}_3(\tilde{x}_3^{\Delta}(c,a,\epsilon))$ in Σ_3^{out}, and we denote by $y_2^{\mathcal{T}}(c,a)$ the y_2 coordinate in Σ^m of the backwards evolution of the basepoint on $\mathcal{Z}_\epsilon(c,a)$ corresponding to the fiber containing the solution on $\mathcal{Y}^{\pitchfork}(c,a,\epsilon)$ passing through $(\tilde{x}_3^{\pitchfork}, \widehat{z}_3(\tilde{x}_3^{\pitchfork}))$ in Σ_3^{out}. With these definitions, we see that the assertions of the proposition hold in the section Σ^m. □

Proof of Lemma 4.7. The estimates (4.31) are shown in §4.4.1. Hence it remains to show that the transversality of $\mathcal{Y}^{\pitchfork}(c,a,\epsilon)$ with respect to the fibers of $\mathcal{Z}_\epsilon(c,a)$ in Σ^m includes the fibers through all points on the backwards evolution of $\mathcal{B}(s;c,a)$. By Proposition 4.5, this amounts to proving (4.32). As in the proof of Proposition 4.5, we work in a neighborhood of the Airy point and determine transversality conditions in the section Σ_3^{out} and use this information to deduce what happens in Σ^m.

Here we consider pulses of Type 2, 3 so $s \in (w_R(\Delta_w), w^\dagger + \Delta_w)$. Evolving $\mathcal{B}(s;c,a)$ backwards from $\Sigma^{h,\ell}$, these solutions are already exponentially contracted to $\mathcal{M}_\epsilon^m(c,a)$ *above* the Airy point, and we see that they eventually enter the chart $\mathcal{K}_3$ via the section Σ_{23} where their $(\tilde{x}, \tilde{z})$-coordinates are *already* $\mathcal{O}(e^{-q/\epsilon})$ uniformly in (c,a).

Suppose we take any such solution which enters Σ_{23} at a point $(\tilde{x}^b_{3,0}, \tilde{z}^b_{3,0}) = \mathcal{O}(e^{-q/\epsilon})$ where we drop the dependence on (c, a). This solution reaches Σ_3^{out} at $(\tilde{x}_3, \tilde{z}_3) = (\tilde{x}^b_{3,1}, \tilde{z}^b_{3,1})$ where

$$\begin{aligned} \tilde{x}^b_{3,1} &= \tilde{x}^b_{3,0} \exp\left(\beta_+^2(\rho, \delta, \epsilon) + \eta_+^2(\rho, \delta, \tilde{x}^b_{3,0}, \tilde{z}^b_{3,0}, \epsilon)\right) \\ \tilde{z}^b_{3,1} &= \tilde{z}^b_{3,0} \exp\left(\beta_-^2(\rho, \delta, \epsilon) + \eta_-^2(\rho, \delta, \tilde{x}^b_{3,0}, \tilde{z}^b_{3,0}, \epsilon)\right), \end{aligned} \tag{5.151}$$

We then need to show that $\mathcal{Y}^{\pitchfork}(c, a, \epsilon)$ is transverse to the fiber in Σ_3^{out} passing through the point $(\tilde{x}^b_{3,1}, \tilde{z}^b_{3,1})$. One way to do this is to find the intersection of this fiber with $\mathcal{Y}^{\pitchfork}(c, a, \epsilon)$ and show that it occurs for some $\tilde{x}_3 > \tilde{x}_3^{\pitchfork}$, where we know this transversality holds.

The fiber through $(\tilde{x}_3, \tilde{z}_3) = (\tilde{x}^b_{3,1}, \tilde{z}^b_{3,1})$ is given by the graph $\tilde{x}_3 = f_3^s(\tilde{z}_3; \tilde{x}^b_{3,1}, \tilde{z}^b_{3,1}, c, a, \epsilon)$, where

$$f_3^s(\tilde{z}^b_{3,1}; \tilde{x}^b_{3,1}, \tilde{z}^b_{3,1}, c, a, \epsilon) = \tilde{x}^b_{3,1} \tag{5.152}$$

and

$$\frac{df_3^s}{d\tilde{z}_3}(\tilde{z}_3; \tilde{x}^b_{3,1}, \tilde{z}^b_{3,1}, c, a, \epsilon) \to 0 \quad \text{as} \quad |(\epsilon, \tilde{x}^b_{3,1}, \tilde{z}^b_{3,1}, \tilde{z}_3)| \to 0 \tag{5.153}$$

We can solve for when this intersects $\mathcal{Y}^{\pitchfork}(c, a, \epsilon)$ by substituting the expressions $(\tilde{x}_3, \tilde{z}_3) = (\tilde{x}_3, \widehat{z}_3(\tilde{x}_3; c, a, \epsilon))$ to obtain

$$\tilde{x}_3 = f_3^s(\widehat{z}_3(\tilde{x}_3); \tilde{x}^b_{3,1}, \tilde{z}^b_{3,1}, c, a, \epsilon), \tag{5.154}$$

which we can solve by the implicit function theorem to find an intersection at

$$\tilde{x}_3^* = \mathcal{O}\left(\exp\left(\beta_+^2(\rho, \delta, \epsilon) - \eta/\epsilon\right)\right), \tag{5.155}$$

which indeed satisfies $\tilde{x}_3^* > \tilde{x}_3^{\pitchfork}$. As the chosen solution on $\mathcal{B}(s; c, a)$ was arbitrary, this shows that $\mathcal{Y}^{\pitchfork}(c, a, \epsilon)$ is transverse to the fibers passing through each solution on $\mathcal{B}(s; c, a)$ in the section Σ_3^{out} for all $(c, a) \in I_c \times I_a$.

As in the proof of Proposition 4.5, we track these solutions in backwards time from Σ_3^{out} to Σ^m to deduce that the transversality holds there also. We recall that $y_2^{\mathcal{T}}(c, a)$ denotes the y_2 coordinate in Σ^m of the backwards evolution of the basepoint on $\mathcal{Z}_\epsilon(c, a)$ in Σ_3^{out} corresponding to the fiber containing the solution on $\mathcal{Y}^{\pitchfork}(c, a, \epsilon)$ passing through $(\tilde{x}_3^{\pitchfork}, \widehat{z}_3(\tilde{x}_3^{\pitchfork})$. Hence following the solutions on $\mathcal{B}(s; c, a)$ from Σ_3^{out} to Σ^m in backwards time gives the result (4.32). □

Proof of Lemma 4.9. For the case of type 4 pulses, the argument proceeds as in the proof of Lemma 4.7. To treat the case of type 5 pulses, more care is needed. Using Proposition A.1 and the fact that $\mathcal{Y}(c, a, \epsilon)$ coincides with $\mathcal{Z}_\epsilon(c, a)$ for $w \leq w_A - \Delta_w$, the transversality result (4.43) hold easily for type 5 pulses with $s \in (2w^\dagger - w_A + \Delta_w, 2w^\dagger - \Delta_w)$, that is, with secondary right pulses of height $w \in (\Delta_w, w_A - \Delta_w)$. For type 5 pulses with $s \in (2w^\dagger - w_A - \Delta_w, 2w^\dagger - w_A + \Delta_w)$, that is, with secondary height $w \in (w_A - \Delta_w, w_A + \Delta_w)$ the backwards evolution of $\mathcal{B}(s; c, a)$ interacts with the Airy point before reaching the section Σ^m, and hence the result (4.43) is not clear.

For type 5 pulses with secondary height $w \in (w_A - \Delta_w, w_A + \Delta_w)$, the manifolds $\mathcal{B}(s; c, a)$ in fact approach the Airy point exponentially close to $\mathcal{W}_\epsilon^{s,r}(c, a)$ in backwards time. Hence these trajectories reach Σ_3^{out} after passing through different charts, as with $\mathcal{Y}(c, a, \epsilon)$. We need to ensure that $\mathcal{Y}^{\pitchfork}(c, a, \epsilon)$ is transverse to the fibers in Σ_3^{out} passing through each point on the intersection of $\mathcal{W}_\epsilon^{s,r}(c, a)$ with Σ_3^{out}. Similar to the above analysis for tracking $\mathcal{Y}^{\pitchfork}(c, a, \epsilon)$, the manifold $\mathcal{W}_\epsilon^{s,r}(c, a)$ intersects Σ_3^{out} curve defined in terms of Airy functions which winds around the origin in an exponentially decaying manner.

We focus on the part of $\mathcal{W}_\epsilon^{s,r}(c, a)$ which reaches Σ_3^{out} after passing through the charts $\mathcal{K}_1 \to \mathcal{K}_2 \to \mathcal{K}_3$ (see §5.5.1) as solutions entering $\mathcal{K}_3$ via different charts do not cause issues. From Lemma 5.9, we have that $\mathcal{W}_\epsilon^{s,r}(c, a)$

intersects Σ_3^{out} in a curve parameterized by $y_{2,0}$ as

$$\begin{aligned}\tilde{x}_{3,1}^r(y_{2,0}) &= \tilde{x}_{3,0}^r(y_{2,0}) \exp\left(\beta_+^2(\rho,\delta,\epsilon) + \eta_+^2(\rho,\delta,\tilde{x}_{3,0}^r,\tilde{z}_{3,0}^r,\epsilon)\right)\\ \tilde{z}_{3,1}^r(y_{2,0}) &= \tilde{z}_{3,0}^r(y_{2,0}) \exp\left(\beta_-^2(\rho,\delta,\epsilon) + \eta_-^2(\rho,\delta,\tilde{x}_{3,0}^r,\tilde{z}_{3,0}^r,\epsilon)\right),\end{aligned} \tag{5.156}$$

where

$$\tilde{x}_{3,0}^r(y_{2,0}) = \frac{\sqrt{\pi}e^{-\frac{\frac{1}{\delta^{2/3}}+y_{2,0}}{k\epsilon^{1/3}}}}{k^{1/6}\delta^{1/6}}\tilde{X}_3^r(y_{2,0}), \quad \tilde{z}_{3,0}^r(y_{2,0}) = \frac{\sqrt{\pi}e^{-\frac{\frac{1}{\delta^{2/3}}+y_{2,0}}{k\epsilon^{1/3}}}}{k^{1/6}\delta^{1/6}}\tilde{Z}_3^r(y_{2,0}), \tag{5.157}$$

and

$$\begin{aligned}\tilde{X}_3^r(y_{2,0}) &= \left(\mathrm{Ai}\left(-\frac{y_{2,0}}{k^{2/3}}\right) + k^{1/3}\delta^{4/3}\,\mathrm{Ai}'\left(-\frac{y_{2,0}}{k^{2/3}}\right)z_{2,0}^r(y_{2,0})\right)e^{\frac{2}{3}\frac{1}{k\delta}}\left(2+\mathcal{O}(\delta)\right)\\ &\quad + \mathcal{O}(\delta)\left(\mathrm{Bi}\left(-\frac{y_{2,0}}{k^{2/3}}\right) + k^{1/3}\delta^{4/3}\,\mathrm{Bi}'\left(-\frac{y_{2,0}}{k^{2/3}}\right)z_{2,0}^r(y_{2,0})\right)e^{-\frac{2}{3}\frac{1}{k\delta}} + \mathcal{O}(\epsilon^{2/3})\\ \tilde{Z}_3^r(y_{2,0}) &= \left(\mathrm{Bi}\left(-\frac{y_{2,0}}{k^{2/3}}\right) + k^{1/3}\delta^{4/3}\,\mathrm{Bi}'\left(-\frac{y_{2,0}}{k^{2/3}}\right)z_{2,0}^r(y_{2,0})\right)e^{-\frac{2}{3}\frac{1}{k\delta}}\left(1+\mathcal{O}(\delta)\right)\\ &\quad + \mathcal{O}(\delta)\left(\mathrm{Ai}\left(-\frac{y_{2,0}}{k^{2/3}}\right) + k^{1/3}\delta^{4/3}\,\mathrm{Ai}'\left(-\frac{y_{2,0}}{k^{2/3}}\right)z_{2,0}^r(y_{2,0})\right)e^{\frac{2}{3}\frac{1}{k\delta}} + \mathcal{O}(\epsilon^{2/3}).\end{aligned} \tag{5.158}$$

The fiber through $(\tilde{x}_3,\tilde{z}_3) = (\tilde{x}_{3,1}^r(y_{2,0}),\tilde{z}_{3,1}^r(y_{2,0}))$ is given by the graph $\tilde{x}_3 = f_3^s(\tilde{z}_3;\tilde{x}_{3,1}^r(y_{2,0}),\tilde{z}_{3,1}^r(y_{2,0}),c,a,\epsilon)$, where

$$f_3^s(\tilde{z}_{3,1}^r(y_{2,0});\tilde{x}_{3,1}^r(y_{2,0}),\tilde{z}_{3,1}^r(y_{2,0}),c,a,\epsilon) = \tilde{x}_{3,1}^r(y_{2,0}) \tag{5.159}$$

and

$$\frac{df_3^s}{d\tilde{z}_3}(\tilde{z}_3;\tilde{x}_{3,1}^r(y_{2,0}),\tilde{z}_{3,1}^r(y_{2,0}),c,a,\epsilon) \to 0 \quad \text{as} \quad |(\epsilon,\tilde{x}_{3,1}^r(y_{2,0}),\tilde{z}_{3,1}^r(y_{2,0}),\tilde{z}_3)| \to 0 \tag{5.160}$$

We can solve for when this intersects $\mathcal{Y}^{\pitchfork}(c,a,\epsilon)$ by plugging in $(\tilde{x}_3,\tilde{z}_3) = (\tilde{x}_3,\widehat{z}_3(\tilde{x}_3))$ to obtain

$$\tilde{x}_3 = f_3^s(\widehat{z}_3(\tilde{x}_3);\tilde{x}_{3,1}^r(y_{2,0}),\tilde{z}_{3,1}^r(y_{2,0}),c,a,\epsilon) \tag{5.161}$$

which we can solve by the implicit function theorem to find an intersection at

$$\tilde{x}_3^*(y_{2,0}) = \tilde{x}_{3,1}^r(y_{2,0}) + \mathcal{O}\left(\exp\left(\beta_+^2(\rho,\delta,\epsilon) - \eta/\epsilon\right)\right), \tag{5.162}$$

provided $\tilde{x}_3^* > \tilde{x}_3^{\pitchfork}$ (i.e. we need to be careful not to leave the domain on which $\widehat{z}_3(\tilde{x}_3;c,a,\epsilon)$ is both well-defined and transverse to the fibers of $\mathcal{Z}_\epsilon(c,a)$). To determine this, we note that the minimum possible $\tilde{x}_3^*(y_{2,0})$-value achieved is at a value of $y_{2,0}$ which is exponentially close to that which gives the minimum value of $\tilde{x}_{3,1}^r(y_{2,0})$. We hence proceed as above by computing the first 'turning point' on this curve, that is, the minimum (or largest negative) $\tilde{x}_3$-value achieved by $\tilde{x}_{3,1}^r(y_{2,0})$.

Similar to the proof of Lemma 5.10, we search for the first zero of $(\tilde{x}_{3,1}^r)'(y_{2,0})$, which amounts to solving for the first zero of

$$\left(\tilde{X}_3^r(y_{2,0}) - k\epsilon^{1/3}(\tilde{X}_3^r)'(y_{2,0}) + \mathcal{O}\left(\delta\tilde{x}_{3,0}^r(y_{2,0})\left(|\tilde{X}_3^r| + |\tilde{Z}_3^r| + \mathcal{O}(\epsilon^{1/3})\right)\right)\right) = 0, \tag{5.163}$$

which occurs when

$$y_{2,0} = y_{2,0}^r + k\epsilon^{1/3} + \mathcal{O}(\epsilon^{2/3}), \tag{5.164}$$

where $y_{2,0}^r$ is the first zero of $\tilde{X}_3^r(y_{2,0})$. Hence the minimum of $\tilde{x}_3^*(y_{2,0})$ occurs at some

$$y_{2,0}^{*,r} = y_{2,0}^r + k\epsilon^{1/3} + \mathcal{O}(\epsilon^{2/3}). \tag{5.165}$$

We now note that for $y_{2,0}$ near $y_{2,0}^r$, for all sufficiently small ϵ, we have that

$$\begin{aligned}\tilde{X}_3^r(y_{2,0}) = \tilde{X}_3^\ell(y_{2,0}) + \Bigg(& k^{1/3}\delta^{4/3}\,\mathrm{Ai}'\left(-\frac{y_{2,0}}{k^{2/3}}\right) e^{\frac{2}{3}\frac{1}{k\delta}}\left(2+\mathcal{O}\left(\delta\right)\right) \\ & + \mathcal{O}\left(\delta e^{-\frac{2}{3}\frac{1}{k\delta}}\left(k^{1/3}\delta^{4/3}\,\mathrm{Bi}'\left(-\frac{y_{2,0}}{k^{2/3}}\right)\right)\right)\Bigg)\left(z_{2,0}^r(y_{2,0}) - z_{2,0}^\ell(y_{2,0})\right) + \mathcal{O}(\epsilon^{2/3}),\end{aligned} \tag{5.166}$$

and hence

$$\begin{aligned}0 = \tilde{X}_3^r(y_{2,0}^r) = (\tilde{X}_3^\ell)'(y_{2,0}^\ell)(y_{2,0}^r - y_{2,0}^\ell) + \mathcal{O}\left((y_{2,0}^r - y_{2,0}^\ell)^2, \epsilon^{2/3}\right) \\ + \Bigg(k^{1/3}\delta^{4/3}\,\mathrm{Ai}'\left(-\frac{y_{2,0}^r}{k^{2/3}}\right) e^{\frac{2}{3}\frac{1}{k\delta}}\left(2+\mathcal{O}\left(\delta\right)\right) \\ + \mathcal{O}\left(\delta e^{-\frac{2}{3}\frac{1}{k\delta}} k^{1/3}\delta^{4/3}\,\mathrm{Bi}'\left(-\frac{y_{2,0}^r}{k^{2/3}}\right)\right)\Bigg)\left(z_{2,0}^r(y_{2,0}^r) - z_{2,0}^\ell(y_{2,0}^r)\right),\end{aligned} \tag{5.167}$$

from which we deduce that

$$y_{2,0}^r - y_{2,0}^\ell = \mu\left(z_{2,0}^r(y_{2,0}^r) - z_{2,0}^\ell(y_{2,0}^r)\right) + \mathcal{O}\left((z_{2,0}^r(y_{2,0}^r) - z_{2,0}^r(y_{2,0}^r))^2, \epsilon^{2/3}\right), \tag{5.168}$$

for some constant $\mu > 0$ bounded away from zero uniformly in ϵ. Hence we have

$$y_{2,0}^{*,r} - y_{2,0}^{\pitchfork} = \mu\left(z_{2,0}^r(y_{2,0}^r) - z_{2,0}^\ell(y_{2,0}^r)\right) + \mathcal{O}\left((z_{2,0}^r(y_{2,0}^r) - z_{2,0}^r(y_{2,0}^r))^2, \epsilon^{2/3}\right). \tag{5.169}$$

Finally, using (5.131), (5.163), (5.169), Lemma 5.9, and the definitions of $y_{2,0}^{*,r}, y_{2,0}^{\pitchfork}$, we have that

$$\begin{aligned}\tilde{X}_3^r(y_{2,0}^{*,r}) - \tilde{X}_3^\ell(y_{2,0}^{\pitchfork}) &= k\epsilon^{1/3}\left((\tilde{X}_3^r)'(y_{2,0}^{*,r}) - (\tilde{X}_3^\ell)'(y_{2,0}^{\pitchfork})\right) + \mathcal{O}\left(\epsilon^{2/3}\right) \\ &= \mathcal{O}\left(\epsilon^{1/3}\left(y_{2,0}^{*,r} - y_{2,0}^{\pitchfork}\right), \epsilon^{2/3}\right).\end{aligned} \tag{5.170}$$

We now estimate

$$\begin{aligned}\tilde{x}_3^* - \tilde{x}_3^{\pitchfork} &= \tilde{x}_{3,1}^r(y_{2,0}^{*,r}) - \tilde{x}_3^{\pitchfork} + \mathcal{O}\left(e^{\beta_+^2(\rho,\delta,\epsilon) - \eta/\epsilon}\right) \\ &= \tilde{x}_{3,0}^r(y_{2,0}^{*,r}) \exp\left(\beta_+^2(\rho,\delta,\epsilon) + \eta_+^2(\rho,\delta,\tilde{x}_{3,0}^r(y_{2,0}^{*,r}), \tilde{z}_{3,0}^r(y_{2,0}^{*,r}), \epsilon)\right) \\ &\quad - \tilde{x}_{3,0}(y_{2,0}^{\pitchfork}) \exp\left(\beta_+^2(\rho,\delta,\epsilon) + \eta_+^2(\rho,\delta,\tilde{x}_{3,0}^\ell(y_{2,0}^{\pitchfork}), \tilde{z}_{3,0}^\ell(y_{2,0}^{\pitchfork}), \epsilon)\right) + \mathcal{O}\left(e^{\beta_+^2(\rho,\delta,\epsilon) - \eta/\epsilon}\right) \\ &= \left(\tilde{x}_{3,0}^r(y_{2,0}^{*,r})(1+\mathcal{O}(\epsilon^{2/3})) - \tilde{x}_{3,0}^\ell(y_{2,0}^{\pitchfork})(1+\mathcal{O}(\epsilon^{2/3})) + \mathcal{O}\left(e^{-\eta/\epsilon}\right)\right) e^{\beta_+^2(\rho,\delta,\epsilon)} \\ &= \left(e^{-\frac{\frac{1}{\delta^{2/3}} + y_{2,0}^{*,r}}{k\epsilon^{1/3}}} \tilde{X}_3^r(y_{2,0}^{*,r})(1+\mathcal{O}(\epsilon^{2/3})) - e^{-\frac{\frac{1}{\delta^{2/3}} + y_{2,0}^{\pitchfork}}{k\epsilon^{1/3}}} \tilde{X}_3^\ell(y_{2,0}^{\pitchfork})(1+\mathcal{O}(\epsilon^{2/3})) + \mathcal{O}\left(e^{-\eta/\epsilon}\right)\right) \frac{\sqrt{\pi} e^{\beta_+^2(\rho,\delta,\epsilon)}}{k^{1/6}\delta^{1/6}} \\ &= \left(\tilde{X}_3^r(y_{2,0}^{*,r})(1+\mathcal{O}(\epsilon^{2/3})) - e^{\frac{y_{2,0}^{*,r} - y_{2,0}^{\pitchfork}}{k\epsilon^{1/3}}} \tilde{X}_3^\ell(y_{2,0}^{\pitchfork})(1+\mathcal{O}(\epsilon^{2/3})) + \mathcal{O}\left(e^{-\eta/\epsilon}\right)\right) \frac{\sqrt{\pi} e^{-\frac{\frac{1}{\delta^{2/3}} + y_{2,0}^{*,r}}{k\epsilon^{1/3}}}}{k^{1/6}\delta^{1/6}} e^{\beta_+^2(\rho,\delta,\epsilon)} \\ &= \Bigg(\left(\tilde{X}_3^\ell(y_{2,0}^{\pitchfork}) + \mathcal{O}\left(\epsilon^{1/3}\left(y_{2,0}^{*,r} - y_{2,0}^{\pitchfork}\right), \epsilon^{2/3}\right)\right)(1+\mathcal{O}(\epsilon^{2/3})) - e^{\frac{y_{2,0}^{*,r} - y_{2,0}^{\pitchfork}}{k\epsilon^{1/3}}} \tilde{X}_3^\ell(y_{2,0}^{\pitchfork})(1+\mathcal{O}(\epsilon^{2/3}))\Bigg) \\ &\quad \times \frac{\sqrt{\pi} e^{-\frac{\frac{1}{\delta^{2/3}} + y_{2,0}^{*,r}}{k\epsilon^{1/3}}}}{k^{1/6}\delta^{1/6}} e^{\beta_+^2(\rho,\delta,\epsilon)} \\ &= \left(\tilde{X}_3^\ell(y_{2,0}^{\pitchfork})\left(1 - e^{\frac{y_{2,0}^{*,r} - y_{2,0}^{\pitchfork}}{k\epsilon^{1/3}}}(1+\mathcal{O}(\epsilon^{2/3}))\right) + \mathcal{O}\left(\epsilon^{1/3}\left(y_{2,0}^{*,r} - y_{2,0}^{\pitchfork}\right), \epsilon^{2/3}\right)\right) \frac{\sqrt{\pi} e^{-\frac{\frac{1}{\delta^{2/3}} + y_{2,0}^{*,r}}{k\epsilon^{1/3}}}}{k^{1/6}\delta^{1/6}} e^{\beta_+^2(\rho,\delta,\epsilon)} \\ &> \left(\epsilon^{1/3}(\tilde{X}_3^\ell)'(y_{2,0}^{\pitchfork})\left(-\frac{\mu\kappa(\rho)}{\delta} + \mathcal{O}\left(\left(\frac{\kappa(\rho)}{\delta}\right)^2\right)\right) + \mathcal{O}\left(\epsilon^{2/3}\log\epsilon\right)\right) \frac{\sqrt{\pi} e^{-\frac{\frac{1}{\delta^{2/3}} + y_{2,0}^{*,r}}{k\epsilon^{1/3}}}}{k^{1/6}\delta^{1/6}} e^{\beta_+^2(\rho,\delta,\epsilon)} \\ &> 0,\end{aligned}$$

for all sufficiently small $\epsilon > 0$. From this we deduce that $\tilde{x}_3^* > \tilde{x}_3^{\pitchfork}$ as required. The remainder of the proof follows as in the proof of Lemma 4.7.

□

6 Discussion

In this paper, we described a phenomenon, previously observed numerically in [6, 12, 13], in which the branch of fast pulse solutions to (1.2) described in [5] turns sharply when continued numerically in the parameters (c, a) for fixed $\epsilon > 0$. This sharp turn is associated with a transition in the pulse solutions as the oscillations in the tails of the pulses grows into a secondary excursion, culminating in a double pulse solution which resembles two copies of the primary pulse.

Using geometric singular perturbation theory and blow-up techniques, we constructed this transition analytically. For each sufficiently small $\epsilon > 0$, we proved the existence of a continuous one-parameter family of homoclinic solutions to (1.2) forming a bridge between the pulses with oscillatory tails constructed in [5] and double pulses which are $\mathcal{O}(\sqrt{\epsilon})$-close to two copies of the primary singular pulse. Our construction of the double pulses was shown to break down near a Belyakov transition (1.3), which corresponds to numerical observations in which the branch of double pulses terminates near this Belyakov transition (see Figure 5 and [6]).

We showed that the sharp single-to-double-pulse transition is due to a canard-explosion-type mechanism organized by the equilibrium at the origin, which in a local center manifold takes the form of a canard point in the terminology of [22]. The homoclinic solutions were then constructed in a similar manner as in the case of a canard explosion of periodic orbits as in [23], using blow-up techniques and geometric matching.

The main complications which arise are twofold. Firstly, the problem is inherently three-dimensional: the setup requires three dimensions in order to construct homoclinic orbits with oscillatory tails. This complicates the matching procedure and also necessitates a framework in which both the hyperbolic and nonhyperbolic components of the flow can be tracked and matched accordingly in local neighborhoods of the nonhyperbolic fold points. To accomplish this, we capitalized on the exchange lemma and the techniques used in [5] to construct single pulses with oscillatory tails.

Secondly, constructing the tails of the solutions proved to be a significant technical challenge. We showed that the behavior of the tails was heavily influenced by the structure of the middle branch of the critical manifold, specifically the existence of what we refer to as an Airy point, encompassing the transition from node to focus behavior. We studied the flow near this point in great detail, utilizing blow-up techniques and invariant manifold theory, and we used this analysis to show that each transitional pulse can be matched with a tail lying in the stable manifold of the equilibrium. This analysis also explained the phenomenon previously observed numerically in which many of the transitional pulses appear to have nearly identical tails (see Figure 4).

While much of the construction is tailored to this particular problem, the techniques used are quite general and can be used to construct many different homoclinic or periodic solutions, both within the FitzHugh–Nagumo system and otherwise. A direct application within the FitzHugh–Nagumo system would be to construct N-pulses with oscillatory tails. On each successive excursion, exponentially small variations in the parameters (c, a) allow the associated matching conditions to be solved, ending with a solution in the tail manifold.

Beyond the FitzHugh–Nagumo system, this geometric matching procedure can be used to construct a wide variety of solutions in different systems. Of particular interest is the notion of a canard explosion as being a mechanism for spike-adding [11, 27, 28, 25, 24, 8]. In this sense, one can think of the canard mechanism in the FitzHugh–Nagumo system as allowing for the addition of a second pulse or spike to the primary pulse [8]. An interesting extension would be to determine if these techniques could be transferred to the case of a slow passage through such a transition, to obtain a full analytical construction of a dynamic spike-adding mechanism.

Finally, we comment on the PDE stability of the transitional pulses. While the pulses with small oscillatory tails (corresponding to those constructed in [5]) were shown to be stable in [4], our expectation is that the pulses lose stability as the oscillations in the tail grow sufficiently large, as the bifurcation curve resembles a "global" saddle-node bifurcation. A full study of the (loss of) PDE stability of these solutions is an interesting direction for future work.

Acknowledgements: The authors thank the referees and editor for their constructive and detailed comments. PC would like to thank Martin Wechselberger for helpful discussions during an initial stage of this project. PC was supported by the NSF under grant DMS-1148284. BS was partially supported by the NSF through grant DMS-1409742.

A Layer analysis of fronts

In this section we prove the following proposition regarding heteroclinic connections between the equilibria p_i for values of $w \in [0, w^\dagger]$ in the system (2.10). The results of Proposition A.1 are shown in Figure 7.

Proposition A.1. *Consider the system (2.10) for $(c, a) = (1/\sqrt{2}, 0)$. For each $w \in (0, w^\dagger)$, there exists a front $\phi_\ell(w)$ connecting the equilibria p_2 and p_1, and a front $\phi_r(w)$, connecting the equilibria p_2 and p_3. Furthermore,*

(i) For $w \in (0, w_A)$, the front ϕ_ℓ leaves p_2 along a weak unstable direction and remains in $\{(u, v) : u_1(w) < u < u_2(w), v < 0\}$. The front ϕ_r leaves p_2 along ϕ_ℓ, then crosses into the half space $v > 0$, where it remains until arriving at p_3.

(ii) When $w = w_A$, the fronts ϕ_ℓ, ϕ_r leave p_2 along the line $v = \dfrac{u - u_2(w)}{2\sqrt{2}}$ in the half space $v < 0$. There exist A_ℓ, A_r and $B_\ell, B_r > 0$ such that ϕ_ℓ, ϕ_r satisfy

$$\begin{aligned} u(t) &= u_2(w) + (A_j + B_j t)e^{\frac{t}{2\sqrt{2}}} + \mathcal{O}(t^2 e^{\frac{t}{\sqrt{2}}}) \\ v(t) &= \frac{1}{2\sqrt{2}}(A_j + B_j t)e^{\frac{t}{2\sqrt{2}}} + B_j e^{\frac{t}{2\sqrt{2}}} + \mathcal{O}(t^2 e^{\frac{t}{\sqrt{2}}}), \end{aligned} \tag{A.1}$$

$j = \ell, r$, asymptotically as $t \to -\infty$. There exists $\Delta > 0$ such that these solutions can be written as graphs $v = v_j(u), j = \ell, r$, for $u \in [u_2(w) - \Delta, u_2(w)]$ with $v_r(u) > v_\ell(u)$ for all $u \in [u_2(w) - \Delta, u_2(w)]$.

(iii) When $w = w^\dagger - w_A$, the fronts ϕ_ℓ, ϕ_r leave p_2 along the line $v = \dfrac{u - u_2(w)}{2\sqrt{2}}$ in the half space $v > 0$.

(iv) For $w \in (w^\dagger - w_A, w^\dagger)$, the front ϕ_r leaves p_2 along a weak unstable direction and remains in $\{(u, v) : u_2(w) < u < u_3(w), v > 0\}$. The front ϕ_ℓ leaves p_2 along ϕ_r, then crosses into the half space $v < 0$, where it remains until arriving at p_1.

Proof. We prove (i) and (ii); the remaining two assertions follow from the symmetry of the cubic nonlinearity. The claims regarding the front ϕ_ℓ follow from analysis of traveling fronts [2, 14, 10].

It remains to show the properties of the front ϕ_r. We first consider the case of small w. When $w = 0$, the equilibria p_1 and p_2 collide, and p_1 and p_3 are connected by the Nagumo front ϕ_f. Hence for small $w > 0$ property (i) follows from the fact that ϕ_f breaks regularly as w increases; this can be shown in a manner similar to the proof of [5, Proposition 5.2]. Hence the result holds for $w \in (0, \Delta_w)$ sufficiently small.

We next examine the linearization of (2.10) at the equilibria p_2, p_3. At p_i, the linearization of (2.10) is given by

$$J_2 = \begin{pmatrix} 0 & 1 \\ -f'(u_i(w)) & c \end{pmatrix}, \tag{A.2}$$

which has eigenvalues

$$\lambda_i^{\pm} = \frac{c \pm \sqrt{c^2 - 4f'(u_i(w))}}{2}. \tag{A.3}$$

For all $w \in (0, w_A)$ and all $c \geq 1/\sqrt{2}$, p_2 is an unstable node (which is degenerate in the critical case of $w = w_A, c = 1/\sqrt{2}$) with corresponding eigenvectors

$$e_2^{\pm} = \begin{pmatrix} 1 \\ \dfrac{c \pm \sqrt{c^2 - 4f'(u_2(w))}}{2} \end{pmatrix}. \tag{A.4}$$

For $w \in (0, w_A)$, the equilibrium p_2 has a well defined strong unstable eigenspace with nonzero (u, v)-components. Hence the front ϕ_r leaves the equilibrium along a trajectory tangent to this subspace with u initially either increasing or decreasing. Proving (i) amounts to showing that the former is always the case.

For all $w \in (0, w_A)$ and all $c \geq 1/\sqrt{2}$, p_3 is a saddle with corresponding eigenvectors

$$e_2^{\pm} = \begin{pmatrix} 1 \\ \dfrac{c \pm \sqrt{c^2 - 4f'(u_3(w))}}{2} \end{pmatrix}. \tag{A.5}$$

Hence for each $w \in (\Delta_w, w_A)$ and each $c \geq 1/\sqrt{2}$, the equilibrium p_2 has a well defined strong unstable manifold $\mathcal{W}^{uu}(p_2)$, and the equilibrium p_3 has a well defined stable manifold $\mathcal{W}^s(p_3)$. If a front were to exist as an intersection of $\mathcal{W}^{uu}(p_2)$ and $\mathcal{W}^s(p_3)$ lying in the half space $v > 0$ for some $c_w \geq \sqrt{2}$, then by monotonicity of the flow with respect to c, this connection will break upon varying c: for $c < c_w$, we must have that $\mathcal{W}^{uu}(p_2)$ lies below $\mathcal{W}^s(p_3)$ and vice-versa for $c > c_w$, and hence this value of c_w for which a connection exists is unique among $c \geq 1/\sqrt{2}$. We show that for each $w \in (0, w_A)$, such a value $c_w > 1/\sqrt{2}$ exists by explicitly constructing the associated front.

Using the ansatz $v = b(u - u_2(w))(u - u_3(w))$, we deduce that there is a front connecting p_2 and p_3 given by

$$\begin{aligned} u(t) &= \frac{u_3(w) + u_2(w)}{2} + \frac{u_3(w) - u_2(w)}{2} \tanh\left(\frac{u_3(w) - u_2(w)}{2\sqrt{2}} t\right) \\ v(t) &= \frac{(u_3(w) - u_2(w))^2}{4\sqrt{2}} \operatorname{sech}\left(\frac{u_3(w) - u_2(w)}{2\sqrt{2}} t\right), \end{aligned} \tag{A.6}$$

with wave speed

$$\begin{aligned} c &= \frac{1}{\sqrt{2}} \left(u_2(w) + u_3(w) - 2u_1(w)\right) \\ &= \frac{1}{\sqrt{2}} \left(u_1(w) + u_2(w) + u_3(w) - 3u_1(w)\right) \\ &= \frac{1}{\sqrt{2}} \left(1 - 3u_1(w)\right) \\ &> \frac{1}{\sqrt{2}}, \end{aligned} \tag{A.7}$$

for all $w \in (\Delta_w, w_A)$. Hence for each $w \in (\Delta_w, w_A)$, for $c = 1/\sqrt{2}$, we must have that $\mathcal{W}^{uu}(p_2)$ lies below $\mathcal{W}^s(p_3)$.

Finally, we can apply the same argument as above to the case of $w = w_A$. For $c = 1/\sqrt{2}$, there is a unique trajectory decaying exponentially in backwards time along the eigenvector

$$e_2^A = \begin{pmatrix} 1 \\ \dfrac{1}{2\sqrt{2}} \end{pmatrix}, \tag{A.8}$$

with exponential rate $e^{\frac{t}{2\sqrt{2}}}$, whereas all other trajectories decay with algebro-exponential rate $te^{\frac{t}{2\sqrt{2}}}$. We abuse notation and refer to this trajectory as $\mathcal{W}^{uu}(p_2)$. For $c > 1/\sqrt{2}$, p_2 is an unstable node, and as above we can find a front solution connecting $\mathcal{W}^{uu}(p_2)$ and $\mathcal{W}^{s}(p_3)$ at with wave speed

$$\begin{aligned} c &= \frac{1}{\sqrt{2}}\left(1 - 3u_1(w_A)\right) \\ &> \frac{1}{\sqrt{2}}, \end{aligned} \tag{A.9}$$

and hence, by the above monotonicity argument, we deduce that $\mathcal{W}^{uu}(p_2)$ lies below $\mathcal{W}^{s}(p_3)$ for $c = 1/\sqrt{2}$, $w = w_A$, which completes the proof of (ii). □

B Way-in-way-out function estimates

Proof of Lemma 3.6. For (i), we note that $0 < -u_1(w) < u_2(w) < \frac{2}{3}$ for all $w \in (0, w^\dagger)$; hence for $\gamma > 0$ and $w \in (0, w_A)$, we have that

$$\begin{aligned} R(w,w) &> \frac{1}{2}\int_{u_1(w)}^{-u_1(w)} \left(c - \sqrt{c^2 - 4f'(u)}\right)(2-3u)du \\ &= \frac{1}{2}\int_{0}^{-u_1(w)} 2c - (1-3u/2)\sqrt{c^2-4f'(u)} - (1+3u/2)\sqrt{c^2-4f'(-u)}du \end{aligned} \tag{B.1}$$

For $a = 0$, we have $f'(u) = 2u - 3u^2$. Letting $I(u)$ denote the integrand in the above expression, we compute

$$\begin{aligned} I'(u) &= \frac{3}{2}\left(c^2 - 8u + 12u^2\right)^{1/2} + \left(4 - 18u + 18u^2\right)\left(c^2 - 8u + 12u^2\right)^{-1/2} \\ &\quad - \frac{3}{2}\left(c^2 + 8u + 12u^2\right)^{1/2} - \left(4 + 18u + 18u^2\right)\left(c^2 + 8u + 12u^2\right)^{-1/2} \\ I''(u) &= \left(c^2 - 8u + 12u^2\right)^{-1/2}(54u - 24) + \left(16 - 120u + 288u^2 - 216u^3\right)\left(c^2 - 8u + 12u^2\right)^{-3/2} \\ &\quad - \left(c^2 + 8u + 12u^2\right)^{-1/2}(24 + 54u) + \left(16 + 120u + 288u^2 + 216u^3\right)\left(c^2 + 8u + 12u^2\right)^{-3/2} \\ &= \left(c^2 - 8u + 12u^2\right)^{-3/2}(16 - 24c^2 + 54uc^2 + 72u - 432u^2 + 432u^3) \\ &\quad + \left(c^2 + 8u + 12u^2\right)^{-3/2}(16 - 24c^2 - 54uc^2 - 72u - 432u^2 - 432u^3) \\ &> 8\left(c^2 + 8u + 12u^2\right)^{-3/2}(4 - 6c^2 - 108u^2) \end{aligned}$$

We have that $I(0) = I'(0) = 0$ and we have that $I''(u) > 0$ for any $u < \sqrt{\frac{4-6c^2}{108}}$. We recall that w_A is defined by $w = f(u_A)$ where u_A is the smaller root of the equation $c^2 = 4f'(u)$. We can solve to find $u_A = \frac{1}{3} - \frac{1}{6}\sqrt{4-3c^2}$, and hence for $c \in I_c$, we have $u_A < \sqrt{\frac{4-6c^2}{108}}$. Therefore $R(w,w) > 0$ for any $w \in (0, w_A)$.

For (ii), for $a = 0$ and $\gamma < 4$, we compute

$$\begin{aligned} R(w^\dagger, w_A) &= \frac{1}{2}\int_{u_1(w^\dagger)}^{u_2(w_A)} \left(c - \sqrt{c^2 - 4f'(u)}\right)\frac{f'(u)}{u - \gamma f(u)}du \\ &= \frac{1}{2}\int_{-1/3}^{u_A} \left(c - \sqrt{c^2 - 4f'(u)}\right)\frac{2-3u}{1-\gamma u(1-u)}du \\ &< \frac{1}{2}\frac{2-3u_A}{1-\gamma u_A(1-u_A)}\int_0^{u_A}\left(c - \sqrt{c^2-4f'(u)}\right)du + \frac{1}{2}\int_0^{1/3}\left(c - \sqrt{c^2-4f'(-u)}\right)\frac{2+3u}{1+\gamma u(1+u)}du \\ &< u_A^{3/2}\frac{2-3u_A}{1-4u_A(1-u_A)} + \frac{1}{2}\left(\frac{1}{3} - u_A\right)(c - 4u_A^{1/2})\frac{2+3u_A}{1+4u_A(1+u_A)} \\ &< 0. \end{aligned}$$

For (iii), we note that

$$\frac{dR}{dw^-}(w^-,w^+) = \frac{1}{2}\left(\sqrt{c^2-4f'(u_1)}-c\right)\frac{f'(u_1)}{u_1-\gamma f(u_1)}\frac{du_1}{dw^-}, \qquad u_1 = u_1(w^-) < 0,$$

and we see that $f'(u_1) < 0$, $u_1 - \gamma f(u_1) < 0$, and $\frac{du_1}{dw^-} < 0$, which implies that $\frac{dR}{dw^-} < 0$ as claimed. Similarly, we have

$$\frac{dR}{dw^+}(w^-,w^+) = \frac{1}{2}\left(c-\sqrt{c^2-4f'(u_2)}\right)\frac{f'(u_2)}{u_2-\gamma f(u_2)}\frac{du_2}{dw^+}, \qquad u_2 = u_2(w^+) > 0,$$

and we have $f'(u_2) > 0$, $u_2 - \gamma f(u_2) > 0$, and $\frac{du_2}{dw^+} > 0$, which implies $\frac{dR}{dw^+} > 0$. □

C Balance of exponential contraction/expansion in $\mathcal{Z}_\epsilon$

In this section, we provide a proof of Proposition 3.9.

Proof of Proposition 3.9. We begin with the proof of (i). We wish to determine the fate of another family of canard solutions γ_ϵ at the same parameter values $(c,a) = (c_\epsilon^\diamond, a_\epsilon^\diamond)$, also continuous in ϵ, which enters at height w_ϵ^{in}, where $\lim_{\epsilon\to 0} w_\epsilon^{in} = w_0^{in} < w^-$. In particular, we must show property (i) of Definition 3.7. Since $R(w^-,w^+) > 0$ and $w_0^{in} < w^-$, we have that $w^+ > w^b$, where w^b is the value of $w > 0$ which satisfies $R(w_0^{in}, w) = 0$. We now fix any sufficiently small $\delta > 0$ with $\delta < \min\{|w^+ - w^b|, |w^- - w_0^{in}|\}$. We claim that for all sufficiently small $\epsilon > 0$, corresponding exit height w_ϵ^{out} of γ_ϵ satisfies $|w_\epsilon^{out} - w^b| < \delta$. Equivalently, we have $w_0^{out} = \lim_{\epsilon\to 0} w_\epsilon^{out} = w^b$.

We first consider the flow in a neighborhood of $\mathcal{M}_\epsilon^{\ell,\mathcal{Z}}(c_\epsilon^\diamond, a_\epsilon^\diamond)$ for $\Delta_w < w < w^- - \delta$ for Δ_w sufficiently small; essentially we perform coordinate transformations to explicitly determine the contraction along $\gamma_\epsilon^\diamond$ away from the fold at the origin. Away from the origin, $\gamma_\epsilon^\diamond$ is $\mathcal{O}(e^{-q/\epsilon})$-close to $\mathcal{M}_\epsilon^{\ell,\mathcal{Z}}(c_\epsilon^\diamond, a_\epsilon^\diamond)$; hence we can parametrize $\gamma_\epsilon^\diamond$ by w, that is, in a neighborhood of $\mathcal{M}_\epsilon^{\ell,\mathcal{Z}}(c_\epsilon^\diamond, a_\epsilon^\diamond)$ the solution $\gamma_\epsilon^\diamond$ is given as a graph

$$\begin{aligned} u &= H(w,\epsilon) = f^{-1}(w) + \epsilon h(w,\epsilon) \\ v &= G(w,\epsilon) = \epsilon g(w,\epsilon), \end{aligned} \tag{C.1}$$

where we take the negative root $u_1(w)$ for $f^{-1}(w)$, and the functions H, G satisfy

$$\begin{aligned} \epsilon D_w H(w,\epsilon)(H(w,\epsilon) - \gamma w) &= G(w,\epsilon) \\ \epsilon D_w G(w,\epsilon)(H(w,\epsilon) - \gamma w) &= c_\epsilon^\diamond G(w,\epsilon) - f(H(w,\epsilon)) + w, \end{aligned} \tag{C.2}$$

and the flow along $\gamma_\epsilon^\diamond$ is given by

$$\dot{w} = \epsilon(H(w,\epsilon) - \gamma w). \tag{C.3}$$

We now write

$$\begin{aligned} u &= \tilde{u} + H(w,\epsilon) \\ v &= \tilde{v} + G(w,\epsilon), \end{aligned} \tag{C.4}$$

and compute the flow nearby for small $\tilde{u}, \tilde{v}$ as

$$\begin{aligned} \dot{\tilde{u}} &= \tilde{v} - \epsilon\tilde{u} D_w H(w,\epsilon) \\ \dot{\tilde{v}} &= c_\epsilon^\diamond \tilde{v} - \tilde{u} f'(H(w,\epsilon)) - \epsilon\tilde{u} D_w G(w,\epsilon) + \mathcal{O}(\tilde{u}^2) \\ \dot{w} &= \epsilon(\tilde{u} + H(w,\epsilon) - \gamma w). \end{aligned} \tag{C.5}$$

We consider the linearization of the two-dimensional $(\tilde{u}, \tilde{v})$ system about $(\tilde{u}, \tilde{v}, \epsilon) = (0, 0, 0)$ for each w. There is one stable and one unstable eigenvalue

$$\lambda^{\pm} = \frac{c_0 \pm \sqrt{c_0^2 - 4f'(f^{-1}(w))}}{2}, \tag{C.6}$$

where $c_0 := \lim_{\epsilon \to 0} c_\epsilon^\diamond$, with corresponding eigenvectors

$$e^{\pm} = \begin{pmatrix} 1 \\ \lambda^{\pm} \end{pmatrix}. \tag{C.7}$$

We now introduce the coordinates

$$\begin{aligned} U &= \tilde{v} - \lambda^+ \tilde{u} \\ V &= \tilde{v} - \lambda^- \tilde{u}, \end{aligned} \tag{C.8}$$

which, using the identities

$$\begin{aligned} \lambda^+ \lambda^- &= f'(f^{-1}(w)) \\ \lambda^{\pm} &= c_0 - \lambda^{\mp}, \end{aligned} \tag{C.9}$$

results in the system

$$\begin{aligned} \dot{U} &= \lambda^- U + F^-(U, V, w, \epsilon) \\ \dot{V} &= \lambda^+ V + F^+(U, V, w, \epsilon) \\ \dot{w} &= \epsilon(f^{-1}(w) - \gamma w + F^s(U, V, w, \epsilon)), \end{aligned} \tag{C.10}$$

where

$$\begin{aligned} F^{\pm}(U, V, w, \epsilon) &= \mathcal{O}\left(\epsilon U, \epsilon V, U^2, UV, V^2\right) \\ F^s(U, V, w, \epsilon) &= \mathcal{O}(U, V, \epsilon), \end{aligned} \tag{C.11}$$

and $\gamma_\epsilon^\diamond$ is given by $U = V = 0$.

We now identify the part of the manifold $\mathcal{Z}_\epsilon(c_\epsilon^\diamond, a_\epsilon^\diamond)$ which intersects this neighborhood as a graph of a function $V = V^*(U, w, \epsilon)$ which is C^1 in (U, w) and continuous in ϵ and is tangent to the plane $V = 0$ at $U = \epsilon = 0$, so that $V_U(0, w, 0) = 0$. Since by assumption $\gamma_\epsilon^\diamond$ is a solution on this manifold, we have also have $V(0, w, \epsilon) = 0$. Thus we can write $V(U, w, \epsilon) = \hat{V}(U, w, \epsilon)U$ where $\lim_{(U,\epsilon) \to 0} \hat{V}(U, w, \epsilon) = 0$.

Setting $\tilde{V} = V - V^*(U, w, \epsilon)$ and restricting to the flow on $\mathcal{Z}_\epsilon(c_\epsilon^\diamond, a_\epsilon^\diamond)$, i.e. $\tilde{V} = 0$, we arrive at the system

$$\begin{aligned} \dot{U} &= (\lambda^- + \tilde{F}^-(U, w, \epsilon))\tilde{U} \\ \dot{w} &= \epsilon(f^{-1}(w) - \gamma w + \tilde{F}^s(U, w, \epsilon)), \end{aligned} \tag{C.12}$$

where $\tilde{F}^-, \tilde{F}^s$ are continuous with

$$\begin{aligned} \lim_{(U,\epsilon) \to 0} \tilde{F}^-(U, w, \epsilon) &= 0 \\ \lim_{(U,\epsilon) \to 0} \tilde{F}^s(U, w, \epsilon) &= 0. \end{aligned} \tag{C.13}$$

Fix $0 < \Delta \ll \Delta_w$ sufficiently small; by assumption, the solution γ_ϵ starts in $\Sigma^{h,\ell}$ at $w = w_\epsilon^{in}$ and thus reaches $U = \Delta$ at some height $w_\epsilon^{in} + \mathcal{O}(\epsilon)$ provided $\epsilon \ll \Delta$. We can now estimate the contraction rate $\Lambda^\ell(w_\epsilon^{in}, \Delta_w)$ of the trajectory γ_ϵ on $\mathcal{Z}_\epsilon(c_\epsilon^\diamond, a_\epsilon^\diamond)$ between heights w_ϵ^{in} and Δ_w. We compute

$$\begin{aligned} \Lambda^\ell(w_\epsilon^{in}, \Delta_w) &= \int_{w_\epsilon^{in}}^{\Delta_w} \frac{\lambda^- + \tilde{F}^-(U, w, \epsilon)}{\epsilon(f^{-1}(w) - \gamma w + \tilde{F}^s(U, w, \epsilon))} dw \\ &= \int_{w_\epsilon^{in}}^{\Delta_w} \frac{c_0 - \sqrt{c_0^2 - 4f'(f^{-1}(w))}}{2\epsilon(f^{-1}(w) - \gamma w)} \left(1 + h(U, w, \epsilon)\right) dw, \end{aligned} \tag{C.14}$$

where $\lim_{(U,\epsilon)\to 0} h(U,w,\epsilon) = 0$. Therefore, by changing variables we have

$$\Lambda^{\ell}(w_\epsilon^{in}, \Delta_w) = \frac{1}{\epsilon}\left(\int_{u_1(w_0^{in})}^{u_1(\Delta_w)} \frac{c_0 - \sqrt{c_0^2 - 4f'(u)}}{2(u-\gamma f(u))} f'(u)du + \mathcal{H}^{\ell}\right), \tag{C.15}$$

where $|\mathcal{H}^{\ell}| \to 0$ as $(\Delta,\epsilon) \to 0$. Hence, by fixing $\Delta_w > 0$ small, and then taking $\Delta, \epsilon > 0$ sufficiently small, we obtain an estimate on the contraction along $\gamma_\epsilon^{\diamond}$ near the left slow manifold $\mathcal{M}_\epsilon^{\ell,\mathcal{Z}}(c_\epsilon^{\diamond}, a_\epsilon^{\diamond})$.

We can repeat this procedure along the middle slow manifold $\mathcal{M}_\epsilon^{m,\mathcal{Z}}(c_\epsilon^{\diamond}, a_\epsilon^{\diamond})$ to show that the expansion along $\gamma_\epsilon^{\diamond}$ between $w = \Delta_w$ and some yet to be determined exit height $w = w_\epsilon^{out}$ is given by

$$\Lambda^{m}(\Delta_w, w_\epsilon^{out}) = \frac{1}{\epsilon}\left(\int_{u_2(\Delta_w)}^{u_2(w_0^{out})} \frac{c_0 - \sqrt{c_0^2 - 4f'(u)}}{2(u-\gamma f(u))} f'(u)du + \mathcal{H}^{m}\right), \tag{C.16}$$

where $|\mathcal{H}^{m}| \to 0$ as $(\Delta,\epsilon) \to 0$.

The final piece to estimate is the passage near the canard point. However, we can bound the expansion/contraction in this region by taking Δ_w sufficiently small. Hence the total expansion/contraction experienced by the solution γ_ϵ along $\gamma_\epsilon^{\diamond}$ is given by

$$\begin{aligned}
\Lambda(w_\epsilon^{in}, w_\epsilon^{out}) &= \Lambda^{\ell}(w_\epsilon^{in}, \Delta_w) + \Lambda^{m}(\Delta_w, w_\epsilon^{out}) + \mathcal{O}(\eta/\epsilon) \\
&= \frac{1}{\epsilon}\left(\int_{u_1(w_0^{in})}^{u_2(w_0^{out})} \frac{c_0 - \sqrt{c_0^2 - 4f'(u)}}{2(u-\gamma f(u))} f'(u)du + \mathcal{H}\right) \\
&= \frac{1}{\epsilon}\left(R(w_0^{in}, w_0^{out}) + \mathcal{H}\right)
\end{aligned} \tag{C.17}$$

where $|\mathcal{H}| \to 0$ as $(\Delta, \Delta_w, \epsilon) \to 0$ and R is the way-in-way-out function.

This now allows us to determine the height w_0^{out}. By assumption the solution γ_ϵ reaches the section $\Sigma^{h,\ell}$ at $w = w_\epsilon^{in}$. By the above analysis, by balancing the exponential contraction/expansion via the function $\Lambda(w_\epsilon^{in}, w_\epsilon^{out})$, we can ensure that for all sufficiently small $\epsilon > 0$, γ_ϵ must return to $\Sigma^{h,\ell}$ at $w = w_\epsilon^{out}$ where $|w_\epsilon^{out} - w^b| < \delta$. Equivalently, we must have that $\lim_{\epsilon\to 0} w_\epsilon^{out} = w^b$.

We now consider the statement (ii). We set $w_b^- < w^-$ to be the unique value satisfying $R(w_b^-, w^+) = 0$ and again consider another family of canard solutions γ_ϵ at the same parameter values $(c,a) = (c_\epsilon^{\diamond}, a_\epsilon^{\diamond})$, also continuous in ϵ, which enters at height w_ϵ^{in}. Demonstrating property (i) of Definition 3.7 follows exactly as in the proof of (iii) above. It only remains to show Definition 3.7 (ii) (the remaining property Definition 3.7 (iii) follows similarly by considering the flow in reverse time).

Hence we assume that the entry heights w_ϵ^{in} satisfy $\lim_{\epsilon\to 0} w_\epsilon^{in} = w_0^{in} > w_b^-$. Fix $\delta > 0$ sufficiently small with $\delta < \min\{|w_0^{in} - w_b^-|, |w^- - w_b^-|\}$. Using similar arguments as above, by balancing the exponential contraction/expansion along the manifolds $\mathcal{M}_\epsilon^{\ell/m,\mathcal{Z}}(c_\epsilon^{\diamond}, a_\epsilon^{\diamond})$, for all sufficiently small $\epsilon > 0$, it is possible to obtain a bound $\Lambda(w_\epsilon^{in}, w_\epsilon^{out}) \le -\dfrac{\eta}{\epsilon}$ for any $w_\epsilon^{out} < w^+ - \delta$ and some $\eta > 0$. Hence we must have $w_\epsilon^{out} > w^+ - \delta$.

To show that w_ϵ^{out} also satisfies $w_\epsilon^{out} < w^+ + \delta$, we argue by contradiction. Suppose $w_\epsilon^{out} \ge w^+ + \delta$. By considering the flow in reverse time, we can measure the expansion/contraction experience by the trajectory $\gamma_\epsilon^{\diamond}$ along γ_ϵ (that is, we reverse the flow direction and interchange the roles of $\gamma_\epsilon^{\diamond}, \gamma_\epsilon$ in the argument used in the proof of (iii)). In reverse time, $\gamma_\epsilon^{\diamond}$ "enters" at height $w^+ < w_\epsilon^{out} - \delta$. By balancing the exponential/contraction as in the proof of (iii), in reverse time the trajectory should "exit" at a height w_ϵ^{C} satisfying $\lim_{\epsilon\to 0} w_\epsilon^{C} = w_b^-$. This gives the desired contradiction as by assumption $w_\epsilon^{C} = w^- > w_b^- + \delta$.

Therefore, we must have $|w_\epsilon^{out} - w^b| < \delta$, and the proof of (ii) is complete.

Finally, the proof of (iii) is similar to that of (ii) by considering the flow in reverse time.

□

D Contraction/expansion rates along $\mathcal{M}_\epsilon^\ell$, $\mathcal{M}_\epsilon^r$

To construct pulses of type $4, 5$, we need more explicit bounds on the rates of contraction and expansion along solutions near the slow manifolds $\mathcal{M}_\epsilon^\ell(c,a)$, $\mathcal{M}_\epsilon^r(c,a)$. We consider the flow in neighborhoods of each of these slow manifolds in which they are normally hyperbolic, and we make coordinate transformations to put the equations in a preliminary Fenichel normal form which identifies the stable/unstable subspaces and corresponding contraction/expansion rates.

The ultimate goal is to show that the manifold $\mathcal{B}(s;c,a)$ is well defined and exponentially close to $\gamma^{\text{se}}(s;c,a)$ in $\Sigma^{h,r}$ for each $(c,a) \in I_c \times I_a$. The existence of the solution $\gamma^{\text{se}}(s;c,a)$ for $(c,a) \in I_c \times I_a$ is clear; however, it is not immediately obvious that the fiber of this solution in the section Σ^m is exponentially contracted to $\gamma^{\text{se}}(s;c,a)$ in backwards time to $\Sigma^{h,r}$. Along the manifold $\mathcal{W}_\epsilon^{s,\ell}(c,a)$, this is clear as this fiber is defined by the fact that it contracts exponentially to $\gamma^{\text{se}}(s;c,a)$ in backwards time. However, after passing near the fold, in backwards time, $\gamma^{\text{se}}(s;c,a)$ is near the slow manifold $\mathcal{M}_\epsilon^r(c,a)$ and solutions near $\gamma^{\text{se}}(s;c,a)$ undergo exponential expansion. We claim that the contraction along $\mathcal{W}_\epsilon^{s,\ell}(c,a)$ compensates for this expansion.

We proceed by determining the balance of contraction/expansion along the slow manifolds $\mathcal{M}_\epsilon^{r/\ell}(c,a)$ in backwards time from Σ^m to $\Sigma^{h,r}$. We break this into three pieces: first the transition from Σ^m to Σ^{out}, where $\gamma^{\text{se}}(s;c,a)$ exits a neighborhood $\mathcal{U}_F$ of the upper right fold point along the fast jump ϕ_b, second the transition from Σ^{out} to $\Sigma^{i,-}$ encompassing the passage near the fold point, and finally the transition from $\Sigma^{i,-}$ to $\Sigma^{h,r}$ describing the passage near the right slow manifold $\mathcal{M}_\epsilon^r(c,a)$.

We first follow $\gamma^{\text{se}}(s;c,a)$ backwards from Σ^m into a neighborhood of $\mathcal{M}_\epsilon^\ell(c,a)$ at a height $w = \Delta_w$, so that we are away from the lower fold point. By construction $\gamma^{\text{se}}(s;c,a)$ lies in $\mathcal{W}_\epsilon^{s,\ell}(c,a)$ and remains in this neighborhood of $\mathcal{M}_\epsilon^\ell(c,a)$ until some height $w = w^\dagger + \mathcal{O}(\epsilon^{2/3}, a)$ corresponding to the fast jump to Σ^{out} in the neighborhood $\mathcal{U}_F$ of the upper right fold point. During this entire passage, solutions corresponding to the fiber $\{(0, y_2^{\text{se}}(s;c,a), z) : |z| \le \Delta_z\}$ in the section Σ^m are contracted exponentially to $\gamma^{\text{se}}(s;c,a)$ in backwards time, and hence we have the following.

Lemma D.1. *For each sufficiently small Δ_w, there exists $\Delta > 0, \epsilon_0 > 0$ and sufficiently small choice of the intervals I_c, I_a, such that for each $0 < \epsilon < \epsilon_0$, each $(c,a) \in I_c \times I_a$, and each $s \in (w^\dagger + \Delta_w, 2w^\dagger - \Delta_w)$, the following holds. The backwards evolution $\mathcal{B}(s;c,a)$ of the fiber $\{(0, y_2^{\text{se}}(s;c,a), z) : |z| \le \Delta_z\}$ in Σ^m reaches the section Σ^{out} near the upper right fold point in a curve which is $\mathcal{O}\left(e^{\Lambda^\ell(\Delta_w, w^\dagger - \Delta_w)}\right)$ close to $\gamma^{\text{se}}(s;c,a)$ uniformly in $(c,a,z_{\text{end}}) \in I_c \times I_a \times [-\Delta_z, \Delta_z]$ where*

$$\begin{aligned}\Lambda^\ell(\Delta_w, w^\dagger - \Delta_w) &= \int_{u_1(\Delta_w)}^{u_1(w^\dagger - \Delta_w)} \frac{c + \sqrt{c^2 - 4f'(u)}}{2\epsilon(u - \gamma f(u))} f'(u) du \\ &< 0.\end{aligned} \tag{D.1}$$

Furthermore the derivatives of the transition map from Σ^m to Σ^{out} for solutions on $\mathcal{B}(s;c,a)$ with respect to (c,a,z_{end}) are also $\mathcal{O}\left(e^{\Lambda^\ell(\Delta_w, w^\dagger - \Delta_w)}\right)$.

Proof. To see this, we consider the flow in a neighborhood of $\mathcal{M}_\epsilon^\ell(c,a)$; essentially we perform coordinate transformations to explicitly determine the expansion along $\mathcal{W}_\epsilon^{s,\ell}(c,a)$ away from the fold at the origin. Away from the origin, we can parametrize $\mathcal{M}_\epsilon^\ell(c,a)$ by w, and using arguments as in the proof of Proposition 3.9, the flow near $\mathcal{M}_\epsilon^\ell(c,a)$ can be reduced to the system

$$\begin{aligned}\dot{U} &= \lambda^- U + F^-(U,V,w,\epsilon) \\ \dot{V} &= \lambda^+ V + F^+(U,V,w,\epsilon) \\ \dot{w} &= \epsilon(f^{-1}(w) - \gamma w + F^s(U,V,w,\epsilon)),\end{aligned} \tag{D.2}$$

where

$$
\begin{aligned}
F^{\pm}(U,V,w,\epsilon) &= \mathcal{O}\left(\epsilon U, \epsilon V, U^2, UV, V^2\right) \\
F^{s}(U,V,w,\epsilon) &= \mathcal{O}(U,V,\epsilon),
\end{aligned}
\tag{D.3}
$$

and $\mathcal{M}_\epsilon^\ell(c,a)$ is given by $U=V=0$.

We now identify the part of $\mathcal{W}_\epsilon^{s,\ell}(c,a)$ which intersects this neighborhood as a graph $V=V^*(U,w,\epsilon)$. This manifold is foliated by strong unstable fibers tangent to lines (U,w) =const for $\epsilon=0$. Setting $\tilde{V}=V-V^*(U,w,\epsilon)$ and performing a coordinate change

$$
\begin{pmatrix} U \\ w \end{pmatrix} \to \begin{pmatrix} \tilde{U} \\ \tilde{W} \end{pmatrix} = \begin{pmatrix} U \\ w \end{pmatrix} + \mathcal{O}(\tilde{V}),
\tag{D.4}
$$

to straighten out the unstable fibers, we arrive at the system

$$
\begin{aligned}
\dot{\tilde{U}} &= \lambda^- \tilde{U} + \tilde{F}^-(\tilde{U},\tilde{W},\epsilon) \\
\dot{\tilde{V}} &= \lambda^+ \tilde{V} + \tilde{F}^+(\tilde{U},\tilde{V},\tilde{W},\epsilon)\tilde{V} \\
\dot{\tilde{W}} &= \epsilon(f^{-1}(\tilde{W}) - \gamma\tilde{W} + \tilde{F}^s(\tilde{U},\tilde{W},\epsilon)),
\end{aligned}
\tag{D.5}
$$

where

$$
\begin{aligned}
\tilde{F}^-(\tilde{U},\tilde{W},\epsilon) &= \mathcal{O}\left(\tilde{U}^2, \epsilon\tilde{U}\right) \\
\tilde{F}^+(\tilde{U},\tilde{V},\tilde{W},\epsilon) &= \mathcal{O}\left(\tilde{U},\tilde{V},\epsilon\right) \\
\tilde{F}^s(\tilde{U},\tilde{W},\epsilon) &= \mathcal{O}(\tilde{U},\epsilon).
\end{aligned}
\tag{D.6}
$$

We can now estimate the contraction rate $\Lambda^\ell(\tilde{W}_1,\tilde{W}_2)$ in backwards time along the fiber of a given trajectory lying on $\mathcal{W}_\epsilon^{s,\ell}(c,a)$ between heights $\tilde{W}_1$ and $\tilde{W}_2$, under the assumption that this trajectory remains in a small neighborhood of $\mathcal{M}_\epsilon^\ell(c,a)$, say $|\tilde{U}|,|\tilde{V}|\le\Delta\ll 1$, for $\tilde{W}\in[\tilde{W}_1,\tilde{W}_2]$. We compute

$$
\begin{aligned}
\Lambda^\ell(\tilde{W}_1,\tilde{W}_2) &= \int_{\tilde{W}_1}^{\tilde{W}_2} \frac{\lambda^+ + \tilde{F}^+(\tilde{U},\tilde{V},\tilde{W},\epsilon)}{\epsilon(f^{-1}(\tilde{W}) - \gamma W + \tilde{F}^s(\tilde{U},\tilde{W},\epsilon))} d\tilde{w} \\
&= \int_{\tilde{W}_1}^{\tilde{W}_2} \frac{\lambda^+}{\epsilon(f^{-1}(\tilde{W}) - \gamma\tilde{W})} \left(1+\mathcal{O}(\epsilon,\Delta)\right) d\tilde{W} \\
&= \int_{\tilde{W}_1}^{\tilde{W}_2} \frac{c+\sqrt{c^2-4f'(f^{-1}(\tilde{W}))}}{2\epsilon(f^{-1}(\tilde{W}) - \gamma\tilde{W})} \left(1+\mathcal{O}(\epsilon,\Delta)\right) d\tilde{W} \\
&= \int_{u_1(\tilde{W}_1)}^{u_1(\tilde{W}_2)} \frac{c+\sqrt{c^2-4f'(u)}}{2\epsilon(u-\gamma f(u))} f'(u) \left(1+\mathcal{O}(\epsilon,\Delta)\right) du.
\end{aligned}
\tag{D.7}
$$

Hence, by fixing $\Delta_w>0$ small, and taking $\Delta,\epsilon>0$ sufficiently small, we obtain the result. □

We proceed by considering the flow near the upper right fold point. Using the analysis in [22, 5], it is clear that the transition in backwards time from Σ^{out} to $\Sigma^{i,-}$ in the neighborhood $\mathcal{U}_F$ of the upper right fold point can be bounded by $e^{\eta/\epsilon}$ for each $\eta>0$ by taking the neighborhood $\mathcal{U}_F$ sufficiently small, that is, by shrinking Δ_w. The derivatives of the transition map also satisfy the same bounds.

Finally, we consider the transition from $\Sigma^{i,-}$ to $\Sigma^{h,r}$. We first prove the following technical lemma.

Lemma D.2. *For each sufficiently small Δ_w and $(c,a)\in I_c\times I_a$, we have that*

$$
\int_{u_1(w^\dagger-\Delta_w)}^{u_1(\Delta_w)} \frac{c+\sqrt{c^2-4f'(u)}}{u-\gamma f(u)} f'(u)du + \int_{u_3(-\Delta_w)}^{u_3(w^\dagger)} \frac{c-\sqrt{c^2-4f'(u)}}{u-\gamma f(u)} f'(u)du > 0.
\tag{D.8}
$$

Proof. We first write

$$\int_{u_3(-\Delta_w)}^{u_3(w^\dagger)} \frac{c-\sqrt{c^2-4f'(u)}}{u-\gamma f(u)} f'(u)du = \int_{u_3(\Delta_w)}^{u_3(w^\dagger-\Delta_w)} \frac{c-\sqrt{c^2-4f'(u)}}{u-\gamma f(u)} f'(u)du + \mathcal{O}(\Delta_w). \tag{D.9}$$

Hence it suffices to show that there exists $C>0$ such that

$$\int_{u_1(w^\dagger-\Delta_w)}^{u_1(\Delta_w)} \frac{c+\sqrt{c^2-4f'(u)}}{u-\gamma f(u)} f'(u)du + \int_{u_3(\Delta_w)}^{u_3(w^\dagger-\Delta_w)} \frac{c-\sqrt{c^2-4f'(u)}}{u-\gamma f(u)} f'(u)du > C, \tag{D.10}$$

for $(c,a)=(1/\sqrt{2},0)$ uniformly in $\Delta_w>0$ sufficiently small; the result then follows by continuity provided Δ_w and the intervals I_c, I_a are sufficiently small. For $(c,a)=(1/\sqrt{2},0)$, we have that $w^\dagger=\dfrac{4}{27}$, and the following identities hold for each $w\in(0,w^\dagger)$ and $u<0$.

$$\begin{aligned} u_3(w) &= \frac{2}{3} - u_1(w^\dagger - w) \\ f(u) &= \frac{4}{27} - f\left(\frac{2}{3}-u\right) \\ f'(u) &= f'\left(\frac{2}{3}-u\right). \end{aligned} \tag{D.11}$$

Hence

$$\begin{aligned} \int_{u_3(\Delta_w)}^{u_3(w^\dagger-\Delta_w)} \frac{c-\sqrt{c^2-4f'(u)}}{u-\gamma f(u)} f'(u)du &= \int_{\frac{2}{3}-u_1(w^\dagger-\Delta_w)}^{\frac{2}{3}-u_1(\Delta_w)} \frac{c-\sqrt{c^2-4f'(u)}}{u-\gamma f(u)} f'(u)du \\ &= -\int_{u_1(w^\dagger-\Delta_w)}^{u_1(\Delta_w)} \frac{c-\sqrt{c^2-4f'\left(\frac{2}{3}-u\right)}}{\frac{2}{3}-u-\gamma f\left(\frac{2}{3}-u\right)} f'\left(\frac{2}{3}-u\right) du \\ &= \int_{u_1(w^\dagger-\Delta_w)}^{u_1(\Delta_w)} \frac{c-\sqrt{c^2-4f'(u)}}{u-\gamma f(u)+\frac{4\gamma}{27}-\frac{2}{3}} f'(u)du \\ &> \int_{u_1(w^\dagger-\Delta_w)}^{u_1(\Delta_w)} \frac{c-\sqrt{c^2-4f'(u)}}{u-\gamma f(u)} f'(u)du, \end{aligned} \tag{D.12}$$

since $0<\gamma<4$. We therefore have that

$$\begin{aligned} &\int_{u_1(w^\dagger-\Delta_w)}^{u_1(\Delta_w)} \frac{c+\sqrt{c^2-4f'(u)}}{u-\gamma f(u)} f'(u)du + \int_{u_3(\Delta_w)}^{u_3(w^\dagger-\Delta_w)} \frac{c-\sqrt{c^2-4f'(u)}}{u-\gamma f(u)} f'(u)du \\ &> \int_{u_1(w^\dagger-\Delta_w)}^{u_1(\Delta_w)} \frac{c+\sqrt{c^2-4f'(u)}}{u-\gamma f(u)} f'(u)du + \int_{u_1(w^\dagger-\Delta_w)}^{u_1(\Delta_w)} \frac{c-\sqrt{c^2-4f'(u)}}{u-\gamma f(u)} f'(u)du \\ &= \int_{u_1(w^\dagger-\Delta_w)}^{u_1(\Delta_w)} \frac{c}{u-\gamma f(u)} f'(u)du \\ &> C, \end{aligned} \tag{D.13}$$

uniformly in $\Delta_w>0$ sufficiently small, which completes the proof. □

In combination with the above results, we can now prove Lemma 4.8.

Proof of Lemma 4.8. In a neighborhood of $\mathcal{M}_\epsilon^r(c,a)$, we can put the flow into the Fenichel normal form

$$\begin{aligned} \dot{U} &= -\lambda^- U + F^-(U,V,\tilde{w},\epsilon)U \\ \dot{V} &= -\lambda^+ V + F^+(U,V,\tilde{w},\epsilon)V \\ \dot{\tilde{w}} &= \epsilon(-f^{-1}(\tilde{w}) + \gamma\tilde{w} + F^{sl}(U,V,\tilde{w},\epsilon)), \end{aligned} \tag{D.14}$$

where

$$\begin{aligned} F^-(U,V,\tilde{w},\epsilon) &= \mathcal{O}\left(U,V,\epsilon\right) \\ F^+(U,V,\tilde{w},\epsilon) &= \mathcal{O}\left(U,V,\epsilon\right) \\ F^{sl}(U,V,\tilde{w},\epsilon) &= \mathcal{O}(UV,\epsilon), \end{aligned} \tag{D.15}$$

$$\lambda^{\pm} = \frac{c \pm \sqrt{c^2 - 4f'(f^{-1}(\tilde{w}))}}{2}, \tag{D.16}$$

and $f^{-1}(\tilde{w})$ refers to the largest root $u_3(\tilde{w})$ of $f(u) = \tilde{w}$. We note that the flow is now in *backwards* time. By construction, up to a reparameterization of $\gamma^{\text{se}}(s;c,a)$ according to the smooth coordinate transformation $(u,v,w) \to (U,V,\tilde{w})$, in backwards time $\gamma^{\text{se}}(s;c,a)$ exits at height $\tilde{w} = 2w^\dagger - s$. Between $\tilde{w} = 2w^\dagger - s$ and $\tilde{w} = w^\dagger - \Delta_w$, $\gamma^{\text{se}}(s;c,a)$ is given as a solution

$$\begin{aligned} U &= U^{\text{se}}(t;c,a,\epsilon) \\ V &= V^{\text{se}}(t;c,a,\epsilon) \\ \tilde{w} &= \tilde{w}^{\text{se}}(t;c,a,\epsilon) \end{aligned} \tag{D.17}$$

where $|U^{\text{se}}|, |V^{\text{se}}| \leq \Delta$ for $\tilde{w} \in (2w^\dagger - s, w^\dagger - \Delta_w)$. We now obtain estimates on this solution and its derivatives. We first recall/comment on how the solution $\gamma^{\text{se}}(s;c,a)$ is constructed.

For a given value of (s,c,a), $\gamma^{\text{se}}(s;c,a)$ is defined as the unique transverse intersection of the forward evolution of the line $\{u = 2/3, w = 2w^\dagger - s\}$ with the manifold $\mathcal{W}_\epsilon^{s,\ell}(c,a)$. Equivalently, for the same effect we could have worked in this Fenichel neighborhood of $\mathcal{M}_\epsilon^r(c,a)$ and considered constructing $\gamma^{\text{se}}(s;c,a)$ as the unique transverse intersection of the forward evolution of the line $\{U = \Delta, |V| \leq \Delta, \tilde{w} = 2w^\dagger - s\}$ with the manifold $\mathcal{W}_\epsilon^{s,\ell}(c,a)$. Using arguments similar to those in [5, §5] in the proof of Proposition 2.7, we obtain the solution $\gamma^{\text{se}}(s;c,a) = (U^{\text{se}}, V^{\text{se}}, \tilde{w}^{\text{se}})$ which satisfies $(U^{\text{se}}, V^{\text{se}}) = (\mathcal{O}(e^{-q/\epsilon}), \mathcal{O}(e^{-\eta/\epsilon}))$ at $\tilde{w} = w^\dagger - \Delta_w$ and $(U^{\text{se}}, V^{\text{se}}) = (\Delta, \mathcal{O}(e^{-q/\epsilon}))$ at $\tilde{w} = 2w^\dagger - s$, where $q > \eta > 0$. Furthermore, the derivatives with respect to (c,a) of these boundary values satisfy similar bounds, where q, η may need to be taken slightly smaller.

We now obtain more precise bounds for this solution and its derivatives. We write $\tilde{w} = w^* + W$ where $w^*(t)$ is the solution to

$$\dot{\tilde{w}} = \epsilon(-f^{-1}(\tilde{w}) + \gamma\tilde{w} + F^{sl}(0,0,\tilde{w},\epsilon)), \tag{D.18}$$

satisfying $\tilde{w}(0) = w^\dagger - \Delta_w, \tilde{w}(T) = 2w^\dagger - s$, where we note that $\epsilon/C < T < C/\epsilon$ for some $C > 0$. This results in the equations

$$\begin{aligned} \dot{U} &= \Lambda^u(t)U + G^-(U,V,W,\epsilon)U \\ \dot{V} &= -\Lambda^s(t)V + G^+(U,V,W,\epsilon)V \\ \dot{W} &= \epsilon(-(f^{-1})'(w^*)W + \gamma W + F^{sl}_{\tilde{w}}(0,w^*,\epsilon)W + G^{sl}(U,V,W,\epsilon)), \end{aligned} \tag{D.19}$$

where

$$\begin{aligned} \Lambda^u(t) &= -\lambda^-(w^*(t)) + \mathcal{O}(\epsilon) \\ \Lambda^s(t) &= \lambda^+(w^*(t)) + \mathcal{O}(\epsilon) \\ G^-(U,W,\epsilon) &= \mathcal{O}\left(U,V,W\right) \\ G^+(U,V,W,\epsilon) &= \mathcal{O}\left(U,V,W\right) \\ G^{sl}(U,V,W,\epsilon) &= \mathcal{O}(UV,W^2). \end{aligned} \tag{D.20}$$

We now define for each sufficiently small $\delta > 0$ the functions

$$\begin{aligned}
\beta_\delta^-(t,s) &= \int_s^t \Lambda^u(\tau) - \delta d\tau \\
\beta_\delta^+(t,s) &= \int_s^t -\Lambda^s(\tau) + \delta d\tau \\
\beta^{sl}(t,s) &= \epsilon \int_s^t -(f^{-1})'(w^*(\tau)) + \gamma + F_{\tilde{w}}^{sl}(0, w^*(\tau), \epsilon) d\tau.
\end{aligned} \tag{D.21}$$

Hence the solution $\gamma^{\text{se}}(s;c,a)$ given by $(U^{\text{se}}, V^{\text{se}}, W^{\text{se}})$, $W^{\text{se}} = \tilde{w}^{\text{se}} - w^*$, solves

$$\begin{aligned}
U(t) &= e^{\beta_0^-(t,T)}\Delta + \int_T^t e^{\beta_0^-(t,s)} G^-(U(s), V(s), W(s), \epsilon) U(s) ds \\
&:= \mathcal{F}^-(U, V, W, \Delta, V_0; c, a)(t) \\
V(t) &= e^{\beta_0^+(t,0)} V_0 + \int_0^t e^{\beta_0^+(t,s)} G^+(U(s), V(s), W(s), \epsilon) V(s) ds \\
&:= \mathcal{F}^+(U, V, W, \Delta, V_0; c, a)(t) \\
W(t) &= \int_T^t \epsilon e^{\beta^{sl}(t,s)} G^{sl}(U(s), V(s), W(s), \epsilon) ds \\
&:= \mathcal{F}^{sl}(U, V, W, \Delta, V_0; c, a)(t).
\end{aligned} \tag{D.22}$$

We define the spaces

$$\begin{aligned}
V_\delta^- &= \left\{ U : [0,T] \to \mathbb{R}^2 : \|U\|_\delta^- = \sup_{t\in[0,T]} e^{\beta_\delta^-(T,t)} |U(t)| < \infty \right\} \\
V_\delta^+ &= \left\{ V : [0,T] \to \mathbb{R} : \|V\|_\delta^+ = \sup_{t\in[0,T]} e^{\beta_\delta^+(0,t)} |V(t)| < \infty \right\} \\
V^{sl} &= \left\{ W : [0,T] \to \mathbb{R} : \|W\|^{sl} = \sup_{t\in[0,T]} |W(t)| < \infty \right\},
\end{aligned} \tag{D.23}$$

and for each fixed small $\delta > 0$ we have that

$$\begin{aligned}
\|\mathcal{F}^-(U, V, W, \Delta, V_0; c, a)\|_\delta^- &= \Delta + \mathcal{O}\left(\|U\|_\delta^- \left(\|U\|_\delta^- + \|V\|_\delta^+ + \|W\|^{sl} \right) \right) \\
\|\mathcal{F}^+(U, V, W, \Delta, V_0; c, a)\|_\delta^+ &= V_T + \mathcal{O}\left(\|V\|_\delta^+ \left(\|U\|_\delta^- + \|V\|_\delta^+ + \|W\|^{sl} \right) \right) \\
\|\mathcal{F}^{sl}(U, V, W, \Delta, V_0; c, a)\|^{sl} &= \mathcal{O}\left((\|W\|^{sl})^2, \|U\|_\delta^- \|V\|_\delta^+ \right),
\end{aligned} \tag{D.24}$$

and hence $\gamma^{\text{se}}(s;c,a)$ satisfies

$$\begin{aligned}
\|U^{\text{se}}\|_\delta^- &= \mathcal{O}(\Delta) \\
\|V^{\text{se}}\|_\delta^+ &= \mathcal{O}(V_0) = \mathcal{O}(e^{-\eta/\epsilon}) \\
\|W^{\text{se}}\|^{sl} &= \mathcal{O}\left(e^{-\eta/\epsilon} \right).
\end{aligned} \tag{D.25}$$

Taking derivatives of (D.22) with respect to the parameters (c,a) and taking δ slightly larger and η slightly smaller if necessary, we can bound the derivatives

$$\begin{aligned}
\|D_\nu U^{\text{se}}\|_\delta^- &= \mathcal{O}(\Delta) \\
\|D_\nu V^{\text{se}}\|_\delta^+ &= \mathcal{O}(e^{-\eta/\epsilon}) \\
\|D_\nu W^{\text{se}}\|^{sl} &= \mathcal{O}\left(e^{-\eta/\epsilon} \right),
\end{aligned} \tag{D.26}$$

for $\nu = (c,a)$.

To determine the contraction/expansion of solutions along $\gamma^{\text{se}}(s;c,a)$, we write

$$\begin{aligned} U &= U^{\text{se}}(t;c,a,\epsilon) + \tilde{U} \\ V &= V^{\text{se}}(t;c,a,\epsilon) + \tilde{V} \\ W &= W^{\text{se}}(t;c,a,\epsilon) + \tilde{W} \end{aligned} \tag{D.27}$$

and obtain the equations

$$\begin{aligned} \dot{\tilde{U}} &= \Lambda^u \tilde{U} + \tilde{G}_1^-(\tilde{U},\tilde{V},\tilde{W},\epsilon)\tilde{U} + \tilde{G}_2^-(\tilde{U},\tilde{V},\tilde{W},\epsilon)U^{\text{se}} \\ \dot{\tilde{V}} &= -\Lambda^s \tilde{V} + \tilde{G}_1^+(\tilde{U},\tilde{V},\tilde{W},\epsilon)\tilde{V} + \tilde{G}_2^+(\tilde{U},\tilde{V},\tilde{W},\epsilon)V^{\text{se}} \\ \dot{\tilde{W}} &= \epsilon(-(f^{-1})'(w^*)\tilde{W} + \gamma\tilde{W} + F^{sl}_{\tilde{w}}(0,w^*,\epsilon)\tilde{W} + \tilde{G}^{sl}(\tilde{U},\tilde{V},\tilde{W},\epsilon)), \end{aligned} \tag{D.28}$$

where

$$\begin{aligned} \tilde{G}_1^-(\tilde{U},\tilde{V},\tilde{W},\epsilon) &= \mathcal{O}\left(U^{\text{se}},V^{\text{se}},W^{\text{se}},\tilde{U},\tilde{V},\tilde{W}\right) \\ \tilde{G}_2^-(\tilde{U},\tilde{V},\tilde{W},\epsilon) &= \mathcal{O}\left(\tilde{U},\tilde{V},\tilde{W}\right) \\ \tilde{G}_1^+(\tilde{U},\tilde{V},\tilde{W},\epsilon) &= \mathcal{O}\left(U^{\text{se}},V^{\text{se}},W^{\text{se}},\tilde{U},\tilde{V},\tilde{W}\right) \\ \tilde{G}_2^+(\tilde{U},\tilde{V},\tilde{W},\epsilon) &= \mathcal{O}\left(\tilde{U},\tilde{V},\tilde{W}\right) \\ \tilde{G}^{sl}(\tilde{U},\tilde{W},\epsilon) &= \mathcal{O}(\tilde{U}V^{\text{se}},U^{\text{se}}\tilde{V},\tilde{U}\tilde{V},\tilde{W}W^{\text{se}},\tilde{W}^2). \end{aligned} \tag{D.29}$$

We can write this as the integral equation

$$\begin{aligned} \tilde{U}(t) &= e^{\beta_0^-(t,T)}\tilde{U}_T + \int_T^t e^{\beta_0^-(t,s)}\tilde{G}_1^-(\tilde{U}(s),\tilde{V}(s),\tilde{W}(s),\epsilon)\tilde{U}(s) + \tilde{G}_2^-(\tilde{U}(s),\tilde{V}(s),\tilde{W}(s),\epsilon)U^{\text{se}}(s)ds \\ \tilde{V}(t) &= e^{\beta_0^+(t,0)}\tilde{V}_0 + \int_0^t e^{\beta_0^+(t,s)}\tilde{G}_1^+(\tilde{U}(s),\tilde{V}(s),\tilde{W}(s),\epsilon)\tilde{V}(s) + \tilde{G}_2^+(\tilde{U}(s),\tilde{V}(s),\tilde{W}(s),\epsilon)V^{\text{se}}(s)ds \\ \tilde{W}(t) &= e^{\beta^{sl}(t,0)}\tilde{W}_0 + \int_0^t \epsilon e^{\beta^{sl}(t,s)}\tilde{G}^{sl}(\tilde{U}(s),\tilde{V}(s),\tilde{W}(s),\epsilon)ds. \end{aligned} \tag{D.30}$$

Provided $|\tilde{U}_T|$, $|\tilde{V}_0|$, and $|\tilde{W}_0|$ are sufficiently small, we can solve this by the implicit function theorem and obtain a solution satisfying

$$\begin{aligned} \|\tilde{U}\|_\delta^- &= \mathcal{O}\left(|\tilde{U}_T| + \Delta(|\tilde{V}_0| + |\tilde{W}_0|)\right) \\ \|\tilde{V}\|_\delta^+ &= \mathcal{O}\left(|\tilde{V}_0| + e^{-\eta/\epsilon}(|\tilde{U}_T| + |\tilde{W}_0|)\right) \\ \|\tilde{W}\|^{sl} &= \mathcal{O}\left(|\tilde{W}_0| + e^{-\eta/\epsilon}|\tilde{U}_T| + \Delta|\tilde{V}_0|\right). \end{aligned} \tag{D.31}$$

Taking derivatives of (D.30) with respect to the parameters (c,a) and taking δ slightly larger if necessary, we can bound the derivatives

$$\begin{aligned} \|D_\nu\tilde{U}\|_\delta^- &= \mathcal{O}\left(|\tilde{U}_T| + |D_\nu\tilde{U}_T| + \Delta(|\tilde{V}_0| + |D_\nu\tilde{V}_0| + |\tilde{W}_0| + |D_\nu\tilde{W}_0|)\right) \\ \|D_\nu\tilde{V}\|_\delta^+ &= \mathcal{O}(|\tilde{V}_0| + |D_\nu\tilde{V}_0| + e^{-\eta/\epsilon}(|\tilde{U}_T| + |D_\nu\tilde{U}_T| + |\tilde{W}_0| + |D_\nu\tilde{W}_0|)) \\ \|D_\nu\tilde{W}\|^{sl} &= \mathcal{O}\left(|\tilde{W}_0| + |D_\nu\tilde{W}_0| + e^{-\eta/\epsilon}(|\tilde{U}_T| + |D_\nu\tilde{U}_T|) + \Delta(|\tilde{V}_0| + |D_\nu\tilde{V}_0|)\right), \end{aligned} \tag{D.32}$$

for $\nu = (z_{\text{end}}, c, a)$.

By Lemma D.1, at $t=0$ the manifold $\mathcal{B}(s;c,a)$ is $\mathcal{O}(e^{\Lambda^\ell(\Delta_w, w^\dagger - \Delta_w)})$-close to $\gamma^{\text{se}}(s;c,a)$. That is, the solutions on $\mathcal{B}(s;c,a)$ can be represented in the above coordinates by solutions $(\tilde{U},\tilde{V},\tilde{W})$ satisfying

$$(\tilde{U},\tilde{V},\tilde{W})(0) = (\tilde{U}_0^B, \tilde{V}_0^B, \tilde{W}_0^B) = \mathcal{O}(e^{\Lambda^\ell(\Delta_w, w^\dagger - \Delta_w)})$$

uniformly along with their derivatives with respect to (z_{end}, c, a). We now solve for the solution to (D.30) which satisfies $(\tilde{V}_0, \tilde{W}_0) = (\tilde{V}_0^B, \tilde{W}_0^B)$ and

$$\tilde{U}_0^B = e^{\beta_0^-(0,T)}\tilde{U}_T + \int_T^0 e^{\beta_0^-(0,s)}\tilde{G}_1^-(\tilde{U}(s), \tilde{V}(s), \tilde{W}(s), \epsilon)\tilde{U}(s) + \tilde{G}_2^-(\tilde{U}(s), \tilde{V}(s), \tilde{W}(s), \epsilon)U^{\text{se}}(s)ds. \tag{D.33}$$

Provided $e^{\beta_0^-(T,0)}\tilde{U}_0^B$ is sufficiently small, we can find a solution $\tilde{U}_T$ satisfying (D.33). Performing a similar computation as in the proof of Lemma D.1 shows that the expansion $\beta_0^-(T,0)$ in backwards time from $w = w^\dagger - \Delta_w$ to $w = 2w^\dagger - s$ can be estimated by

$$\Lambda^r(w^\dagger - \Delta_w, 2w^\dagger - s) = \int_{u_3(w^\dagger - \Delta_w)}^{u_3(2w^\dagger - s)} \frac{c - \sqrt{c^2 - 4f'(u)}}{2\epsilon(u - \gamma f(u))}\left(1 + \mathcal{O}(\epsilon, \Delta)\right) f'(u)du. \tag{D.34}$$

Using this in combination with the $\mathcal{O}(e^{\Lambda^\ell(\Delta_w, w^\dagger - \Delta_w)})$ bounds on $\tilde{U}_0^B, \tilde{V}_0^B, \tilde{W}_0^B$ for the contraction/expansion from Σ^m to Σ^{out} and Σ^{out} to $\Sigma^{i,-}$ and Lemma D.2, we deduce that $\mathcal{B}(s; c, a)$ is $\mathcal{O}(e^{-q/\epsilon})$-close to $\gamma^{\text{se}}(s; c, a)$ in $\Sigma^{h,r}$. □

References

[1] Milton Abramowitz and Irene A Stegun, editors. *Handbook of mathematical functions: with formulas, graphs, and mathematical tables*. Dover, 1964.

[2] Donald G Aronson and Hans F Weinberger. Multidimensional nonlinear diffusion arising in population genetics. *Advances in Mathematics*, 30(1):33–76, 1978.

[3] G Carpenter. A geometric approach to singular perturbation problems with applications to nerve impulse equations. *J. Differential Equations*, 23(3):335–367, 1977.

[4] P Carter, B de Rijk, and B Sandstede. Stability of traveling pulses with oscillatory tails in the FitzHugh–Nagumo system. *Journal of Nonlinear Science*, 2016. http://dx.doi.org/10.1007/s00332-016-9308-7.

[5] P Carter and B Sandstede. Fast pulses with oscillatory tails in the FitzHugh–Nagumo system. *SIAM J. Math. Anal.*, 47(5):3393–3441, 2015.

[6] AR Champneys, V Kirk, E Knobloch, BE Oldeman, and J Sneyd. When Shil'nikov meets Hopf in excitable systems. *SIAM J. Applied Dynamical Systems*, 6(4):663–693, 2007.

[7] Peter De Maesschalck and Freddy Dumortier. Time analysis and entry–exit relation near planar turning points. *Journal of Differential Equations*, 215(2):225–267, 2005.

[8] M Desroches, TJ Kaper, and M Krupa. Mixed-mode bursting oscillations: Dynamics created by a slow passage through spike-adding canard explosion in a square-wave burster. *Chaos: An Interdisciplinary Journal of Nonlinear Science*, 23(4):046106, 2013.

[9] N Fenichel. Geometric singular perturbation theory for ordinary differential equations. *J. Differential Equations*, 31(1):53–98, 1979.

[10] Th Gallay. Local stability of critical fronts in nonlinear parabolic partial differential equations. *Nonlinearity*, 7(3):741, 1994.

[11] J Guckenheimer and C Kuehn. Computing slow manifolds of saddle type. *SIAM Journal on Applied Dynamical Systems*, 8(3):854–879, 2009.

[12] J Guckenheimer and C Kuehn. Homoclinic orbits of the FitzHugh-Nagumo equation: The singular-limit. *Discrete and Continuous Dynamical Systems Series S*, 2(4):851, 2009.

[13] J Guckenheimer and C Kuehn. Homoclinic orbits of the FitzHugh-Nagumo equation: Bifurcations in the full system. *SIAM J. Applied Dynamical Systems*, 9(1):138–153, 2010.

[14] Hermann Haaf. *Existence of periodic travelling waves to reaction-diffusion equations with excitable-oscillatory kinetics.* PhD thesis, University of Warwick, 1993.

[15] SP Hastings. On the existence of homoclinic and periodic orbits for the FitzHugh-Nagumo equations. *Quarterly J. Mathematics*, 27(1):123–134, 1976.

[16] Morris W Hirsch, Charles Chapman Pugh, and Michael Shub. *Invariant manifolds*, volume 583. Springer, 1977.

[17] Alan L Hodgkin and Andrew F Huxley. A quantitative description of membrane current and its application to conduction and excitation in nerve. *The Journal of physiology*, 117(4):500, 1952.

[18] AJ Homburg and B Sandstede. Homoclinic and heteroclinic bifurcations in vector fields. *Handbook of Dynamical Systems*, 3:379–524, 2010.

[19] CKRT Jones. Stability of the travelling wave solution of the FitzHugh-Nagumo system. *Trans. American Mathematical Society*, 286(2):431–469, 1984.

[20] CKRT Jones, N Kopell, and R Langer. Construction of the FitzHugh-Nagumo pulse using differential forms. In *Patterns and dynamics in reactive media*, pages 101–115. Springer, 1991.

[21] M Krupa, B Sandstede, and P Szmolyan. Fast and slow waves in the FitzHugh-Nagumo equation. *J. Differential Equations*, 133(1):49–97, 1997.

[22] M Krupa and P Szmolyan. Extending geometric singular perturbation theory to nonhyperbolic points—fold and canard points in two dimensions. *SIAM J. Mathematical Analysis*, 33(2):286–314, 2001.

[23] M Krupa and P Szmolyan. Relaxation oscillation and canard explosion. *J. Differential Equations*, 174(2):312–368, 2001.

[24] J Nowacki, HM Osinga, and K Tsaneva-Atanasova. Dynamical systems analysis of spike-adding mechanisms in transient bursts. *The Journal of Mathematical Neuroscience (JMN)*, 2(1):1–28, 2012.

[25] HM Osinga and KT Tsaneva-Atanasova. Dynamics of plateau bursting depending on the location of its equilibrium. *Journal of Neuroendocrinology*, 22(12):1301–1314, 2010.

[26] S Schecter. Exchange lemmas 2: General exchange lemma. *J. Differential Equations*, 245(2):411–441, 2008.

[27] D Terman. Chaotic spikes arising from a model of bursting in excitable membranes. *SIAM Journal on Applied Mathematics*, 51(5):1418–1450, 1991.

[28] K Tsaneva-Atanasova, HM Osinga, T Rieß, and A Sherman. Full system bifurcation analysis of endocrine bursting models. *Journal of Theoretical Biology*, 264(4):1133–1146, 2010.

[29] E Yanagida. Stability of fast travelling pulse solutions of the FitzHugh-Nagumo equations. *J. Mathematical Biology*, 22(1):81–104, 1985.

[30] EP Zemskov, IR Epstein, and Adrian Muntean. Oscillatory pulses in fitzhugh–nagumo type systems with cross-diffusion. *Mathematical Medicine and Biology*, 28(2):217–226, 2011.